AWS/TR-79/006
Revised

THE USE OF
THE SKEW T, LOG P DIAGRAM
IN ANALYSIS AND FORECASTING

DECEMBER 1979

Revised March 1990

(This June 1995 reprinting includes all errata and revisions to date, including a minor change to the convective gust potential forecast procedure on Page 5-41)

APPROVED FOR PUBLIC RELEASE;

DISTRIBUTION IS UNLIMITED

# AIR WEATHER SERVICE
Scott Air Force Base, Illinois 62225-5008
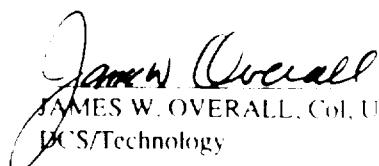
REVIEW AND APPROVAL STATEMENT

AWS/TR-79/006, December 1979 (revised March 1990), *The Use of the Skew T, Log P Diagram in Analysis and Forecasting*, has been reviewed and is approved for public release. There is no objection to unlimited distribution of this document to the public at large, or by the Defense Technical Information Center (DTIC) to the National Technical Information Service (NTIS).

ROGER C. WHITON, Lt Col, USAF
Directorate of Aerospace Development

FOR THE COMMANDER

JAMES W. OVERALL, Col, USAF
DCS/Technology

REPORT DOCUMENTATION PAGE

2. Report Date: December 1979 (Revised March 1990)

3. Report Type: Technical Report

4. Title: *The Use of the Skew T, Log P Diagram in Analysis and Forecasting*

7. Performing Organization Name and Address: HQ AWS/XT, Scott AFB, IL 62225-5008

8. Performing Organization Report Number: AWS/TR-79/006 (Revised)

11. Supplementary Notes: Reprinted in March 1990 to incorporate the following: November 1987 revision that updates obsolete references and adds new stability indices and formulas; August 1988 and March 1989 errata; and a March 1990 revision that adds new stability indices and fog forecasting techniques. Supersedes AD-A195862.

12. Distribution/Availability Statement: Approved for public release; distribution is unlimited.

13. Abstract: Describes the DoD Skew T, Log P diagram and provides instructions on its use. Instructions include how to plot data on the diagram and how to use the data to determine unreported meteorological elements and atmospheric stability. Also tells how to analyze discontinuities, stable layers, and clouds, as well as how to use the plotted diagram to help forecast meteorological phenomena such as aircraft icing and severe convective storms. Revised in November 1987 to add several new stability indices and provide instructions for plotting and using pressure altitude curves. The March 1990 revision adds several new stability indices and forecasting techniques currently displayed on the Satellite Data Handling System (SDHS), the Automated Weather Distribution System (AWDS), and microcomputer Skew T programs.

14. Subject Terms: METEOROLOGY, WEATHER, WEATHER FORECASTING, WEATHER ANALYSIS, UPPER AIR, SOUNDING, atmospheric sounding, atmospheric stability, stability index, meteorological sounding, meteorological analysis, Skew T, Log P diagram.

15: Number of Pages: 153

17. Security Classification of Report: Unclassified

18. Security Classification of this Page: Unclassified

19. Security Classification of Abstract: Unclassified

20. Limitation of Abstract: UL

Standard Form 298

PREFACE

This report (originally issued on 1 September 1952 as AWSM 105-124) was converted to an Air Weather Service Technical Report (AWS/TR-79/006) in December 1979. Surprisingly, there have been only minor changes in the basic procedures for plotting, analyzing, and using the Skew T, Log P diagram over the past 35 years. The two recent revisions (November 1987 and March 1990) are primarily concerned with new stability indices. This reprint, which incorporates all revisions and errata to date, was necessary to replenish stock and fill outstanding orders for this venerable document.

Many of the changes in the 1987 revision had to do with updating obsolete references, but instructions for plotting and using the pressure altitude curve were also added, as paragraph 3.7. A major change was the addition (in Chapter 5) of several new stability indices, along with their descriptions and formulas. For the latter, AWS thanks Bill Henry of the National Weather Service Training Center, whose pamphlet (*The Skew T, Log P, Diagram*) provided most of the material.

The 1990 revision adds several new stability indices currently displayed on the Satellite Data Handling System (SDHS), the Automated Weather Distribution System (AWDS), and microcomputer Skew T programs. For the microcomputer indices, AWS/XTX used the very recently published *Skew-T Professional*, Version 2.3, 2 November 1989. This revision also includes procedures for determining a Fog Stability Index, a Fog Point value, and a Fog Threat value.

This printing (March 1990) also incorporates August 1988 and March 1989 errata.

Readers may note that many of the equipment references in Chapter 7 seem obsolete. These references (along with some of the equipment) are being reviewed for possible updating in subsequent revisions.

Contents

FIGURES

TABLES

INTRODUCTION

1.1. Organization of the Manual. This manual is issued in one volume. A planned second volume to cover the use of atmospheric soundings in forecasting proved impracticable to compile. Also, the general use of computer-produced analysis and prognostic charts has greatly decreased the direct application of soundings in forecasting. However, Chapter 8 is added to note some uses of soundings in techniques for forecasting certain phenomena. The manual opens with a description of the DOD Skew T, Log P Diagram (chapters 1 and 2) and instructions for plotting soundings on it (chapter 3). The procedures for evaluating, on the diagram, certain basic quantities from the sounding are then outlined in chapter 4. Up to this point, the treatment is designed for guidance of both observers and forecasters. The rest of the manual is a text for forecasters on the principles and procedures of analyzing raobs on the Skew T, Log P Diagram for stability, fronts, inversions, and clouds. This material is not a review of the conventional standard textbook approach, but a selection and evaluation of topics which recent experience and empirical studies indicate are of direct application to practical forecasting under present operating conditions in ordinary detachments. In chapter 8 various empirical forecasting procedures involving use of the soundings plotted on Skew T, Log P Diagrams are mentioned with respect to clouds, fog, precipitation, showers, temperature, hail, icing, contrails, and turbulence.

1.2. Reason for Choosing the Skew T, Log P Diagram. The Skew T, Log P Diagram was selected by AWS as the most convenient thermodynamic diagram for general use. It was chosen in preference to numerous other diagrams because it is easier to use in many meteorological procedures and computations.

Such thermodynamic diagrams as the Emagram, Tephigram, Stüve Diagram[1] and the Skew T, Log P Diagram all express the same physical relationships [33] and show isobars, isotherms, dry adiabats, saturation adiabats, and saturation mixing-ratio lines. They differ only in the arrangement of these coordinates (see Figures 1a through 1d).

For convenience and utility, it is desired to have a diagram on which: a) the important isopleths are straight rather than curved, b) the angle between adiabats and isotherms is large enough to facilitate estimates of the stability, c) the ratio of area on the chart to thermodynamic energy is the same over the whole diagram, d) an entire sounding to levels inside the stratosphere can be plotted, and e) the vertical in the atmosphere approximates the vertical coordinate of the diagram. Both the skewed version of the Tephigram and the Skew T, Log P Diagram have most of these advantages, but the latter is preferred because its isobars are straight, which makes it easier to estimate pressure altitudes. The Skew T, Log P Diagram was developed[2] from the Emagram by "skewing" the isotherms of that diagram to nearly 45 degrees

---

[1] In the United States, the Stüve Diagram came to be known as "The Pseudo-Adiabatic Diagram." Actually, all of the diagrams mentioned are "pseudo-adiabatic diagrams," in that they are derived by assuming that the latent heat of condensation is used to heat the air parcel, and that condensed moisture falls out immediately (see pars. 2.4 and 5.3).

[2] The coordinate system of the Skew T, Log P Diagram was first suggested by N. Herlofson [30], a Norwegian meteorologist.
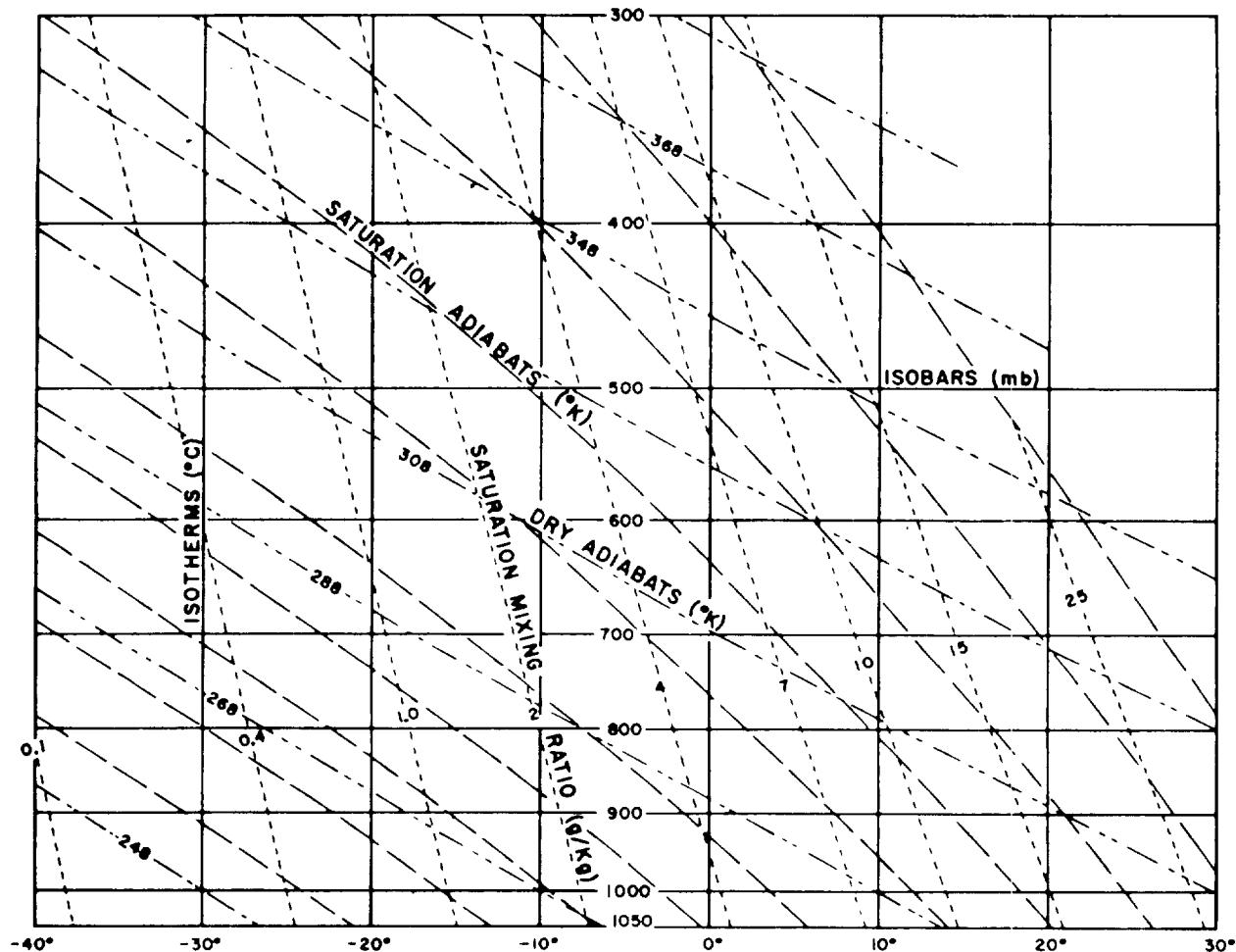
Figure 1a. Coordinate System of the Emagram.

from the vertical to increase the angle between isotherms and adiabats. On the Skew T, Log P Diagram, both the isotherms and isobars are straight lines. The desired relationship between energy and diagram area is also essentially fulfilled, so that thickness scales are easily prepared for any given layer. In addition, a convenient color scheme has been selected, and auxiliary scales have been added to further enhance the value of the diagram. A detailed description of the Skew T, Log P Diagram is given in Chapter 2.

1.3. Different Versions of the DOD Skew T, Log P Diagram. The DOD Skew T, Log P Diagram - hereafter referred to as the

"Skew-T Chart" - is printed by the Aeronautical Chart and Information Center (ACIC), and can be requisitioned by USAF activities in accordance with instructions in the DOD *Catalog of Weather Plotting Charts* published by ACIC. The Skew-T Chart is available in five versions:

a. A full-scale chart for general use (DOD WPC 9-16), printed on a sheet 28 x 30 inches. This version now includes the Appleman contrail forecasting curves (see AWSM 105-100) which were on the formerly issued WPC 9-16B.

b. A small-scale chart (DOD WPC 9-16-1), photographically reduced from the full-scale chart, and printed on a sheet 17 x 15

1—2
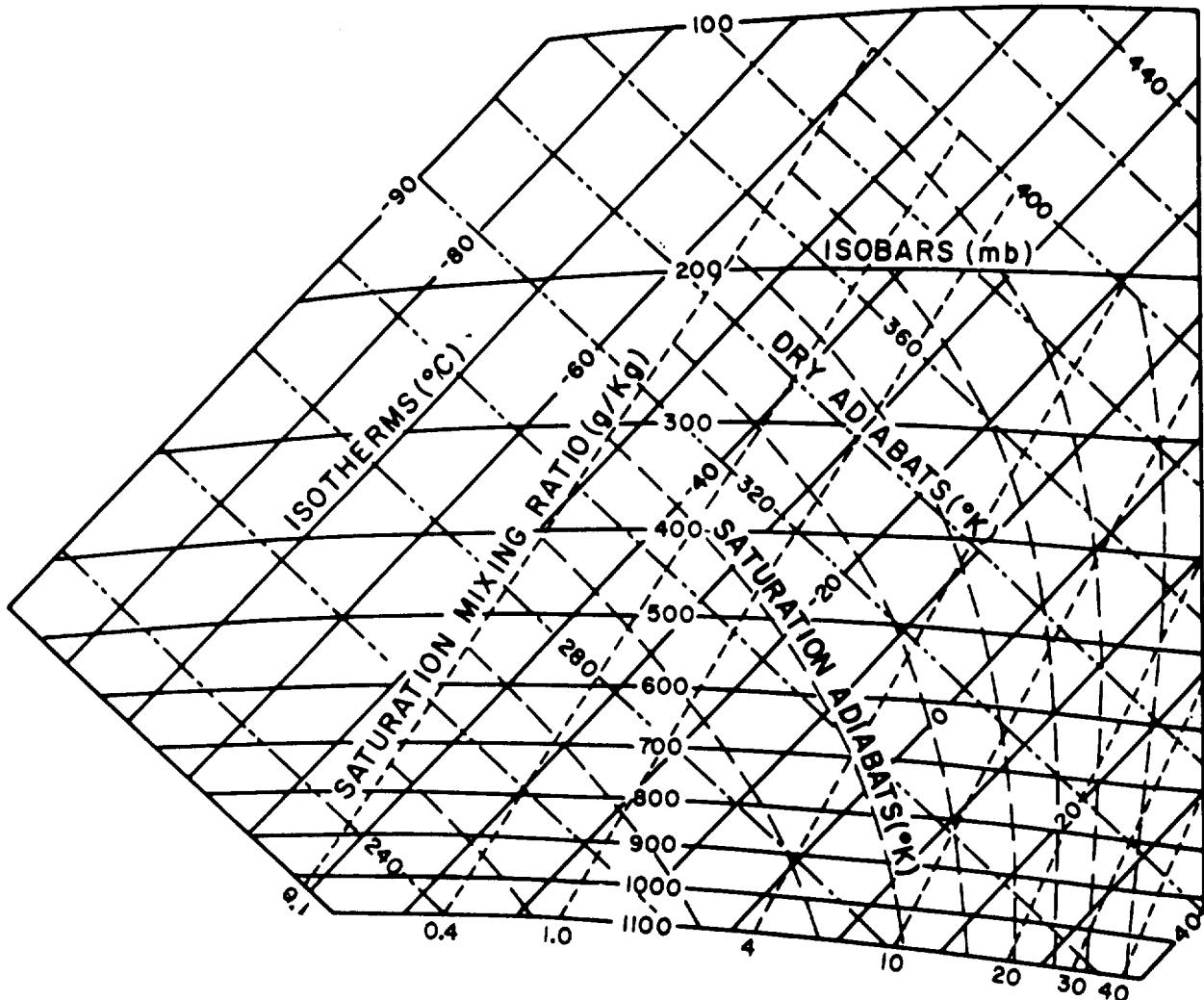
Figure 1b. Coordinate System of the Tephigram.

inches. This version eliminates several of the auxiliary scales and overprints, and is intended for use where these scales are not required and display or handling problems make a smaller sheet essential. Overlays designed for use on the full-scale version must be reduced by one-third to adapt them to this small-scale chart.

c. A "modified" version (DOD WPC 9-16A), printed on a sheet 20.5 x 15.5 inches. This is a cut-out from the full-scale chart, enlarged (but not photographically), and extending only from 1050 to 400 mb, and from -20°C to +50°C at the base. The auxiliary scales on the left and top are omitted, and of the overprinted material only the virtual tem-

perature marks are included. This version was designed for the special requirements of the Military Weather Warning Center.

d. A "High Altitude" version

printed on a sheet 24.7 x 24.3 inches. It extends the chart up to 1 mb starting at 150 mb, thus overlapping the basic version from 150 to 100 mb. The analysis block overprints and the scale are the same as on the WPC 9-16-1. The standard atmosphere curve reaches to the stratopause (47 km). This chart is designed for special activities concerned with analysis of the upper portion of high radiosonde flights and the lower portion of rocketsonde flights.

1—3
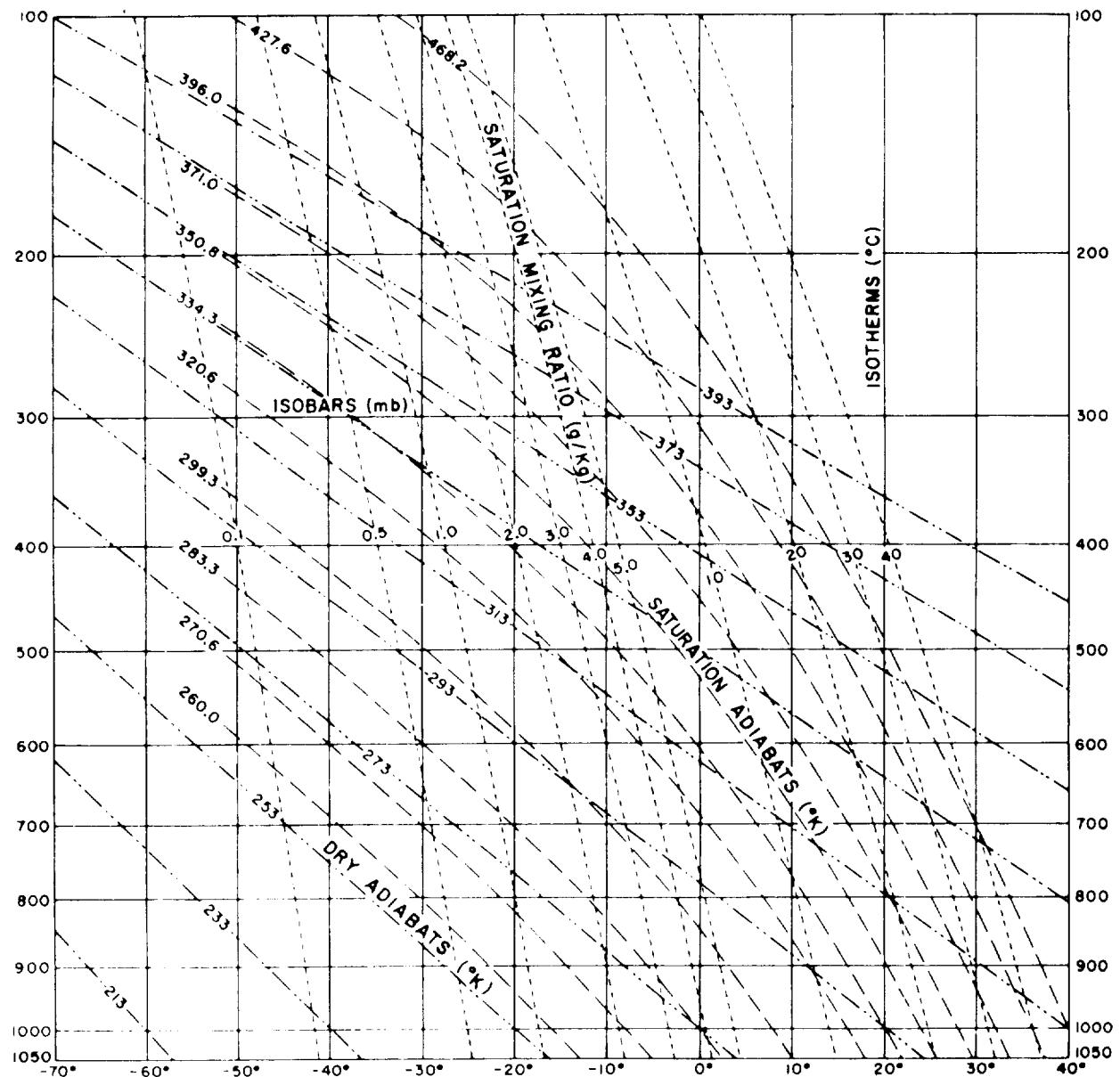
Figure Ic. Coordinate System of the Stüve ("Pseudo-Adiabatic") Diagram.

e. A version of WPC 9-16, identified as DOD WPC 9-16-2, with a refractivity overprint. This is an aid in computing estimates of anomalous radar propagation. The basis and use of the overprint is described in AWS TR 169 and in AWS TR 183.
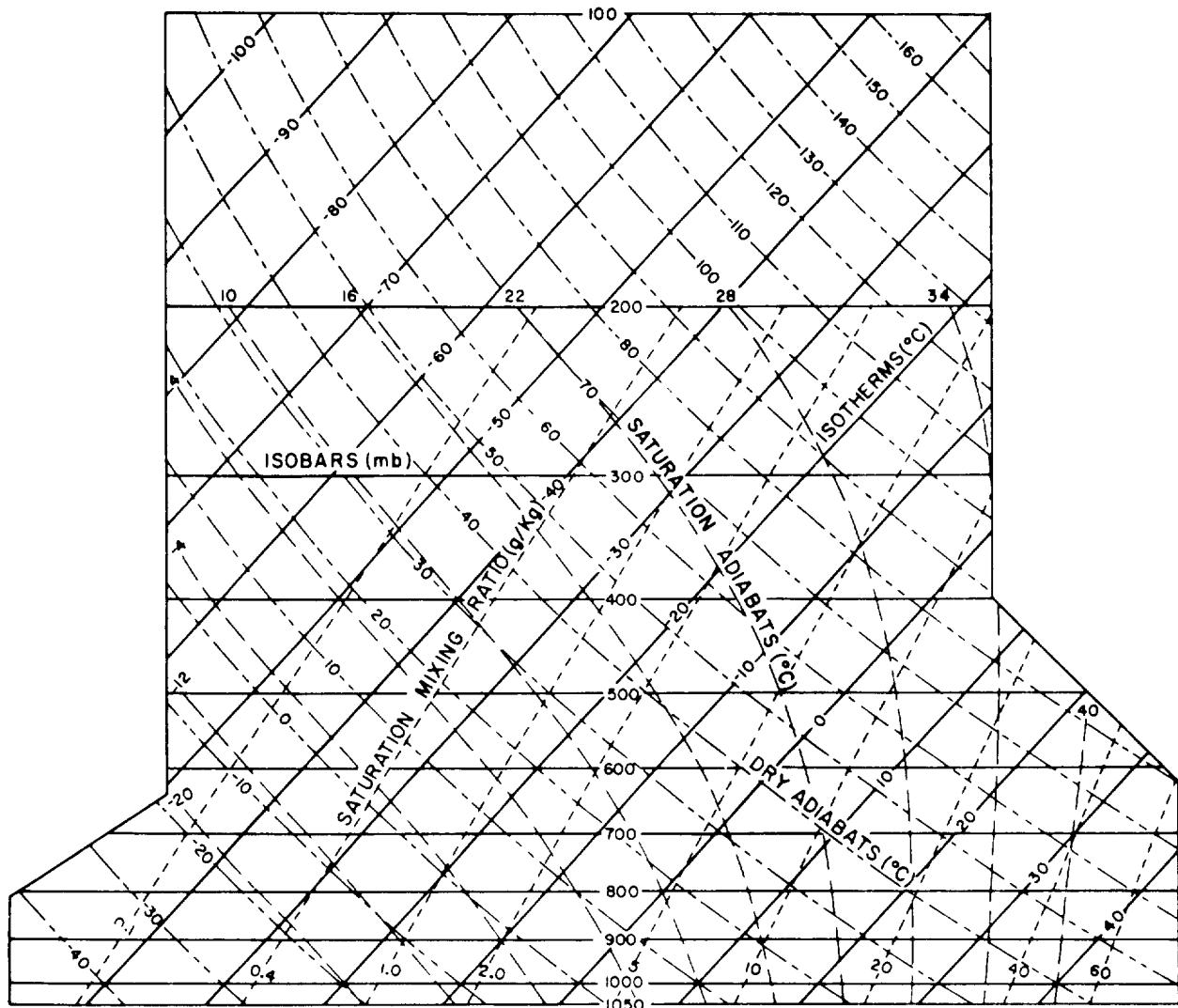
Figure Id. Coordinate System of the Skew T, Log P Diagram.

DESCRIPTION OF THE SKEW-T CHART

2.1. Isobars. Isobars on the Skew-T Chart are horizontal, solid, brown lines spaced logarithmically for 10-mb intervals. Pressure-value labels are printed at both ends and in the center of isobars for each 50-mb interval from 1050 to 100 mb as shown in Figure 2. The upper portion of the chart from 400 to 100 mb is also used for pressure values from 100 to 25 mb. Labels for the latter range are printed in brackets at the ends of the appropriate isobars. In case it should be desired to plot as high as 10 mb it is suggested that the range 1000 mb to 100 mb be used for the range 100 to 10 mb, and the scale values for the latter be written by hand beside the printed 1000- to 100-mb values at the left of the diagram.

ICAO Standard Atmosphere height values are shown under appropriate isobar labels on the left side. The values are given in both feet (in parentheses) and meters [in brackets]. The height values for the range from 1000 to 100 mb are printed to the right of the left edge of the grid; those for the range from 100 to 25 mb are printed to the left of this boundary.

2.2. Isotherms. Isotherms (see Figure 3) are straight, solid, brown lines, sloping from the lower left to upper right. The isotherm spacing is the same over the entire chart. Isotherms are labeled for 5°C intervals, and alternate 10°C temperature bands are tinted green. A Fahrenheit temperature scale is printed along the bottom edge of the chart to coincide with the appropriate isotherms.

The scale of temperature in the region around 100 mb does not extend to values low enough to accommodate some of the colder soundings that occur in the tropical-tropopause region. To plot such soundings, it is suggested that for the upper part of the sounding (above 100 mb) the temperature scale be shifted to the right by 10°C or 20°C and the isotherms in the area concerned be relabeled accordingly by hand. The slope of the dry adiabats will no longer be exactly correct for such a shifted scale, but the resultant error is small and of no consequence because one seldom is interested in detailed stability analysis at such heights (usually in the stratosphere). Where the plot of a sounding passes off the left side of the chart, start the continuation of the sounding at the pressure where this occurs but offset 10° or 20°C to the right on the temperature scale.

2.3. Dry Adiabats. The dry adiabats (see Figure 4) are the slightly-curved, solid, brown lines sloping from the lower right to upper left. They indicate the rate of temperature change in a parcel of dry air rising or descending adiabatically, i.e., with no loss or gain of heat by the parcel. The dry adiabat for each multiple of 10°C is labeled, as shown in the figure, with the Celsius temperature value of its point of intersection with the 1000-mb isobar. (Note that the dry adiabats are labeled in °C, rather than °K as on many other thermo dynamic diagrams, and care must be taken not to confuse these labels with those for the ordinary isotherms which are also labeled in °C.) The dry adiabats for the upper portion of the chart are labeled twice, to include the values (in parentheses) for the 100- to 25-mb pressure range. On the chart, the spacing between the dry adiabats decreases as their numerical value increases.

2.4. Saturation Adiabats. Saturation adiabats (illustrated in Figure 5) are the
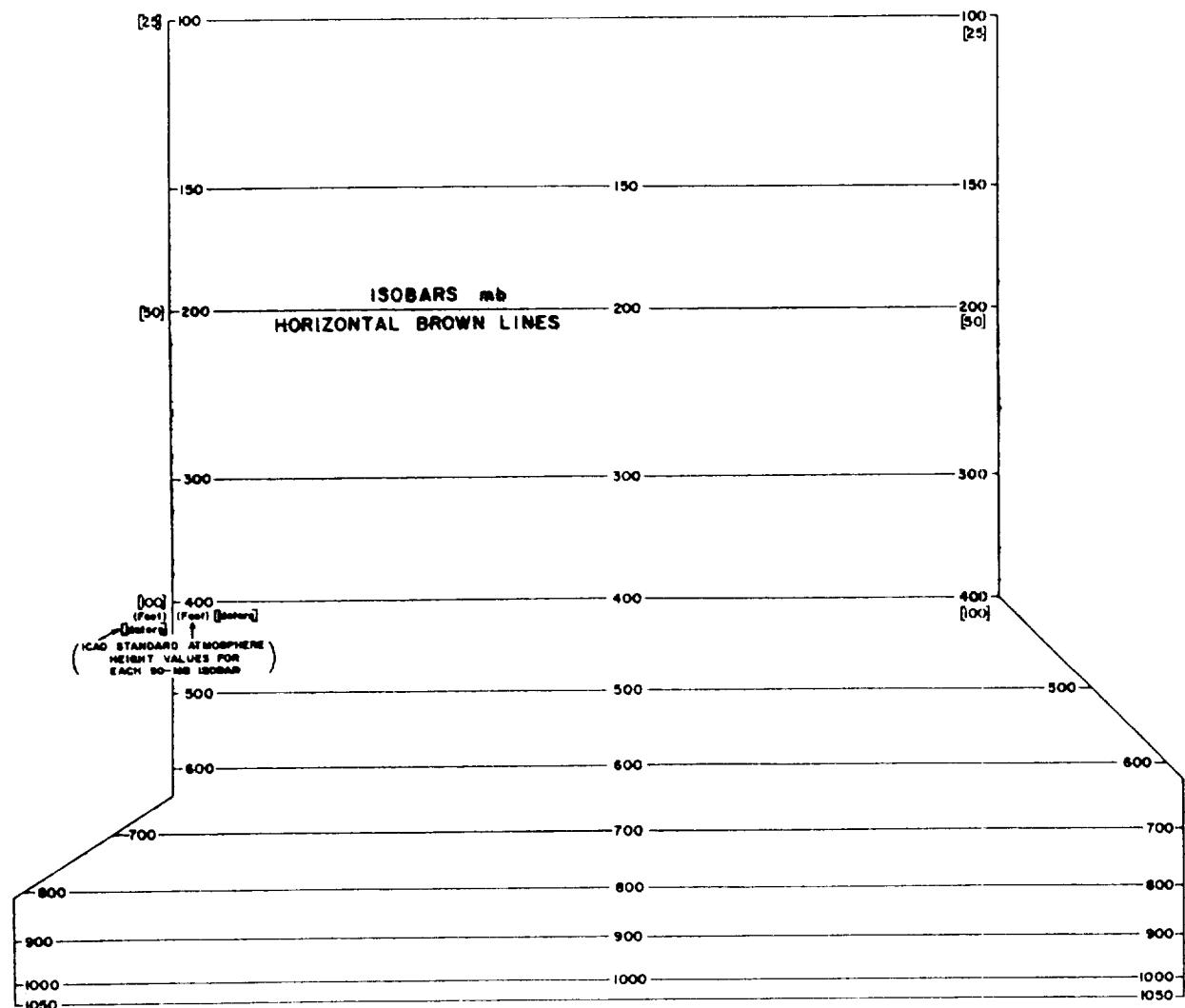
Figure 2. Isobars on the Skew-T Chart.

slightly-curved, solid, green lines sloping from the lower right to upper left. They are paths that the saturated air follows, and represent the rate of temperature change in a parcel of saturated air rising pseudo-adiabatically — pseudo-adiabatic means all the condensed water vapor is assumed to fall out immediately as the parcel rises (see par. 5.3 of this manual, and pp. 68-70 of [33]). The condensation at all temperatures is assumed to be liquid water and therefore no latent heat of fusion is included (see par. 5.3). Each saturation adiabat is labeled with the Celsius temperature value of its point of

intersection with the 1000-mb isobar. The saturation adiabats tend to become parallel to the dry adiabats at low values of moisture, temperature, and pressure. They extend only to the 200-mb isobar, because humidity observations are not routinely obtainable from higher altitudes with present standard equipment.

2.5. Saturation Mixing-Ratio Lines. The saturation mixing-ratio lines (see Figure 6) are the slightly-curved, dashed, green lines sloping from the lower left to upper right. They are labeled in grams per kilogram; i.e.,
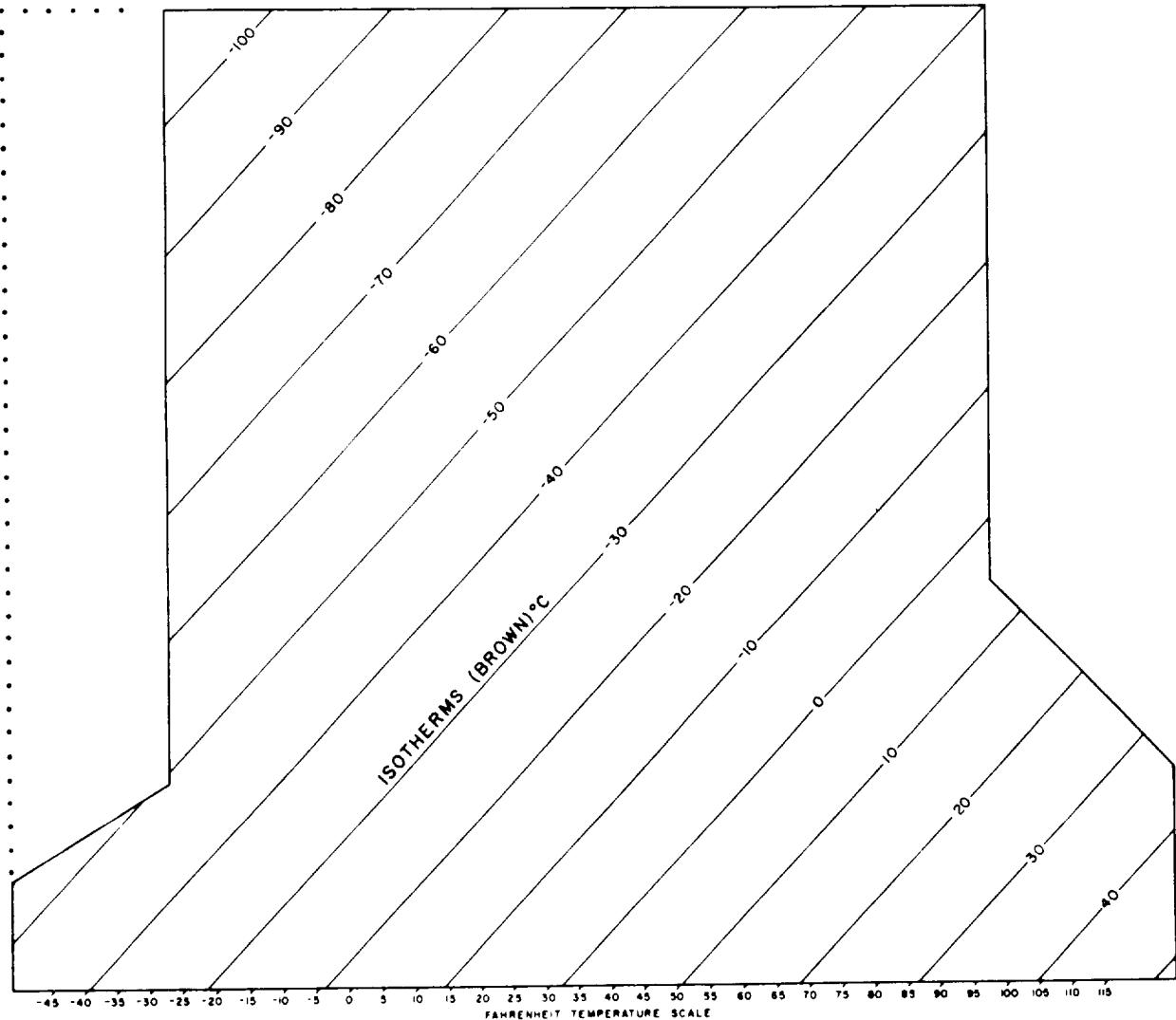
Figure 3. Isotherms on the Skew-T Chart.

in parts of water vapor per 1000 parts of dry air. The spacing between the saturation mixing-ratio lines decreases as their numerical value increases. The mixing ratio at all temperatures is computed from the vapor pressure over a plane water surface. Like the saturation adiabats, the mixing-ratio lines are extended only to the 200-mb isobar.

2.6. Thickness Scales. The nine thickness scales on the Skew-T Chart (illustrated in Figure 7) are the horizontal, graduated,

black lines, each of which is placed midway between the two standard-pressure isobars to which it applies. The bounding pressures of the layer for each scale are labeled at its left end. Scales are included for the following layers: 1000 to 700 mb, 1000 to 500 mb, 700 to 500 mb, 500 to 300 mb, 300 to 200 mb, 200 to 150 mb, 150 to 100 mb, 100 to 50 mb, and 50 to 25 mb. The scales are graduated along the top in 20's or 10's and labeled in hundreds of geopotential feet; along the bottom they are graduated in 10's and labeled in
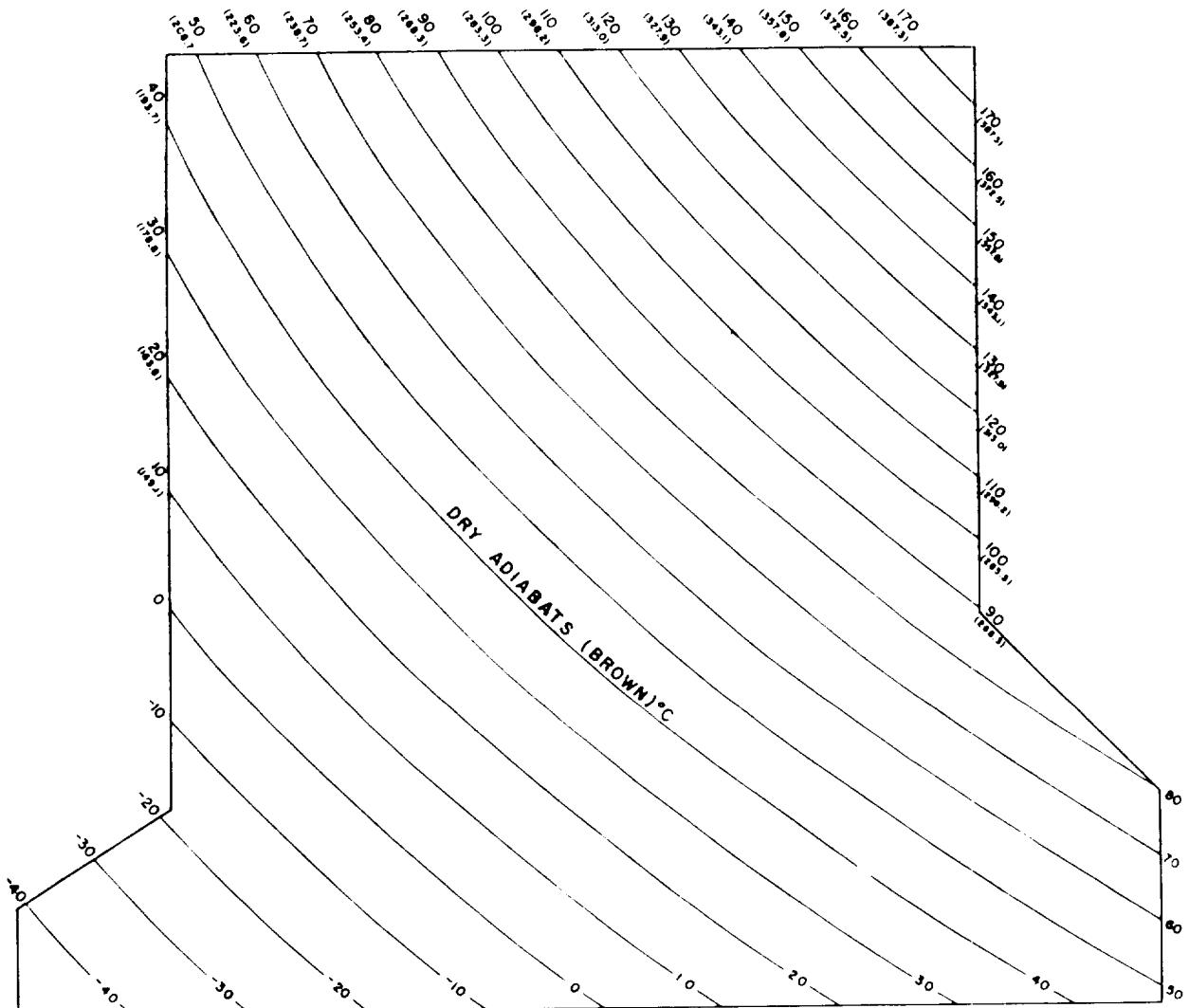
Figure 4. Dry Adiabats on the Skew-T Chart.

100's of geopotential meters[4]. Each thickness scale may be used also for layers other than that for which it is labeled, provided that the ratio of the boundary pressures is the same; paragraph 4.14 explains this procedure. If needed, additional thickness scales may also be constructed locally for any desired layer (see pp. 109-116 of [33]).

2.7. The 1000-mb Height Nomogram. The 1000-mb height nomogram, printed on the full-scale version (DOD WPC 9-16) only, as shown in Figure 8, consists of three black scales:

a. A temperature scale in whole °C and °F, extending horizontally along the top of the chart.

---

[4]For meteorological purposes, geopotential feet and meters can be considered as geometric feet or meters with very little error. (The exact relationship is explained in the *Smithsonian Meteorological Tables*, Sixth Revised Edition [60], which tabulates the resulting errors for all heights and latitudes.)

2—4
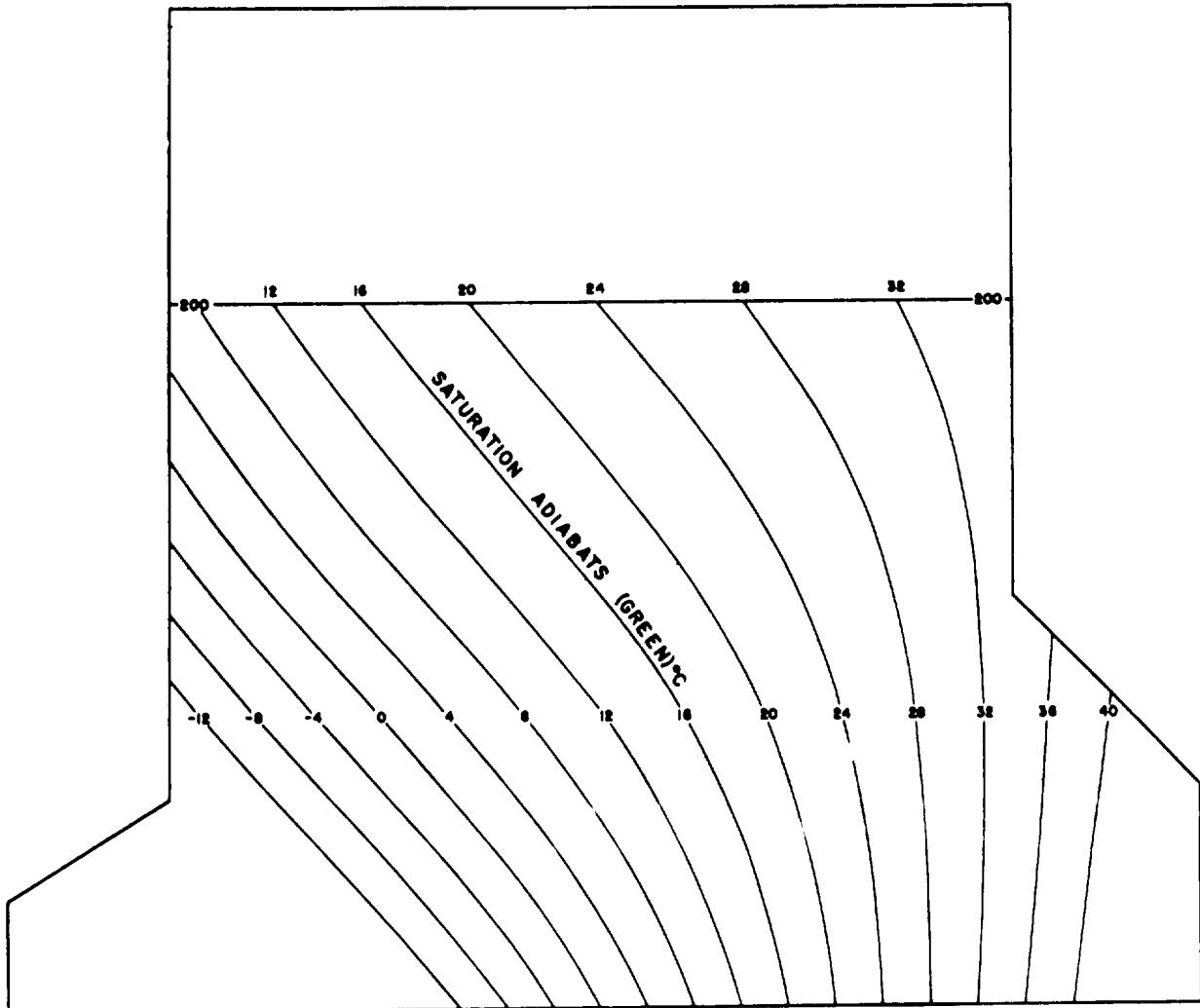
Figure 5. Saturation Adiabats on the Skew-T Chart.

b. A pressure scale in whole millibars, extending vertically along the left side of the chart.

c. A height scale in geopotential whole feet and meters, parallel to the pressure scale.

2.8. Standard Atmosphere Data. The ICAO Standard Atmosphere lapse rate is shown on the Skew-T Chart as a heavy brown line passing through the point at 1013 mb and 15°C. The position of this line is also illustrated in Figure 8. The heights of pressure surfaces in this standard atmosphere up to 100 mb are indicated on the vertical scale (labeled ICAO STANDARD ATMOSPHERE ALTITUDE) printed on the right side of the chart. This scale is graduated in geopotential meters and feet (see Footnote 4). The heights of standard-pressure surfaces are also printed at the left margin of the chart beneath each pressure value (1000, 950, 900,...etc., to 10 mb).
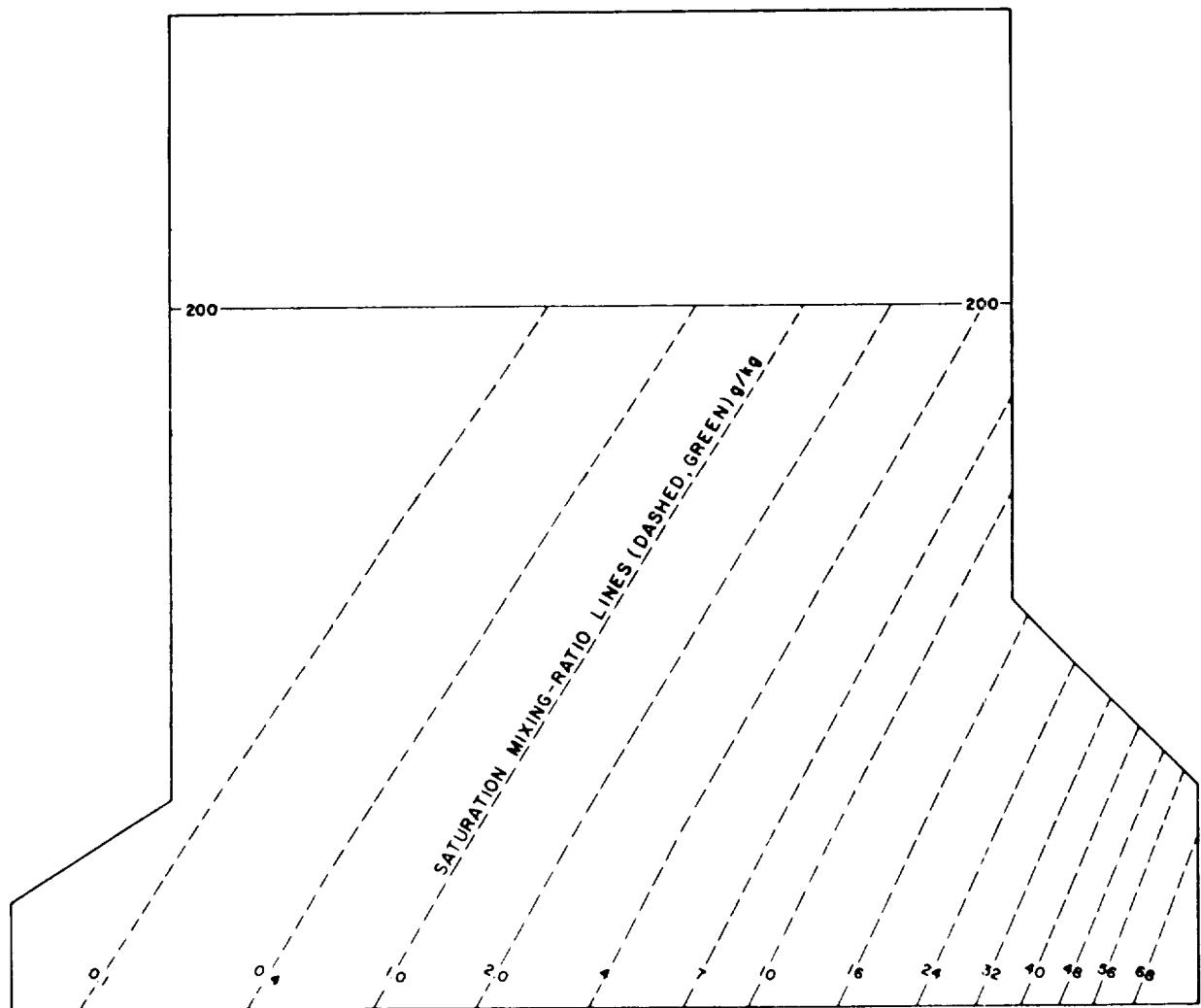
Figure 6. Saturation Mixing-Ratio Lines on the Skew-T Chart.

2.9. Wind Scale. Three vertical staffs labeled WIND SCALE are printed along the right side of the chart for use in plotting upper-wind data. Solid circles on the staffs indicate heights for which wind data are usually reported; the open circles on the staffs are for wind data for mandatory pressure surfaces.

2.10. Contrail-Formation Curves. Printings following the May 1959 edition of the full-scale version (DOD WPC 9-16) of the Skew-T Chart are overprinted in thin black lines with two sets of four lines each. taken from AWS/TR-81/001. These are labeled with the theoretical critical relative-humidity values

separating the categories for forecasting probability or absence of contrails from jet aircraft. The solid set of lines is for use between the 500- and 100-mb surfaces, and the dashed set for use between the 100- and 10-mb surfaces. The application of these "curves" is explained in AWS/TR-81/001.

2.11. Analysis Blocks. To facilitate and standardize entry of sounding analyses, a form as shown in Figure 9 has been printed on the right-hand side of DOD WPC 9-16, 9-16-2, and on the left-hand side of DOD WPC 9-16-1. The DOD WPC 9-16A does not have this feature.

THICKNESS SCALES (BLACK)
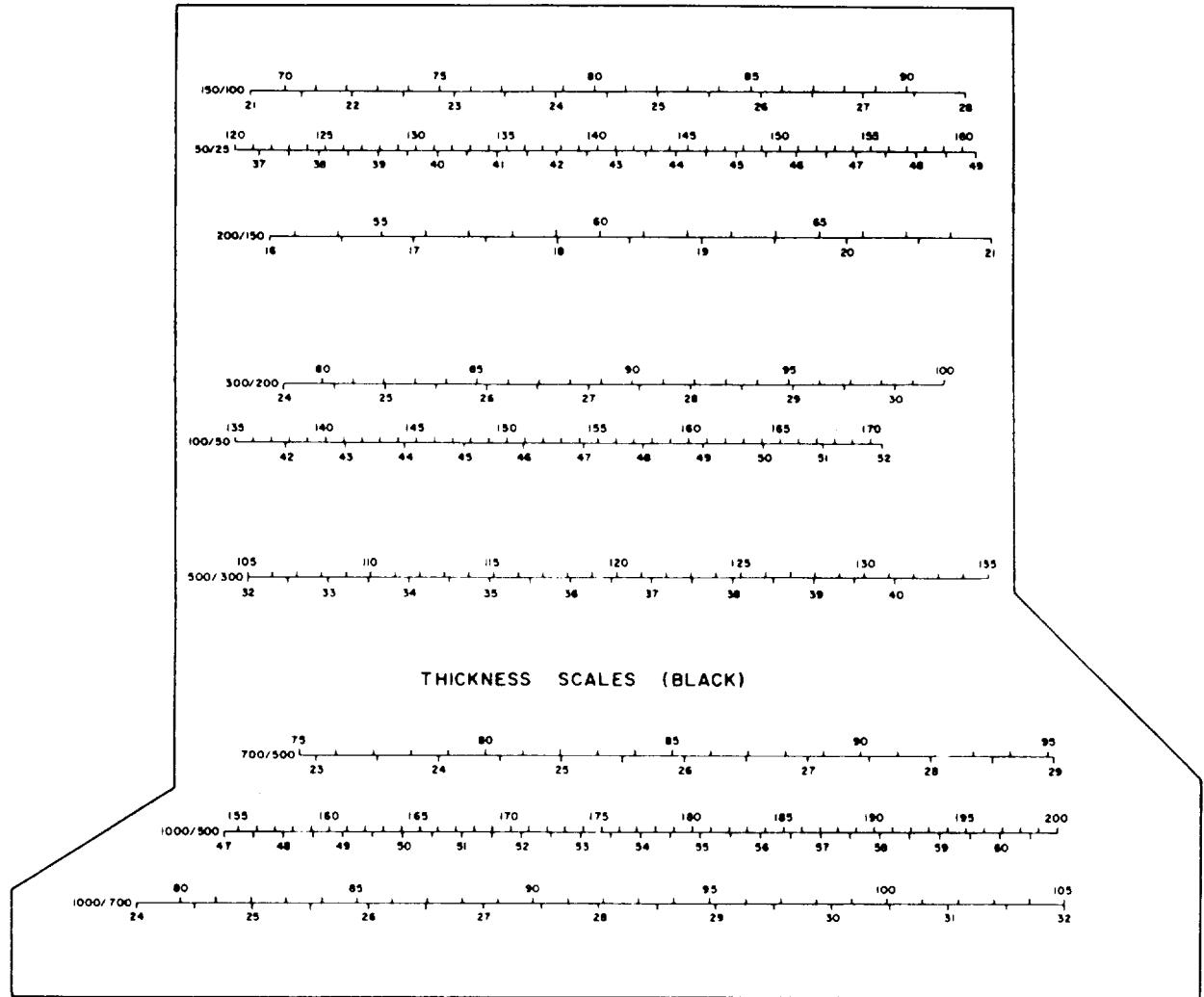
Figure 7. Thickness Scales on the Skew-T Chart.
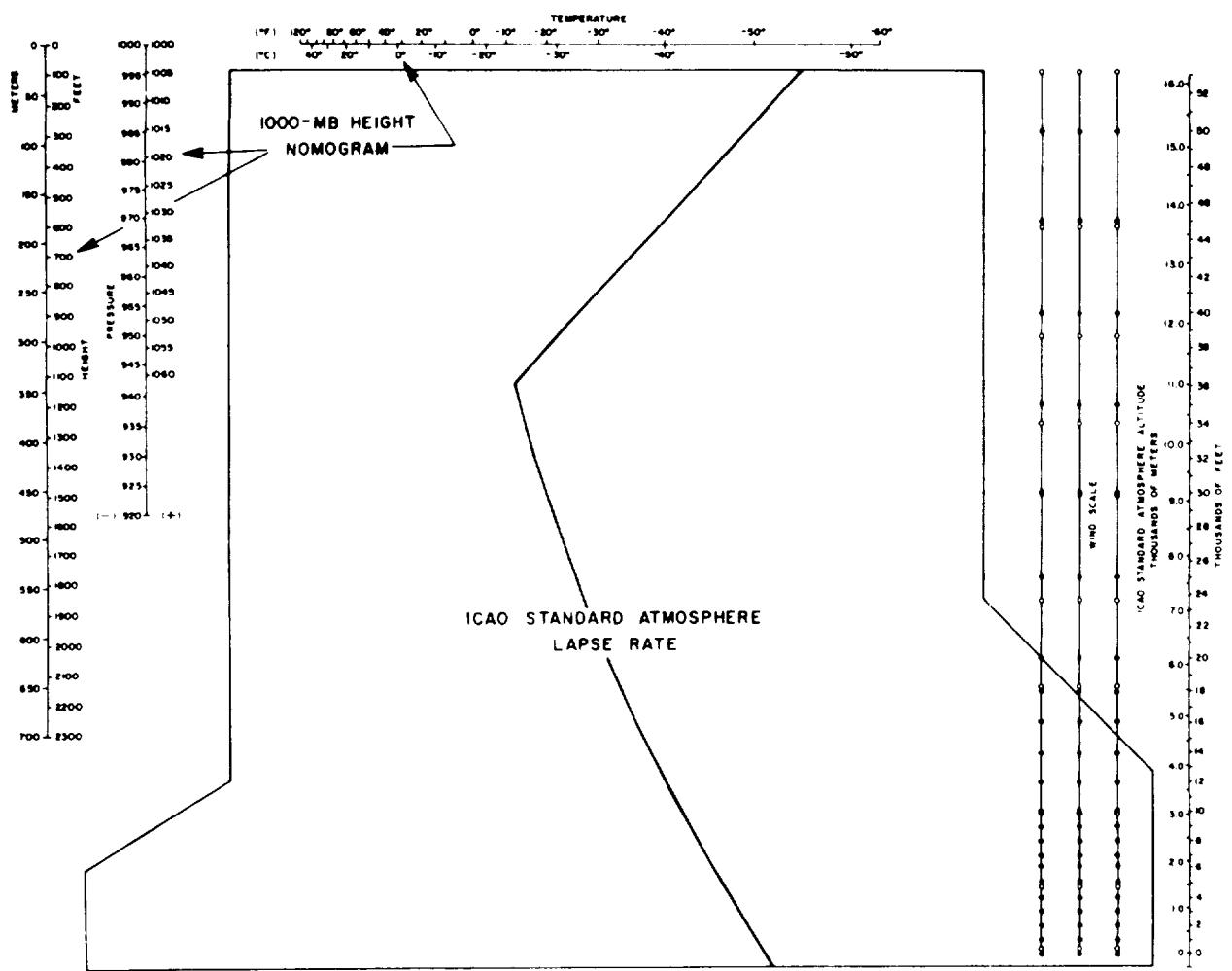
Figure 8. Auxiliary Scales on the Skew-T Chart.

SKEW T - LOG P ANALYSIS

TIME	TIME

AIRMASS ANALYSIS

TYPE BOUNDARY ———— FT. TYPE BOUNDARY ———— FT. TYPE	———— FT. ———— FT.

FREEZING LEVEL(S)	

INVERSIONS

FRONTAL	
RADIATION	
SUBSIDENCE	
TROPOPAUSE	
L.C.L.	
C.C.L.	
L.F.C.	

SIGNIFICANT WIND

MAX.	
MIN.	
LEVELS OF SHEAR	

STABILITY

INDEX		INDEX	
TO		TO	
TO		TO	
TO		TO	

CLOUDS

TYPE						
AMOUNT						
BASES						
TOPS						

ICING

TYPE	
SEVERITY	
BOUNDARIES	

CONTRAILS

PERSISTENCE	
HEIGHT	

TURBULENCE

DEGREE	
HEIGHT(S)	
MAX WIND GUSTS	
HAIL SIZE	

TEMPERATURES

MAX.	
MIN.	

CUMULUS CLOUD FORMATION AT TEMP_____ TIME_____

DISSIPATION OF LOW LEVEL INVERSION AT_____ TIME_____

REMARKS

FORECASTER	FORECASTER

Figure 9. Analysis Block on the Skew-T Chart.

PLOTTING SOUNDING DATA ON THE SKEW-T CHART

3.1. General. The data used for plotting thermodynamic diagrams such as the Skew-T Chart are obtained from a variety of sources, including radiosondes, dropsondes, aircraft soundings, rocketsondes, and upper-wind reports of pibals or rawins. The plotter should refer to the appropriate FMH, WBAN, or WMO publications for decoding instructions applicable to the type of report in question. The plotting instructions given in this chapter pertain to all six versions of the Skew-T Chart.

3.2. Number of Soundings Plotted Per Chart. One chart is used for each reporting station, and normally no more than two soundings from new data are plotted on it. A trace from a previous sounding should be entered on the chart for continuity purposes. There should be a 6-hour or a 12-hour time interval between each set of curves, determined by the individual forecasting unit. Thus, if four soundings per day from a given station are plotted, two charts would normally be used. For a 12-hour time interval, plot one chart for the 0000Z and 1200Z soundings plus the trace of the previous day's 1200Z sounding and plot one for the 0600Z and 1800Z soundings plus the preceding 1800Z trace. Use of a 12-hour interval permits the analyst to see from one chart the changes in air mass that occur at a particular station between successive primary upper-air analysis times. For a 6-hour time interval, plot one chart for the 0000Z and 0600Z soundings plus the trace for the previous day's 1800Z trace, and one for the 1200Z and 1800Z soundings plus the preceding 0600Z sounding.

3.3. Choice of Color. The temperature and dew-point curves from the preceding ("continuity") sounding should be traced in black ink or pencil without transcription of data or circling of any point. This is usually done before the first new sounding is plotted. The first new sounding (6 or 12 hours) after the "trace" should be plotted in blue pencil; the second new sounding (12 or 24 hours) after the "trace" in red pencil. This procedure is suggested since the use of red for the third set of curves emphasizes the latest data. All supplementary data for a sounding should be in the same color as the plotted curves; e.g., legend, tropopause, etc.

3.4. Plotting Individual Elements. A free-air temperature curve and a dew-point curve should be plotted for each sounding. Curves of other types of moisture representation may be plotted if desired.

The points to be plotted on the chart are located by reference to the pressure and temperature (either free air or dew point) of the level. Pressures are plotted in whole millibars; temperatures are plotted to the nearest tenth of a degree or whole degree according to local policy and chart scale. Each point on the curve of temperature or dew point is presented by a small dot located at the proper temperature and pressure. A small circle will be drawn around each dot on the temperature and dew-point curves (note that, for clarity, the points on temperature curves in the figures in this manual have been indicated by large solid dots). This circle will aid in locating the points when drawing the connecting lines; and the circles further aid in identifying significant points on the curves. If other moisture curves are plotted (for example, the wet-bulb curve) small triangles or other symbols should be drawn around the dots on these curves to distinguish them from the dew-point curve.

The free-air temperature curve will always be represented by a solid line; while the moisture curves will be dashed lines. Use

a straightedge when drawing the connecting lines between the plotted points.

Through strata of *doubtful* data, draw the free-air temperature and moisture-representation curves in the normal manner. Indicate the limits of such strata in the space above the legend (e.g., TEMP DBT FL 615-550 MB), in the same color as is used for plotting the curves.

Where there is a stratum of *missing* data, terminate the curves at the lower boundary of the stratum, and start the curves again at the upper boundary of the stratum. Enter the symbol MISDA in the middle of the stratum of missing data in the same color as is used for plotting the curves. When humidity data are missing, it is desirable to enter 10168 or 10169, when applicable, below the symbol MISDA. This procedure will inform the analyst whether the missing humidity data are due to dry, cold air, or are the result of some other factor (frequently non-meteorological). Often, humidity data do not appear again at higher levels after they have been indicated as missing at lower ones. In these cases, it is desirable to enter M ABOVE or 10168 ABOVE, as applicable, just above the last reported humidity point.

Enter the height of each mandatory level on the isobar to which it pertains. Make this entry just inside either edge of the diagram for levels from 1000 mb to 100 mb, and just inside the opposite edge of the diagram for levels above 100 mb.

If necessary, the position of height entries may be adjusted to avoid conflict with other plotted data. Enter height values exactly as they are received. For example, plot 436 for an 850-mb height reported as 85436 and plot 175 for a 200-

mb height reported as 20175. Plot maximum wind and tropopause data when reported within the levels plotted. For the pressure level of the tropopause, extend the isobar into the margin of the side on which the mandatory-level heights are entered.

3.5. Plotting Wind Data. Wind data at the mandatory levels, as received in the rawinsonde report, should always be plotted on the open circles on the wind staffs in the same color as the corresponding sounding curves. Wind data at other levels, taken from the winds-aloft report for the same time, may be plotted on the solid dots if desired. The conventions specified in AWSR *105-22* (i.e., north is at the top of the diagram, a full barb equals 10 knots, etc.) should be followed when plotting winds. Use the right-hand staff for the first wind report, and plot succeeding reports on the middle and/or left-hand staffs. The winds for the continuity trace are not normally copied unless the analyst specifically desires them; in which case, they should be located on the right-hand staff.

3.6. Legend. A legend will be entered for each sounding plotted. Enter the station index number (or location identifier), station name, time (Z), and date (Z), and initials of plotter in the identification box(es). Use the same color for legend entries as was used for the corresponding sounding curves.

When a scheduled sounding is not received, complete the legend entries and enter the $101A_{df}A_{df}$ group identifying the reason for no observation in the space above the legend in the appropriate color. If a $101A_{df}A_{df}$ group is not received, enter "..... Z MISG."

3.7 Construction and Use of the Pressure-Altitude Curve.

The pressure-altitude (P-A) curve is used to help forecasters determine heights of various elements more accurately. Using the P-A curve accounts for atmospheric soundings that are warmer or colder than the standard atmosphere.

STEP 1--Along the bottom of a Skew T, log p diagram, start converting isotherms to equal height (isohypsic) lines by relabeling the 50°C isotherm as "0" meters. Continue to relabel each 10-degree isotherm in 1,000-meter increments (the 30° isotherm, for example, is now labeled "2,000 meters"). Continue labeling up the left side of the diagram until the -100°C isotherm now represents 15,000 meters.

STEP 2--Using the height values encoded in the rawinsonde observation bulletin, enter the height of each mandatory level on the right-hand side of the diagram next to the pressure level associated with that height.

STEP 3--Plot the observed height of each mandatory level on the isotherms that you relabeled as isohypsic lines in Step 1. Since each isohypsic line represents 100 meters, you will have to interpolate. Enclose each plotted point in a small box.

STEP 4--As shown in the example, connect the plotted points with a solid line. The line should be smooth, with a gradual curve to the right with increasing height.

STEP 5--Determine the feature of interest and the pressure level at which it lies. With a straightedge, follow the pressure level horizontally until it intersects the P-A curve constructed in Step 4. Make a small tick mark at the intersection.

STEP 6--Using the relabeled isohypsic scale on the bottom or left edge of the diagram, read the value of the tick mark made in Step 5. Each relabeled isotherm, remember, now equals 100 meters. Convert meters to feet with the scale on the right side of the diagram.
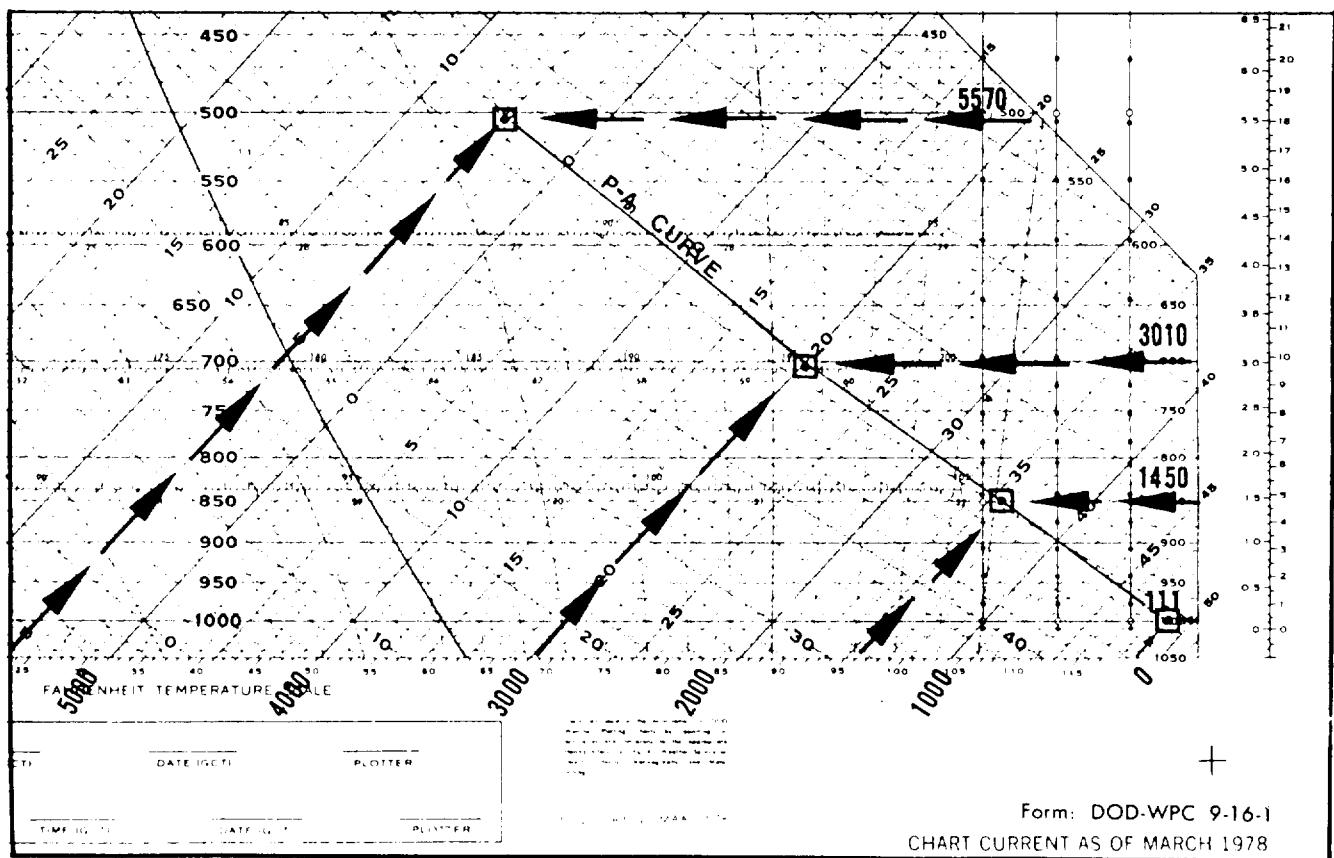
FIGURE 9A. Example Skew T, Log P diagram with P-A Curve Plotted. If the P-A curve constructed in Step 4 extends beyond the left edge of the diagram below a feature of interest, the upper part of the curve can be extended as shown in Steps 7 through 10, next page.

STEP 7--Determine the height of the highest reported mandatory level, which is probably 100 mb. Round that height up to the nearest 1,000 meters. At the top of the chart, relabel the -100°C isotherm with the rounded height value.

STEP 8--Continuing to the right across the top of the diagram, relabel each 10-degree isotherm in decreasing 1,000-meter increments. For example: if the 100-mb height is 17,400 meters, the -100°C isotherm is relabeled "18,000 meters"; the -80°C isotherm, "16,000 meters."

STEP 9--Plot the observed heights and construct the "upper" P-A curve in the same way as in Steps 3 and 4, using the isotherms relabeled in Steps 7 and 8.

STEP 10---Use the "upper" P-A curve to determine heights in the same way as described by Steps 5 and 6, but with the isohypsic scale constructed in Steps 7 and 8.

DETERMINATION OF UNREPORTED METEOROLOGICAL QUANTITIES FROM PLOTTED SOUNDINGS

4.1. Introduction. In accordance with paragraph 3.4, two curves are usually plotted and drawn on the Skew-T Chart for each sounding, as shown in Figure 10. One represents the free-air temperature (T), the other the dew-point temperature (T_d). This chapter outlines procedures for determining certain unreported meteorological quantities which may be evaluated on the Skew-T Chart from such a plotting sounding.

4.2. Mixing Ratio.
Definition: In a sample of moist air, the mixing ratio (w) is the ratio of the mass of water vapor (M_v) to the mass of dry air (M_d), i.e., $w = M_v / M_d$.[6] It is expressed in parts per thousand, usually grams of water vapor per kilograms of dry air.

Procedure: To find the mixing ratio for a given pressure on the plotted sounding, read the value, either directly or by interpolation, of the saturation mixing-ratio line that crosses the T_d curve at that pressure. On the sounding shown in Figure 10, for example, T_d at 700 mb is -13°C; and the saturation mixing-ratio value at 700 mb and -13°C is 2.0 g/kg. Hence, the mixing ratio of the air at the 700-mb level on this sounding is 2.0 g/kg.

4.3. Saturation Mixing Ratio.
Definition: The saturation mixing ratio (w_s) is the mixing ratio a sample of air would have if saturated[7].

Procedure: To find the saturation mixing ratio for a given pressure on the plotted sounding, read the value, either directly or by interpolation, of the saturation mixing-ratio line that crosses the T curve at that pressure. On the sounding shown in Figure 10, T at 700 mb is -5°C; and the saturation mixing-ratio value at 700 mb and -5°C is 3.8 g/kg. Hence, the saturation mixing ratio of the air at the 700-mb level on this sounding is 3.8 g/kg.

4.4. Relative Humidity.
Definition: Relative humidity (RH) is the ratio (in percent) of the amount of water vapor in a given volume of air to the amount that volume would hold if the air were saturated.

Procedure: The relative humidity can be computed from the mixing ratio (w) and the saturation mixing ratio (w_s) by the following equation:

---

[6]The "specific humidity" (q), where $q = M_v/(M_v + M_d)$, the mass of water vapor per mass of moist air, often is preferable for very precise physical and theoretical work. For synoptic purposes, however, the mixing ratio is sufficiently representative, and is easier to evaluate.

[7]Moist air at temperature T and at total pressure p is said to be saturated if its composition is such that it can co-exist in neutral equilibrium with a plane surface of pure condensed phase (water or ice) at the same temperature and pressure [65].
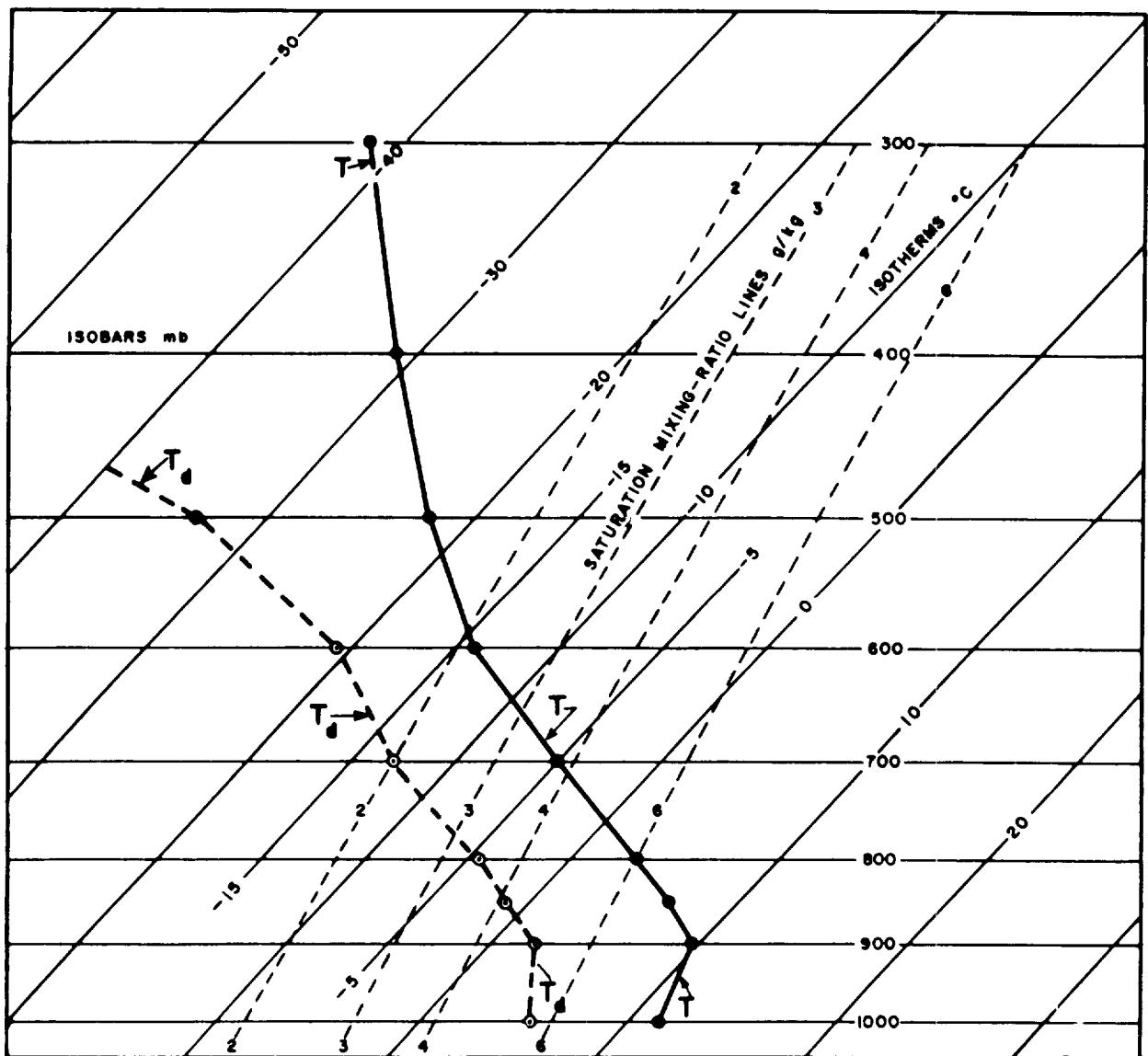
Figure 10. Sample Sounding on the Skew-T Chart.

$$RH = 100(w/w_s)$$

On the sounding shown in Figure 10, w and w_s at 700 mb are 2.0 and 3.8 g/kg, respectively. Therefore the relative humidity at the 700-mb level on that sounding is $100\frac{2.0}{3.8} = 53\%$.

Alternate Procedure: There is also a procedure, shown in Figure 11 to find graphically

on the Skew-T Chart the relative humidity for a given pressure on the sounding. It is as follows:

Step 1. From the T_d curve at the given pressure, follow the saturation mixing-ratio line to the 1000-mb isobar.

Step 2. From this intersection, draw a line parallel to the isotherms.

4−2
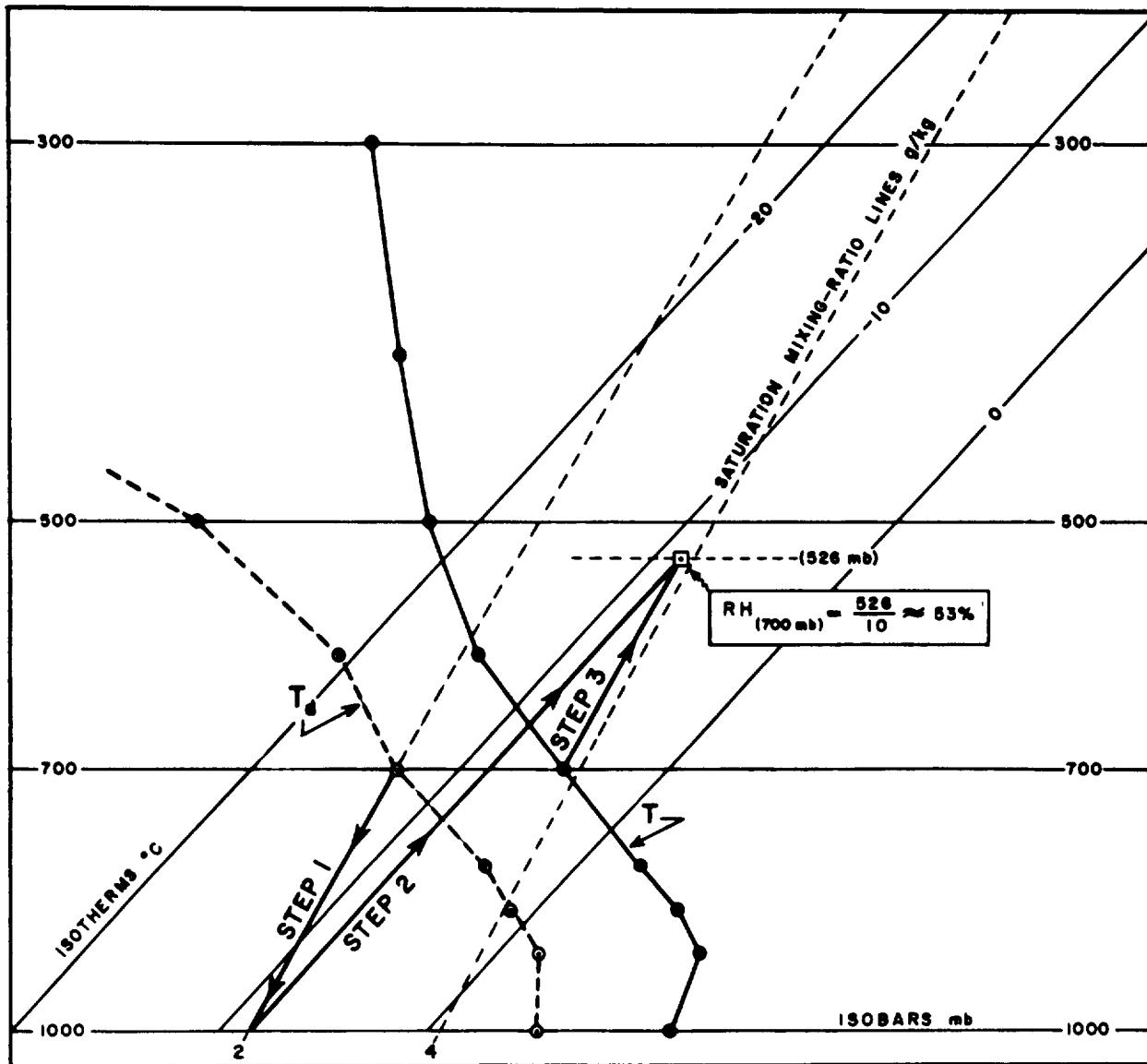
Figure 11. Alternate Procedure for Finding Relative Humidity (RH).

Step 3. From the T curve at the given pressure, follow the saturation mixing-ratio lines to the intersection with the line drawn in Step 2. The numerical value of the isobar through this last intersection point is divided by ten. The quotient is the relative humidity at the given pressure.

4.5. Vapor Pressure.

Definition: The vapor pressure (e) is that part of the atmospheric pressure which water vapor contributes to the total atmospheric pressure.

Procedure: From the T_d curve at the given pressure on the sounding (for example, at 700

4—3
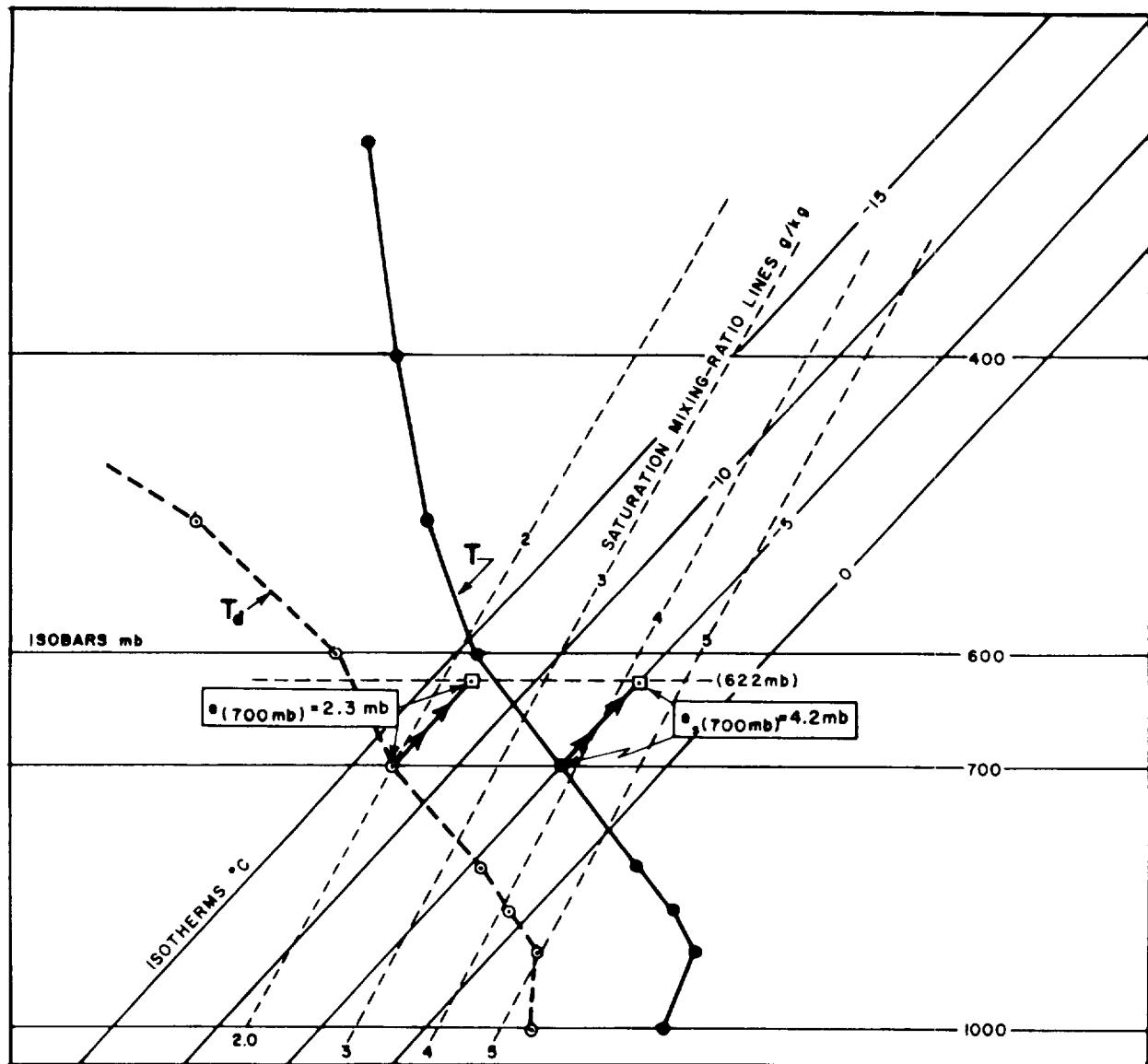
Figure 12. Determination of the Vapor Pressure (e) and the Saturation Vapor Pressure (e_s).

mb in Figure 12), follow the isotherms to the 622-mb isobar[x]. The value of the saturation mixing-ratio line, read by interpolation if necessary, through this point at 622 mb gives the vapor pressure in millibars at the given pressure.

4.6. Saturation Vapor Pressure.

Definition: The saturation vapor pressure (e_s) is the partial pressure which water vapor would contribute to the total atmospheric pressure if the air were saturated.

---

[x]The theoretical basis for choosing this particular isobar is explained on pages 60-63 of[33].

Procedure: Referring again to Figure 12, from the *T* curve at the given pressure (700 mb), follow the isotherms to the 622-mb isobar. The value of the saturation mixing-ratio line, read by interpolation if necessary, through this point at 622 mb gives the saturation vapor pressure in millibars at the given pressure.

4.7. Comments on Temperature Parameters.
At times in the past, various authors have given a slightly different name and definition to the same temperature parameter. This has resulted in a confusion which is more annoying than serious. The names and definitions for the various temperature parameters used in this manual were taken from the WMO standard names and definitions [65] whenever possible, or from the most logical and practical designations now in use.

4.8. Potential Temperature.
Definition: The potential temperature *(θ)* is the temperature that a sample of air would have if it were brought dry-adiabatically to a pressure of 1000 mb.

Procedure: The procedure is shown in Figure 13. From the *T* curve at the given pressure (700mb), follow the dry adiabat to the 1000-mb isobar. The isotherm value of this adiabat at 1000mb is equal to the potential temperature of the air parcel at the given pressure. The dry adiabat is an isotherm of constant potential temperature.

In the example shown in Figure 13, $θ_{(700)}$ = 24°C or 297°K.

4.9. Wet-Bulb Temperature.
Definition: The wet-bulb temperature (T_w) is the lowest temperature to which a volume of air at constant pressure can be cooled by evaporating water into it. This assumes that the heat required for evaporation is taken from the air itself. (WMO definition [65].) Physically, the wet-bulb temperature is the temperature of the wet-bulb thermometer rather than of the air.

Procedure [9]: Figure 14 illustrates the method of finding the wet-bulb temperature at a given pressure on the sounding. The steps are:

Step 1. From the T_d curve at the given pressure, in this case 700 mb, draw a line upward along a saturation mixing-ratio line.

Step 2. From the *T* curve at the given pressure (700 mb), draw a line upward along a dry adiabat until it intersects the line drawn in Step 1. (The height of this intersection is the "lifting condensation level," as described in par. 4.20.)

Step 3. From this point of intersection, follow a saturation adiabat back to the given pressure, 700 mb. The isotherm value at this pressure is equal to the wet-bulb temperature.

In the example shown in Figure 14, $T_w{(700)}$ = -8°C.

4.10. Wet-Bulb Potential Temperature.
Definition: The wet-bulb potential temperature $(θ_w)$ is the wet-bulb temperature a sample of air would have if it were brought saturation-adiabatically to a pressure of 1000 mb.

---

[9] The procedure given here is for the adiabatic wet-bulb temperature. The "true" (i.e., isobaric) wet-bulb temperature is almost identical (see p. 78 of [33]).
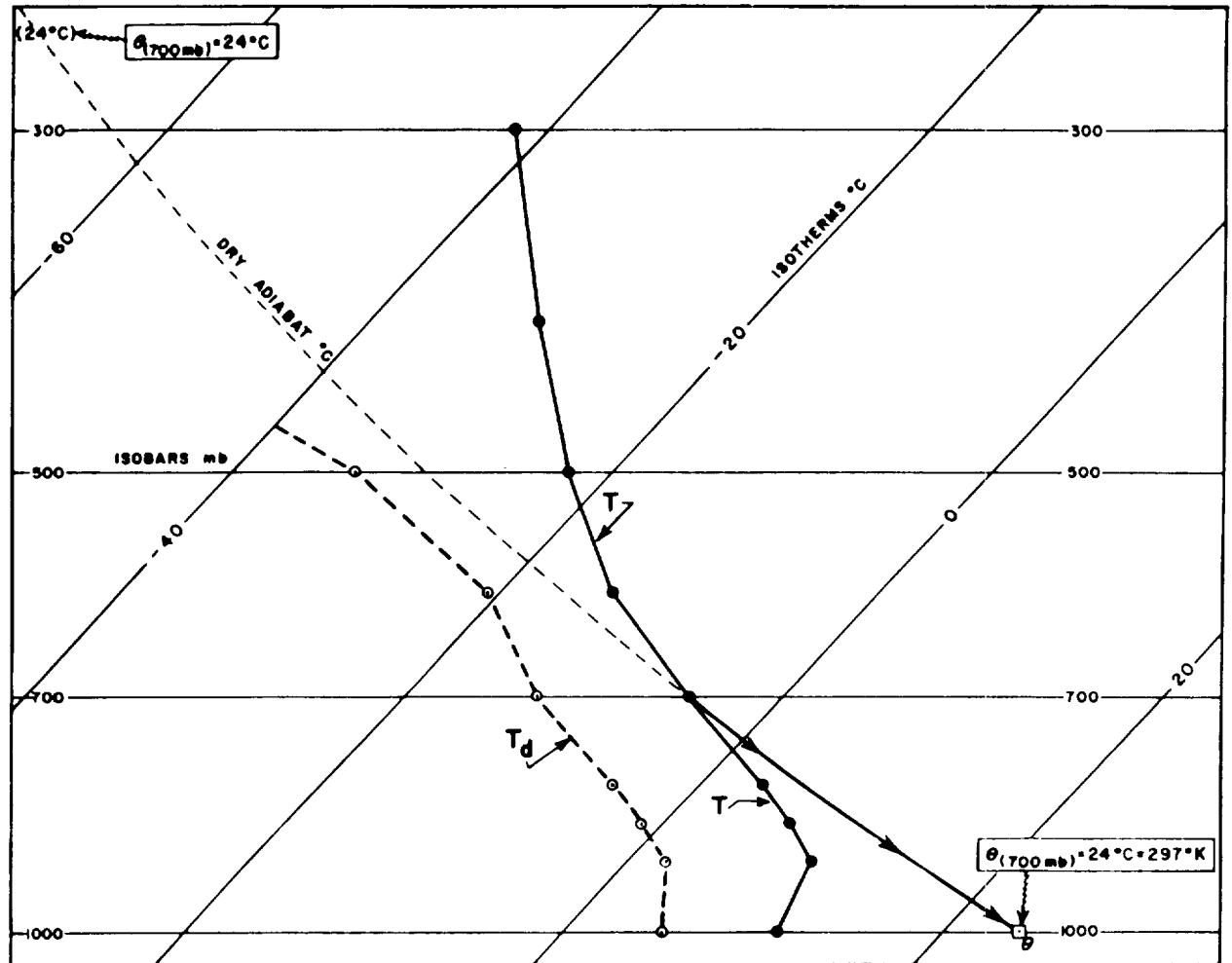
Figure 13. Determination of the Potential Temperature (θ).

Procedure: Find the wet-bulb temperature as in paragraph 4.9 and shown in Figure 14. The value of the saturation adiabat through this wet-bulb temperature point is equal to the wet-bulb potential temperature.

Alternate Procedure: Another procedure is also illustrated in Figure 14. Find the wet-bulb temperature as in paragraph 4.9. From the T_w point, follow the saturation adiabat to the 1000-mb isobar. The isotherm value at this intersection is equal to the wet-bulb potential temperature at the given pressure.

In the example shown in Figure 14, $\theta_{w(700)} = 9.5°C$.[10]

4.11. Equivalent Temperature.

Definition: The equivalent temperature (T_E) is the temperature a sample of air would have if all its moisture were condensed out by a pseudo-adiabatic process (i.e., with the latent heat of condensation being used to heat the air sample), and the sample then brought dry-adiabatically to its original pressure. This equivalent temperature is sometimes

---

[10] In theoretical and physical meteorology it is customary to express θ_w in °K (i.e., by adding 273° to the Celsius temperature value).
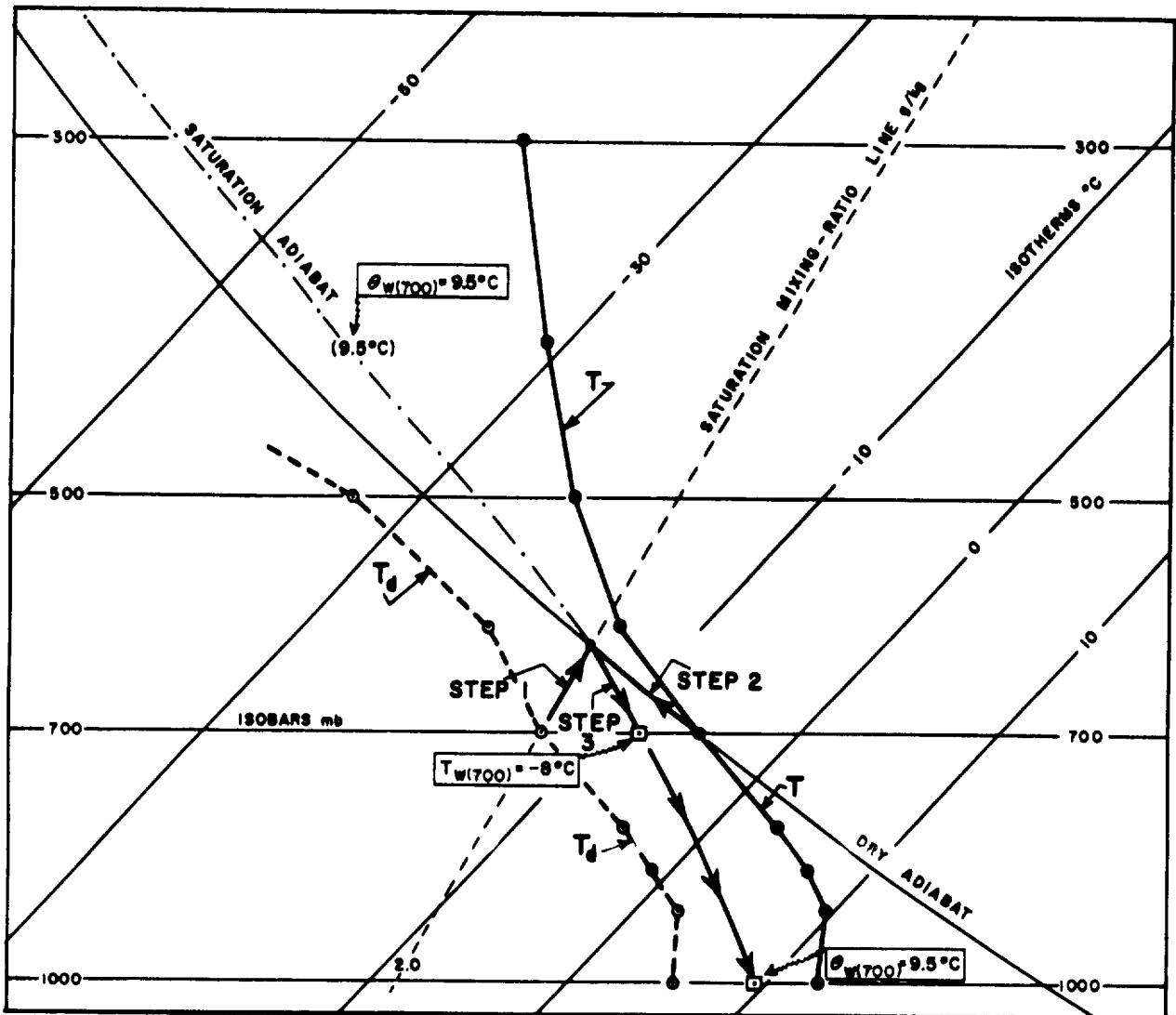
Figure 14. Determination of the Wet-Bulb Temperature (T_w) and the Wet-Bulb Potential Temperature (θ_w).

termed the "adiabatic equivalent tempera-ture," and should not be confused with the "isobaric equivalent temperature" which is always slightly lower.

Procedure: Figure 15 illustrates the method of finding T_E for a given pressure on the sounding. The steps are:

Step 1. From the T_d curve at the given pres-

    sure, in this case 700 mb (Point P'), draw a line upward along a saturation mixing-ratio line. Also, from the T

curve at the given pressure (Point P), draw a line upward along a dry adiabat until it intersects the line drawn first. (The height of this intersection is the "lifting condensation level," see par. 4.20.)

Step 2. From this intersection, follow a saturation adiabat upward to a pressure where both the saturation and dry adiabats become parallel; i.e., to a pressure where all the moisture has been condensed out of the sample.
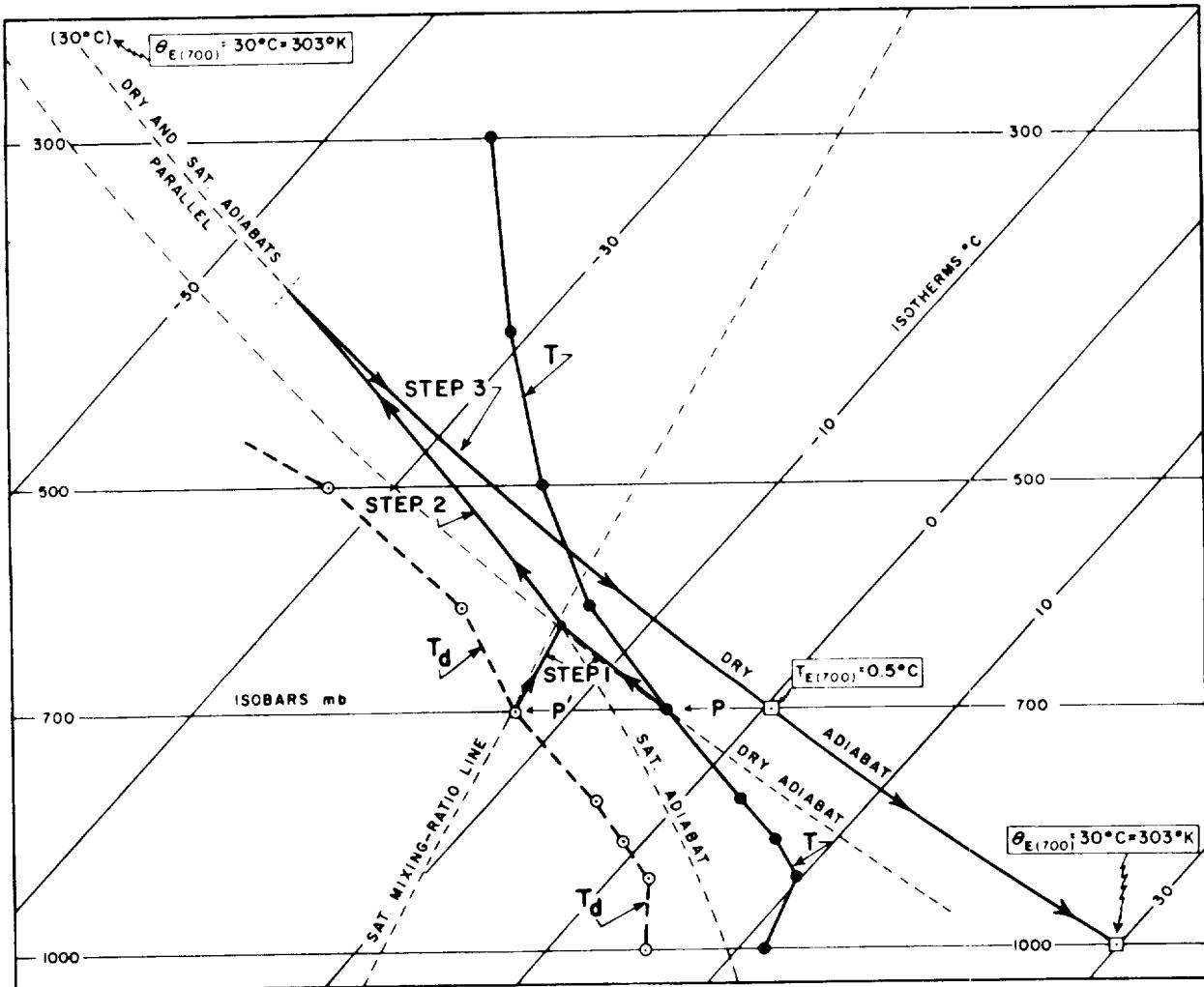
Figure 15. Determination of the Equivalent Temperature (T_E) and the Equivalent Potential Temperature (θ_E).

Step 3. From this pressure, follow a dry adiabat back to the original pressure, 700 mb. The isotherm value at this point is equal to the equivalent temperature (T_E).

In the example shown in Figure 15, $T_{E\,(700)} = +0.5\,^\circ C$.

4.12. Equivalent Potential Temperature.

Definition: The equivalent potential temperature (θ_E) is the temperature a sample of air would have if all its moisture were condensed out by a pseudo-adiabatic process (i.e., with

the latent heat of condensation being used to heat the air sample), and the sample then brought dry-adiabatically back to 1000 mb.

Procedure: Find the equivalent temperature for the given pressure, in this case 700 mb, as described in paragraph 4.11, and as shown in Figure 15. From the T_E point, follow the dry adiabat to the 1000-mb isobar. The isotherm value at this point is equal to the equivalent potential temperature (θ_E) at the given pressure. θ_E can also be read directly from the value of the dry adiabat through the T_E point at the given pressure.

4-8
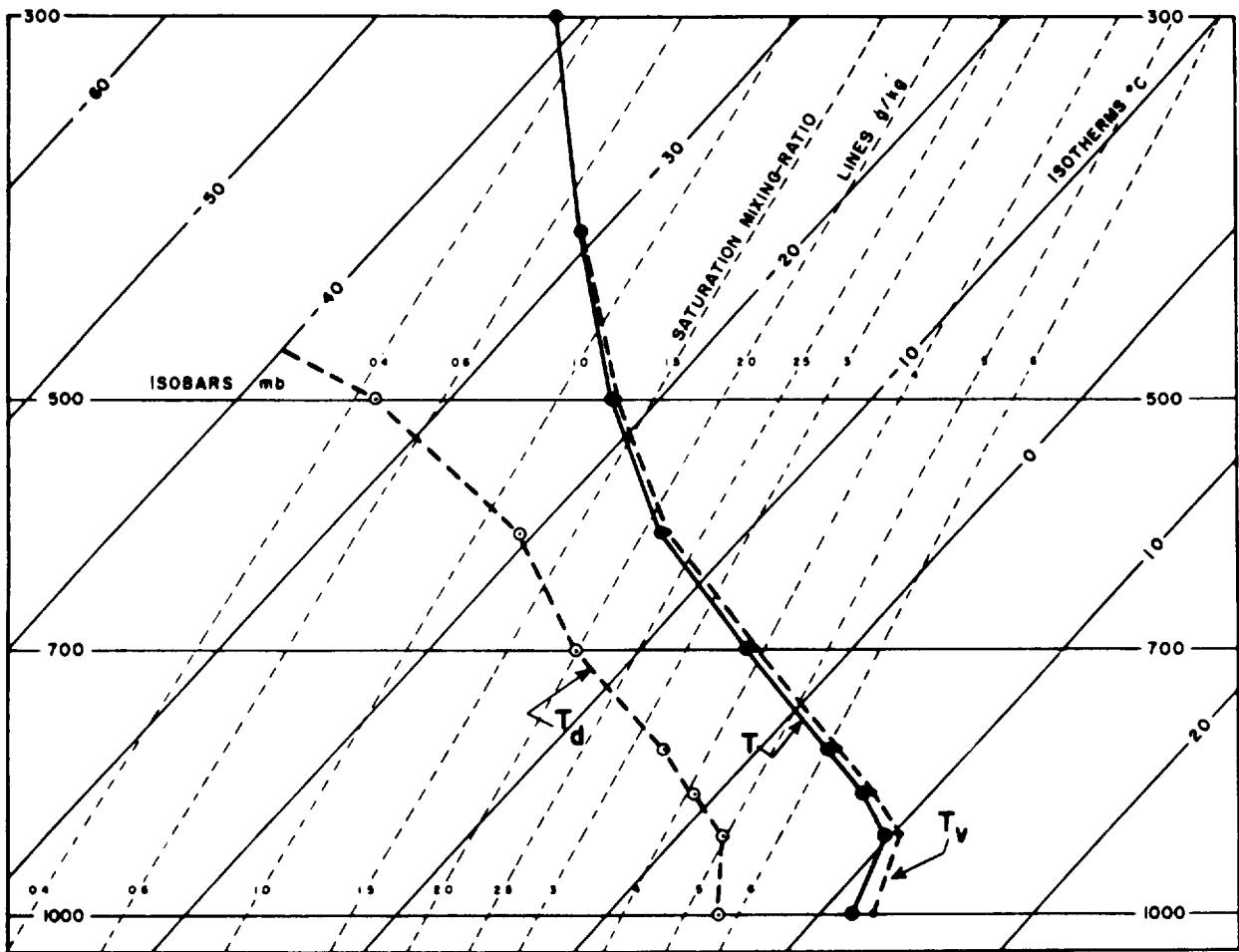
Figure 16. Comparison Between the Observed-Temperature and Virtual-Temperature Curves.

In the example shown in Figure 15,

$\theta_{E(700)}$ = 30°C or 303°K.

4.13. Virtual Temperature.

Definition: The virtual temperature (T_v) of a moist air sample is defined as the temperature at which *dry* air at the same pressure, would have the same density as the moist air.

Procedure: At a given pressure on a sounding, the difference (in °C) between the observed and virtual temperatures (i.e., $T_v - T$) is approximately equal to 1/6 of the numerical value of the saturation mixing-ratio line passing through the T_d curve at that pressure. Hence, the virtual temperature may be computed at each appropriate pressure by adding this numerical difference $(w/6)$ to that pressure's temperature (T).

An example of the relationship between the T and T_v curves is shown in Figure 16. At the lower moisture values; i.e., above 500 mb, the T and T_v curves are almost identical.

For detailed work, a more accurate determination of the virtual temperature can be made by using the following formula (see p. 63 of [33] for the derivation of this equation):

$$T_v = T(1 + 0.6w)$$

4—9

4.14. Thickness of a Layer.

Definition: The thickness of a layer between any two pressure surfaces is equal to the difference in the geopotential heights of these surfaces.

Procedure: Figure 17 illustrates the procedure for finding the thickness of a given layer:

Step 1. Construct a T_v curve for the given layer, in this case the 1000- to 700-mb layer, based upon the corresponding T and w values at the appropriate points of the original sounding (see paras. 4.2 and 4.13).

Step 2. Draw a straight line through the given layer, so that the areas confined by the T_v curve and the straight line balance to the right and the left of of the line. The straight line can have any orientation, but it is easiest to balance the areas when they are small, so choose an orientation that minimizes the areas.

Step 3. The thickness of the layer is read at the point where the straight line of Step 2 crosses the thickness scale for the given layer.

The label at the left end of each thickness scale on the Skew-T Chart specifies the layer for which that scale is primarily intended. However, each scale is also applicable in determining the thickness of certain other layers, namely, layers for which the numerical ratio of the boundary-pressure values is equal to the ratio indicated by the label of the printed scale. For example, the scale for the 500- to 300-mb layer (labeled "500/300") can also be used to determine the thickness of the layers 50 to 30 mb, 250 to 150 mb, 1000 to 600 mb, etc. The thickness scales printed on the Skew-T Chart thus provide for a thickness determination of any layer whose boundary-pressures ratio is equal to 2/1, 3/2, 4/3, 5/3, 7/5, or 10/7; there are six unique ratios.

The thickness of the layer between any two pressure surfaces is directly proportional to the mean virtual temperature[11] of the layer. This can be seen from the hypsometric equation, upon which all thickness computations are based, and which may be written in the form:

$$\text{Thickness} = \frac{R_d}{g} \, \overline{T_v} \, \text{Ln} \left(\frac{P_1}{P_2} \right)$$

where $\overline{T_v}$ is the mean virtual temperature of the layer (in °K); R_d is the gas constant for dry air; g is the gravity constant; P_1 and P_2 are the boundary pressures of the layer; and Ln indicates the natural logarithm (to the base e). Once the boundary-pressure values are chosen, the natural logarithm of their ratio becomes a constant; and thus the thickness varies only with the mean virtual temperature. This may also be shown on the Skew-T Chart. For example, the thickness of the 1000- to 500-mb layer with a mean virtual temperature of -40°C is read from that thickness scale as 15,540 feet. The thicknesses of both the 100- to 50-mb and 50- to 25-mb layers (which each have the same ratio of pressures, 2/1) with the same mean virtual temperature of -40°C are also read from their thickness scales

---

[11] Although the T and T_v curves are almost the same for layers of low moisture content, the difference between T and T_v becomes more important when warm, moist air is involved. If thickness calculations for the summer soundings at Miami, Fla., for instance, were based on T values, rather than T_v values, thickness errors in a moist 1000- to 700-mb layer of as much as 100 feet could result.

as 15,540 feet. Thus, if the boundary-pressures ratio of a nonstandard layer fits one of the six unique thickness-scale pressure ratios printed on the Skew-T Chart and if the mean virtual temperature of the nonstandard layer is known, its thickness can be read from that particular thickness scale at the intersection of the proper isotherm value.

In the example shown in Figure 17, the thickness of the 1000- to 700-mb layer is approximately 9550 geopotential feet, or 2910 geopotential meters when read from the bottom scale.

4.15. Height of the 1000-mb Surface.

Definition: This is the height of the 1000-mb pressure surface in geopotential feet above mean sea level (MSL).

Procedure: The 1000-mb Height Nomogram described in paragraph 2.7, printed in the upper left-hand corner of the Skew-T Chart, is used to obtain this value. An example of the use of this nomogram is shown in Figure 18. Locate the surface-air temperature value (40°F) on the TEMPERATURE scale along the top of the chart. Then locate the *sea-level* pressure (1025 mb) on the PRESSURE scale at the left side of the chart. Next, lay a straightedge between these two points so that it intersects the HEIGHT scale. The value at this point of intersection of the HEIGHT scale (660 feet) is the height of the 1000-mb surface above MSL. When the sea-level pressure is less than 1000 mb, the indicated height value is negative; i.e., the 1000-mb surface is below MSL.

The height of the 1000-mb surface above the station can also be calculated from this nomogram. To do this, the station pressure is used on the PRESSURE scale instead of the sea-level pressure. The height read is then the height above the station (or below the station, if the station pressure is less than 1000 mb).

4.16. Pressure Altitude.

Definition: Pressure altitude is defined as the altitude at which a given pressure is found in a standard atmosphere[12]. When an aircraft altimeter is set at 29.92 inches (1013 mb), its height-scale reading indicates the pressure altitude in the particular standard atmosphere upon which its calibration is based. (Most U.S. aircraft altimeters are based on the old NACA standard atmosphere, which does not differ significantly from the ICAO standard atmosphere except above the tropopause.)

Procedure: To find the pressure altitude at a given pressure on a sounding, read the value, in feet or meters as desired, of the ICAO STANDARD ATMOSPHERE ALTITUDE scale (at the right side of the chart) at that pressure. The exact heights of pressures divisible by 50 mb are given in geopotential feet (in parentheses) and in geopotential meters [in brackets] below the pressure-surface values printed along the left border of the chart. For example, the pressure-altitude height for 500 mb is 18,289 feet; for 700 mb it is 9,882 feet.

4.17. Density Altitude.
Density altitude is defined as the altitude in a standard atmosphere at which a given density is found. This parameter is frequently used in meteorological and operational problems related to aircraft performance, airport design, etc.

---

[12] A standard atmosphere is a hypothetical vertical distribution of atmospheric temperature, pressure, and density which, by national or international agreement, is taken to be representative of the atmosphere for purposes of pressure-altimeter calibration, aircraft-performance calculations, aircraft and missile design, ballistic tables, etc.(refer to the *Glossary of Meteorology* for further discussion). The scales on the Skew-T Chart are based on the ICAO Standard Atmosphere, adopted in November 1952 (see *AWS-TR-232*   and *U. S. Standard Atmosphere, 1962,* for a table of height values.
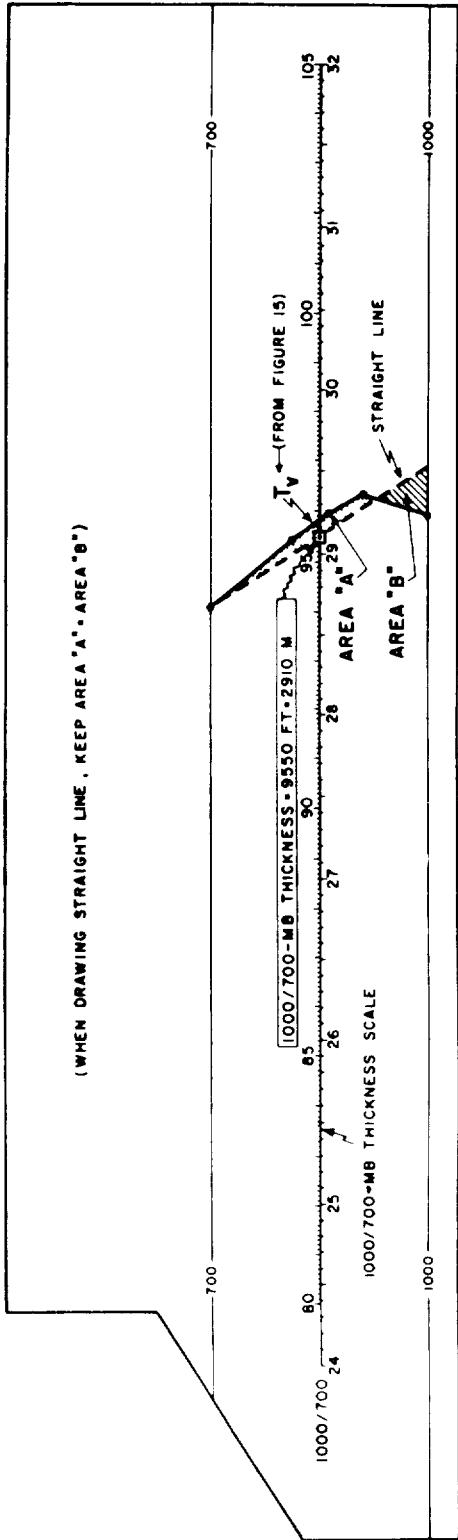
Figure 17. Determination of the Thickness of the 1000- to 700-mb Layer.

Computation of the density altitude c a n be easily accomplished on an edition of the full-scale Skew-T Chart which has a density-altitude nomogram overprinted on it. This edition and instructions for its use are available in *AWS TR 105-101*. (See para. 1.3f)

4.18. Convection Condensation Level.

Definition: The convection condensation level (CCL) is the height to which a parcel of air, if heated sufficiently from below, will rise adiabatically until it is just saturated (condensation starts). In the commonest case, it is the height of the base of cumuliform clouds which are or would be produced by thermal convection solely from surface heating.

Procedure: To determine the CCL on a plotted sounding, proceed upward along the saturation mixing-ratio line t h r o u g h the surface dew-point temperature until this line intersects the T curve on the sounding. The CCL is at the height of this intersection. Figure 19 illustrates this procedure.

When there is much variation in moisture content in the layers near the surface, an average moisture value of the lower layer may be used in place of the surface-parcel moisture value in computing the CCL (see for examples, paras. 5.24.1 through 5.24.3).

4.19. Convection Temperature.

Definition: The c o n v e c t i o n temperature (T_c) is the surface temperature that must be reached to start the formation of convection clouds by solar heating of the surface-air layer.

Procedure: Determine the CCL on the plotted sounding, as described in paragraph 4.18. From the CCL point on the T curve of the sounding, proceed downward along the dry adiabat to the surface-pressure isobar. The temperature read at this intersection is the
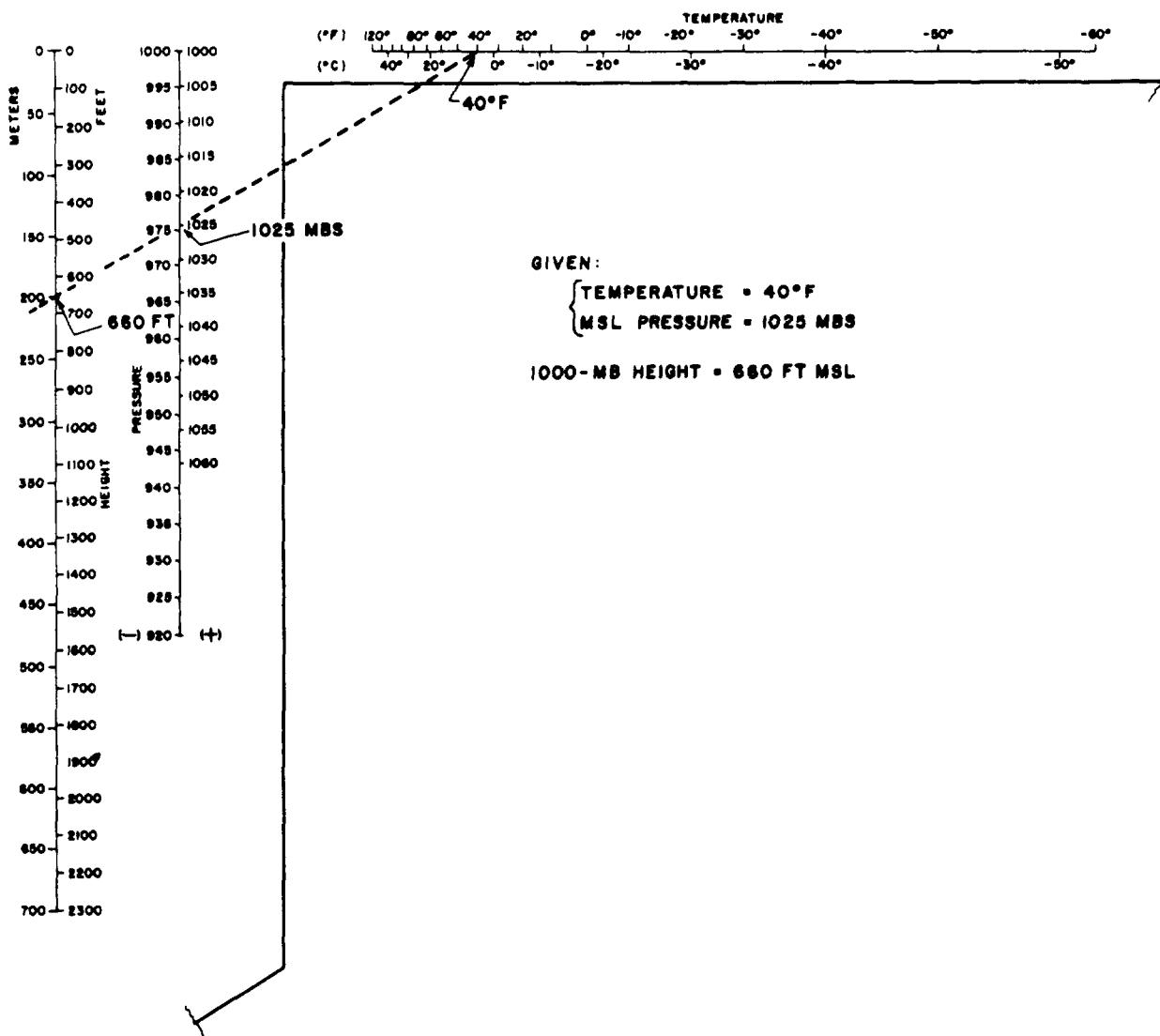
Figure 18. Determination of the Height of the 1000-mb Surface Above (or Below) Mean Sea Level.

GIVEN:

{ TEMPERATURE = 40°F
{ MSL PRESSURE = 1025 MBS

1000-MB HEIGHT = 660 FT MSL

convection temperature (T_c) . This procedure is illustrated in Figure 19.

4.20. Lifting Condensation Level.

Definition: The lifting condensation level (LCL) is the height at which a parcel of air becomes saturated when it is lifted dry-adiabatically. The LCL for a surface parcel is always found at or below the CCL; note that when the lapse rate is, or once it becomes, dry adiabatic from the surface to the cloud base, the LCL and CCL are identical.

Procedure: The LCL is located on a sounding at the intersection of the saturation mixing-ratio line through the surface dew-point temperature with the dry adiabat through the surface temperature. This procedure is also illustrated in Figure 19.

4.21. Mixing Condensation Level.

Definition: The mixing condensation level (MCL) is the lowest height, in a layer to be mixed by wind stirring, at which saturation occurs after the *complete* mixing of the layer; it is located at the intersection of the saturation mixing-ratio line through the mean mixing ratio of the layer with the mean dry adiabat of the mixed layer.

4—13
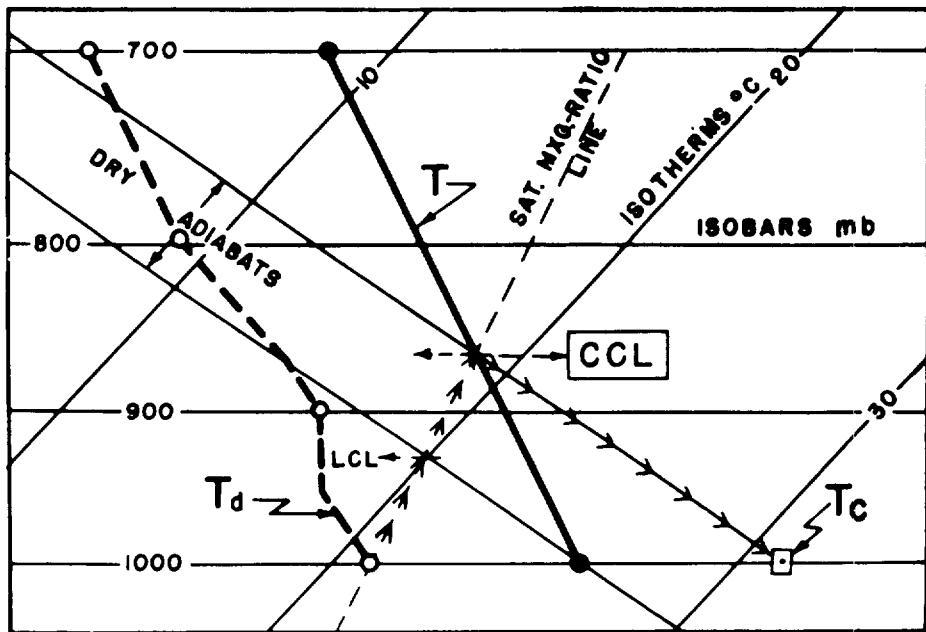
Figure 19. Procedure for Locating the Convection Condensation Level, the Convection Temperature, and the Lifting Condensation Level.

Procedure: The determination of the MCL first requires an estimate or forecast of the height of the top of the layer to be mixed. There is no known objective way to determine this height. However, a subjective estimate based on local experience which considers such things as the expected lower-level wind speeds, the terrain roughness, and the original sounding through the lower layers, will usually suffice (see par. 6.7 for a discussion of this).

Once the top of the mixed layer is estimated, the procedure is as follows. Since the potential temperature and the mixing ratio of a completely mixed unsaturated layer are constant from the ground to the top of the layer, an equal-area approximation of its mean temperature and moisture can be used. Determine the mean dry adiabat (an isotherm of potential temperature) of the mixed layer from the original T curve on the sounding by the equal-area method shown in Figure 20. Then, determine for the mixed layer the mean saturation mixing-ratio line through the T_d curve by the equal-area method as shown in Figure 20. If an MCL exists, it will be found at the point of intersection

(*within* the mixed layer) of the mean saturation mixing-ratio line with the mean dry adiabat of the mixed layer. If there is no intersection of these two lines *within* the mixed layer, then the mixed air is too dry to reach saturation by the mixing process.

4.22. Level of Free Convection.

Definition: The level of free convection (LFC) is the height at which a parcel of air lifted dry-adiabatically until saturated and saturation-adiabatically thereafter would first become warmer (less dense) than the surrounding air. The parcel will then continue to rise freely above this level until it becomes colder (more dense) than the surrounding air.

Procedure: The LFC for a given parcel which becomes saturated by *lifting* is located at the height where the saturation adiabat through the initial wet-bulb temperature of the parcel intersects the sounding temperature curve at a higher level. If the parcel is to be *heated* to make it rise, then the wet-bulb temperature corresponding to the convection temperature must be used (see par. 4.9 for

4—14
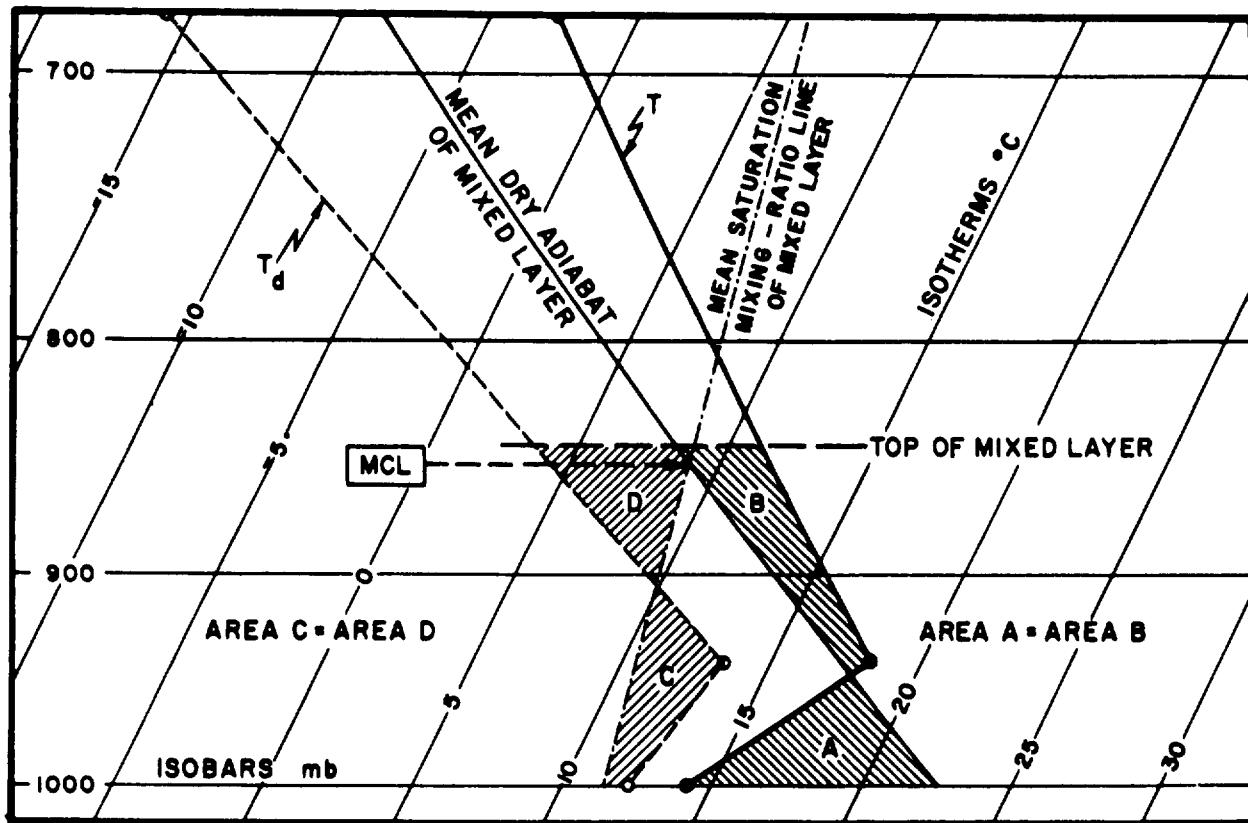
Figure 20. Determination of the Mixing Condensation Level on a Sounding.

graphical determination of wet-bulb temperature).

For determining the LFC, the result is often more realistic if one uses the wet-bulb temperature corresponding to the moisture content of the lower layer(s) of the atmosphere instead of the surface wet-bulb temperature (see for examples, pars. 5.24.1 through 5.24.3).

4.23. Positive and Negative Areas. On a thermodynamic diagram such as the Skew-T Chart, a given area can be considered proportional to a certain amount of kinetic energy of a vertically and adiabatically moving air parcel.

Definition of NEGATIVE Area: When a parcel on a sounding lies in a stable layer, energy has to be supplied to it to move it either up or down. The area between the path of such a parcel moving along an adiabat and the sounding curve is proportional to the amount of kinetic energy that must be supplied to move it. This is called a "negative (energy) area."

Definition of POSITIVE Area: When a parcel can rise freely because it is in a layer where the adiabat it follows is warmer than the surrounding environment, the area between the adiabat and the sounding is proportional to the amount of kinetic energy the parcel gains from the environment. This is called a "positive (energy) area."

The negative and positive areas are not uniquely defined on any given sounding. They depend on the parcel chosen and on whether the movement of the chosen parcel is assumed to result from heating (insolation at the ground, release of latent heat of condensation, etc.), or from forcible lifting (convergence, orographic effects, etc.).

Procedure for the Surface-Parcel-Heating Case: The plotted sounding is analyzed to find the CCL according to procedure of paragraph 4.18. A saturation adiabat is then constructed upwards from the CCL to well beyond the point where it intersects the sounding again the equilibrium level (EL - see par. 4.24); and a dry adiabat is constructed through the CCL down to its intersection with the surface-pressure isobar. The negative and positive areas are then labelled and colored or shaded as in the example in Figure 21. (Note that many soundings have no lower negative area, as when the lower layers are already adiabatic, but only a positive area; and also that many soundings show only a deep negative area without any positive area as when the CCL is extremely high.) The areas determined by the above procedure are indicative of conditions under the assumption that the surface temperature does not rise after the CCL has been reached - if the surface temperature does rise further then it is readily seen that the areas change somewhat because the cloud base rises and the surface humidity decreases.

Procedure for the Lifted Surface-Parcel Case: In this instance, the surface parcels are lifted by some mechanical process, such as orographic or frontal lifting or convergence. The first step is a determination, from the plotted sounding, of the LCL for the lifted surface parcel by the procedure given in paragraph 4.20. Then, from this LCL draw a line upward parallel to the nearest saturation adiabat (i.e., construct the saturation adiabat through the LCL) to well beyond the EL. An example is shown in Figure 22. The point at which this line first intersects the *T* curve of the sounding is the LFC. Then the negative area is the area on the chart below the LFC bounded on the right by the sounding curve, at the bottom by the surface point, and on the left by the dry adiabat from the surface point to the LCL and by the saturation adiabat from the LCL to the LFC. This negative area represents the energy that the lifting mechanism must supply to the lifted surface parcel to raise it to the LFC. The positive area is the area

above the LFC bounded on the left by the sounding curve, on the right by the saturation adiabat through the LFC, and terminated at the top by the EL. This positive area represents the energy gained by the lifted parcel after it rises above the LFC. There is also an upper negative area above the EL.

Procedure for the Case Where an Upper-Level Parcel is Lifted: In the event that the analyst wishes to determine the positive and negative areas that will result when an air parcel initially at some upper level is lifted by a mechanism such as frontal overrunning, upper-level convergence, etc., the procedure is exactly analogous to that used in the lifted surface-parcel case. That is, first determine the LCL for the parcel in question, then construct the saturation adiabat upward through this LCL through the LFC to well beyond the EL. The negative area, representing the energy that must be supplied to the parcel to raise it to its LFC, is the area below the LFC bounded by the sounding curve on the right, and by the dry and saturation adiabats on the left. The positive area, representing the energy gained by the parcel after it rises above the LFC, is the area above the LFC bounded by the sounding curve on the left, and the saturation adiabat through the LFC on the right, and terminating at the EL.

4.24. Equilibrium Level.

Definition: The equilibrium level (EL) is the height where the temperature of a buoyantly rising parcel again becomes equal to the temperature of the environment.

Procedure: Determine the positive area for the parcel of interest according to the proper procedure outlined in paragraph 4.23. The EL is then found at the top of the positive area where the *T* curve and the saturation adiabat through the LFC again intersect. The location of an EL is shown in both Figures 21 and 22.
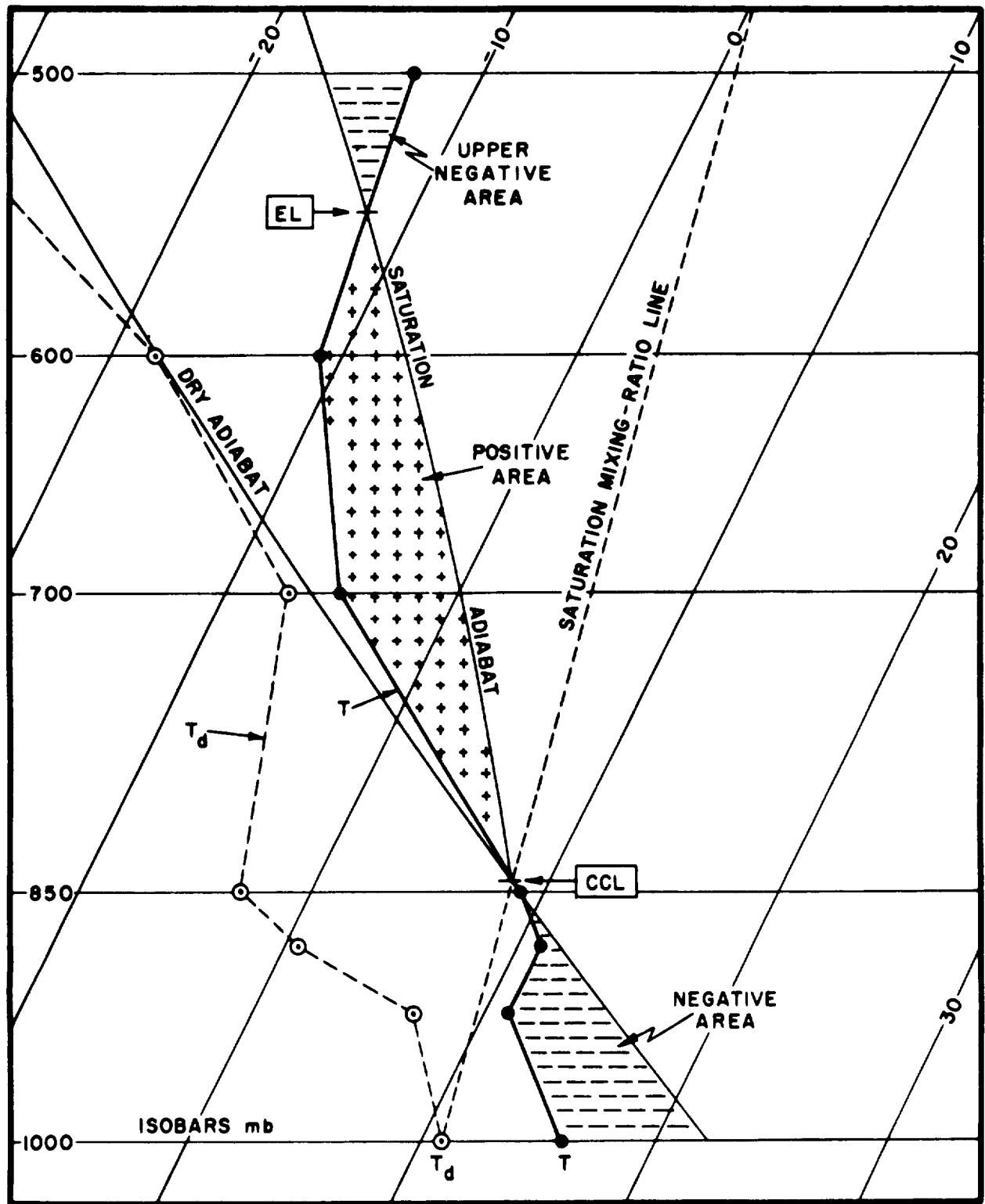
Figure 21. Determination of the Positive and Negative Areas on a Sounding Due to the Heating of a Surface Parcel.
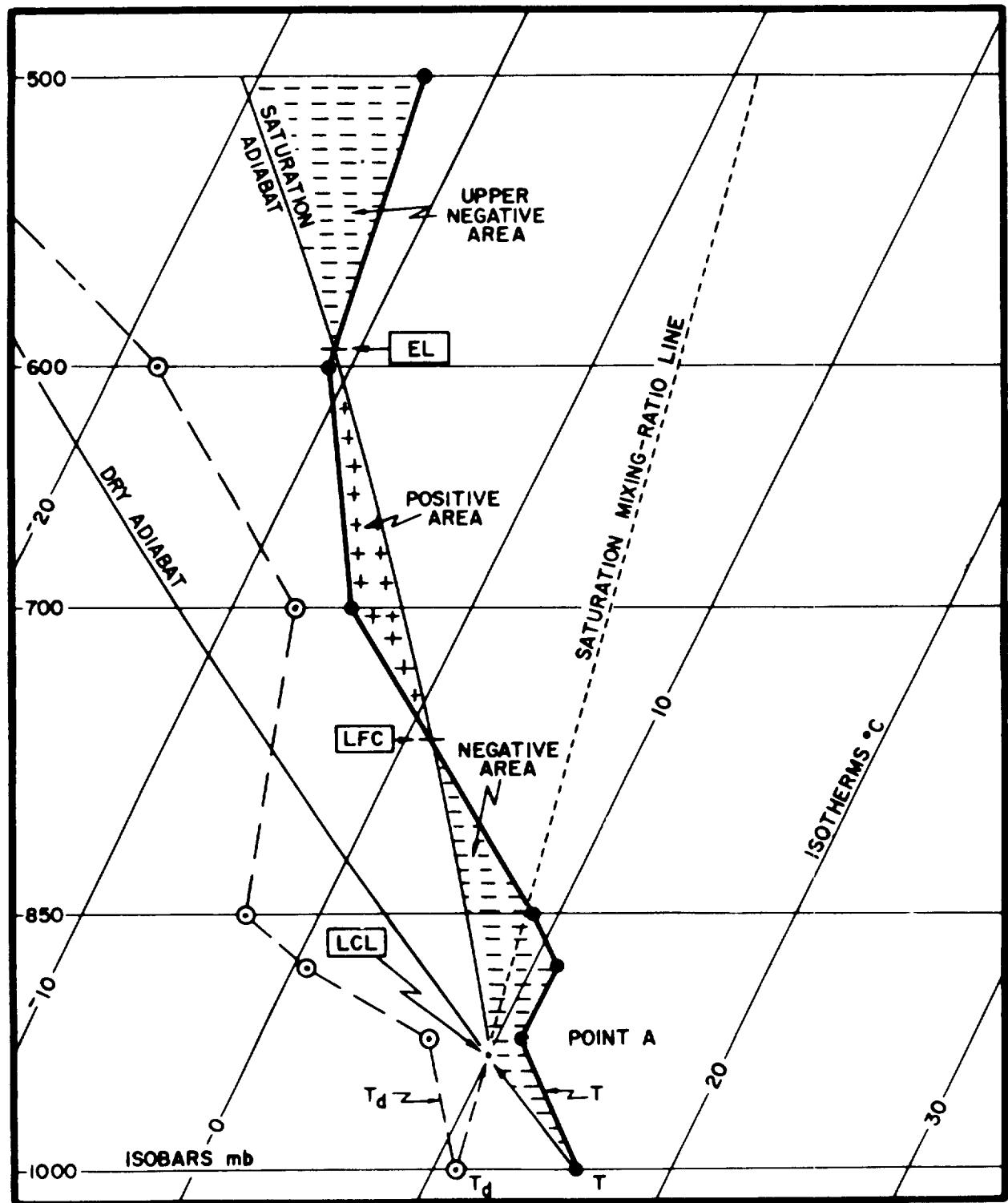
Figure 22. Determination of the Positive and Negative Areas on a Sounding Due to the Lifting of a Surface Parcel.

4.25. Energy Determinations on the Skew-T Chart. When positive or negative areas have been located on the Skew-T Chart in accordance with the procedures given in paragraph 4.23, the energies involved may be computed by the following relationships:

a. One square centimeter on the DOD WPC 9-16 chart equals 0.280×10^6 ergs.

or 0.0280 joules, per gram of air in the sample under consideration.

b. One square inch on the DOD WPC 9-16 chart equals 1.808×10^6 ergs, or 0.1808 joules, per gram of air in the sample.

DETERMINATION OF STABILITY

5.1. The "Parcel" Theory as a Basis for Determining Stability and Instability. Nearly all the procedures routinely used to evaluate and analyze the stability of the atmosphere are manipulations of the so-called "parcel" method, which is a particular way of applying certain physical laws of hydrostatics and thermodynamics. It is simply a theory which assumes an over-simplified model of the behavior of the atmosphere. We do not yet know just how closely this model corresponds to reality. Only recently have serious attempts been made to analyze the physics of clouds and atmospheric convection in more realistic and quantitative detail. These studies provide some useful corrections and modifications to parcel-method procedures, as will be shown in Chapter 8 of this manual. The theory of the parcel-method will now be described briefly and qualitatively along with general indications of its unrealistic assumptions and their effects on the practical utility of the method.

The temperature of a minute parcel of air is assumed to change adiabatically as the parcel is displaced a small distance vertically from its original position. If the parcel is unsaturated, its virtual temperature (see pars. 4.13 and 5.8) is assumed to change at the dry-adiabatic rate; if the parcel is saturated, the change will occur at the saturation-adiabatic rate. In addition, it is assumed that the moving parcel neither affects, nor is affected by, the atmosphere through which it moves; i.e., the parcel does not "mix" with nor disturb the surrounding air.

If, after the vertical displacement, the parcel has a higher virtual temperature (i.e., lower density) than the surrounding atmosphere, the parcel is subjected to a *positive buoyancy force* and will be further accelerated upwards; conversely, if its virtual temperature has become lower than that of the surrounding air, the parcel will be denser than its environment (subjected to a *negative buoyancy force*) and will be retarded and eventually return to the initial or equilibrium position.

The atmosphere surrounding the parcel is said to be *stable* if the displaced parcel tends to return to its original position; *unstable* if the displaced parcel tends to move farther away from its original position; and *in neutral equilibrium* when the displaced parcel has the same density as its surroundings.

According to the parcel theory, the behavior of a parcel which, once it is saturated, becomes warmer than its environment through the release of the latent heat of condensation, is as follows. The parcel ascends under acceleration from the positive buoyancy force. If the saturated parcel continues to rise through an atmosphere in which the lapse rate exceeds the saturation adiabatic, the speed of the ascent increases. This acceleration persists until the height is reached where the saturation-adiabatic path of the parcel crosses the temperature sounding; i.e., where the parcel temperature becomes equal to the environment temperature. This height has been defined as the equilibrium level (EL) in paragraph 4.24. The rising parcel at this point has its maximum momentum. It now passes above the EL, becomes colder than the environment (negative buoyancy) and is decelerated in the *upper negative area*, until it comes to rest at some unspecified distance above the EL ("overshooting"). The acceleration and speed of the parcel at any point can

be computed from the temperature excess of the parcel over the environment by the buoyancy formula — but it usually gives a very unrealistic result.

5.2. General Comment on the Effect of the Assumptions in the Parcel Theory on the Utility of Parcel-Method Techniques.

Meteorologists of a generation ago experimented extensively with the use of parcel-method techniques for analysis and forecasting of air masses, fronts, and convection weather. There was, at that time, little knowledge of cloud physics and convection mechanisms. Ideas of air-mass and frontal analysis predominated in the forecaster's routine, and the forecasters were eager to use soundings in place of indirect aerology. In more recent years, experience has shown that while identification of air-mass type is no longer a problem requiring soundings, the analysis of the soundings for temperature, moisture, and stability characteristics of the air remains one of the basic tools for weather forecasting. But this kind of analysis *by itself* has not proved very useful for forecasts of over six hours, and the necessity of also considering circulation characteristics and dynamics is now generally recognized [2] (and *A WS TR200*).

Parcel methods are useful because there are definite empirical relations between the results of parcel computations and the observed atmospheric behavior. Also, the parcel computations can provide a sort of standard of reference against which various more realistic procedures or forecasts may be compared to see if they are an improvement over the pure parcel computations.

In Chapter 8, considerable information from recent observational, theoretical, and experimental studies of convection and cloud physics will be referenced that appears to have a practical value in adapting parcel procedures to the real atmosphere and in appreciating their limitations. At this point it will suffice to note that the main effects observed in real convection and clouds which are not accounted for by the parcel theory are:

a. Lateral mixing of the convection-thermal or cumulus cloud with its environment ("dynamic entrainment"), which reduces the water content and buoyancy — at least of the outer parts of the convection column.

b. Vertical mixing, within the convection-thermal or cloud cell itself and with the environment at the top; in the cumulus cloud this is manifested by downdrafts, "holes," etc., and causes redistribution of condensed water and departures from the saturation-adiabatic lapse rate locally and for the cloud as a whole — these effects may be more important than those of lateral mixing.

c. Cooling from evaporation of falling precipitation; e.g., the lapse rate in rising saturated air which is being cooled by melting of falling snow or hail is 9°C to 14°C per kilometer.

d. Skin-friction and form-drag (dynamical interaction) between the rising thermal or cloud and the surrounding winds — especially when there is strong vertical-wind shear in the environment.

e. The compensatory subsidence in the environment of a rising convection current (see par. 5.23).

f. Internal viscous friction (can be neglected).

g. Radiation to or from cloud boundaries (see par. 5.11.0).

h. Different effects for coalescence versus ice-crystal precipitation process.

i. Cellular structure.

j. Reduction in buoyancy due to weight of condensed water (see par. 5.3).

k. Drag of falling precipitation on upward vertical motion.

Although the theory for many of these effects permits estimates of the right order of magnitude, observations of most of the parameters required for such computations are either not routinely obtainable or are not specifiable in sufficient detail and accuracy. In empirical forecast studies, the effects of the above factors are often indirectly "built-in" by correlating the actual weather occurrences with parcel-method-derived parameters or with combinations of such parameters and synoptic parameters. In general, the parcel-theory assumption of

solid, continuous, adiabatic ascents in clouds results in much higher values for updraft speed, water content, and temperature than would be found in actual observations. But since these departures have a largely systematic character, the parcel-method procedures are useful in an empirical way. This relationship is probably fortuitous, and especially so for forecasters.

5.3. The Parcel-Theory Assumptions Used In the DoD Skew T Chart.

Any thermodynamic diagram designed for use in atmospheric studies is simply a graphic means for presenting the parcel theory for such applications. However, there are actually a number of differences in the assumptions incorporated into the various adiabatic diagrams used by meteorologists. Apart from the choice of physical constants, which has long been standardized by WMO [65], these differences have chiefly concerned the assumptions about what happens to the condensed water after saturation takes place, and about the change in state due to freezing of the condensed water.

On older adiabatic diagrams, saturation adiabats at temperatures below 0°C were computed from vapor pressures over an ice surface. But newer diagrams (such as the current DoD Skew T chart, the Navy's "Arowagram," and the NWS's pseudo-adiabatic charts) are based on the assumption of vapor pressure over water at all temperatures, an assumption considered more realistic in view of the predominance of supercooling in clouds, at least down to -20°C. Therefore, evaluations of stability and parcel temperatures for lifting or heating effects on newer diagrams will differ from results obtained from older ones. In some cases, these differences will be considerable.

The error due to the pseudoadiabatic assumption that all other condensation products immediately fall out is

small (<1°C) in the case of a cloud that does not precipitate as long as the ascent of the saturated parcel is not more than 200 mb and no freezing takes place [54]. In a real cloud, however, the latent heat of fusion (freezing) adds considerable buoyancy to the parcel at temperatures below -10°C (compared to the water pseudoadiabatic assumption) [54]. Direct fallout of most condensed water (as precipitation) does, of course, occur from many clouds; but in large cumuliform varieties, much of the precipitation from one portion may be evaporated into another, causing a marked redistribution of buoyant energy.

5.4. Identifying Basic Types of Stability and Instability for Small Parcel Displacements In a Sounding Plotted on the Skew T Chart.

The stability of an air parcel in a given layer of the atmosphere, according to elementary parcel theory, is indicated on a thermodynamic diagram by comparing the lapse rate of the T_v curve for the given layer with the lapse rate of the corresponding dry adiabat (for an unsaturated parcel), or the saturation adiabat (for a saturated parcel).

In present forecasting practice, however, the ambient (free air) T curve is almost always used for these comparisons instead of the more exact T_v curve to eliminate the laborious point-by-point computation required for the latter and to allow faster evaluation of stability or instability. In this report, the T curve is used in making all lapse rate comparisons unless otherwise specified. It should be noted, however, that under certain conditions, the substitution of T for T_v can be a source of significant error in evaluating stability; a discussion of such error is given in paragraph 5.8. A detailed discussion of the exact (mathematical) form of the stability criteria according to parcel theory is found in many standard meteorology texts, an example of which is at [33].
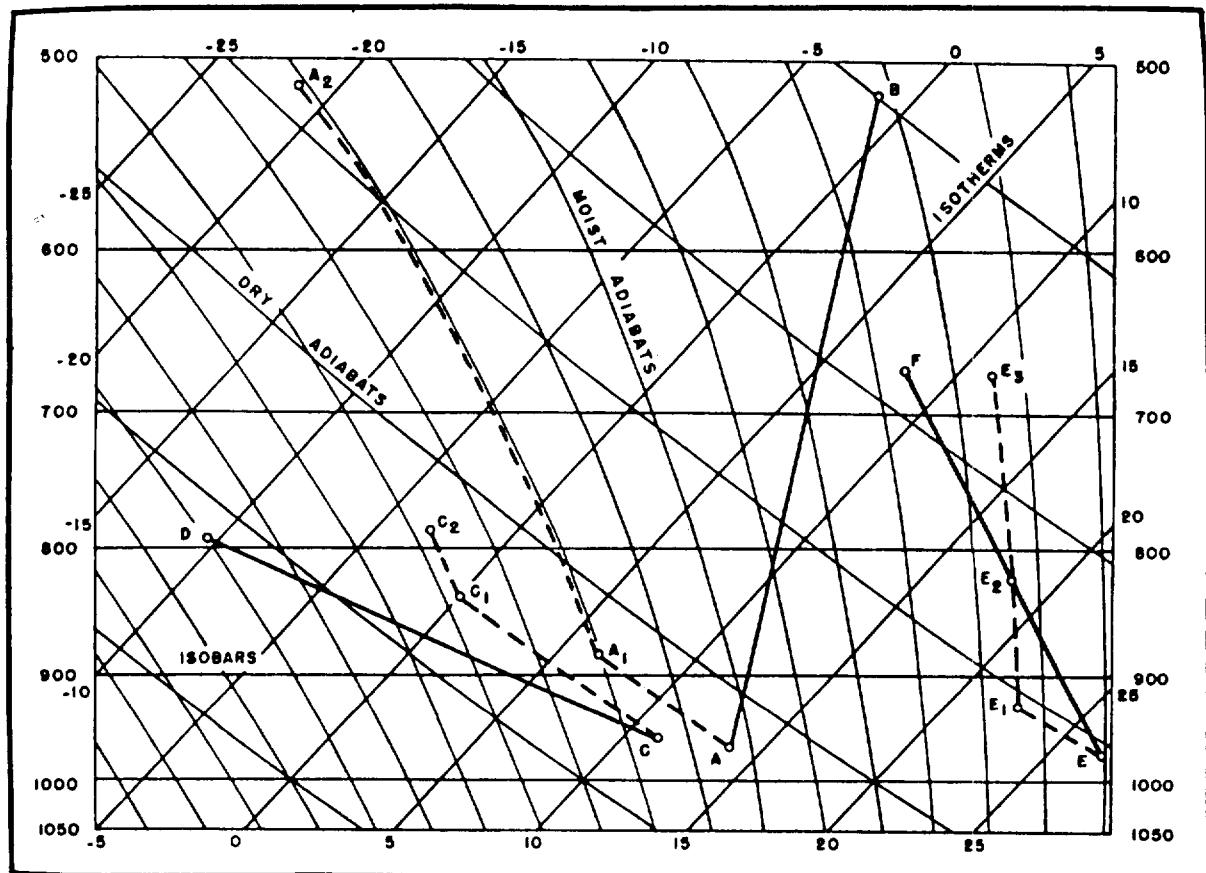
Figure 23. Stability Classification.
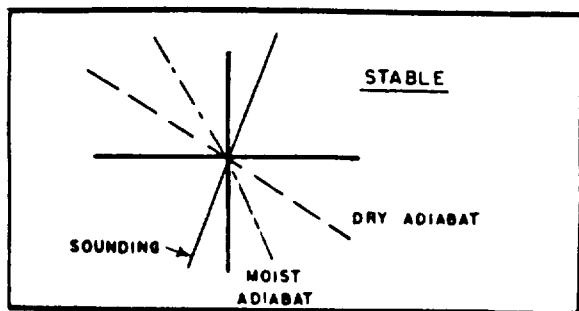
Figure 23a. Environmental (Sounding) Lapse Rate Less Than Lapse Rates of Dry and Moist Adiabats.
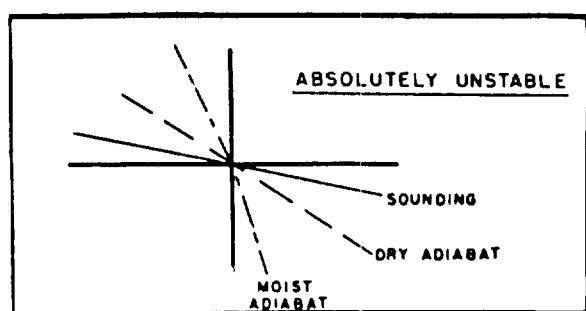
Figure 23b. Environmental (Sounding) Lapse Rate Greater Than Lapse Rates of Dry and Moist Adiabats.
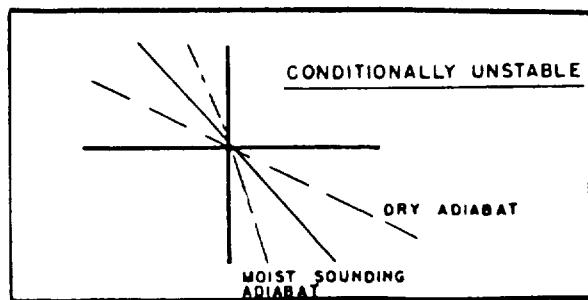
Figure 23c. Environmental (Sounding) Lapse Rate Less than Lapse Rate of Dry Adiabat, but Greater than Lapse Rate of Moist Adiabat

5.5. Description of Stability Criteria. The stability of any given layer for small parcel displacements is classified as follows:

a. Stable. Referring to Curve AB in Figure 23: If a particle of air at Point A is lifted, it will move along the dry adiabat until it reaches saturation. Assuming that this occurs at Point A_1, and the particle is lifted further, it will then ascend along the moist adiabat to Point A_2. At every point in its ascent, it is apparent that the particle is colder than the surrounding air. For example, at Point A_2 it would have a temperature of about minus 22°C, while the surrounding air (at Point B) would have a temperature of minus 2°C. Thus the air along the path $A-A_1-A_2$ will always be more dense (and heavier) than the surrounding air and will always tend to return to its original state. This air is said to be *stable*; see Figure 23a.

b. Absolutely Unstable. Referring to Curve CD in Figure 23: If a particle of air at Point C is lifted, it will move along the dry adiabat until it reaches saturation. Assuming that this occurs at Point C_1, and the particle is lifted further, it will move along the moist adiabat to Point C_2. At every point in its ascent, the particle is warmer than the surrounding air, whose temperature distribution is given by Line CD. As a result, the air along path $C-C_1-C_2$, being warmer and less dense than the surrounding air, will continue to rise of its own accord. This air is said to be *absolutely unstable*; see Figure 23b.

c. Conditionally Unstable. Referring to Curve EF in Figure 23: If a particle of air at Point E is lifted, it will move along the dry adiabat until it reaches saturation. Assuming that this occurs at Point E_1, and the particle is lifted further, it will move along the moist adiabat to Point E_2. Prior to reaching Point E_2, the air is colder and denser than its surroundings, and in the area $E-E_1-E_2$, may be considered to be *stable*. However, after passing Point E_2, the air is always warmer and less dense than its surroundings and is therefore *unstable*. This "combination" condition is referred to as *conditional instability*, with "conditional" referring to the fact that the air must be lifted past Point

E_2 in order for it to continue to rise of its own accord; see Figure 23C.

d. Autoconvection Lapse Rate. There are superadiabatic lapse rates where the temperature decrease with altitude is so great that the density of the air is either constant or increasing with altitude. The density of air is constant with height when the lapse rate is equal to 3.42°C per 100 meters. This is known as the *autoconvective lapse rate* or the *autoconvection gradient.* When this lapse rate is reached or slightly exceeded, the denser air above will spontaneously sink into the less dense air below. This spontaneous overturning of the atmosphere is called *autoconvection* because it represents the self-convection of air without an external impulse being applied.

e. Conditional State. If the lapse rate of the T curve is greater than that of the dry adiabat but less than that of the saturation adiabat (as along Curve EF of Figure 23), such a layer is often termed "conditionally stable" or "conditionally unstable," meaning that it is stable if unsaturated and unstable if saturated. If a saturated parcel at Point F (in Figure 23) were displaced upward, its temperature change would follow the saturation adiabat. The parcel would then be warmer than the surrounding air and would be accelerated upward; the layer would therefore be *unstable.* If the displaced parcel were unsaturated, however, its temperature change would follow the dry adiabat. In its new position, the parcel would be colder than its surroundings and would sink back to its original position; the layer would be *stable.* In the case of downward displacement, the temperature of both saturated and unsaturated parcels (under the pseudo-adiabatic assumption) would follow the dry adiabat. In its new position, the parcel would be warmer than its environment, and would tend to rise back to its original position. In other words, parcels in a conditional layer are actually stable for all downward displacements, whether initially saturated or unsaturated and regardless of moisture content. (In real clouds, evaporation of suspended water droplets will cause downward displacements to follow the saturation adiabat until the drops have evaporated, but if the layer has a lapse rate less steep than the saturation adiabat, such parcels will be stable, and tend to return upward.)

f. Neutral Equilibrium. If the T curve parallels an adjacent saturation adiabat, the layer is in *neutral equilibrium* for the upward displacement of saturated parcels; i.e., the upward displacement of saturated parcels will be neither aided nor hindered by the surrounding atmosphere. (However, for upward displacement of unsaturated parcels and downward pseudo-adiabatic displacement of all parcels, this curve is stable.) Similarly, if the T curve parallels an adjacent dry adiabat, the layer is in neutral equilibrium for the displacement of unsaturated parcels (but unstable for upward displacement of saturated parcels.) These two conditions of equilibrium are frequently termed "Saturation Indifferent" and "Dry Indifferent," respectively.

5.6. Discussion of Superadiabatic Lapse Rates. Many investigations have shown that genuine superadiabatic lapse rates frequently occur within the first 1,000 feet off the surface. However, when absolutely unstable lapse rates are reported in the troposphere above the gradient wind level, as shown between Points C and D of Figure 23, they are often rejected as erroneous data [32]. Such rejection arises from the assumption that measurement defects or spurious effects, such as condensed water evaporating from either the radiosonde instrument housing or the thermistor, must be causing the excessive cooling. Presumably, this generally occurs while the instrument is emerging from the top of a cloud layer into the very dry air of a capping inversion. This is, in fact, where superadiabatic lapse rates are frequently reported. Admittedly, the resulting error is more likely with some makes of radiosonde than with others, and does actually account for some of the cases of superadiabatic lapse rates reported. However, there is now

sufficient evidence to indicate that valid cases of superadiabatic lapse rates can occur through a fairly shallow layer sandwiched between stable layers in the troposphere [26] [32].

There are two processes which can explain the occurrence of such real superadiabatic lapse rates:

a. Sufficient destabilization due to rapid lifting at a saturated/dry-air interface within the lifted layer.

b. High rate of evaporation at the top of a cloud layer. The simultaneous occurrence of both processes is also likely.

Thus, when a superadiabatic lapse rate is included in a raob report, the possibility of it being a valid observation can no longer be ignored. A study of the synoptic conditions occurring in the area of the raob ascent to determine the causal process is preferable

to a routine rejection of the report. When rapid lifting of tropospheric layers is likely, due to either the rapid movement of a cold front or orographic lifting, there is a rather high probability of finding a shallow layer with a transitory superadiabatic lapse rate. Altocumulus castellanus reports on the surface chart are often noted in the area of such activity. (See also par. 5.20.2 for further details on the effects of lifting on the lapse rate.)

5.7. Oscillation of a Parcel as a Function of Stability. It is a corollary of the classical parcel theory of stability that a parcel given a forced or buoyancy impulse may be assumed to oscillate about its EL rather than return to EL immediately. The period of such an oscillation is given by an equation analogous to that for simple harmonic oscillation of a pendulum, i.e., approximately:

$$2\pi/\text{period} = \sqrt{\frac{(\text{gravity})}{(\text{temperature})}} \times (\text{"delta" lapse rate})$$

where "delta" lapse rate is the difference between the dry-adiabatic lapse rate and the actual lapse rate in the region of the oscillation. Actually, of course, in a stable layer the parcel's oscillation amplitude will be damped with time so that finally the parcel comes to rest at the EL. In an unstable layer, however, the oscillation period and amplitude in effect increase with time, and the period tends to approach asymptotically an equilibrium value at which the parcel oscillates between top and bottom of the unstable layer (i.e., continuous convectional overturning). The latter case is interesting because it seems to confirm the potentialities of empirical parcel-theory applications to atmospheric convection phenomena. Thus, Priestley [50] found a relation between the observed cumulus top-height oscillations and the environment lapse rate which agreed in a general way with the theory. Radar and

photographic studies of cloud growth show that each cell builds up with a periodic pulsating motion.

5.8. Note on Errors Caused by Use of the Observed-Temperature (T) **Curve for the Virtual-Temperature** (T_v) **Curve in Stability Determinations.** The use of the T curve in lieu of the T_v curve for stability determinations (see par. 5.4) causes a certain amount of misrepresentation of the stability. The discrepancy will be greatest where a layer of high moisture content is adjacent to a dry one. Use of the T curve will affect stability determinations as follows:

a. If T_d (moisture content) *decreases* rapidly with height, using the T curve will indicate too much stability.[15]

_____

[15] The moisture condition described here frequently occurs at the top of a stratus deck located just below a temperature inversion.
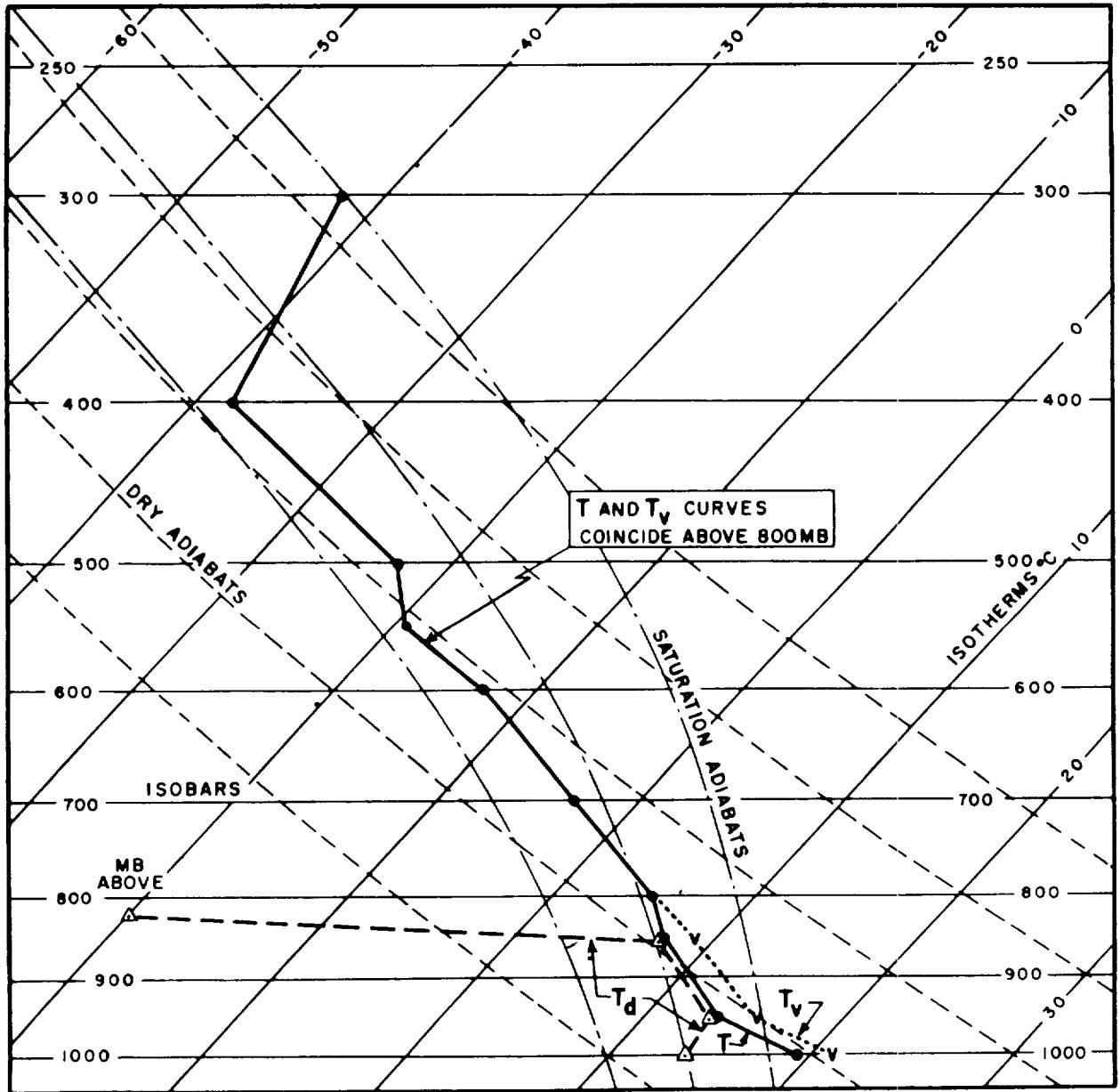
Figure 24. Sample Sounding for Stability Analysis.

b. If T_d *increases* rapidly with height, the T curve will indicate too much instability. This frequently occurs at the base of a warm front.

The example of a sounding on which the difference between the use of the T and T_v curves would introduce an appreciable error into the stability analysis of a layer is shown from 850 to 800 mb in Figure 24. Through this layer, the lapse rate of the T curve is more stable than the T_v curve indicates.

If T_v curves should actually be computed, and should it be desired to use them in moisture-stability analysis, then the sounding

5—8

T_v curve should be compared with *virtual saturation adiabats* rather than with the ordinary saturation adiabats. The virtual saturation adiabats are not available, but they would have a steeper (more unstable) lapse rate than the ordinary saturation adiabats. As an approximation, one can assume [49] that the virtual saturation adiabats starting at a condensation level computed using the T_v of the parcel will asymptotically approach at about -20°C the ordinary saturation adiabat for the same parcel but started at its condensation level computed using ordinary T and T_d .

The weight of the suspended water in a saturated parcel reduces the virtual temperature somewhat; in the hypothetical pseudo-adiabatic process this effect is eliminated by definition, but in the full adiabatic process, as might be approached in a real cloud, it might be important. We can define a *cloud virtual temperature* as the temperature at which dry air would have the same density as the cloud air (i.e., weight of moist cloud air plus water or ice particles). This cloud virtual temperature for an adiabatic parcel rise of over 100 mb can be approximately 1 °C to 2°C colder than the temperature indicated by a similar rise under the pseudo-adiabatic assumption (as on the Skew-T Chart) [54] .

5.9. An Example of Stability Determinations (for Small Parcel Displacements) on a Skew-T Chart.

The plotted sounding shown in Figure 24 might represent conditions above a station some distance behind a cold front. The frontal zone is indicated by the stable layer just below 500 mb. The drying out above 850 mb is a result of subsidence in the cold air as it moves south. The T_v curve is shown as the dashed line from 1000 to 800 mb. Above 800 mb, it parallels the T curve. The stability of the sounding according to the principles of paragraph 5.5., is analyzed as follows:

a. *1000 to 950 mb*. The slopes (see Footnote 13) of the T and T_v curves are both

greater than the slope of the dry adiabat. Therefore, this layer is absolutely unstable (in fact, superadiabatic); i.e., it is unstable regardless of its moisture content (actually, the T and T_d curves show the layer to be unsaturated).

b. *950 to 850 mb*. The slopes of the T and T_v curves are both less than the slope of the dry adiabats, but greater than that of the saturation adiabats. Therefore, this layer is in a conditional state. Since the T and T_d curves practically coincide, the layer is saturated. The slopes of both the T and T_v curves when compared with that of the saturation adiabats, show the layer to be unstable as long as it remains saturated.

c. *850 to 800 mb*. The slope of the T_v curve is greater than that of the saturation adiabats, and slightly less than that of the dry adiabats, indicating that this layer is also conditional. (The T and T_d curves indicate that the layer is definitely unsaturated.) A comparison of the T_v curve and the dry adiabats show the layer to be stable. The T curve indicates greater stability than the T_v curve.

d. *800 to 600 mb*. The layer is unsaturated, and the slope of the T curve is less than that of the dry adiabats; hence, the layer is stable.

e. *600 to 550 mb*. Through this unsaturated layer, the T curve is parallel to the dry adiabats; hence, the layer is in equilibrium for small upward and downward displacements of parcels within it. (The effect of large upward displacements that would saturate the parcel or bring it into the layer above 550 mb have to be considered by the procedures of par. 5.23.)

f. *550 to 500 mb*. The slope of the T curve is less than those of the dry or saturation adiabats. Hence, the layer is absolutely stable.

g. *500 to 400 mb.* This layer is in equilibrium since the T curve parallels the dry adiabats and the air is unsaturated. The remarks on the 600- to 550-mb layer apply here also.

h. *400 to 300 mb.* The air is absolutely stable above 400 mb.

5.10. Processes Which Change the Lapse Rate.

It is not feasible to obtain an optimum, routinely-applied stability analysis of radiosonde ascents unless the processes that tend continually to change the lapse rate are well understood. Since their effects will be referred to throughout the rest of this manual, a general discussion of them is introduced at this point.

It is desirable for proper understanding to distinguish the four basic kinds of *physical* processes that can change the lapse rate at a point or in a given local vertical:

a. Non-adiabatic heating and cooling (due to radiation, conduction, evaporation, and condensation).

b. Solid (or non-shearing) advection of an air column with a lapse rate different from that already over the station.

c. "Differential (or shearing) advection" of temperature due to vertical wind-shear.

d. Vertical motion (orographic, convergence, divergence, and penetrative convection).

The combined effect of these processes may be visualized in the form of an equation, each term of which may be positive or negative:

The Local Change of the Lapse Rate with Time
= a (The Local Change with Height of the Additions or Subtractions of Heat per Unit Time)
+ b (The Advection of the Lapse Rate)
+ c (The Differential Advection of Temperature Due to Vertical Wind-Shear)
+ d (The Local Change of Temperature Due to Vertical Motion).

Figure 25 illustrates the effects of these four terms schematically. In addition, Attachment 2 contains a mathematical discussion of the above equation, which is not found in textbooks. In the following paragraphs, some comments are made on the synoptic importance of these processes, and on how they can be evaluated in practice. In actual synoptic situations, several of these processes are usually operating simultaneously at the same location, and it may be difficult or impossible to evaluate their effects separately. Empirical and subjective judging of the combined effects is often practiced.

5.11.0. Non-Adiabatic Heating and Cooling Effects.

These are generally important only at the ground surface and within some clouds. The formation of low-level stability (or inversions) by nocturnal radiation, and of low-level instability by isolation, are discussed in paragraphs 5.11.1 and 5.11.2. Radiation in the free air and at cloud tops, however, is slow and its effect on the lapse rate is generally negligible for short-term forecasting. The release of the latent heat of condensation (and fusion) has important local effects readily observable whenever condensation takes place at sufficiently high temperature so that the resulting buoyant energy leads to deep convection. The latent heat is also an important source of kinetic energy in the stratiform-cloud shields formed by upward vertical motion organized on a large scale; but here the effect of the release of the latent heat on the lapse rate occurs evenly over thick layers and wide areas and is masked by the effects of the vertical motion on the temperature, so that it is not easily identifiable in the soundings. Evaporational-cooling and melting effects have a trivial direct effect on lapse rates except locally in heavy precipitation (see [64]

5.11.1. Instability from Surface Heating.

The ground absorbs solar radiation causing the surface temperature to rise. This heats the surface air parcels by conduction. These heated parcels tend to organize into large "bubbles" that ascend by virtue of their buoyancy relative to the surrounding unheated or

$$\left[\begin{matrix} \text{LOCAL CHANGE OF LAPSE} \\ \text{RATE WITH TIME} \end{matrix} \right] =$$

(a)

(a)

$$= \left[\begin{matrix} \text{LOCAL CHANGE WITH HEIGHT} \\ \text{OF ADDITION OR SUBTRACTION OF} \\ \text{HEAT PER UNIT TIME} \end{matrix} \right]$$

(b)

(b)

$$+ \left[\begin{matrix} \text{THE ADVECTION OF THE} \\ \text{LAPSE RATE} \end{matrix} \right]$$

(c)

(c)

$$+ \left[\begin{matrix} \text{THE DIFFERENTIAL ADVECTION} \\ \text{OF TEMPERATURE BY THE} \\ \text{VERTICAL WIND SHEAR} \end{matrix} \right]$$

(d)

(d)

$$+ \left[\begin{matrix} \text{THE LOCAL CHANGE} \\ \text{OF TEMPERATURE BY} \\ \text{VERTICAL MOTION} \end{matrix} \right]$$
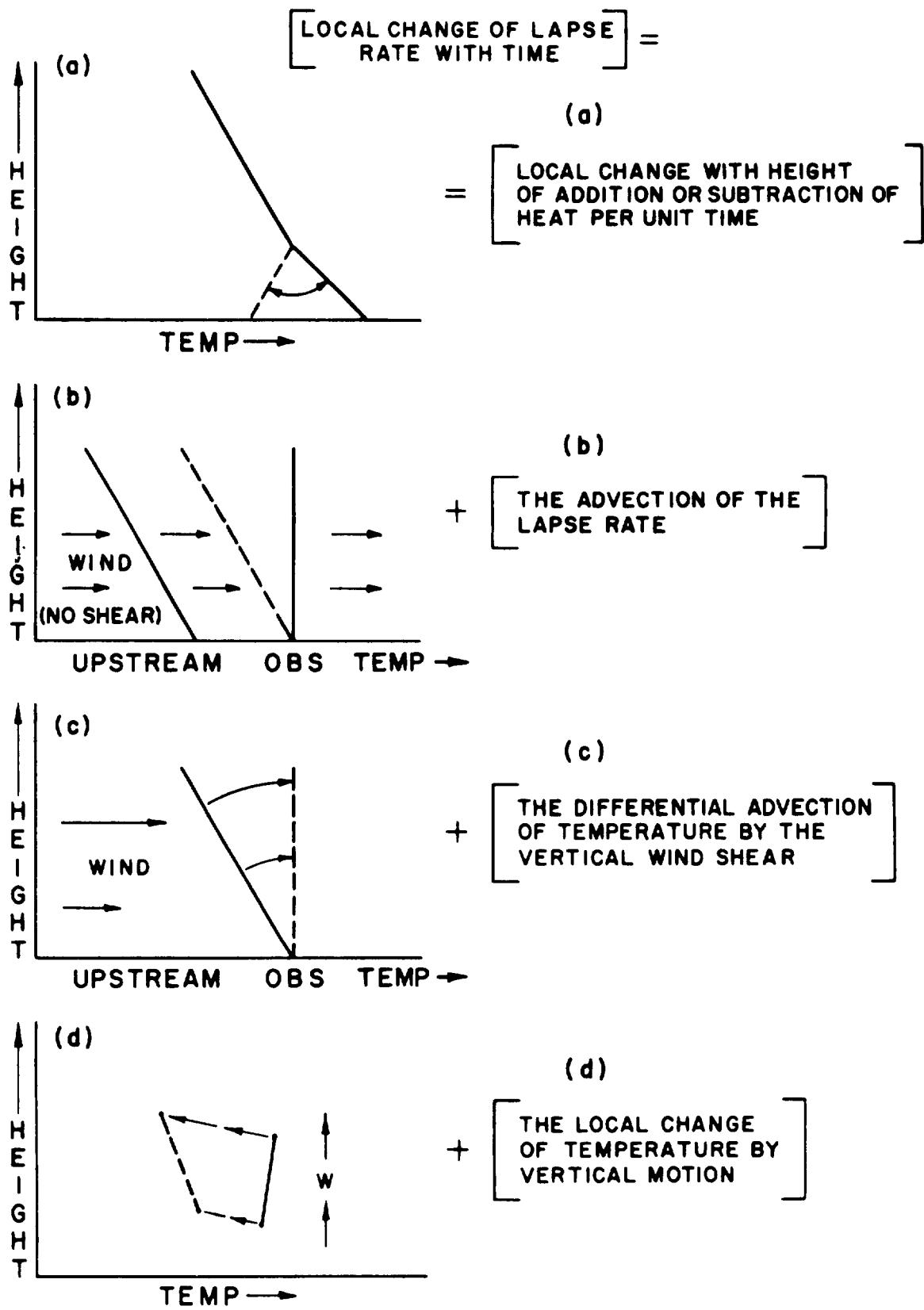
Figure 25. Schematic Illustration of the Four Effects Which Affect the Local Change of the Lapse Rate with Time.

5–11
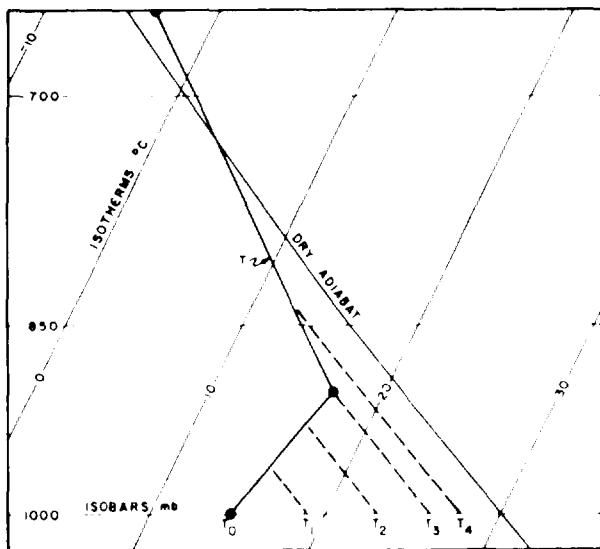
Figure 26. The Successive Changes of the Temperature Lapse Rate Due to Solar Heating of the Ground with Time (t).

less-heated parcels. If the lapse rate is already adiabatic (or superadiabatic), the "bubbles" rise rapidly until a stable region is reached which resists further rise. If the initial lapse rate is stable, then the rise of the surface-heated parcels is resisted from the start. Once some of the "bubbles" of heated parcels at the base of the stable region acquire sufficient buoyancy from a small excess of temperature over their neighboring parcels, or as soon as some of them are impelled upward by mechanical turbulence, their momentum causes them to penetrate some distance into the overlying stable region.

Through such penetrative convection (really a form of vertical motion whose effects on lapse rate will be discussed more generally in par 5.16), heated "bubbles" of air can successively rise and mix at higher and higher altitudes in the stable layers above, thereby slowly extending the dry-adiabatic lapse rate to greater altitudes and allowing the surface temperatures to rise, as shown in Figure 26.

Thus surface heating creates instability indirectly through the intermediate mechanism of vertical motion. However, the amount of heat absorbed and conducted to the air by the ground sets an upper limit for the magnitude

of the penetrative-convection effect on the lapse rate. For this reason, when Sir Napier Shaw popularized the tephigram he attempted to induce forecasters to compute on the diagram the heat-energy input in ergs required to make stable surface layers unstable and clouds to form, etc. The energy in ergs expected from the surface heating could then be compared with the energy in ergs required for penetrative convection to a given depth, i.e., could be compared with the ergs equivalent of a negative energy area on the diagram. (Note: The energy equivalent in ergs for a unit area on a given thermodynamic diagram can be readily determined—see par. 4.25 for such evaluations on the DOD Skew-T Chart.) This approach has been found feasible and has been used successfully to some extent for maximum-temperature forecasting (USWB Forecasting Guide No.4). However, usually there are practical difficulties in obtaining the proper data on radiation properties of the ground (albedo, conductivity, wetness, etc.), which affect the proportion of the insolation that goes into heating the air.

Another way of judging the heat transferred from ground to air, one which obviates computations in energy units, has come into more general use by forecasters. This is based on the assumption that the rise of surface air temperature is a measure of the amount of energy taken up by the air from the ground. From Figure 26, it will be seen how the stable lapse rate or the so-called negative-energy area is wiped out or reduced by surface heating as the surface temperature rises. The amount of the negative area removed is proportional to the surface temperature rise. However, the *rate* of increase of the surface temperature depends also on the shape of the negative area and on the structure of the initial lapse rate. This use of the surface temperature also has the advantage that the progress of the heating effect can be followed continuously, whereas soundings are available only one to four times a day.

The case of air moving over warmer ground may be considered analogous to that of local surface heating, except that the upstream

distribution of the ground-surface temperature then becomes the main factor in determining the amount of the change in surface air temperature. This is often called an "advection effect" in synoptic parlance, but from the physical point of view it is mainly a non-adiabatic heating effect.

5.11.2. Stability from Surface Cooling (and the Effect of Wind Stirring).

The lapse rate that characteristically results from pure nocturnal-radiation effects in a calm air mass, is a shallow inversion based at the ground. The depth of the inversion layer increases as the duration of the cooling, and the steepness of the inversion (degree of negative lapse rate) increases as the degree of cooling. However, over a snow cover, long cooling (as during the Polar night) also tends to develop an isothermal layer above the inversion [63]. The effects of cooling of the ground (by radiation, or by passage of air over colder ground) on the lapse rate of the lower atmosphere are complicated by wind. Wind, by turbulent mixing of the air cooled at the ground with warmer air above, tends to establish a surface layer with an adiabatic lapse rate and a turbulence inversion above it, as described in Chapter 6. (Note: In this particular case, the wind does not change the overall stability, but merely shifts the inversion base to a higher level.) All sorts of intermediate conditions and combinations between the ground inversion and the turbulence inversion can occur, depending on the relative degrees of wind and cooling. The movement of air over cooler ground, of course, implies wind, and usually results in a turbulence layer and inversion. Further complications arise when saturation results from the surface cooling, leading to fog or stratus (see chapter 8 and *AWS-TR-239*). However, unlike the case of condensation in cumulus clouds, the latent heat released in fog or stratus is usually too small to increase greatly the depth of mixing. On the other hand, the formation of fog or stratus greatly reduces or stops the further radiational cooling of the ground, though there is some radiational cooling at the top of the fog or stratus which tends to promote instability (or lessen stability) below the top.

The use of the parcel-method analysis to estimate quantitatively the stabilization effect of surface cooling is greatly limited in practice by the deficiencies in the available means of estimating the radiation flux and the wind mixing, though these factors can often be successfully accounted by indirect empirical methods.

5.12. Advection Effects.

Advection, both at the surface and aloft, has a strong influence on the lapse rate through a given region of the atmosphere. Before a forecast is made from a sounding, consideration should therefore be given to the lapse-rate changes which will result from the effects of advection during the forecast period.

The advection effects, as indicated in paragraph 5.10, may be visualized as two processes: a) the advection of air of a different lapse rate, and b) "differential advection" of temperature due to vertical wind shear. (Do not confuse these with the effect of "advection" of horizontally homogeneous air over warmer or colder ground, which is mostly a non-adiabatic heating or cooling effect; see pars. 5.11.1 and 5.11.2.)

The first effect is the easier to visualize. An air mass with a different lapse rate may move into the area of interest and the typical weather associated with the imported lapse rate also accompanies the air mass, often with little modification. This can happen even without vertical shear, as shown schematically in Figure 25b.

The second effect is less obvious and also more difficult to evaluate on synoptic charts. This effect is often present even when the lapse rate is uniform horizontally throughout the air mass (see Figure 25c). It is due to ageostrophic winds. For this reason it is useless to use the geostrophic wind in attempting to estimate the shearing advection effect, since in a regime of geostrophic winds (at all heights) all shears are parallel to the isotherms and the shearing motion does not change the lapse rate. It is the vertical shear of the ageostrophic-wind components that accomplishes advectional change of the lapse
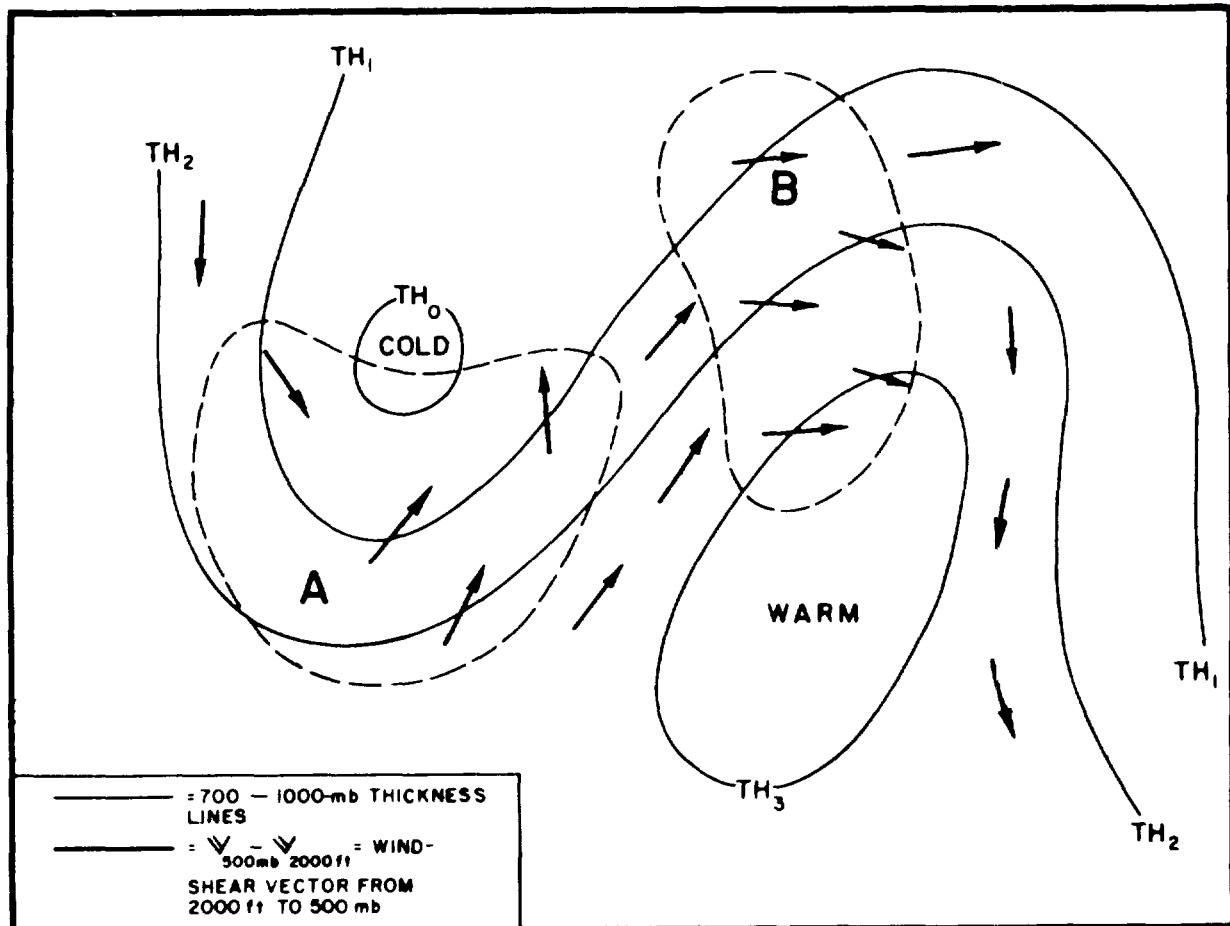
Figure 27. The Effect of Shearing Motion on the Lapse Rate. Stabilization of the lapse rate occurs where the shear vector crosses the thickness lines towards lower thickness: $\left(\frac{\partial V}{\partial Z} \cdot \nabla T < 0 \right)$, as in Area A; destabilization occurs where the shear vector crosses thickness lines towards higher thickness: $\left(\frac{\partial V}{\partial Z} \cdot \nabla T > 0 \right)$, as in Area B.

rate, and this shear must have a component normal to the isotherms to give any change of the lapse rate. So in practice, we should estimate the temperature advections at the two levels concerned by using actual winds and not the geostrophic winds. The rule is simply: *Where more rapid cooling is indicated at the upper than at the lower level, stability is decreasing, and vice versa.*

There are regions on some upper-air charts where the ageostrophic-wind components are so strong that the influence of the "differential advection" can be assessed directly by

inspection. But most of the time, the actual flow cannot be clearly distinguished from the geostrophic wind, and then the lapse-rate change due to shear cannot be reasonably judged.

One way of judging the shear effect would be to plot the actual wind-shear vector of the layer from 2000 feet above the surface to 500 mb on a chart which contains the 1000- to 500-mb thickness analysis; wherever the shear vectors are directed towards warmer regions, a decrease of stability should be taking place, and vice versa. If the winds were

geostrophic at all levels in the layer the shear vectors would blow along the thickness lines and no stability change would be taking place. Unfortunately, no experience with this approach is- available. The principle is illustrated in Figure 27.

In actual practice, many forecasters estimate the total advective change of stability on a given sounding by estimating the temperature advection at several levels in the troposphere using the actual winds and isotherms. This procedure takes into account the combined lapse-rate advection and shear effects, if both are present.

5.13. Preliminary Remarks on the Effects of Vertical Motion.

The vertical motions which affect the lapse rate may be of any scale or type, from small-scale turbulence to the large-scale mean vertical-motion field associated with macro-synoptic features. As different principles apply to the vertical motion of different scales or types, it is customary to consider the vertical motions of different scales as somewhat distinct phenomena. Accordingly, we will discuss separately in the next few paragraphs: Ascent and subsidence of whole layers, horizontal divergence and convergence on the meso- and macroscale, and penetrative convection. The lifting effects of mountains and fronts involve combinations of these phenomena.

The lapse-rate changes of a layer during ascent or descent are solely a linear function of the change in thickness of the layer resulting from such vertical motion (see Figure 28). For a simple approach to assessing the effects of vertical motion on a layer, it is customary in textbooks to assume no horizontal divergence and, of course, the conservation of mass. However, the assumption of no divergence over any considerable depth and extent is realized in the atmosphere only where there is neither development nor change in the pressure field. Therefore, the attempt to assess the effects of ascent or subsidence under that assumption is so artificial as to greatly limit its practical application. Divergence and

large-scale vertical motion are so intimately associated in the atmosphere that a general discussion of their combined effects on the lapse rate will be given in paragraphs 5.14.0 through 5.14.6. In that discussion the no-divergence case is included as a special case.

5.14.0. Effects of Convergence and Divergence.

The divergence (convergence) is, of course, not necessarily zero in the atmosphere, for in developing pressure systems there must be a more or less marked field of divergence. What are the complications that the divergence introduces in assessing the effects of vertical motion on the lapse rate? The answer is unfortunately not simple, because it depends on the relative magnitudes of the divergence and the rate of ascent or descent.

Let us consider a thin layer defined by a pressure interval, Δp, and the area, A, of its projection on the horizontal plane. Then, for any transformation of the layer under the conservation of mass, the product of Δp and A does not change: $\Delta p_1 A_1 = \Delta p_2 A_2$, where subscript 1 refers to the initial state and subscript 2 to the final state. (This is the equation of continuity.)

By the hydrostatic equation, $\Delta p = -\rho g h$, where ρ is density, g is gravity, and h is the thickness of a layer (in feet or meters). Substituting for Δp and dropping g (which is essentially a constant for our purposes), we may write the equation in ratio form as:

$$\left(\frac{\rho_1}{\rho_2}\right)\left(\frac{h_1}{h_2}\right) = \frac{A_2}{A_1}$$

When convergence (negative divergence) occurs, A_2/A_1 is < 1, and when divergence

5—15
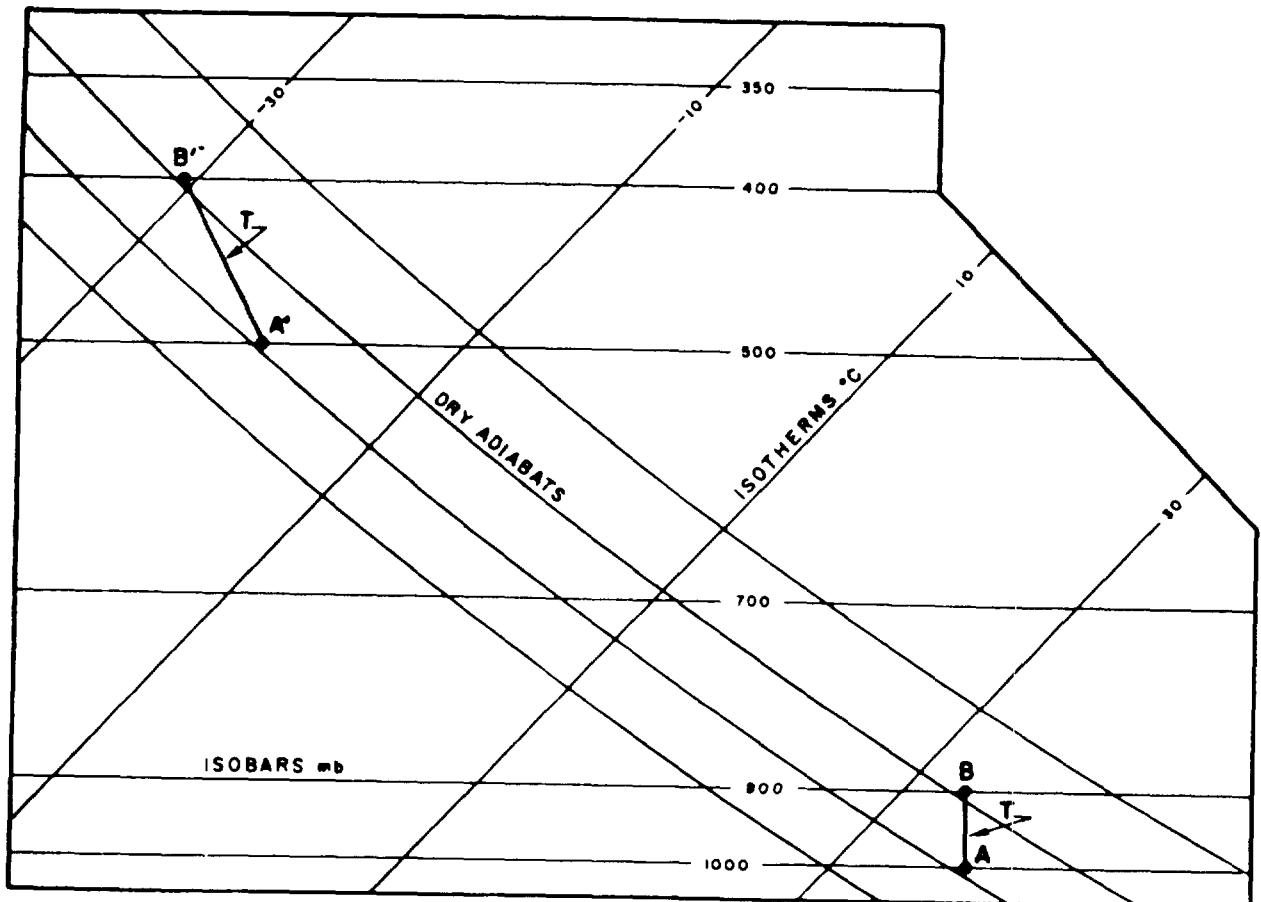
Figure 28. Lapse-Rate Changes Caused by Lifting or Subsidence of a Dry Layer.

occurs it is >1.[16] There are innumerable combinations of the three parameters, ρ, h, and A, that satisfy the above relationship. Before proceeding to the most general case, it is of interest to discuss several "special" cases where one of these parameters remains constant.

5.14.1. Cases Without Vertical Shrinking or Stretching. For example, assume that $h_2 = h_1$ (no vertical stretching or shrinking occurs) and that there is convergence to

the extent that $A_2/A_1 = 0.9$. Then, $\rho_1/\rho_2 = 0.9$ also. Since ρ increases from the initial to the final state, there is descending motion to obtain the density increase. Similarly, if $A_2/A_1 = 1.1$, the area increases from the initial to final state; i.e., divergence exists, ρ decreases and there is ascending motion. Thus, convergence or divergence can be associated with vertical motion without resulting in any change of lapse rate provided only the thickness of the layer remains constant.

---

[16] Physically, divergence has time as one of its dimensions so the actual amount of divergence depends on how long it continues. In the simple demonstration here we are concerned only with its sign.

5—16

5.14.2 Cases With Convergence but Without Vertical Motion. Alternatively, let us assume that $\rho_1 = \rho_2$; i.e., there is no vertical motion, but $A_2/A_1 = 0.9$; i.e., there is convergence. Then $h_1/h_2 = 0.9$ and the thickness increases, since the final state, h_2, must be larger. Also, the lapse rate is changed in the same sense as in the case of ascent without divergence (see par. 5.14.4); that is, the lapse rate tends to approach the dry (or saturation) adiabats.

5.14.3. Cases With Divergence but Without Vertical Motion. If $\rho_1 = \rho_2$; i.e., there is no vertical motion, but $A_2/A_1 = 1.1$; i.e., divergence is occurring, then $h_1/h_2 = 1.1$ also, which means a thickness decrease. Hence, the lapse rate changes in the same sense as for descent without divergence (see par. 5.14.4), that is, the lapse rate tends to depart further from adiabatic.

5.14.4. The No-Divergence (No-Convergence) Case. If there is no divergence or convergence, ρ and h vary according to:

$$\left(\frac{\rho_1}{\rho_2}\right)\left(\frac{h_1}{h_2}\right) = \frac{A_2}{A_1} = 1 \; ; \; \text{or} \; \frac{\rho_1}{\rho_2} = \frac{h_2}{h_1}$$

That is, without convergence or divergence (meaning A does not change), the density and thickness of a layer vary inversely with one another.

If the layer ascends $\rho_2 < \rho_1$, since the density decreases with height in the atmos-

phere; then from the last equation it follows that $h_2 > h_1$; i.e., the layer stretches vertically. For an entirely dry-adiabatic (or entirely saturation-adiabatic) process, the lapse rate will, as a result of vertical stretching, tend to approach the dry (or saturation) adiabatic (respectively).[17] On the other hand, if, again without divergence, the layer descends, $\rho_2 > \rho_1$, and $h_2 < h_1$; i.e., the layer shrinks vertically. In this case, the lapse rate tends to depart further from the adiabatic.[17]

5.14.5. In the Lower Atmosphere. Thus, the effects on the lapse rate of ascent and descent without divergence are the same as those of convergence and divergence without vertical motion. This fact has a practical significance in the *lower* atmosphere, where, because of the constraining boundary at the earth's surface, divergence must always accompany descent and convergence must always accompany ascent. Therefore, in this region it is customary to regard the effects on the lapse rate of divergence-combined-with-descent (or of convergence-combined-with-ascent) to be of the same kind, additive, and for practical purposes, inseparable.

5.14.6. In the Upper Levels. This is not so for the middle and higher levels where the continuity equation can be satisfied by any of the possible categories of combinations of ρ, h, and A, shown in Table 1. This table includes as categories 7-12 the special arbitrary cases, four of which (categories 9-12) were discussed in paragraphs 5.14.1 through 5.14.4, where one of the parameters is held constant: $\rho_1 = \rho_2$, $h_1 = h_2$, or $A_1 = A_2$.

---

[17] These effects of ascent and descent on the lapse rate for the no-divergence or no-convergence assumption are the "rules" often stated in textbooks. Though their limitations are often overlooked, these "rules" are widely used by forecasters. They are generally valid only for qualitative use and for the lower troposphere -- up to 700 mb and sometimes to 500 mb. Nor are they safely applicable to very thick layers or for very large displacements, in view of the fact that vertical motion and divergence usually vary markedly with height and time.

Categories 2 through 5, however, do not occur in the lower atmosphere, where the ground forms a fixed boundary surface.

It is obvious that in the upper levels there is no *a priori* basis for assessing which of the

TABLE 1

Category Number	Divergence	Vertical Motion	Thickness	Change In Lapse Rate (If Initially Stable)
1.	Divergence	Descent	Shrinks	More Stable
2.	Divergence	Ascent	Shrinks	More Stable
3.	Divergence	Ascent	Stretches	Less Stable
4.	Convergence	Descent	Shrinks	More Stable
5.	Convergence	Descent	Stretches	Less Stable
6.	Convergence	Ascent	Stretches	Less Stable
7.	Divergence	None	Shrinks	More Stable
8.	Convergence	None	Stretches	Less Stable
9.	Divergence	Ascent	No Change	No Change
10.	Convergence	Descent	No Change	No Change
11.	None	Ascent	Stretches	Less Stable
12.	None	Descent	Shrinks	More Stable

categories 1, 2, 3, 7, and 9 occurs, assuming one can determine that divergence is present, nor which of the categories 4, 5, 6, 8, and 10 occurs if convergence is present. This is a problem that in practice has to be approached empirically.

5.15. How to Assess the Vertical-Motion Field in Practice. The determination of the distribution, sign, and magnitude of the vertical motion aloft poses some difficulties in routine synoptic practice. The NWP vertical-motion charts (both the synoptic and prognostic) for the layer 850 mb to 500 mb now being transmitted by facsimile from the National Meteorological Center are probably the best answer for the region they cover and the detachments that receive them. (These charts should improve in accuracy and coverage over the next several years.)

There are also several other less satisfactory techniques. One of these is by inspection of the vorticity advection on vorticity charts, such as transmitted on facsimile for the 500-

mb surface over the United States. The principles to be followed in this are well discussed by Cressman [20] ; note that the inference of the vertical motion requires that care be taken to consider the local-change term in the vorticity equation when the vorticity gradients are large. Examples of the inference of vertical motion from vorticity advection at 300 mb are shown in Section 4.2 of *AWS TR 105-130*.

If vorticity charts are not available, it is possible to judge the approximate vorticity advection by inspection of the contour and isotach charts (see *AWS-TR-229*). But here, there is difficulty in inferring the sign of the vertical motion except near the ground.

Without vertical-motion or vorticity charts it is necessary, therefore, to use empirical models such as those of Figures 29 and 30, as well as the well-known Bjerknes-Holmboe model [15] for the relation of the vertical-wind profile to the convergence-divergence pattern (that determines how troughs and ridges move), and the Endlich jet-stream
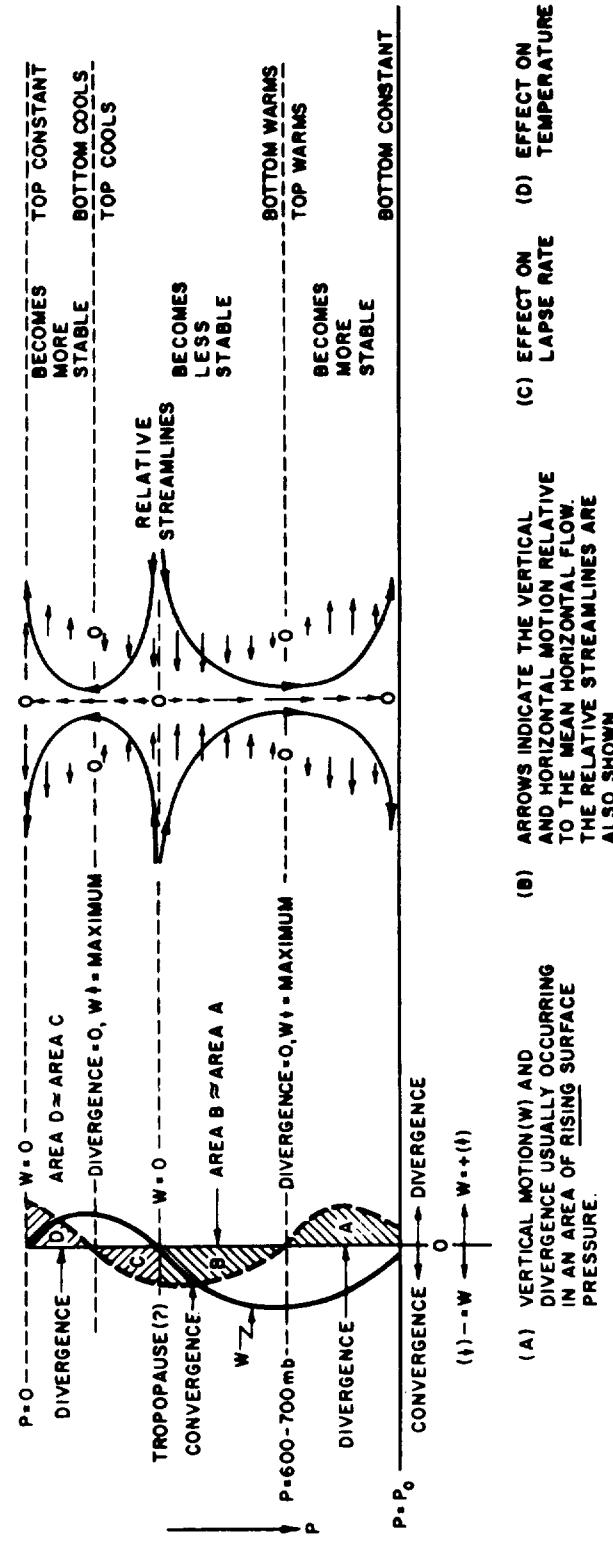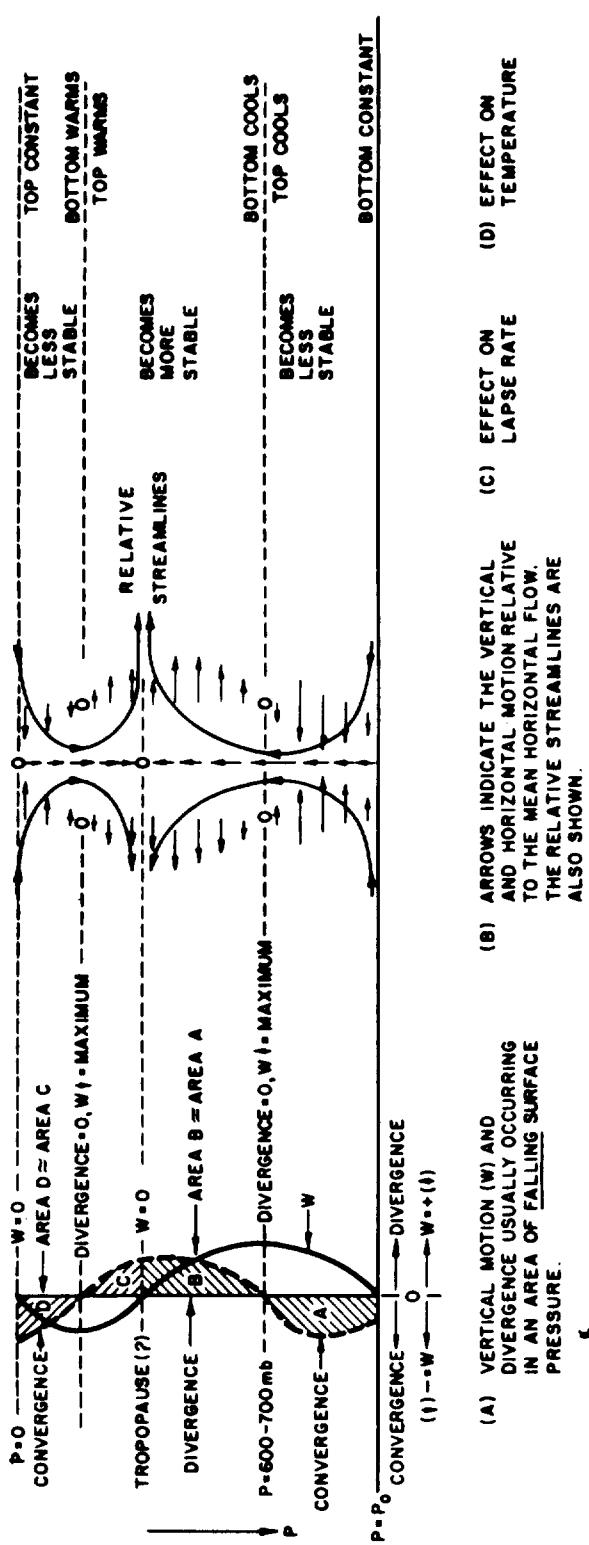
Figure 29. Effect of Divergence and Vertical Motion Upon the Lapse Rate Above an Area of *Falling* Surface Pressure.

Figure 30. Effect of Divergence and Vertical Motion Upon the Lapse Rate Above an Area of *Rising* Surface Pressure.

model [24] . The associated surface-re-ported weather distribution is also often indicative of whether the motion is generally upward or downward.

Figure 29 illustrates the typical distribution of vertical motion, divergence, and lapse-rate change in an area of falling surface pressure, and Figure 30, in an area of rising surface pressure. We see that in the typical case the rise or fall of surface pressure is due to a small net difference in several large-magnitude convergence and divergence regions in the vertical column above the ground. Even in areas without marked surface-pressure tendency, there may be layers aloft with divergence and convergence, but if so, the magnitudes are usually small and they fully compensate one another. Observe in Figures 29 and 30 these rules: *Where the upward motion increases (or downward motion decreases) with height, the lapse rate (if initially stable) tends to become less stable; and where upward motion decreases (or downward motion increases) with height, the lapse rate tends to become more stable.*

Finally, there are the so-called "objective" measures of the divergence and vertical motion computed from a triangle of rawin soundings [11] [22] [28]. These are too sensitive to errors in the rawin equipment to be very accurate, and the usual station spacing is so coarse that the divergence areas of small lateral extent are smoothed out or missed as much as they are on vertical-motion or vorticity charts.

5.16. Penetrative Convection. This is a form of vertical motion in the atmosphere consisting of either random or organized local vertical currents having cross-sections of the order of a few feet to a few miles.* Most of these vertical motions, especially in the lower atmosphere, are due to *thermal convection* initially created by the effect of heating or cooling (e.g., as described

in par. 5.11.1). (The heating or cooling may be non-adiabatic or adiabatic.) The buoyancy forces (see par. 5.1) acting on the parcels in the unstable column or layer lead not only to neighboring up and down currents within the layer but also to ones which (aided by turbulence from shear or friction) penetrate into adjacent more stable layers (above or below). The effect is called *penetrative convection* and is one of the chief processes which tend to change the lapse rate of stable layers towards a less stable or the unstable state. When condensation takes place in the convection column (usually this is an adiabatic heating) additional buoyant energy is provided by the latent heat released, and the penetrative effect is greatly augmented. Besides surface heating (non-adiabatic), convergence and adiabatic ascent also frequently create instability through penetrative convection, especially at the higher levels.

The speed with which the penetrative convection changes the lapse rate varies greatly according to the duration of the convection, the resistance (stability) of the layers affected, the size spectrum and pattern of convection cells, etc. The rate of change is also modified by mixing between the "thermals" or clouds and their environment, as well as by any compensating subsidence which may be spread over a much larger area of the environment than that affected by the updrafts. Ultimately, whole layers can be rendered completely unstable by widespread continued penetrative convection, as frequently happens from thermal convection in the lowest layers near strongly-heated ground or in layers lifted by a front.

5.17. Stability-Instability Criteria for Large Vertical Displacements. The stability criteria of paragraph 5.5 for small parcel displacements, while generally applicable and widely used, are not indicative of what might happen when layers or parcels are

---

*The term "convection" in synoptic practice usually deals explicitly with only the larger vertical currents associated with cumulus clouds, with "thermals," "bumpiness," "turbulence affecting aircraft," etc.

given larger vertical displacements, such as would cause whole layers to change their type of stability over a broad area, or would cause parcels to cool adiabatically to saturation and to penetrate deeply into layers having different stability (i.e., "stability" according to the criteria of par. 5.5). As a result, a number of procedures have been proposed to apply the parcel theory to this problem of large vertical displacements. However, for some reason, more attention has been given to the effects of large displacements from lifting than to those from heating.

Two different approaches to the lifting problem have been developed and appear in most textbooks. The first one involves the concept of *latent instability*, and aims to predict what happens when a parcel is lifted mechanically (as by a front, mountain, or convergence); the other approach involves the concept of *potential instability*, (or *convective instability*) in which the effect of bodily lifting any layer (or the whole atmosphere!) is considered. It will be shown in the next few paragraphs that these two concepts lead to rather different results — see paragraph 5.22 for a comparison summary.

The practical value of the procedures developed from these approaches now seems to be along different lines than originally envisaged by their authors. Most textbooks still present these methods as their originators did, rather than in the light of present-day practice and experience. Unfortunately, the reasoning behind these procedures was never carefully nor fully explored by the proponents of the procedures. Nor have other theoretical meteorologists felt the parcel approach to the problem sufficiently interesting or promising to give it a more thorough and comprehensive formal development. As a result, these procedures have been developed or modified mostly by empirical "trial and error" in forecasting offices to the point where the rational basis for them has become generally obscure. This makes it difficult to give a logical and systematic presentation of the state of this "art."

5.18.0. Latent Instability. Although the analysis for latent instability has not been widely practiced outside of India and its value is controversial, many publications and meteorology courses have represented it otherwise. A discussion of it here is desirable if only to clear up the confusion and misunderstanding.

Normand [46] suggested that for estimating the effects of lifting parcels of a deep layer *which is in the conditional state*, it should be useful to classify the soundings into types. First, he distinguished soundings in which lifting would cause at least some parcels to become unstable (warmer than the environment) from those soundings in which lifting could not result in any parcels becoming unstable. The first type he called *latent instability*. The second type has no latent instability and he designated it as the *stable type* of the conditional state.

Normand then noted that the cases of latent instability fall into two sub-types, one of which should lead to no more than shallow clouds (if any), and the other to thick clouds, showers, or thunderstorms. The first sub-type he called the *pseudo-latent type* (which other writers have called "pseudo-lability" or "pseudo-instability"), and the second sub-type he called the *real-latent type*.

Using the ideas of Sir Napier Shaw, Normand visualized the effect of lifting on these types of conditional soundings in terms of energy. That is, he compared the latent energy of the water vapor in the parcels to be lifted with the kinetic energy needed to lift the parcels high enough to release their latent energy through condensation and any resulting free convection.

Referring to Figure 31, Part A illustrates a sounding of the stable type, i.e., no latent instability. The curve of the ascent of the lifted parcel (the surface parcel in this example), nowhere crosses the environment curve and the Area N is proportional to the energy that has to be provided to lift the parcel. The parcel consumes kinetic energy
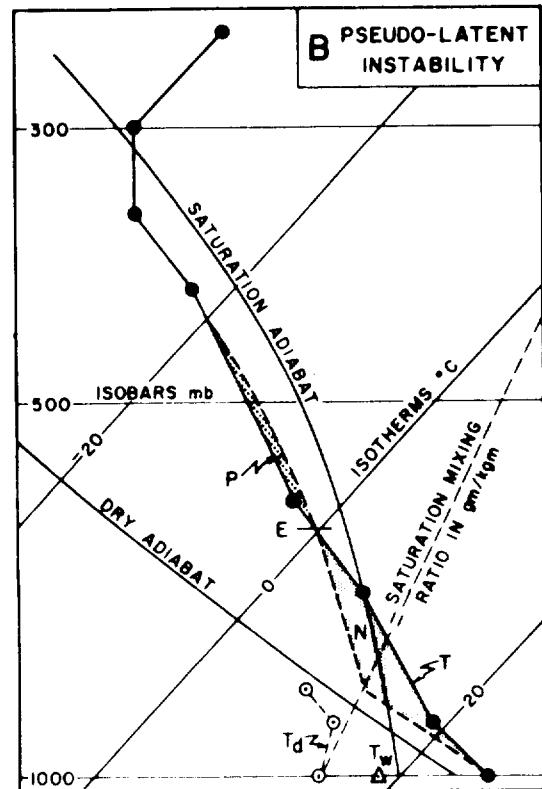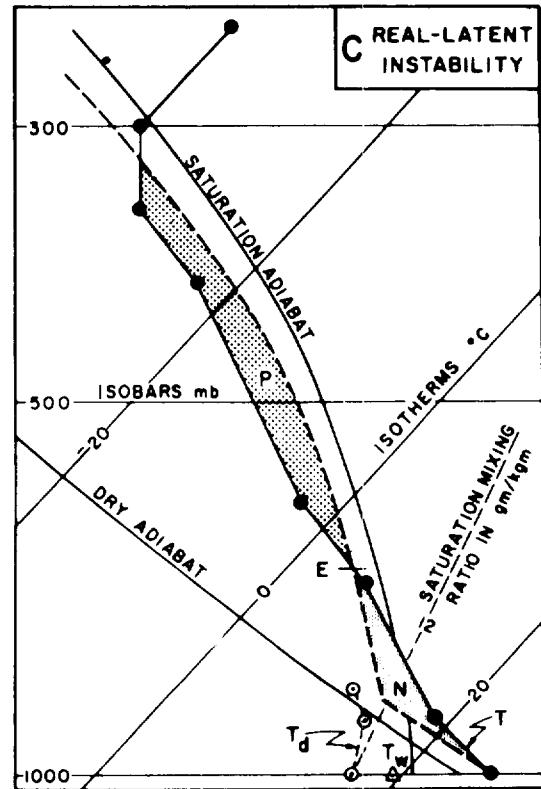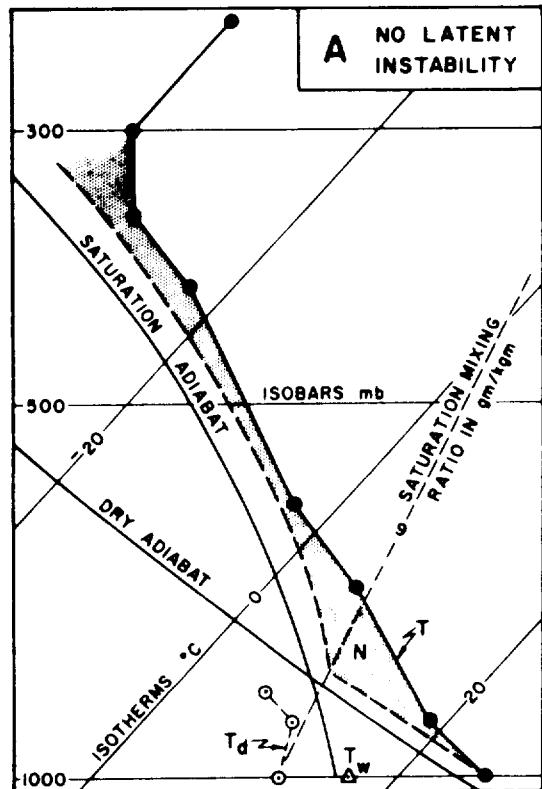
Figure 31. Three Types of Conditional Equilibrium for a Lifting Process. It is assumed that it is the surface parcel that is lifted. Part A shows the stable type with no latent instability; Part B shows a case of pseudo-latent instability; Part C shows a case of real-latent instability. Notice that the temperature lapse-rate curves (T) in all three parts of the figure are the same, and to obtain the types of conditional equilibrium one needs only to vary the moisture content of the lifted surface parcel.

(from the lifting mechanism) all the way up and the Area N is therefore called the *negative energy area* (see par. 4.23). There is no positive energy area in this case. In Part B of Figure 31, above Point E the curve of the temperature of the lifted surface parcel is warmer than the environment and, as explained in paragraph 5.1, the parcel will rise freely from the buoyancy provided by the released latent-heat energy of the water vapor condensed. Outside sources of energy (i.e., the lifting force) were consumed up to Point E, proportional to the negative Area N; above Point E an excess of latent-heat energy is released and the Area P, therefore

called the *positive energy area*, is proportional to its amount. Since the P-area is smaller than the N-area, more energy was used to lift the parcel to Point E than was released for free convection after it reached Point E. Thus, Normand reasoned that this type of sounding would give little or no weather from lifting and therefore should be called "pseudo-latent." Part C of Figure 31 shows a sounding with a much larger positive area than negative area, meaning that much more energy could be released above Point E than was consumed to lift the surface parcel to Point E. This is Normand's "real-latent instability" type.

5.18.1 Validity of Assumption. There are implicit in Normand's ideas certain assumptions which are not valid. The hypothesis that the *relative* size of the positive and the negative areas should be a criterion for the intensity of the convection weather from lifting was purely intuitive as well as a gross oversimplification. Experience has shown that the actual sizes of the negative area and of the positive area are more important for the forecasting of cumulus clouds and showers than is the difference in size between the positive and negative areas [49] . This is because the negative area in every case must first be wiped out before any convection weather can begin, and the negative area may be too large for the available lifting to overcome regardless of the size of the positive area. Also, even a pseudo-latent sounding can sometimes produce very severe weather, such as when both the negative and the positive areas are narrow and deep and there is marked convergence. Strictly speaking, the positive area evaluates only that part of the latent energy which contributes to buoyancy for *free convection*. Normand's criteria fail to account for the additional latent energy released by both the lifting and convergence processes, which often make the difference between weak cumulus development and severe storms. The magnitude of the lifting may also be the critical factor; e.g., even with a small positive area, a sufficiently large lift might cause severe weather. In this connection, note that Normand's criteria imply that the lifting always stops once the CCL or LFC is reached, which is of course arbitrary and unrealistic. Marshall [39] has shown from simple parcel theory how greatly a small amount of lifting could augment the convection in cumulus clouds already existing. In actual clouds, the effect of this energy contribution from lifting is probably often manifested by a greater amount of "overshooting" above the EL than would occur if there were no lifting or convergence, e.g., as in a pure air-mass-heating cumulus.

5.18.2. Procedure for Finding Whether Any Latent Instability is Present. Normand discovered a simple procedure to determine whether a sounding is of the stable type or has some latent instability (of either type). For this procedure it is necessary that the T_w curve for the sounding be plotted on the adiabatic diagram along with the T curve. Figure 32 shows an example.

Step 1. In Figure 32, select the saturation adiabat (γ_s) that is tangent to the T curve, as shown at Point Q.

Step 2. Plot the curve of the wet-bulb temperature (T_w) on the sounding as described in paragraph 4.9. Latently-unstable conditions are indicated for those portions of the sounding where the T_w curve lies to the right of the tangent saturation adiabat (γ_s), and which are below the altitude where γ_s is tangent to the T curve. In Figure 32, latent instability is indicated for the layer below 860 mb.

General use of the above procedure undoubtedly has been discouraged by the fact that now only dew-point temperatures are transmitted in upper-air reports, so that the T_w curve has to be computed by the forecaster. (Note from the T_d curve in Figure 32 that there is no way in which the T_d curve can be used to determine at a glance the layers with latent instability.)
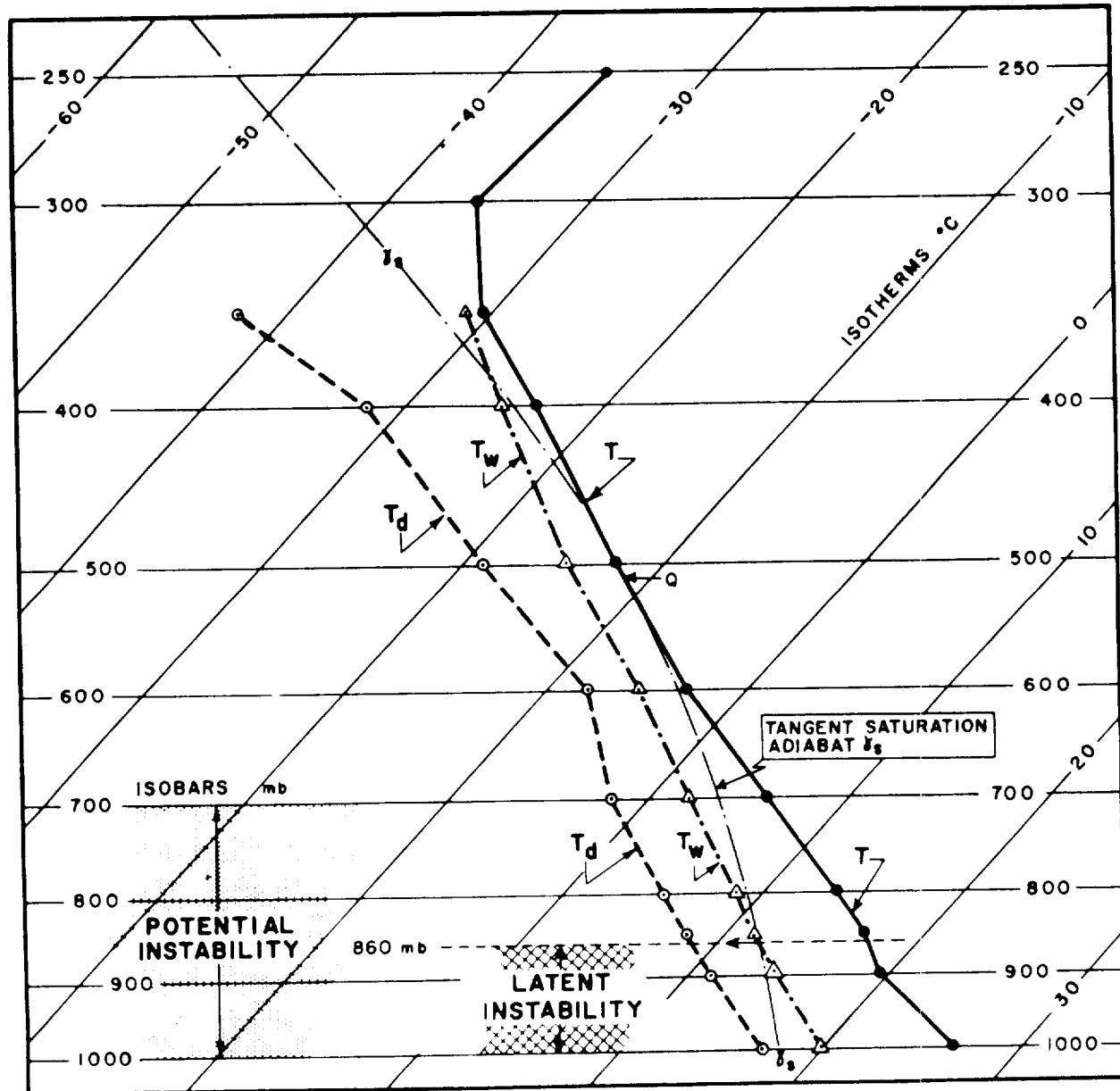
Figure 32. The Determination of the Latent-Instability Layer(s) of a Sounding. The potential-instability layer(s) are also shown for comparison.

5.18.3. The Value of the Distinction Between Pseudo- and Real-Latent Instability.

According to Normand, merely determining which layers have some latent instability does not answer the more important question (to him) as to whether the latent instability is of the pseudo- or real type. The only way to determine this is to analyze on an adi-

abatic diagram the negative and positive areas for lifting of each of those parcels which are shown by the T_w curve to have latent in- stability. The sizes and shapes of the negative and positive areas will often differ consider- ably for different parcels within this layer; without "testing" each parcel in this way one cannot be certain which ones have what type

of latent instability. Obviously the labor of making this evaluation for many parcels and soundings requires much more time than most practicing forecasters can spare for it. Normand and his disciples have not been able to develop any objective procedure to simplify and shorten this procedure — if indeed it is even possible. However, their papers indicate that they consider the surface parcel usually to be sufficiently representative of the whole latently-unstable layer whenever the T_w or T_d curves show that the moisture content decreases regularly but not too rapidly with height in the lowest 100 mb. Furthermore, they generally assume that latent instability is most likely in the surface and lower tropospheric layers, where the moisture content is usually highest. In India, the only region where the criteria for the type of latent instability have been extensively applied, this is probably true; and it also has been the practice there to consider the surface and lower layers as the ones that will always be lifted. In middle latitudes these assumptions seem unnecessarily restrictive, because moisture contents increasing or varying irregularly with height and lifting of upper layers as well as surface layers are frequently observed. Very few reports have appeared on systematic attempts to apply latent-instability-criteria evaluations to the variety of conditions found in middle latitudes. Since the moisture content normally decreases with height, Normand's method of locating the layer(s) with latent instability tends to favor the surface layers and often misses higher layers that have strong potential instability (see par. 5.19.0) releasable with a large but expected lift. It has been suggested that where a temperature sounding plotted on a Skew-T Chart has several pronounced and thick projections of the lapse rate to the left, and/or the moisture curve has several such projections to the right, a separate tangent saturation adiabat should be drawn for each projection or distinctive segment of the temperature curve. In this way, secondary layers of latent instability are revealed which may also be released if there is (as often happens) more convergence in their region than in the lower region of the primary latent instability.

5.18.4. Utility of Latent-Instability Analysis in General.

In the absence of some guidance on how to decide in an economical way which parcel(s) and layer(s) should be tested for latent instability, practicing forecasters have not been inclined to experiment further with the latent-instability concept. In addition, the weaknesses (discussed above in par. 5.18.1) in the assumptions underlying Normand's criteria for latent instability, give reason to doubt that any effort to apply these criteria in practice would be worthwhile.

Nevertheless, the examination of the negative and positive areas for heating *and/or* lifting of the surface or other selected parcel, is a procedure (first advocated by Shaw) which many forecasters find useful in various ways, but entirely without reference to Normand's criteria. Some empirical relations of the energy areas to convective weather have been reported in the literature, but these relations have to be worked out for each local region. "Modifications" of the sounding curve in the lower layers are often made from experience to obtain more representative surface temperature and moisture values for analysis and forecasting of lifting and heating effects (see Chapter 8). These same considerations should be applied to the soundings when analyzing them for latent instability.

Since the value of analyzing for pseudo-versus real-latent instability is questioned, one may ask: Is it still useful to examine soundings with the aid of the T_w curve to determine merely whether latent instability *of any sort* is present? Because the layer(s) with latent instability contain the parcels most liable to cloud formation (not necessarily the unstable or thick clouds) upon uniform lifting of the whole air column, the procedure for identifying these layers might be useful in routine forecasting. (In this connection, mention should be made of a procedure sometimes used in India and British countries for plotting on the diagram the curve of lifting saturation temperature for each significant point of the lower levels of the sounding — variously called an "ST-gram," "estegram," or "Normand curve." This curve shows which levels will have cloud first.) In any case, the
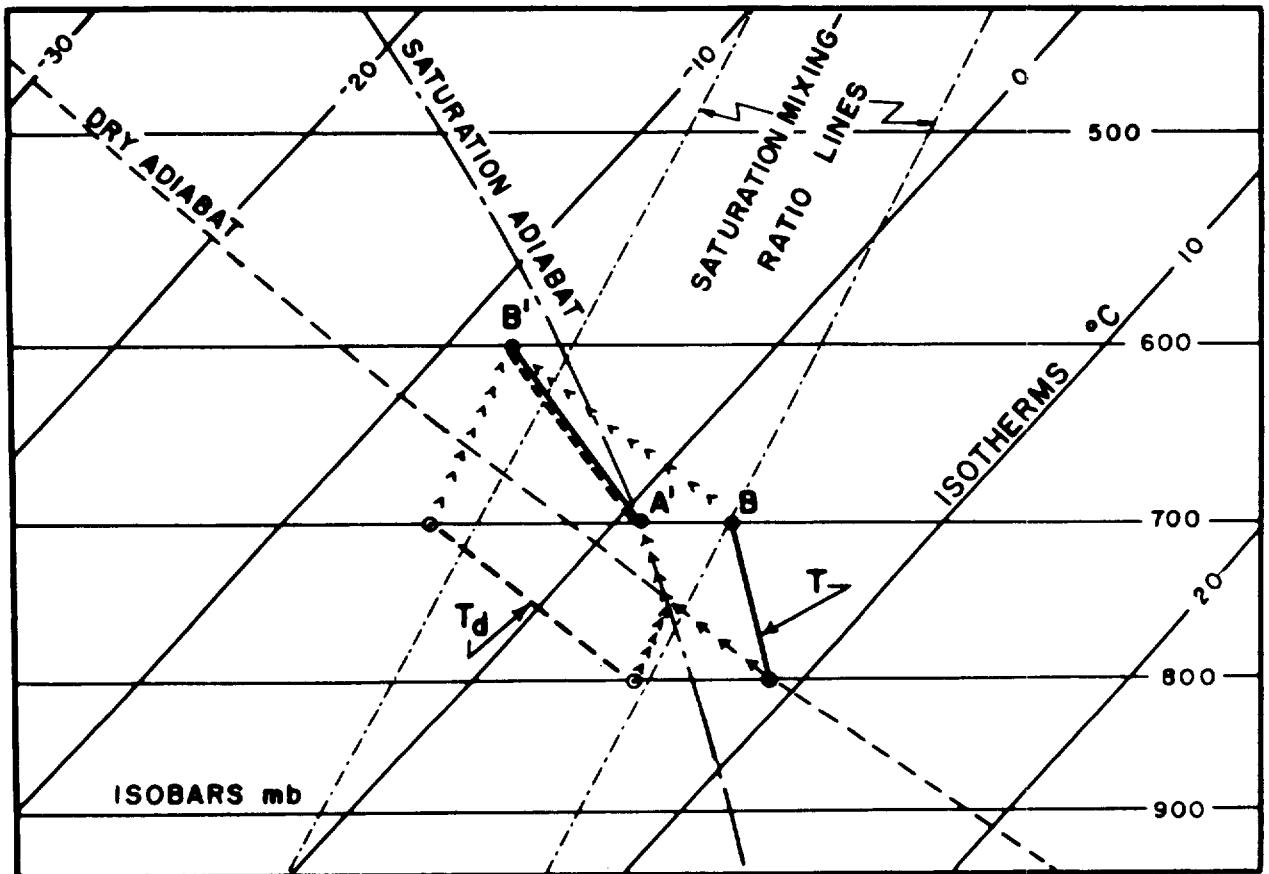
Figure 33. Example of a Stable Layer with Potential Instability.

latent-instability concept should be thought of mainly in this way, rather than as a criterion for "instability" in the usual sense of that term.

5.19. Potential Instability. In the early 1930's, when forecasters were trying to explain as much weather as possible in terms of fronts, Rossby [52] introduced the concept of a criterion for the instability or stability of a layer resulting when it is lifted as a whole, as at a front or mountain. He called the instability released in this way "convective instability," an unfortunate term because it implies that convection does not result from any other type of instability or lifting. Later, Hewson [31] proposed this should be more properly called "potential instability," a more appropriate and less ambiguous term that is gradually coming into

wider use than "convective instability." However, other meteorologists sometimes carelessly use the term "convective instability" to mean absolute instability or even "conditional instability". Hence, some confusion is possible with Rossby's term.

The criteria which Rossby introduced were based on the lapse rate of equivalent potential temperature (see par 4.12). This was a convenient unit in the 1930's when it was customary to plot soundings on a Rossby diagram, which has θ_E as one of its coordinates. As the routine use of Rossby diagrams was never universal (and in time was abandoned entirely) it was pointed out by Petterssen that one could apply Rossby's criteria on any diagram containing the saturation adiabats, which are also lines of constant θ_E (as well as of wet-bulb potential temperature), provided that the
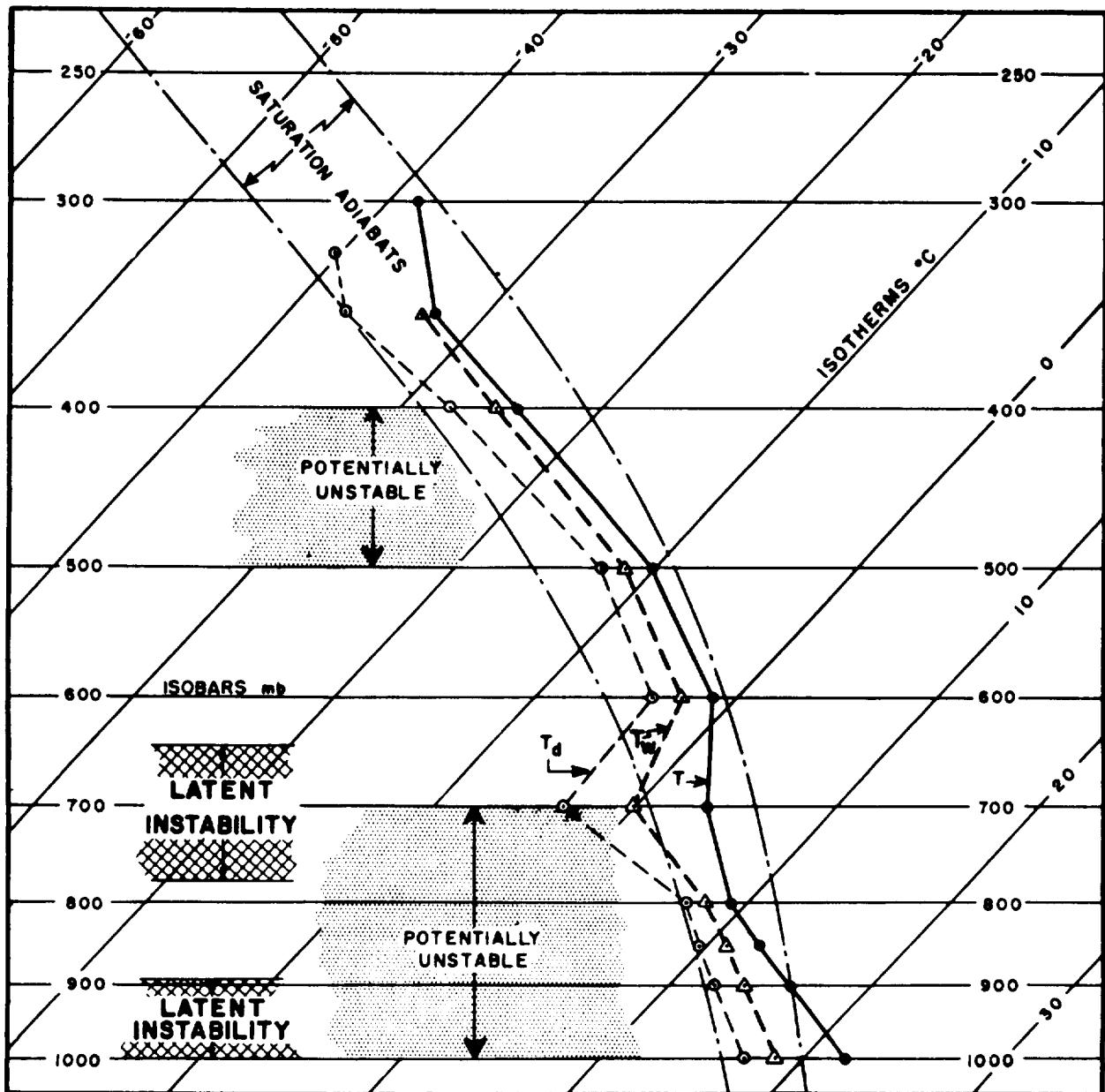
Figure 34. Example of Potentially Unstable Layers, Comparing Use of T_w and T_d Curves for Diagnosis.

T_w curve of the sounding is plotted (see par. 4.9). The Rossby criteria then become:

a. Layers in which the wet-bulb lapse rate is greater than the saturation adiabatic are *potentially unstable.*

b. Layers in which the wet-bulb lapse rate is less than the saturation adiabatic are *potentially stable.* In other words, the slopes of the T_w curve and the saturation adiabats are compared.

Illustrated in Figure 33 is an analysis on a Skew-T Chart to show how a stable layer

5-27

having potential instability, as indicated by the T_w curve becomes unstable when lifted enough. (Note that this demonstration is made by parcel procedures; the use of the potential-instability concept is sometimes referred to as "the layer method" as though it was not derived from the parcel theory, which is a misconception.)

In Figure 33, the unsaturated layer with lapse rate AB is stable in its original position between 700 and 800 mb. However, if the layer were lifted 100 mb, its new lapse rate would be A'B'. (Paths of the parcels from Points A and B are indicated by arrowheads.) The layer is now saturated and its stability is then found by comparing the slope (see Footnote 13) of A'B' with that of the saturation adiabats. Since the slope of A'B' is greater than that of the saturation adiabats, the layer is now unstable. Thus, the original layer AB is potentially unstable, the instability being releasable by a lifting of 100 mb or more.

Potentially-stable layers are all those layers of the sounding which will not become unstable by any amount of lifting.

In Figure 34 is an example of potentially unstable layers identified by the T_w curve, and with the T_d curves added to show what extent one may substitute the latter for the T_w curve to get an approximate idea of where there is potential instability. In layers of marked departure of T_w lapse rate from the saturation adiabats, the T_d curve will usually show the same sign of departure, though the exact top and bottom limits of the potentially unstable layers may not always be determinable from the T_d curve. When the T_w curve is more nearly parallel to the saturation adiabats, the T_d curve becomes quite undependable as an indication of potential instability and the T_w curve must be used.

5.20.0. Effects of Lifting Potentially Unstable and Stable Layers.

The idea of potential instability and stability appears to be very simple and the criteria for them are certainly very easy to use. But the relation of these states to the resulting weather is very complex and not well understood. The "classic" example of the release of potential instability causing severe convection weather (deep cumulus, thunderstorms, hail, and showers) is the lifting of an air mass having a small T_w lapse-rate slope in a strong "dry" inversion or having a rapid drying out above a surface moist layer. There are, however, many other layers with less-marked potential instability (steeper T_w lapse-rate slopes), and it is always a question what kind of weather their lifting will produce. This question has not been given any formal theoretical analysis; but a few inferences can easily be made.

For example, a shallow potentially-unstable layer with deep layers of potentially-stable air both above and below, when lifted to saturation may produce any of the following: A solid stratiform deck of cloud, only scattered shallow cumulus, cumulus and altostratus mixed, or deep cumulus penetrating into the higher stable layers with or without precipitation. Which of these possibilities will actually occur presumably depends on a variety of factors, such as the amount of lifting beyond that just sufficient to start condensation, the steepness of the lapse rate of wet-bulb temperature, the degree of stability of the adjacent layers, the speed and spatial uniformity of the lifting, etc. For many practical purposes there may be little difference in the clouds and weather that result from lifting a shallow potentially-stable layer as compared to those from lifting a shallow potentially-unstable layer. Therefore, there are probably many cases of potential instability in which the "instability" aspect is of trivial significance, especially in winter.

5.20.1. Does the Whole Layer Become Unstable?

When the layer or layers of potential instability are deep, it may be desirable to examine the effect of the lifting

on representative parcels at several heights in the layer to see whether the condensation will start first at the top, or the middle, or the bottom of the layer. One can find cases where considerable more lifting is required to saturate the bottom than the top, or vice versa, and the question then arises: If the lifting expected will not be sufficient to saturate the whole layer, will the convection started in the first-saturated part spread rapidly through the remainder of the layer anyway? It is often assumed that the whole layer will become unstable upon saturation of any part of it, but this presumably cannot happen until the lapse rate of the unsaturated part of the layer becomes conditional[19](if it were not already conditional before lifting — see Figures 35a and 35b). It could also happen that potentially-stable layers adjacent to the potentially-unstable layer saturate first, with the possibility of starting a premature convection in the potentially-unstable layer by mixing and penetration across the boundary. Likewise, surface-heating convection may penetrate into a low-lying potentially-unstable layer while it is being lifted, resulting in local releases of its instability before the layer lifting alone would do so.

For example, on the sounding shown in Figure 35a, an absolutely-stable lapse rate AB exists through the potentially-unstable layer between 800 and 900 mb, where both the dew point and wet bulb decrease rapidly with height. If this layer were lifted by 50 mb, its lapse rate would appear as $A'B'$, and the layer would become saturated and unstable from 850 to about 820 mb. The upper, unsaturated portion of the layer, however, would remain absolutely stable, and the potential instability being released would be confined mostly to the saturated portion of the layer. Under such conditions, the total potential instability of the layer would not be realized until the entire layer had been lifted to saturation. For the
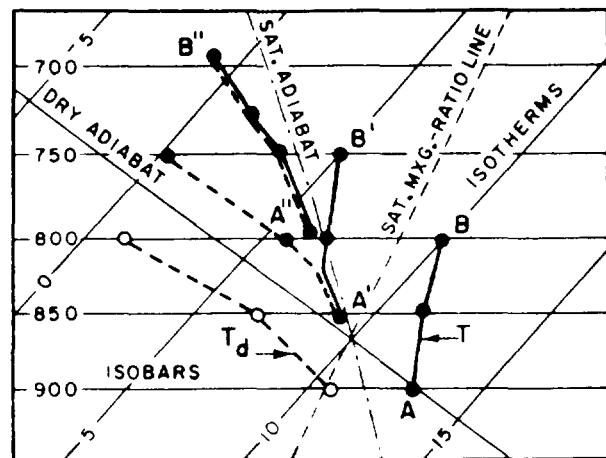
Figure 35a. Effect of Lifting on Absolutely-Stable Layer AB on the Release of Its Potential Instability.
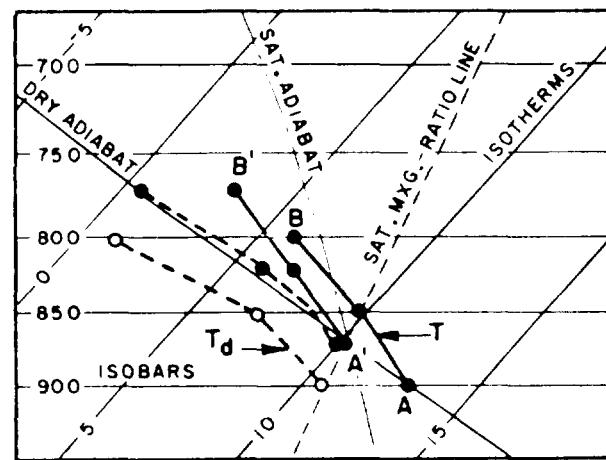
Figure 35b. Effect of Lifting a Conditionally-Unstable Layer on the Release of Its Potential Instability.

example in Figure 35a, this would require lifting by an additional 55 mb, after which the resultant lapse rate would then be $A''B''$.

If, on the other hand, the original temperature lapse rate of the same layer were in a conditional state as shown by the sounding AB of Figure 35b, lifting through only 30 mb would result in lapse rate $A'B'$, enough to saturate the bottom portion of the layer from

------

[19] Note that the lifting of an absolutely-stable layer having potential instability must always first convert the layer to the conditional state (Figure 35a) before the instability can be released.
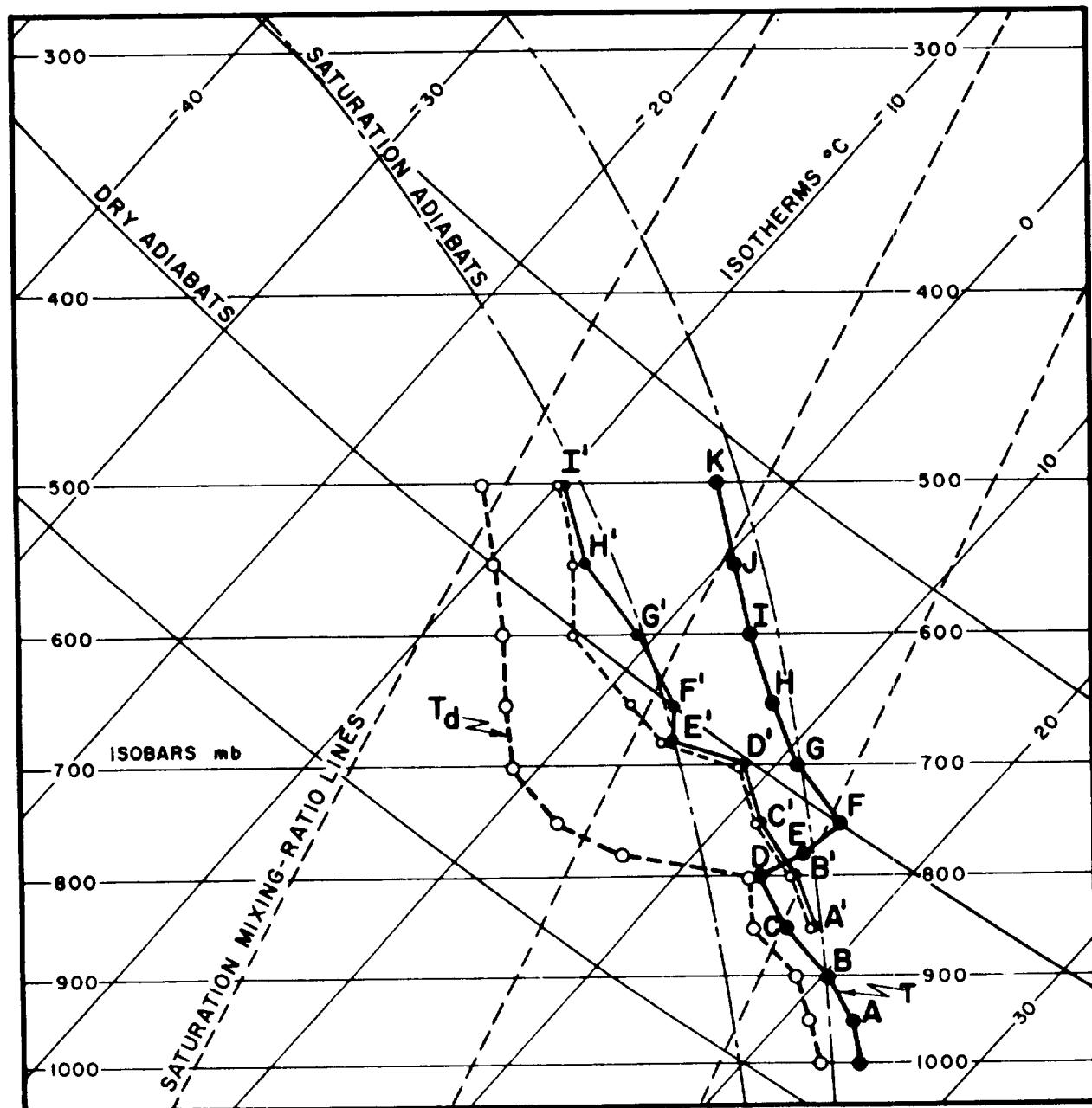
Figure 36. Superadiabatic Lapse Rate (D'E') Resulting from Lifting an Air Mass 100 mb.

about 870 to about 850 mb. The resultant up-
ward acceleration and convection of the satu-
rated portion would then tend to push rapidly
upward into the upper, still unsaturated re-
mainder of the layer without further lifting.

If, however, the dew-point *depression* or wet-
bulb *depression* decreases with height through
a potentially-unstable layer, such as the 1000-
to 800-mb layer shown in Figure 34, lifting
will then release the potential instability first

at the *top* of the layer. As the lifting continues, the height of the release of potential instability will progress downward through the layer; but the total potential instability of the original layer will not be realized until the entire layer has been lifted to saturation.

### 5.20.2. Superadiabatic Lapse Rates from Layer Lifting.
In evaluating on a diagram the effect of lifting of potentially-unstable layers, one sometimes finds cases where a superadiabatic lapse rate appears to result, as illustrated in Figure 36.

A superadiabatic lapse rate (i.e., slope less than the dry adiabats) can result from the lifting of a layer through which the moisture content decreases sharply with height, as in "dry-type inversions" (s u b s i d e n c e, trade wind, etc.).

In Figure 36 the T and T_d curves which include such a layer are shown before and after the sounding is lifted 100 mb. The layer AB is lifted to $A'B'$, the layer BC is lifted to $B'C'$, etc. After each layer is lifted 100 mb, as might be caused by the advance of a fast-moving cold front, a superadiabatic lapse rate results in the layer $D'E'$. The validity of such lapse rates is discussed in paragraph 5.6.

5.20.3 Effects of Divergence.
Divergence has no effect on the potential instability of an unsaturated layer, since the potential wet-bulb temperature is conservative for a dry-adiabatic process. However, the effect of divergence on the temperature lapse rate during a lifting process may speed up or slow down the rate of the lifting, and thus has a bearing on how soon the potential instability might be released. Note also that there may be *potentially-stable* layers that if lifted enough, could become unstable with or without saturation under the combination of convergence or d i v e r g e n c e with vertical stretching (see par. 5.14.6).

5.20.4. How Much Lift is Needed for Release of Instability?
The practical use of potential instability requires that the layer or layers identified as having it be examined to see how much lift is needed for its release. This can be done by choosing in each such layer the parcel with the highest relative humidity (the one where $T - T_d$ is least) and lifting it to saturation on the Skew-T Chart. Perhaps half of the potentially-unstable layers one sees are hardly susceptible to release by the lifts that could be expected. This is why the stability indexes based on the potential-instability concept (see par. 5.24.0, and Chapter 8) are not useful unless combined with other factors or considerations.

5.20.5. Lifting of Potentially-Stable Layers.
The saturation of a *potentially-stable* layer upon lifting may begin at any part of the layer. One can predict the location and final extent of the resulting cloud only by "testing" parcels in different parts of the layer to see which one becomes saturated first by the amount of lifting expected. In addition, potentially-stable layers may be penetrated by clouds formed in the release of potential instability of the layers beneath.

5.21. Processes Which Change the Potential Instability.
In general, those processes which increase the moisture content (wet-bulb or dew-point temperature) of the lower levels, and/or decrease the moisture content at higher levels tend to create or increase potential instability. All the effects that change the lapse rate, as discussed in paragraph 5.14.6, can indirectly change the vertical distribution of potential stability and instability, through their effects on evaporation and diffusion of moisture.

5.22. Relation Between Potential and Latent Instability.
It is evident from the literature that many meteorologists confuse potential with latent instability, or incorrectly assume that they measure essentially the same thing. The relation between latent instability and potential instability is neither simple nor

definite. For example, the following cases may be cited: Layers with latent instability (stability) often overlap or partly coincide with those of potential instability (stability); only the bottom parts of layers of potential instability generally have latent instability; in layers where both types of instability occur, the latent instability is usually of the real-latent type; potentially-stable layers often have latent instability. See Figures 32 and 34 for illustrations of some of these cases.

The basic reason for this lack of close correspondence between latent and potential instability is that the former requires a high relative humidity and assumes the conditional state, whereas the latter does not depend directly on the relative humidity and is independent of the initial lapse rate. It is obvious, therefore, that potential instability is not a substitute for latent instability or vice versa. The main value of potential instability is as an indicator of possible convective overturning from either layer ascent or convergence.

5.23. Slice Method. The assumption in the parcel theory that the parcel moves up or down without disturbing the environment is obviously unrealistic. As the parcel moves, the environment must readjust to some extent flowing into the space evacuated by the parcel and giving way in front of it, causing the distribution of temperature and density in the environment to change slightly. This effect may be considered trivial on the scale of parcels; but when we try to apply the parcel method to convection columns of the size of large cumulus and thunderstorms, the effect greatly limits the practical application. A step towards improving on the parcel theory in this respect, was introduced by J. Bjerknes [14] who considered theoretically the effect of neighboring up and down currents in a horizontal (isobarically bounded) "slice" of the atmosphere on the parcel-stability criteria. Petterssen [48] and Beers [13] developed actual procedures for applying this concept in practice. These procedures are rather cumbersome and time-consuming, even with use of Beers special nomograms. Although several experiments [8] [13] seemed to indicate these procedures give some improvement in thunderstorm forecasting over parcel methods, other studies cast considerable doubt on this conclusion and suggest that the apparent improvement was due to other factors previously overlooked [36] . In any case, the procedures have not been adopted routinely and therefore will not be described here.

The Bjerknes-Petterssen slice approach is incomplete because the effects of mixing, entrainment, and shear across the cloud boundaries are not considered. However, for cumulus forecasting the effects of entrainment and wind shear could probably be estimated empirically, using as a qualitative guide the extensive research literature on cumulus dynamics.

There is a difficulty in choosing a suitable convection model for a valid slice theory. The nature of the compensating subsidence in the environment of a convection updraft is not definitely known. The descent may be largely concentrated close to the boundary of the updraft (the Bjerknes assumption), or spread over a wide area extending far from the updraft, or in case of a cumuliform cloud take place partly inside the cloud (as often actually observed). All three processes probably occur in varying degrees and combinations from case to case.

Petterssen, et al, [49] experimented with an application of his slice method to the analysis of soundings for estimating the amount of cloudiness (sky cover) and the height of cloud tops. In light of later studies [36] it seems doubtful that a better prediction of the cloud tops is given by Petterssen's procedure than by parcel procedures. Nor has it been demonstrated that the cloudiness is satisfactorily predictable by this approach although the slice reasoning seems to account for the statistical fact that in air-mass convection situations, the probability is about 85% that the cloud cover will not exceed four octas.

Cressman [21] derived an interesting and apparently significant extension of Petterssen's analysis to show the effect of horizontal divergence on the cloudiness. When the ratio $(\gamma - \gamma_s) / (\gamma_d - \gamma)$ is small, the effect of the divergence (convergence) on the cloudiness is large; and, when this ratio is large, the effect of the divergence (convergence) is small. (γ is the sounding lapse rate, γ_d, the dry adiabatic, and γ_s, the saturation adiabatic lapse rate.) This would seem to explain the fact that in the oceanic tropics where the lapse rate in the lower troposphere is always close to the saturation adiabatic, the cloudiness may be little or much, depending largely on the presence of general subsidence or convergence.

The slice-method procedures so far developed do not greatly alter the results of the parcel methods and the apparent differences may easily be due to other factors overlooked. The effect on stability criteria by using these slice-method procedures instead of the parcel procedures is to indicate somewhat less instability (or more stability) in that region of the positive area lying above the height where the sounding curve becomes parallel to the saturation adiabats, and somewhat more instability (or less stability) below that height [48] [49]. In empirical forecasting procedures this difference is usually of little or no consequence for the relationships of stability criteria to weather, although the numbers obtained will be different.

The slice method requires a more complete development before its theoretical advantages can be realized in practice.

5.24.0. The Stability Indexes. The overall stability or instability of a sounding is sometimes conveniently expressed in the form of a single numerical value called a *stability index*. Such indexes have been introduced mainly as aids in connection with particular forecasting techniques or studies. Most of the indexes take the form of a difference in T, T_d, $(T - T_d)$, T_w, $(T - T_w)$,

θ, θ_E, θ_w, $(T - \theta_w)$, q, w, pressure, height, etc., between two arbitrarily chosen surfaces (or heights), such as 850 mb and 500 mb, 1000 mb and 700 mb, etc. The indexes of this type have the advantage of ease of computation, flexible choice of the layer most pertinent to the particular problem or area, and a numerical form convenient for ready use in objective studies. On the other hand, details of the lapse-rate structure important to the problem at hand may be smoothed out or completely missed in these indexes, unless the index is carefully chosen and evaluated by statistical studies on many cases. Also, these indexes are generally useful only when combined, either objectively or subjectively, with other data and synoptic considerations [3] [61]. Used alone, they are less useful than the standard stability analyses of the complete sounding by the parcel method described in the preceeding paragraphs of this chapter; in fact, used alone, a stability index is apt to be almost worthless. The greatest value of an index lies in alerting the forecaster to those soundings, routes, or areas, which should be more closely examined by other procedures. One way to apply a stability index for this purpose is to construct a "stability chart" on which the index values for soundings over a large area are plotted and isoplethed (see *AWS TR 200*; also [2] [3] [4] [59]). Such charts offer several possible advantages:

a. Incorrect or unrepresentative indexes may be spotted.

b. Location and movements of stable and unstable air masses can be visualized.

c. Systematic local or regional effects (e.g., orographic) may be discovered.

d. Patterns can be related quickly to other synoptic charts, and some correlations of index values with other parameters may be suggested (for further investigation by objective studies).

However, experience has shown that an index or critical index value which is significant in one region (or season) may not be in another [4] [61]. Hence, the stability chart should be more of an experimental or investigative tool than a routine one, unless extensive
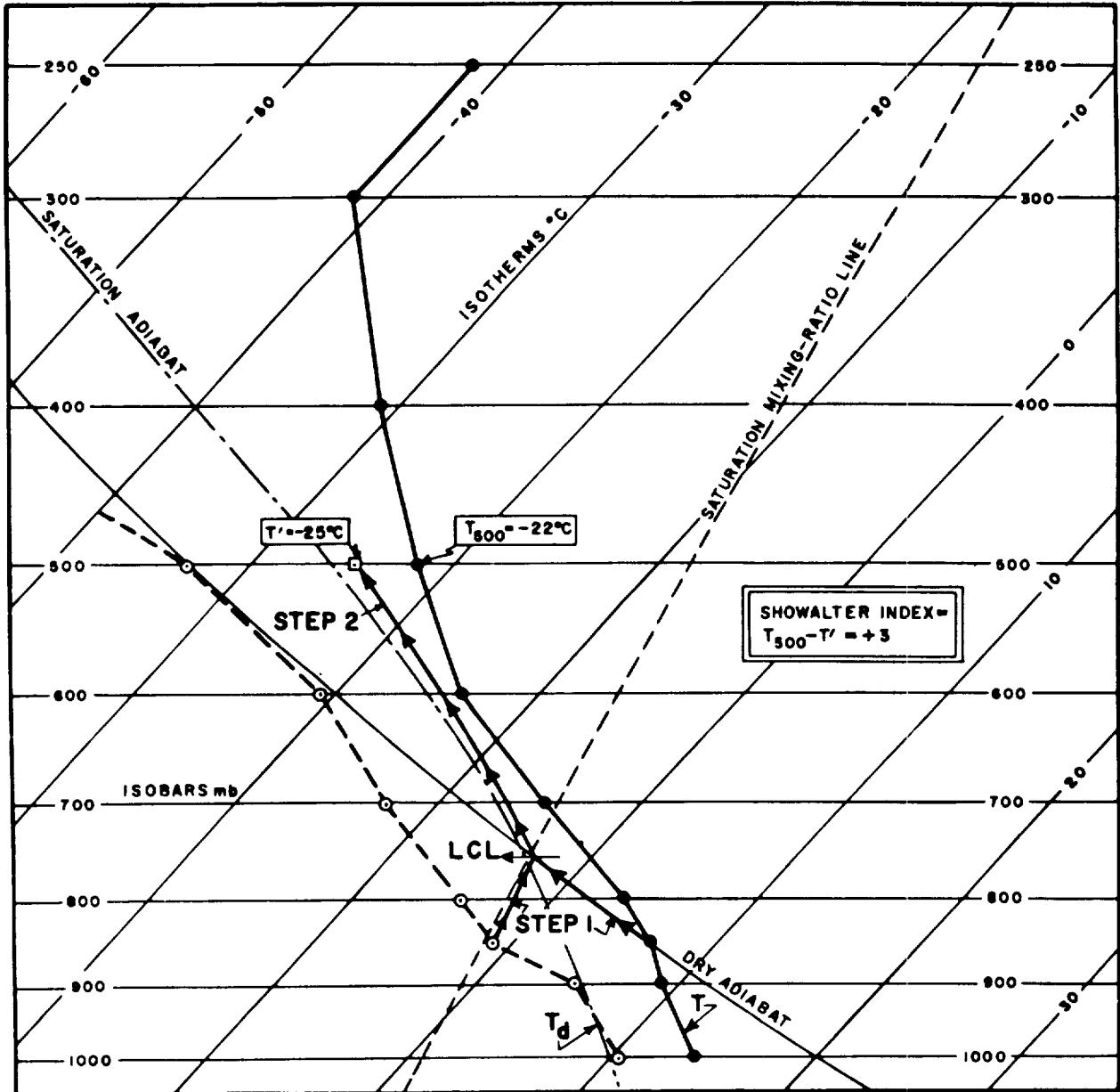
Figure 37. Computation of the Showalter Stability Index.

correlation studies have selected an index significant for the extended general application [4] [61], and the critical index values for various weather conditions have been determined.

The Showalter, Fawbush-Miller, and Lifted Indexes described below are all based on the

potential-instability concept; but many forecasters have applied them to the forecasting of showers in general, from heating as well as from lifting. The fact that the results of such "across-the-board" applications seem to be useful (when combined with other parameters) indicates that these indexes to a considerable extent also reflect conditions

5—34

affecting the formation of showers from surface heating. This is presumably because the θ_E or θ_w lapse rate used in these indexes is partly a function of the ordinary-temperature lapse rate, and hence is partly indicative of the stability criteria for surface-parcel heating.

5.24.1. The Showalter Index. The procedure for computing the Showalter Stability Index (SI) is illustrated in Figure 37.

Step 1. From the 850-mb temperature (T), draw a line parallel to the dry adiabats upward to the LCL (see par. 4.20). (Mountain stations should start with some higher constant-pressure-surface temperature chosen according to circumstances. Such a procedure is incorporated into the instructions given in FMH No. 3 (Circular P) for computing the stability indexes that are transmitted as part of the radiosonde reports from U.S. and Alaskan stations these indexes also appear on the stability index charts transmitted by facsimile from the NMC.)

Step 2. From the LCL, draw a line parallel to the saturation adiabats upward to 500 mb. Let the temperature at this intersection point at 500 mb be called T'.

Step 3. Algebraically subtract T' from the 500-mb temperature. The value of the remainder (including its algebraic sign) is the value of the Showalter Index. (In Figure 37, $T' = -25°C$, $T = -22°C$; the Showalter Index is therefore +3.) This Index is positive when T' lies to the left of the T curve. Positive Index values imply greater stability of the sounding.

For forecasting purposes in the United States, Showalter [58] groups the range of index values as follows:

a. When the Index is +3 or less, showers are probable and some thunderstorms may be expected in the area.

b. The chance of thunderstorms increases rapidly for Index values in the range +1 to -2.

c. Index values of -3 or less are associated with severe thunderstorms.

d. When the value of the Index is below -6, the forecaster should consider the possibility of tornado occurrence. However, the forecasting value of all index categories must, in each case, be evaluated in the light of other synoptic conditions.

5.24.2. The Lifted Index. The arbitrary choice of 850 mb in the Showalter Index makes it difficult to use on a detailed synoptic time and space basis when, as often happens, there is an inversion or rapid drop in moisture which passes through the 850-mb surface between stations or between two successive sounding times. To avoid this difficulty, Galway of the U. S. Weather Bureau SELS Center [2] devised the "Lifted Index" (LI), a modification of the Showalter Index. To evaluate the LI, the mean mixing ratio in the lower 3000 feet of the sounding is determined by equal-area averaging. Then the mean potential temperature in the lower 3000 feet at the time of convection is determined by forecasting the afternoon maximum temperature and assuming that a dry-adiabatic lapse rate will prevail through this 3000-foot layer (if significant heating, or cooling, is not expected during the afternoon, the mean temperature of the lower 3000 feet as shown on the sounding is used). From these mean values the LCL is located (see par. 4.20). Then the saturation adiabat through this LCL is extended upward to 500 mb. The 500-mb temperature thus determined is assumed to be the updraft temperature within the cloud if one develops. The algebraic difference between the environment temperature and the updraft temperature (observed minus computed) at 500 mb defines the LI. LI values are usually algebraically less than SI values.

5.24.3 The Modified Lifted Index (MLI). The arbitrary choice of 500 mb for the Lifted Index (Para 5.24.2) fails to consider the destabilizing effects of cold air aloft; the MLI was developed to correct this problem. To evaluate the MLI, find the LCL in the same way as for the traditional Lifted Index. Extend the saturation adiabat through this LCL upward to the pressure level at which the environmental temperature is -20°C. The temperature thus determined is assumed to be the updraft temperature (T_p) within the cloud, should a cloud develop. The algebraic difference between the environmental temperature (-20°C) and the updraft temperature (T_p) defines the MLI.

$$MLI = -20 - T_p$$

The MLI is not calculated when the -20°C level is above 500 mb (too warm) or below the LCL (too cold). MLI threshold values are the same as those for the Lifted Index. Although the MLI was developed to estimate the potential for severe thunderstorms in Europe, it has been used with success in the CONUS.

5.24.4. The Fawbush-Miller Stability Index (FMI). This index involves consideration of a surface "moist layer." This "moist layer" is defined as a surface stratum whose upper limit is the pressure surface where the relative humidity first becomes less than 65%. If its vertical extent exceeds 6,000 feet, only the lowest 150-mb layer is used to determine the mean wet-bulb temperature of the "moist layer." (Soundings sometime contain shallow dry layers within this defined "moist layer"; e.g., in the lowest 30 mb, or in the top layers of a surface inversion. In such a case, the assumption is made that the normal convective mixing of moisture will wipe out such shallow dry layers, and they are therefore ignored in identifying the "moist layer.")

The procedure for computing the FMI is shown in Figure 38:

Step 1. Compute relative humidity (see Para 4.4) for enough points in the lower part of the sounding to identify the "moist layer." In the sounding shown in Figure 38, the "moist

layer" extends to about 875 mb, since the 65% relative-humidity value is about half-way between 900 mb (where RH = 75%) and 850 mb (where RH = 57%).

Step 2. Plot the T_w curve (see Para 4.9) for the "moist layer." Draw a straight-line approximation of the T_w curve through this layer. The approximation will be sufficiently accurate, if the area between the straight line and the T_w curve is the same on each side of the straight line (equal-area averaging). The isotherm value at the mid-point, (M) of this straight-line approximation of the T_w curve is the average T_w for the layer. (in Figure 38, the "moist layer" average $T_w = 8.7°C$.)

Step 3. From Point M of the straight-line approximation of Step 2, proceed upward parallel to the saturation adiabats to 500 mb. Subtract the isotherm value (T') at this new position from the observed 500-mb temperature indicated by the T curve. The value of the remainder (including its algebraic sign) is the numerical value of the FMI (in Figure 38, the FMI = +1 1/2). Positive values of the FMI indicate stability; minus values, instability. Fawbush and Miller classify the relative stability of soundings as follows:

- FMI greater than +1   Relatively stable
- FMI between 0 and -2:   Slightly unstable
- FMI between -2 and -6   Moderately unstable
- FMI lower than -6   Strongly unstable

Values of FMI and SI are usually quite similar. Occasionally, however, significant differences occur when the moisture value at 850 mb is not as representative of the layer below that pressure as when a subsidence inversion is located just below 850 mb. Since the FMI considers more information about the moisture values, it appears to be more representative that the SI. However, computation of the Showalter Index is much easier, and in many cases is of comparable utility.
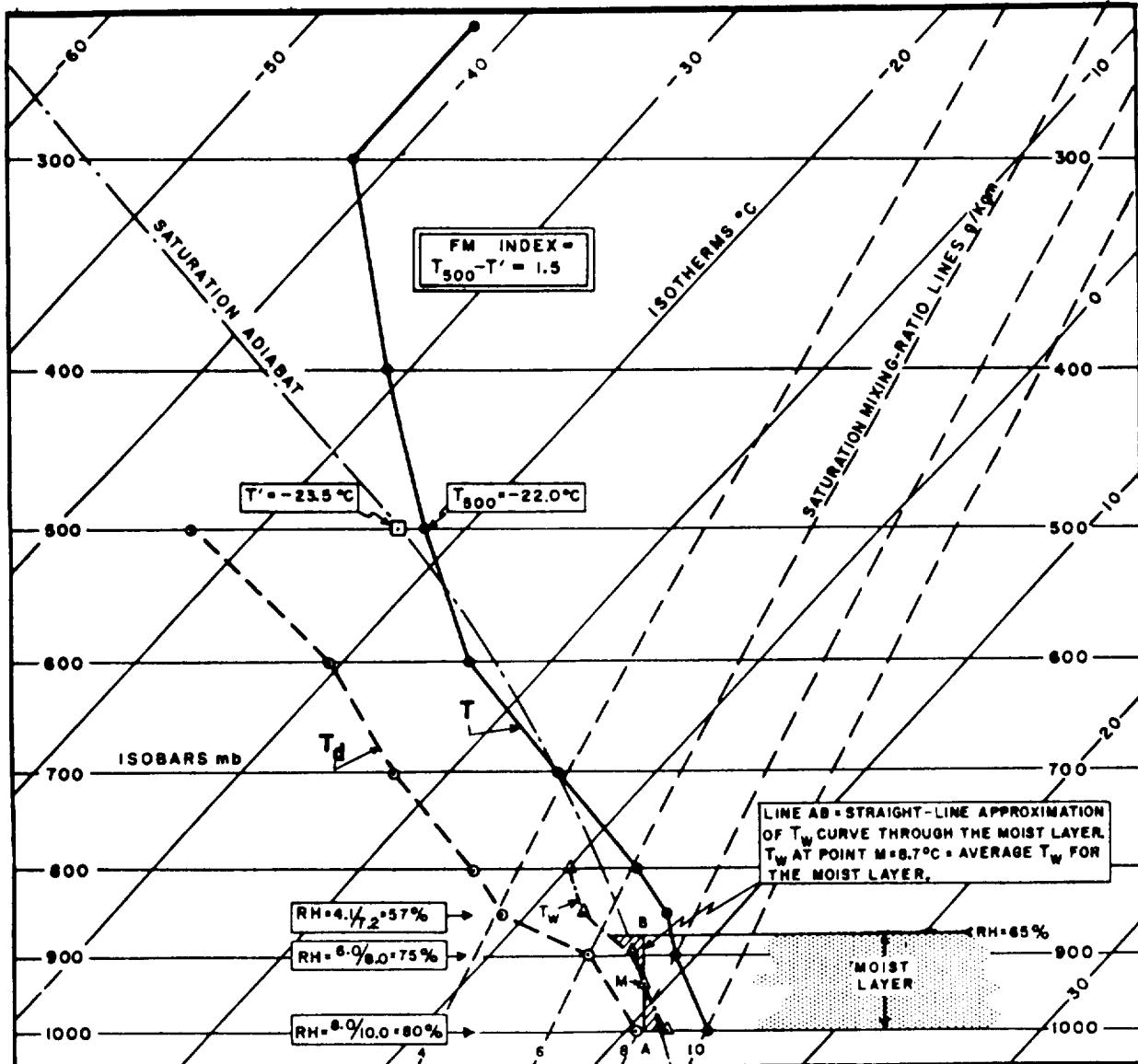
Figure 38. Computation of the Fawbush-Miller Stability Index (FMI).

5.24.5. The Martin Index (MI). This stability index, devised by Delance Martin, is claimed to be more sensitive to low-level moisture than ether the Showalter or FM Indexes [35]. It is evaluated on the Skew T Chart as follows: Draw the saturation adiabat intersecting the temperature-sounding curve at 500 mb past the height of maximum mixing ratio. Find the intersection of this line with the saturation mixing-ratio line through the maximum mixing-ratio value in the sounding. From this intersection, draw a dry adiabat to intersect the 850-mb line. Algebraically subtract the sounding temperature at 850 mb from the temperature at the latter intersection. The resulting number (including its algebraic sign) is the Martin Index. With a marked low-level turbulence or subsidence inversion, the reference height is taken as the height of the base of the inversion instead of 850 mb.

5.24.6. The Best Lifted Index (BLI). The BLI was developed by Fujita, who noted that a lifted index (LI) computed from a fixed level, such as the surface, might misrepresent the stability of the air mass because the base of an updraft or unstable layer will vary from point to point in the lower troposphere.

Procedure: Compute an LI for two or more points in the layer between the surface and 1,600 meters AGL. The algebraic difference between the temperature of the lifted parcel and its environment defines the LI. The BLI is the most unstable value of all LIs computed from different levels. Any number of points between the surface and 1,600 meters could be used.

5.24.7. The Model Lifted Index. The Model Lifted Index procedure uses variables available at initial and forecast times. Lifted Index from the LFM is transmitted in FOUS bulletins (FRH 60-78).

Procedure: The boundary layer mean temperature and relative humidity values apply at mid-layer and are used to determine the dew point and temperature of a parcel at 25 mb above the model terrain at each of the grid points. Parcels at the mid-point of the boundary layer are first lifted dry adiabatically to saturation (LCL), then moist adiabatically to the 500-mb level. The resultant temperatures at 500 mb are compared to the initialized (or forecast) 500-mb temperatures at each grid point to give the initial and forecast Model Lifted Index. The initial or forecast temperature at 500 mb minus the parcel temperature is the Model Lifted Index. The LFM LI can be interpreted as one similar to a surface-based LI.

5.24.8. The NGM Lifted Index is similar to that from the LFM, but the boundary layer (35 mb) is not as thick as that in the LFM (50 mb). The boundary layer NGM LI therefore, represents a surface-based LI even more than does the LFM LI.

5.24.9. The "K" Index is a measure of thunderstorm potential based on vertical temperature lapse rate, moisture content of the lower atmosphere, and vertical extent of the moist layer. It is derived arithmetically and does not require a plotted sounding. The temperature difference between 850 and 500 mb is used to parameterize the vertical temperature lapse rate. The 850-mb dew point provides information on the moisture content of the lower atmosphere. The vertical extent of the moist layer is represented by the 700-mb temperature-dew point depression.

Procedure:

K = (850-mb temp minus 500-mb temp plus 850-mb dew point minus 700-mb dew point depression).

With the K Index, the higher the positive number, the greater the likelihood of thunderstorm development. Inclusion of the 700-mb dew point depression biases it in favor of "air mass" type thunderstorms, and it works better (McNulty, 1983) for non-severe convection. The K Index is also an important index for forecasting heavy rain. Moisture at 850 and 700 mb implies the presence of a deep moist layer; i.e., large values of precipitable water. Note: This index cannot be reliably computed for mountain stations.

Although K Index values can be correlated to a probability of thunderstorm occurrence, these values will vary with seasons, locations, and synoptic settings. The values listed below work best for the central United States in summer.

K INDEX	% PROBABILITY OF THUNDERSTORMS
K < 15	Zero
15 to 20	20%
21 to 25	20-40%
26 to 30	40-60%
31 to 35	60-80%
36 to 40	80-90%
K > 40	Near 100%

5.24.10. The "KO" Index. The German Weather Bureau (Deutsches Wetterdienst) created the KO Index to estimate the potential for thunderstorms in Europe. The index is the average mid-level equivalent potential temperature minus the average low-level equivalent potential temperature. The KO index is more sensitive to moisture than other, more traditional, stability indices.

$$KO = \frac{(\theta_E\,500 + \theta_E\,700)}{2} - \frac{(\theta_E\,850 + \theta_E\,1,000)}{2}$$

where: θ_E = equivalent potential temperature

500=500mb
700=700mb
850=850mb
1,000=1,000mb.

KO INDEX	LIKELIHOOD OF THUNDERSTORMS
>6	Low
2-6	Moderate
<2	High

5.24.11. The Thompson Index (TI). TI is used to determine the severity of thunderstorms in the Rocky Mountains.

$$TI = KI - LI,$$

where KI is the K index (Para 5.24.8) and LI is the lifted index (Para 5.24.2).

TI	THUNDERSTORM INTENSITY
<20	No Thunderstorms
20-29	Isolated, Weak
30-34	Moderate
>35	Severe

5.24.12. Total Totals (TT). The Total Totals index was introduced by Miller (1972) for identifying potential areas of thunderstorm development. Total Totals is actually the sum of two other convective indices: the Vertical Totals (VT) and Cross Totals (CT); that is,

TT = VT plus CT = (850-mb temp plus 850-mb dew point) minus 2(500-mb temp).

Vertical Totals (VT).

VT = 850-mb temp minus 500-mb temp (°C).

The number represented by VT expresses the lapse rate between two constant pressure surfaces. Although VT will usually be 26 or better before convection and thunderstorm activity develops, that value is no guarantee that there will be thunderstorm activity.

In the west, where most thunderstorms are of the orographic or air mass variety, VT correlates with thunderstorm activity best; the greater the VT, the greater the conditional instability. In the west, significant moisture at 700 or 500 mb is sufficient to initiate thunderstorms. "Significant moisture," in this case, is defined as a 700- or 500-mb temperature-dew point spread of 6 degrees or less, a dew point of -17 °C or warmer at 500 mb, or a dew point of 0 °C or warmer at 700 mb.

West of the Rockies, the VT thresholds shown in the following table generally correlate with thunderstorms if mid-level moisture is available. Completely dry soundings may show high vertical totals, but cannot support thunderstorm development without sufficient moisture at some level.

VT	THUNDERSTORM ACTIVITY
28	Isolated
29 to 32	Few
32	Scattered

Cross Totals (CT).

CT = 850-mb dew point minus 500-mb temp (°C).

The value represented by CT combines a measure of low-level moisture with temperatures aloft. Moist 850-mb dew points and cold 500-mb temperatures yield high CT values. Although CT will usually be at or above 18 before thunderstorm activity develops, the value is not a guarantee of thunderstorm development.

As mentioned earlier, VT measures the vertical lapse rate while CT incorporates low-level moisture. Although VT may be a better indicator of thunderstorm activity in one region or during certain situations, and although the CT may carry more weight in certain regions and situations, the Total Totals index has shown itself to be a more reliable predictor of severe weather activity.

The general TT convection threshold is 44. Weak potential for heavy thunderstorms is 50; for moderate, 50 to 55, and for strong, greater than 55. Note, however, that threshold convection values for TT vary considerably across the United States. Forecasters should check NWS Regional Technical Attachments or Technical Memoranda for threshold values applicable to a given area.

NOTE: Use Total Totals with careful attention to either the Cross Totals or the low-level moisture since it is possible to have large Total Totals due to the temperature lapse rate with little supporting low-level moisture.

5.24.13. SWEAT Index. The Severe Weather Threat Index (SWEAT) is used to estimate the severe weather potential of a given air mass. SWEAT is computed from five terms that contribute to severe weather potential; these terms are:

- Low-level moisture (850-mb dew point)
- Instability (Total Totals)
- Low-level jet (850-mb wind speed)
- Upper-level jet (500-mb wind speed)
- Warm advection (veering between 850 and 500 mb)

If the reporting station is higher than 850 mb, use the temperature and depression at the top of the surface layer (surface pressure minus 100 mb) in place of the 850-mb temperature and depression.

Use the wind reported closest to 18,000 ft MSL as the 500-mb wind speed.

$$SWEAT = 12D + 20(T-49) + 2f8 + f5 + 125(S+0.2)$$

where:

D = 850-mb dew point in degrees Celsius (if D is negative, set the term to zero)

f8 = 850-mb wind speed in knots

f5 = 500-mb wind speed in knots

S = Sin (500-mb wind direction - 850-mb wind direction)

T = "Total Totals" in degrees Celsius (if T is less than 49, set the term 20(T-49) to zero)

The entire shear term [125(S+0.2)] is set to zero when any of the following four conditions are <u>not</u> met:

•850-mb wind direction is from 130-250°

•500-mb wind direction is from 210-310°

•500-mb wind direction minus 850-mb wind direction is positive.

•Both the 850- and 500-mb wind speeds are at least 15 knots.

NOTE: No term in the formula may be negative.

Applications:

The USAF developed the SWEAT index initially and remains its chief user. In a USAF study that documented 328 tornado occurrences, none had a SWEAT index of less than 375. In the same study, the lowest value associated with a severe thunderstorm episode was 272. An "occurrence" was said to have taken place only after five events of the type noted were confirmed. Only cases in which severe weather was known to have occurred were considered. Nothing can be inferred about "false alarm" rates.

Commonly accepted SWEAT index threshold values used by the Air Force are usually 300 for severe thunderstorms and 400 for tornadoes. It must be emphasized that the SWEAT index is only an indication of the *potential* for severe weather; that is, a high SWEAT index for a given time and area does not mean that severe weather is occurring or definitely will occur. Although SWEAT shows the potential for severe weather, some kind of triggering mechanism is still necessary to set it off.

Experience has shown that although high SWEAT values can occur in the morning (based on the 1200Z sounding) without concurrent severe convective weather, the potential is usually realized if the predicted value for the afternoon and evening is also high. Although low observed values of the SWEAT index almost certainly mean there is no severe weather occurring, those values can increase dramatically during a 12-hour period.

Note that the SWEAT index attempts to incorporate both thermodynamic information (850-mb dew point, Total Totals) and kinetic information (which favors strong low and mid-level flow with winds veering with height). SWEAT, therefore, is more than a typical "stability" index.

The SWEAT index should not be used to predict ordinary thunderstorms. Use of the shear term and minimum values for the stability (Totals) and wind speed terms were specifically designed to discriminate between ordinary and severe thunderstorms.

5.24.14. Bulk Richardson Number (R). The bulk Richardson number is the ratio of positive buoyant energy within the layer of free convection to one-half the square of the shear vector in the first 6 km above the surface. Values of R less that 50 indicate potential for severe storm development. Values greater than 50 are associated with weaker, multicelled storms. Because of its complexity, R is best calculated on a computer. For more detail, see "The Dependence of Numerically Simulated Convective Storms on Vertical Wind Shear and Buoyancy, by M.L. Weisman and J.B. Klemp, *Monthly Weather Review*, June 1986, pp. 514-520.

$$R = \frac{B}{1/2 \; \overline{U}^2},$$

where U is the shear vector in the lowest 6 km of the atmosphere and B is the buoyancy of a parcel given by:

$$- B = g \int \frac{\theta(z) - \bar{\theta}(z)}{\bar{\theta}(z)} \, dz,$$

where $\theta(z)$ defines the moist adiabatic ascent of a representative surface parcel and the integral is taken over the vertical interval where the lifted parcel is warmer than its environment (positive area on the Skew T). $\bar{\theta}(z)$ represents the environmental potential temperature profile.

5.24.15 The Dynamic Index: This index works best for "air mass" thunderstorms.

Procedure:

Compute the CCL using a mean mixing ratio for the lower 100 mb of the sounding. From the CCL, follow a saturation adiabat to the 500-mb level. Algebraically subtract the 500-mb temperature of the parcel from the observed 500-mb temperature. *Negative* numbers indicate *conditional instability*, and *positive* numbers indicate *stability*.

NOTE: The condition necessary for instability here is that the surface temperature be high enough to allow an air parcel to rise dry adiabatically to at least the height of the CCL before intersecting the temperature curve. If this condition is met, free convection will occur and thunderstorms will develop.

5.24.16. The Upper-Level Instability Index (UI)
was developed by the NWS Western Region as a simple method of assessing the potential for strong gusts associated with high-level thunderstorms (those with bases between 17 and 18 thousand feet), which are fairly common in the western United States from May through September. These storms are often associated with strong, gusty surface winds and "dry lightning." Precipitation, if any, seldom reaches the ground, but virga is common.

Two requirements are necessary for the development of these storms:

- The upper level (above 12,000 ft MSL) must be convectively unstable, and

- The lower level must be dry.

A good measure of lower-level moisture is the 700-mb dew point depression. Determination of upper level stability is determined by a parcel index similar to the Showalter Index. A parcel at 500 mb is lifted to its LCL.

From the LCL, it follows a saturation adiabat through the 400-mb level to the 300-mb level. The index is the sum of the algebraic difference between the ambient temperature and the temperature of the lifted parcel at 400 and 300 mb.

Convective Gust Potential Forecast Procedure:

Step 1. Multiply the 500-mb dew point depression by three and subtract the 700-mb dew point depression from the result. If the number is negative, proceed, but if the number is positive, there is no gust potential.

Step 2. Compute the upper-level instability index (UI) by lifting a parcel from 500 mb to its LCL, then up the moist adiabat through 400 mb to 300 mb.

$$UI = (T_{400\,mb} - T_{500\text{-}mb\ parcel}) + (T_{300\,mb} - T_{500\text{-}mb\ parcel})$$

Step 3. Using the 700-mb depression and the computed UI, locate a point on the graph in Figure 38a.
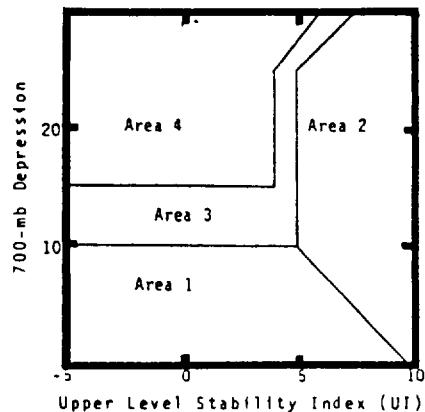
Figure 38a. Convective Gust Potential Graph.

If the point located in Step 3 falls in:

Area 1: It is too moist for strong convective gusts even though thunderstorms may occur.

Area 2: It is too stable for upper level thunderstorms.

Area 3: Consider a met watch advisory for gusts above 30 knots for the period during which thunderstorms are expected.

Area 4: Consider a weather warning for gusts above 40 knots for the period during which thunderstorms are expected.

5-41

5.24.17. Summary of Stability Index Values and Their Results. The summary tables on the next two pages show the more important values to consider when using some of the stability indices discussed in this chapter. The potentials shown are "first guess," and do not reflect mid-level moisture or upper level instability.

LIFTED INDEX (LI)[1]	Thunderstorm Indications
0 to -2	Thunderstorms possible--good trigger mechanism needed
-3 to -5	Unstable--thunderstorms probable
less than -5	Very unstable--heavy to strong thunderstorm potential

SHOWALTER INDEX (SI)[1]	Thunderstorm Indications
3 to 1	Thunderstorm possible--strong trigger needed
0 to -3	Unstable--thunderstorms probable
-4 to -6	Very unstable--good heavy thunderstorm potential
less than -6	Extremely unstable--good strong thunderstorm potential

K INDEX West of Rockies[1]	K INDEX East of Rockies[2]	Airmass Thunderstorm Probability
less than 15	less than 20	None
15 to 20	20 to 25	Isolated thunderstorms
21 to 25	26 to 30	Widely scattered thunderstorms
26 to 30	31 to 35	Scattered thunderstorms
above 30	above 35	Numerous thunderstorms

Note: K value may not be representative of airmass if 850-mb level is near surface. Western U.S. values are forced to approximate area coverage used by George.[2]

WEST OF THE ROCKIES (with adequate moisture):
VERTICAL TOTALS (VT)   **Expect:**

<28	No thunderstorms
29 to 32	Few thunderstorms
>32	Scattered thunderstorms

WEST OF THE ROCKIES:
TOTAL TOTALS (TT)[1]   **Expect:**

48	Isolated or few thunderstorms
52	Scattered thunderstorms, few of moderate intensity
55	Scattered thunderstorms, few of moderate intensity, isolated severe
58	Scattered thunderstorms, few severe, isolated tornadoes
61	Scattered to numerous thunderstorms, few to scattered severe, few tornadoes
64	Numerous thunderstorms, scattered severe, scattered tornadoes

---

EAST OF THE ROCKIES[3] (Total Totals Most Important):

CROSS TOTALS	VERTICAL TOTALS	TOTAL TOTALS	Expect:
18-19*	26 or more*	44	Isolated or few thunderstorms
20-21	26 or more	46	Scattered thunderstorms
22-23	26 or more	48	Scattered thunderstorms, isolated severe thunderstorms
24-25	26 or more	50	Scattered thunderstorms, few severe thunderstorms, isolated tornadoes
26-29	26 or more	52	Scattered to numerous thunderstorms, few to scattered severe thunderstorms, few tornadoes
30	26 or more	56	Numerous thunderstorms, scattered severe thunderstorms, scattered tornadoes

*Except along the immediate Gulf Coast and over the Gulf Stream, where the CT value is only 16 or more, and the VT value is only 23 or more

SUMMARY TABLE REFERENCES

[1] Western Regional Technical Attachment No. 84-14, May 1984, National Weather Service, Salt Lake City, Utah.

[2] George, J.J., *Weather Forecast for Aeronautics*, Academic Press, New York, 1960.

[3] Miller, R.C., *Notes on Analysis and Severe-Storm Forecasting Procedures of the Air Force Global Weather Central*, AWS-TR-200 (revised), Air Weather Service, Scott AFB, IL, May 1972.

ANALYSIS OF DISCONTINUITIES AND STABLE LAYERS IN RAOBS

6.1. Introduction. The prevailing condition of the atmosphere is stable, with stratification into distinct layers. The mean lapse rate, above the surface layer affected by nocturnal radiation inversions and daytime surface heating, is near the saturation adiabatic up to the mid-troposphere, above which the mean lapse rate becomes increasingly stable with altitude. A typical sounding in any region and season will be stable over the greater part of its height and the stable parts will be divided into layers of different degree of stability.

For various reasons the analysis of the stability features of soundings is as important for forecasting as the analysis of the instability features. Although much of the weather that is of operational concern is associated with instability, the forecasting of instability weather generally is made from a currently stable condition and certain features of the stable structure are critical for the possibility of instability developing. Moreover, certain cloud, fog, and visibility conditions are associated with absolute stability. Stable layers are significant as indications of the kind of flow (smooth versus turbulent), of the possibilities for vertical and lateral mixing, and hence for the diffusion and transport of heat, moisture, aerosols, and momentum.

Two properties of the stability are of interest: The degree of stability (as indicated by the lapse rate) and the discontinuities of the lapse rate which mark the boundaries of each layer (so-called "laminar") of different stability.

6.2. Classification of Stable Layers. The types of stability have been described in Chapter 5. Stable layers of two kinds were defined: *absolutely stable* and *conditional.* The absolutely stable layers can be subdivided into three well-recognized types: *inversion*[20], *isothermal*[21], and *stable-lapse*[22] *layers.*

It has been customary to attempt to identify and describe these layers in terms of a single physical process supposedly the cause. The results of this must be rather arbitrary in many cases, because in Nature several of the causes are often operating simultaneously. Moveover, for many of the stable layers the recognition of the cause cannot be made with any assurance from the soundings alone.

---

[20]The free-air temperature normally decreases with altitude in the troposphere. However, frequently soundings show shallow layers where a reversal of the normal lapse rate occurs and the temperature increases with altitude or "inverts." These layers are called "inversions," or more specifically, *temperature inversions.* The prime characteristic of the inversion is the great stability of the air within the inversion layer.

[21]A layer through which the temperature does not change with height.

[22]Any stable layer in which the temperature decreases with height (excludes isothermals and inversions).

The analysis of the stable layers cannot be made independently of their boundary discontinuities (see par. 6.3) even though forecasters freely shift their attention from layer to discontinuity and vice versa as the situation and problem at hand may dictate. Whether one prefers to think of an "inversion" as a layer or as a discontinuity (strictly speaking, the base or top of the inversion) depends on the context and is mainly a difference in emphasis.

6.3. Synoptic Discontinuities. The usually-recognized "synoptic discontinuities" are: *fronts, bases of subsidence and turbulence inversions, and tropopauses.* These are considered "important discontinuities" in routine analysis and forecasting. Their location and identification are only partly made from raob soundings, however, and their importance likewise is judged largely by other factors.

6.4. The "Unexplained Discontinuities." One sees in the soundings many prominent discontinuities (as well as many lesser ones) that are ignored in conventional analysis, because their significance has not been obvious and no acceptable models for their interpretation have been developed. With the present spacing of sounding stations and existing coding procedures, it is difficult to trace any time and space continuity that may exist in many of the discontinuities observed in the transmitted soundings, unless they are obviously accounted for by fronts or other familiar features on synoptic charts.

These "unexplained discontinuities," especially when they are widespread or persistent, may often be of practical importance because of their effect on turbulent diffusion and cloud formation, not to mention errors in analysis resulting from confusing them with fronts, etc.

The fact that many of the unexplained discontinuities seen in the regularly transmitted soundings probably have a synoptic-scale extent and history, is brought out by research studies [23] using a special detailed evaluation and analysis of the raobs. These studies also indicate there are many smaller discontinuities of similar nature which are "smoothed out" by the standard evaluation and coding procedures for raobs. An example of one of these detailed raob analyses will be instructive [23]. Figure 39 shows on a single adiabatic diagram a group of such detailed soundings for 1500Z, 29 March 1956. The great detail in these soundings was obtained by recomputing the evaluations from the original recorder records with less smoothing and retaining additional significant points that would be taken out by the coding procedure. The comparison of the soundings, which lie along a northwest-southeast line from Bismarck to Cape Hatteras, is effected by an extension of the hypothesis, first suggested by Palmén, that individual tropopauses are conservative along potential temperature surfaces [7]. The application of this hypothesis to other non-frontal discontinuities than tropopauses was given considerable justification by the experience with isentropic-chart analysis carried on routinely in the United States during 1938-1942; these charts seemed to show a marked tendency for the air flow and the stratification of the atmosphere to parallel isentropic surfaces, as predicted on theoretical grounds by Shaw and Rossby [45].

Note in Figure 39 that several prominent discontinuities in the troposphere conserve a similar shape and intensity from station to station while sloping through a great range in height. Relating them to the isentropes (dry adiabats) on the diagram, one can readily see that each of these discontinuities lies within small limits along a particular isentrope. The isentropic cross-section for the same soundings shown in Figure 40, reveals this tendency more clearly. The thin, solid lines on the cross-sections are isolines of potential temperature drawn for each whole °K. Packing of the isentropes on a vertical cross-section indicates layers of the atmosphere which are very stable (the greater the packing, the greater the stability). The great spatial extent of many of these stable layers ("laminars"), each associated with essentially the same "bundle" of isentropes, is evident in this figure. The accuracy and
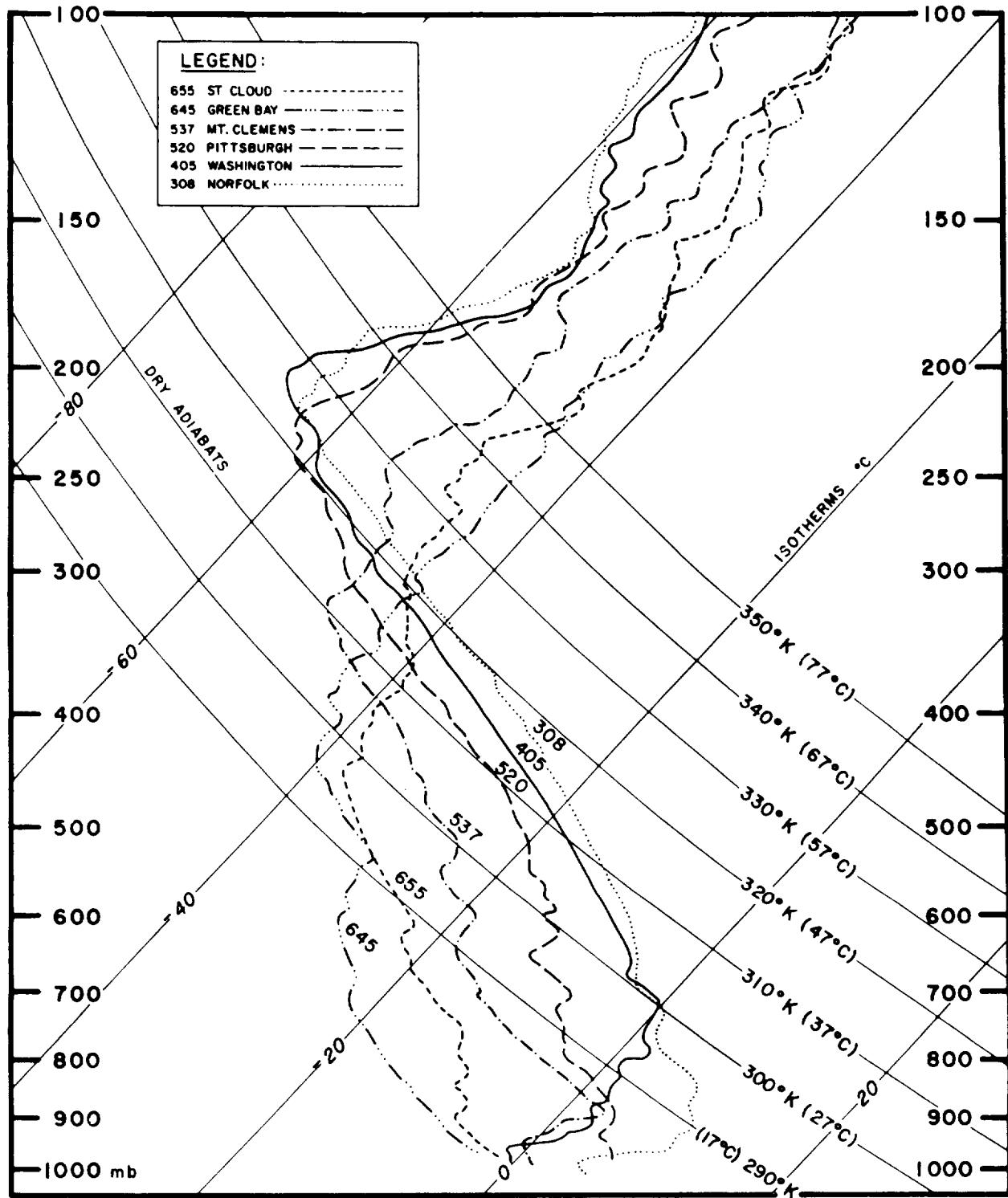
Figure 39. Sounding Curves for Six Stations Along a Line from Bismarck to Cape Hatteras, 1500Z, 29 March 1956 (Danielson [23]).
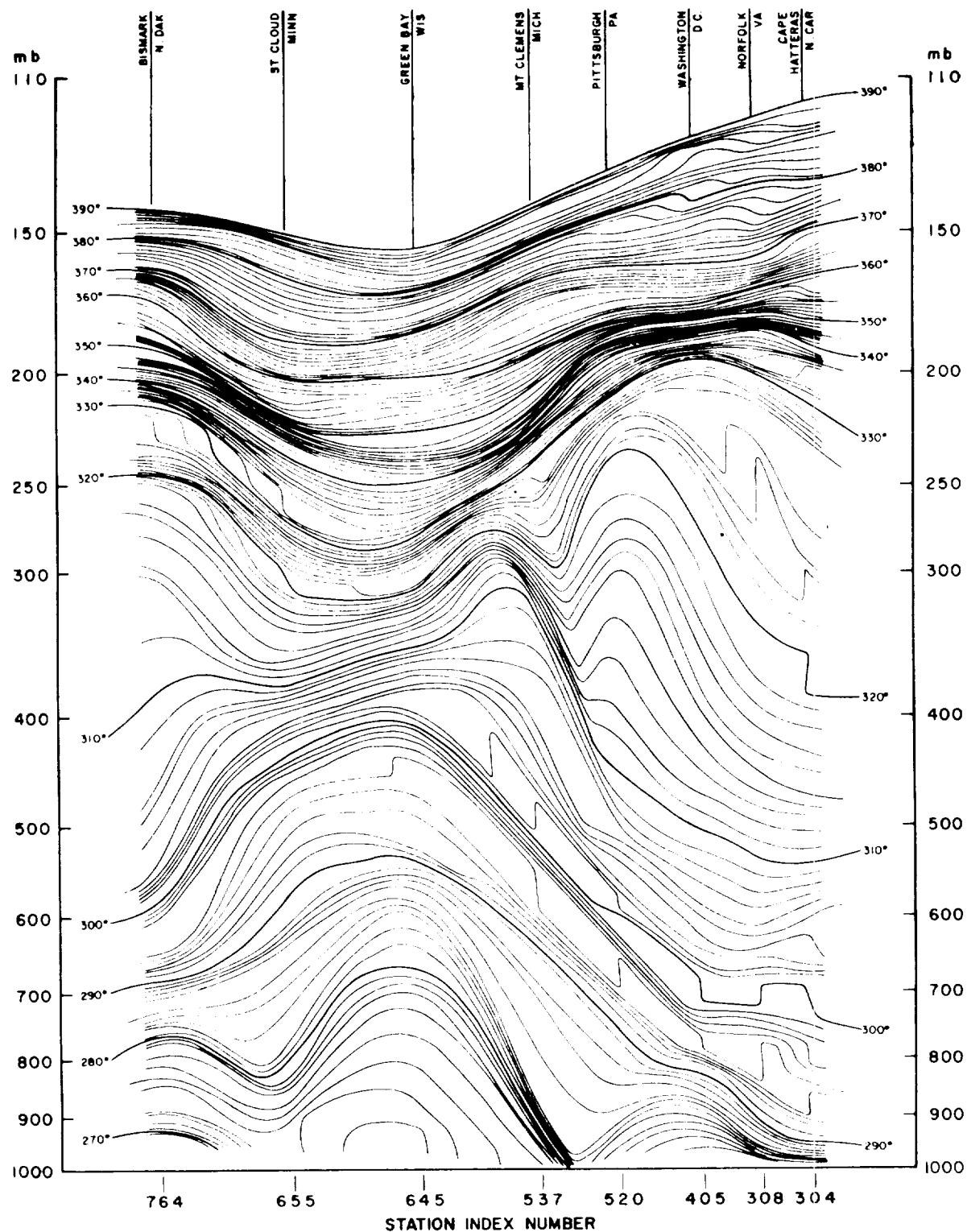
Figure 40. Isentropic Vertical Cross-Section from Bismarck to Cape Hatteras, 1500Z, 29 March 1956. The potential temperature isotherms are drawn for each °K (Danielson [23]).

6—4

spacing of the isentropes on this cross-section anaylsis have been corroborated by the constant-pressure and isentropic charts, trajectory analysis, and use of thermal-wind relationships. Another interesting feature is the continuity of some tropopause "leaves" with discontinuities reaching far down into the troposphere (see par. 6.10.0).

6.5. Radiation Inversions and Layers. Nocturnal and polar radiation inversions are formed when the lowest layers of the atmosphere are cooled by contact with the radiationally-cooled earth's surface (see par. 5.11.2). The depth and lapse rate of the cooled layer will depend on the wind speed, amount of cloud, type of surface, and number of hours of darkness, as well as on the initial temperature difference between the air mass and ground [**63**]. An example of a sounding showing a nocturnal radiation inversion with calm conditions is seen in Figure 41. Wind tends to convert this structure to that of a turbulence inversion (see par. 6.7) which has its base at some level above the ground. All transitions between the two states are commonly observed. Often only a stable ground layer without inversion is found under nocturnal radiation conditions, a "radiation layer" which might be a pre-inversion stage but more probably is a light wind effect.

6.6. Subsidence Inversions and Layers. A subsidence layer is one which has undergone a general sinking. In the lower and middle troposphere, the sinking is manifested by vertical shrinking associated with horizontal divergence, as discussed in paragraph 5.14.6. Since widespread subsidence is directly involved in the creation and maintenance of high-pressure areas, subsidence layers in some degree are evident in nearly all anti-cyclones at some stage of their development. These layers are apt to be deep and pronounced in the so-called "warm highs," both in the tropics and mid-latitudes, in the polar high-pressure caps, and in rapidly equatorward-moving polar air masses ("cold highs").

The most striking feature of a well-developed subsidence layer is the inversion at its base with a strong upward decrease of moisture
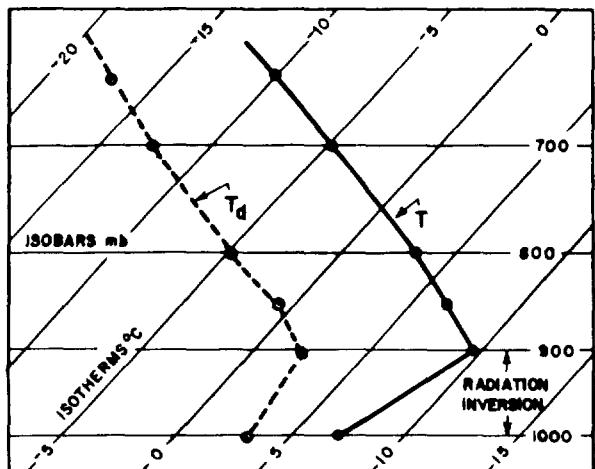

Figure 41. Nocturnal Radiation Inversion (1000 to 900 mb).

through the inversion ("dry inversion") and often continuing a great distance above it, as illustrated in both Figures 42 and 43. Above the discontinuity at the base of the layer (whether an inversion or merely a stabilization) is usually found a rather deep layer of stable, dry air. These features and the location of the sounding station within a high-pressure system are usually sufficient to identify a marked subsidence layer, provided the possibility of confusion with an overlying cold or warm front is carefully eliminated. (The katafront type of cold front can easily be confused with a subsidence inversion; see par. 6.9.1.)

The subsidence layer associated with a subtropical high cell (example in Figure 42) is usually deep and persistent, and over a given portion of the cell, especially in the central and western parts, the height of the inversion base is usually nearly constant. However, the height over a particular point does vary with time, due to the passage of migratory troughs, easterly waves, and the movement of the parent high cell. The subtropical inversion lowers and becomes very strong over the cold waters off the west coast of the continents. In the tropics these inversions are generally known as "trade-wind inversions." However, the term "trade-wind inversion" is also often used colloquially to indicate merely a stable layer associated with a rapid falling off of
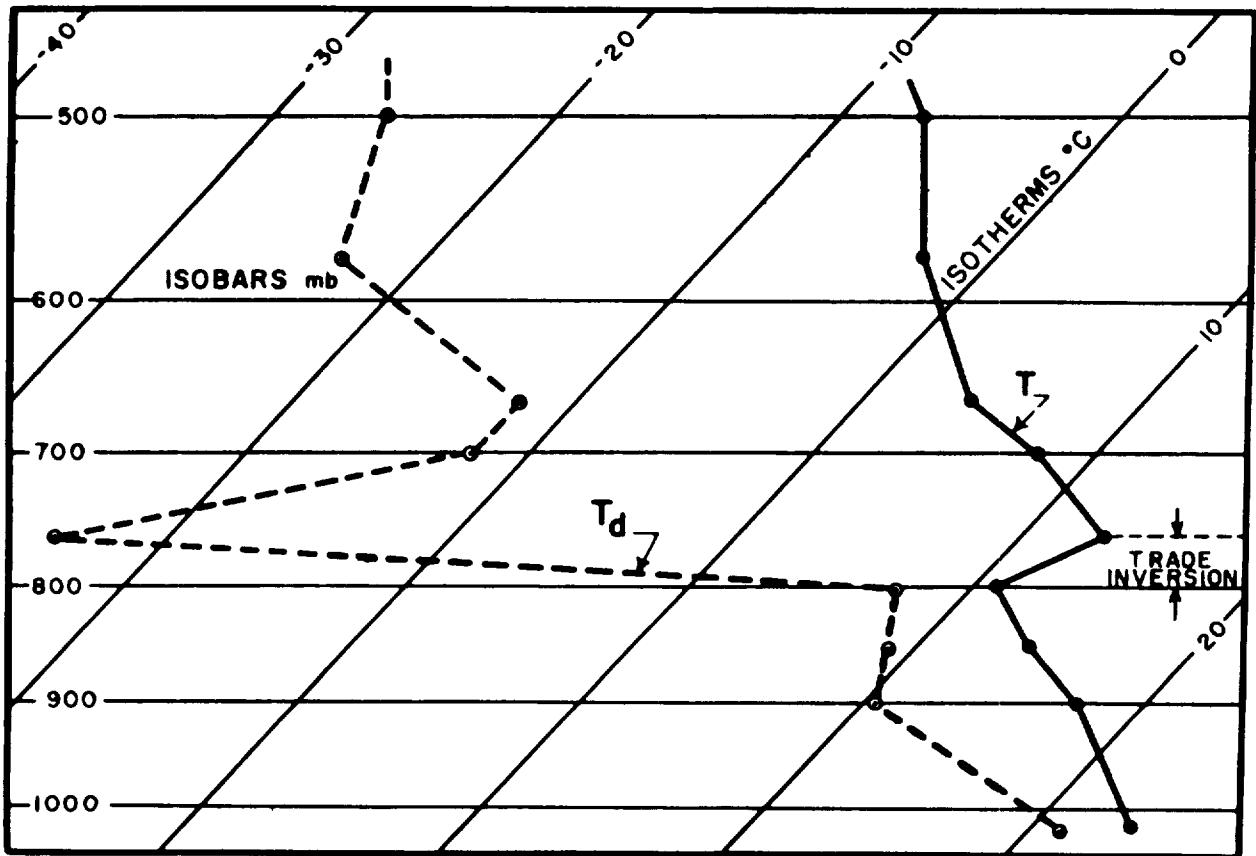
Figure 42. Subsidence ("Trade-Wind") Inversion Over San Juan, Puerto Rico.

moisture with height, rather than actual temperature inversion. The California coastal inversion is an example of a "trade-wind inversion" which persists for long periods in the summer and is removed only by a marked change in the prevailing pressure pattern. Unless the troughs and lows can be forecast, continuity and climatology are the best tools for forecasting the height of subsidence inversions in subtropical highs. (Sources of data on the subtropical inversion are given in [6] [51] and AWS-TR-241).

Figure 43 is an example of a subsidence layer and inversion in a southward moving fresh polar air mass. The surface cold front passed 40 hours previously and is identified in the sounding by the inversion at about 650 mb (see par. 6.9.1).

A subsidence-inversion surface in a large high in the middle latitudes which is under-going conversion from the cold to the warm type is often dome shaped, though the inversion tends to be stronger and lower on the eastern side. Such a subsidence inversion is usually highest over the center of the surface anallobaric (pressure-rise) field. As the high passes over a given station, the inversion base will first be observed to rise and then lower [44].

If it lowers too near the ground, as often happens near the periphery of a high, the inversion is likely to be modified or masked by frontal precipitation and by such surface effects as mixing (turbulence), convection, or radiation. Therefore, in the peripheral region it may be especially difficult to distinguish the subsidence inversion from frontal and turbulence inversions (see pars. 6.7 and 6.9.1).
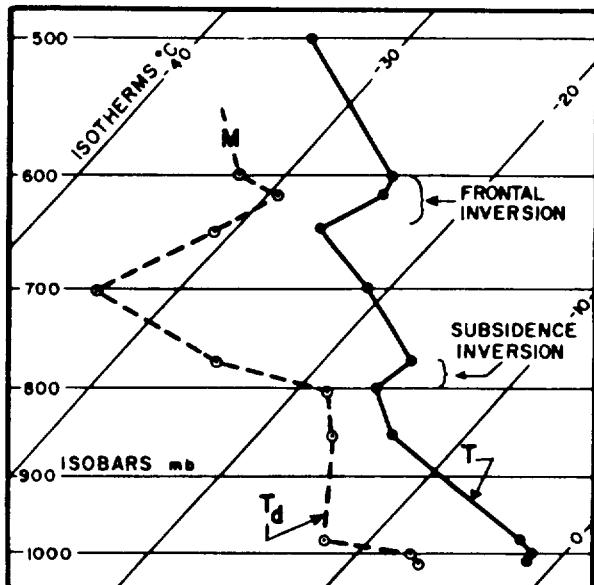
Figure 43. Subsidence Inversion in Polar Air Over Sault Ste. Marie, Michigan.

level mechanical turbulence. As a result, the temperature lapse rate through the layer becomes dry-adiabatic, and an inversion developes at the top of the mixed layer[23] The turbulent mixing also acts to bring the moisture content to a constant value throughout the entire layer. This, in turn, means that the T_d curve for the unsaturated layer becomes parallel to the saturation mixing-ratio lines, that is, the mixing ratio of the turbulently-mixed layer becomes constant with height. The relative humidity is decreased at the bottom and increased at the top of the layer.

The lag in the moisture element on the radiosonde (see pars. 7.5.0 through 7.5.3 and [17]) causes the moisture reported at the top of the mixed layer to be somewhat too low and therefore the plotted T_d curve in such a layer may never actually become completely parallel to the saturation mixing-ratio lines.

If the original moisture content of the mixed layer is sufficiently high and the mixing deep enough, saturation will be reached in the upper portions of the mixed layer. The effect of this process on a sounding is shown in Figure 45. Here the 900- to 850-mb layer becomes saturated as a result of the turbulent mixing of the layer between the surface (1000 mb) and 850 mb.

From a systematic point of view, the decision as to the future formation of a turbulence inversion would revolve around an estimate of the depth of the layer that will mix. The depth estimate depends basically on the expected wind speed, roughness of the underlying terrain, and the original lapse rate in the lower layers. If the overall initial or expected lapse rate indicates only slight stability, turbulent

6.7. Turbulence Inversions and Layers.

The movement of air over an uneven surface causes turbulence and vertical mixing. This mixing, in turn, causes the temperature lapse rate through the mixed layer to change toward the dry adiabatic (or saturation adiabatic if the moisture content and depth of the layer are great enough for the MCL to be reached - see par. 4.21). For an initially stable lapse rate, this means a decrease in temperature at the top of the mixed layer and a temperature increase at its base (i.e., at the surface).

The process is illustrated in Figure 44, which shows how a sounding would be affected by surface-frictional turbulent mixing in the simplest case (no cloud formation, no convergence, evaporation, radiation, nor advection effects).

On this sounding, the layer from the surface to 850 mb has been thoroughly mixed by low-

---

[23]
If the turbulence causing such an inversion is due solely to the roughness of the ground or water surface, the inversion will not be higher than a few thousand feet above the earth's surface. When surface heating becomes an additional factor the inversion may be much higher. High inversions are not known to occur solely as result of turbulence within the "free air," but undoubtedly turbulence helps to accentuate or diffuse some inversions and discontiuities already formed aloft by other processes.
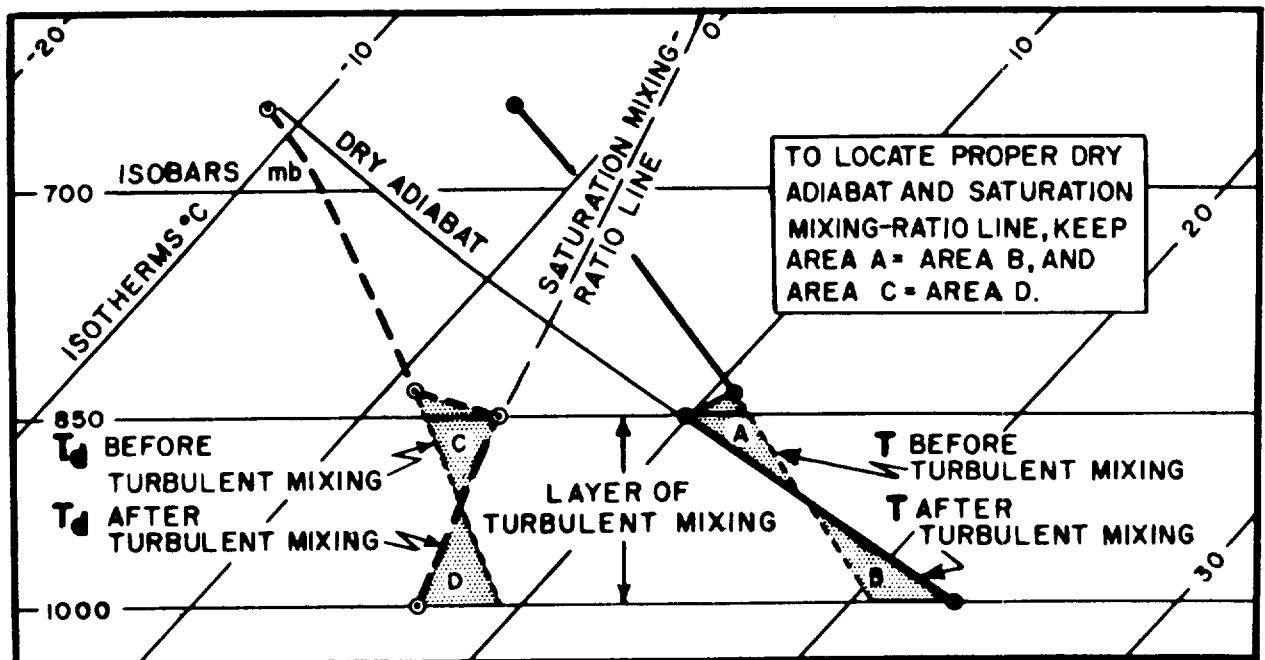
Figure 44. Formation of a Turbulence inversion.
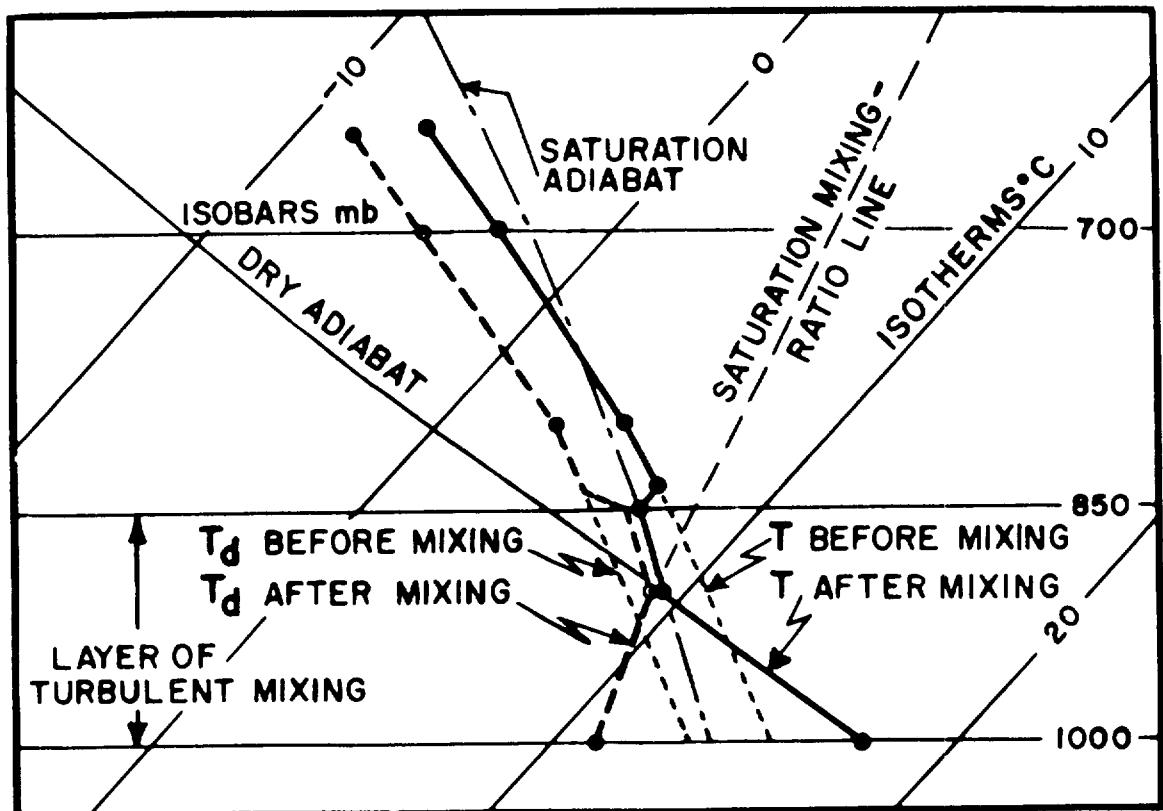
Figure 45. Saturation of a Layer by Turbulent Mixing.

mixing may easily extend to great heights without forming a marked inversion. There are often complicating factors. For example, vigorous cloud formation, convergence, upslope lifting, or additional convection from surface heating, tend to make a deeper mixed layer. On the other hand, divergence or continued radiation cooling tend to make a shallower mixed layer.

In face of these complications, experience is probably the best basis for predicting the depth of the turbulent mixing at any particular station; in this connection it is important to visualize the depth as a function of time, there being an ultimate maximum depth which is approached asymptotically as long as the constellation of factors continues unchanged. Once a first approximation to the expected depth has been estimated, the equal-area method can be used to find the appropriate dry-adiabat and saturation mixing-ratio line. This procedure is illustrated in Figure 44. If these two lines intersect within the layer as shown in Figure 45, the portion of the layer above the intersection is saturated with a lapse rate equal to the saturation adiabatic lapse rate.

The complications mentioned above are due to the fact that turbulent mixing generally occurs in conjunction with various other important atmospheric processes. Typical synoptic combinations are cited by Petterssen [47]. In the common case of warm air moving over cold ground, the mean temperature of the mixed layer gradually decreases and the inversion intensifies and lowers. In cold air moving over a warm surface, the temperature of the mixed layer gradually increases, the inversion weakens and rises, and ultimately may be eliminated.

6.8. Convection Inversions. Often when the troposphere is generally stable with a conditional lapse rate, vigorous dry or moist convection from surface heating or low-level convergence extends well up into the stable region with widespread and continued overshooting (see par. 5.1). The overshooting produces either a slight inversion or more generally a shallow very stable layer just

above or at the top of the convection layer [16]. This effect is difficult to distinguish from effects of subsidence, and in the tropics sometimes the results become identical with low tropopauses [29].

6.9.0. Frontal Surfaces and Zones. The front separates two different air masses [27]. Each air mass has characteristics which were acquired in its source region, but which have been modified through changes caused by vertical motions, surface temperature influences, addition of moisture from evaporation of precipitation falling through the cold air mass, etc.

Frontal zones are often difficult to identify on a plotted sounding. The reasons for this will be brought out in the discussions to follow.

6.9.1. Temperature Characteristics of Frontal Zones. The T curve on the plotted sounding is the basic reference for locating frontal zones aloft. If the front were a sharp discontinuity, the T curve should show a clearcut inversion separating the lapse rates typical of the cold and warm air masses. On the sounding shown in Figure 46, such a frontal inversion is indicated between 700 and 650 mb. However, a shallow isothermal or relatively stable layer (horizontal zone) is the more usual indication of a well-defined front. Frequently, the frontal boundary is so weak, distorted, or confused with other discontinuities, that frontal identification is very uncertain. Some of the conditions responsible for this difficulty are:

a. An air mass is rarely entirely without some internal stratification due to subsidence, shear, turbulence, and advection. This "layering" within an air mass shows up as irregulatities in the temperature sounding (see par. 6.4). The sounding shown in Figure 47 illustrates such minor stratification within an air mass. These effects may combine with others (see below) to create a lapse-rate discontinuity which resembles that of a frontal zone.

b. Vertical motions within the two air masses distort the original temperature contrast across the front, especially in the case of cold fronts. The vertical motion in the air

Figure 46. Frontal Inversion.

Figure 47. Effect of Atmospheric Inhomogeneity on an Otherwise Smooth Lapse Rate [55] .

Figure 48a. Vertical Motion and Clouds Associated with an "Anafront" [25] .

Figure 48b. Temperature Sounding Through an "Anafront."

perature contrast across the front is increased, thus strengthening the frontal discontinuity. Examples of temperature soundings taken through an anafront and through a katafront are shown in Figures 48b and 49b, respectively.

c. The usual subsidence within the southward-moving cold air often creates one or more inversions or discontinuities in lapse rate *below* the frontal inversion (see in Figure 43, the 800- to 770-mb layer). These lower discontinuities can be mistaken for a true frontal zone; also, they may be so close to the frontal zone that only one deep inversion or stable layer is evident. An example of a sounding indicating a frontal layer and a subsidence layer in close proximity is shown in Figure 50. On this sounding, a subsidence layer from 870 to 820 mb is stronger than the frontal layer from 740 to 680 mb. The low T_d values of the 870- to 820-mb layer identify this layer as one caused by subsidence. However, if precipitation were to fall through the layer from above, thus raising the dew point, there might be little or no clear indication of the subsidence origin of the layer.

d. The boundaries of a frontal zone are frequently indistinct because the zone merges gradually into the adjacent air masses. In such cases the T curve changes gradually from a quasi-isothermal lapse rate in the frontal zone to the characteristic lapse rates of the air masses. To determine with assurance which significant point of discontinuity in lapse rate mark the limits of the frontal zones then becomes difficult or impossible. An example of a sounding taken through an indistinct frontal zone is shown in Figure 51. On this sounding, the frontal zone is most clearly evident in the 830- to 780-mb layer, but the exact frontal-zone boundaries (especially the top) are indistinct. In such cases [27] , wind and humidity data, or possibly a temperature comparison with a previous sounding or with a sounding from a nearby station, may help to resolve the problem (see pars. 6.9.2 and 6.9.3). (In practice, the location of fronts should rest more on the analyses of the horizontal-temperature field on the

masses associated with Bergeron's [12] two common types of cold fronts (see also par. 6.9.5) is shown in Figures 48a and 49a. An "anafront," a cold front which produces a widespread band of weather (see Figure 48a), is associated with downslope motion (subsidence and divergence) of the cold air and widespread upslope motion in the overrunning warm air. This process serves to decrease the temperature contrast across the front, thus weakening the frontal discontinuity. However, when condensation (warming) takes place in the warm air mass and there is evaporation of rain falling (cooling) through the cold air, the contrast across the front is likely to be maintained or increased. A "katafront," a cold front which is characterized by a narrow weather band (see Figure 49a), is associated with downslope motion in the warm air over the higher reaches of the frontal surface. The descending warm air mass is warmed adiabatically, and the tem-

6—11

Figure 49a. Vertical Motion and Clouds Associated with a "Katafront" [25].

surface and upper-air charts.) For example, on the sounding shown in Figure 51, the height of the top of the frontal zone could be estimated as most probably 700 mb, although the 640- to 700-mb layer also shows evidence of a temperature gradient from colder air below to warmer air above. If the height of the frontal-zone boundary in question is more clearly defined on a sounding taken at some other not too distant station, the analyst may use the concept of quasi-constant potential temperature along the frontal surface, except in the lower layers; i.e., he may expect the frontal-zone boundaries to be located at or near the same potential-temperature value at both stations.

The lower frontal-zone boundary on the sounding of Figure 51 shows the influence of surface effects; nocturnal radiation had produced a surface inversion, which was being wiped out in the 850- to 1000-mb layer. The remains of the radiation inversion persist and mask the bottom of the frontal zone. Here again, a subjective if not arbitrary judgment is required — the analyst must select the significant point which he believes is most representative of the change from pure air-mass to transition-zone lapse rate. In this case, 860 mb is probably the best estimate because this level separates two layers having
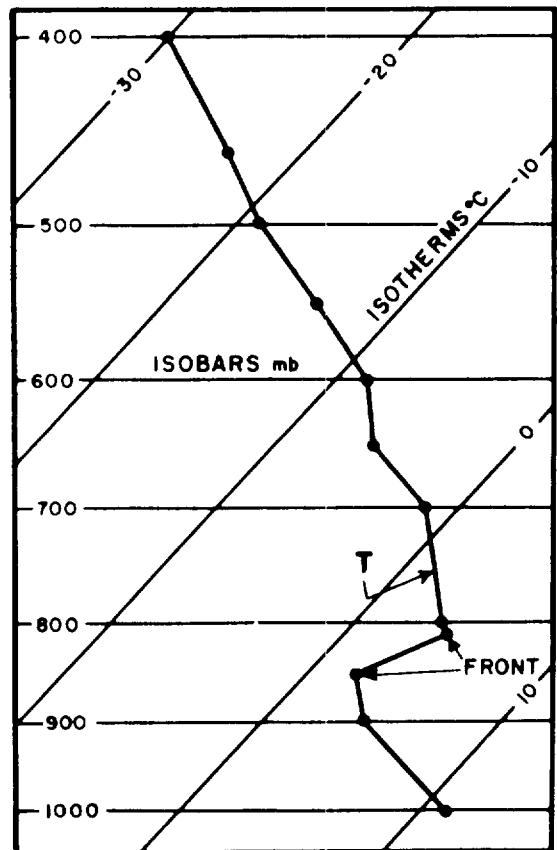
Figure 49b. Temperature Sounding Through a "Katafront."

6— 12
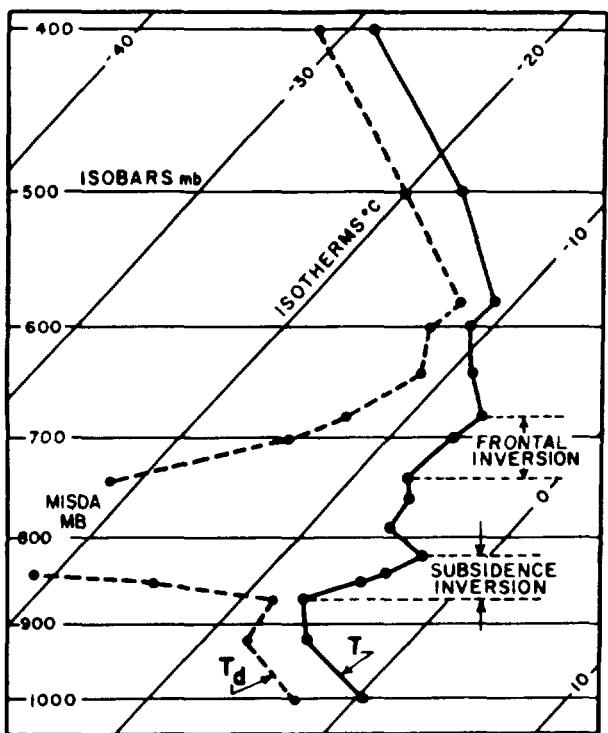
Figure 50. Frontal and Subsidence Inversions.

semi-constant lapse rates, viz., the layers from 950 to 860 mb, and from 860 to 780 mb.

6.9.2. Humidity Characteristics of Frontal Zones.

The relative-humidity curve through a front would, of course, show a saturation or near-saturation where there is a frontal-cloud layer (see Chapter 7), but otherwise there may be no consistent indication of the front in the relative humidity. The mixing ratio, T_d, or T_w curve, however, often has a characteristic behavior. In an ideal case, the T_d curve through the frontal zone will show an inversion or sharp change associated with that of the T curve. On the sounding shown in Figure 52, a dew-point inversion (i.e., increase) is evident between 870 and 790 mb. In this particular case the T_d curve would be a primary aid in locating the frontal zone, since the T curve below 900 mb has been affected by nocturnal radiation to an extent that the location of the frontal inversion on this curve is obscured. Such a marked distribution of humidity through fronts is not

regularly observed, however, because of the following effects:

a. The humidity element of the radiosonde is inaccurate in many respects [17] (see also, *AWS-TR-241* and Chapter 7).

b. The warm air mass may have been dried out, either by subsidence along the frontal slope (see Figure 49a), or by a trajectory past an upstream ridge. The cold air may then show T_d values higher than those of the warm air.

c. The underlying cold air often acquires moisture rapidly through evaporation from a water surface, such as the Great Lakes, and also through evaporation from wet ground or of rain falling from the warm air mass above.

However, these effects usually do not obscure all the more marked differences between frontal inversions and subsidence inversions (see Figure 50).

Sawyer [56], in a study of humidity data obtained on 23 Meteorological Research Flights through fronts over England, found that usually a characteristic tongue of relatively dry air was associated with many of the frontal zones. The dry zone extended downward in the vicinity of the fronts and was tilted in the same direction as the front. An example of this phenomenon is shown in Figure 53, which represents a cross-section of a front observed on one of the flights. The dry zone is indicated by the dew-point-depression maximum just above 600 mb.

The dry zone was less well developed with cold fronts than with warm fronts, and extended down to an average pressure of 700 mb in cold fronts and to 800 mb in warm fronts. In about half of the fronts, the driest air was found within the frontal transition zone itself, but there were also occasions when dry air was found on both the cold and the warm sides of the transition zone. Striking changes of frost point were observed as the aircraft entered the dry zone; about half of the flights showed a sharp transition from moist to dry
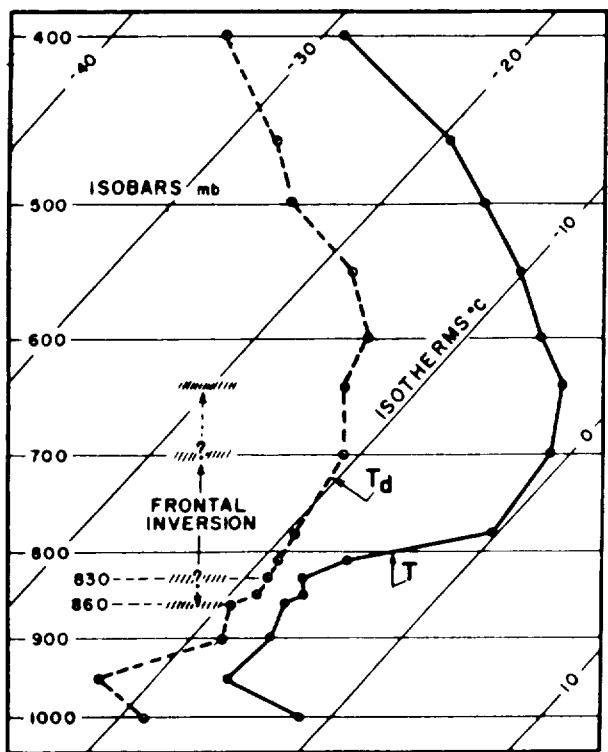
Figure 51. Sounding Showing Indistinct Frontal-Zone Boundaries.

air, with an average frost-point change of about 37°F in 35 miles horizontal distance. Some of the sharpest changes were more than 40°F in 20 miles.

6.9.3. Wind Variations Through Frontal Zones. Because the analysis of the vertical-wind profile through the front is an important and often necessary adjunct to raob analysis in locating fronts, it is desirable to discuss the subject here.

The classical picture of the variation of the wind along a vertical through a frontal zone is shown in Figure 54. Through a cold front, the wind backs with height; through a warm front, the wind veers with height. On the Skew-T Chart shown in Figure 55, the plotted upper winds (above the surface layer) which show the greatest variation are those for the 800- to 650-mb layer. This indication coincides closely with the frontal indications of the T and T_d curves. Since the wind veers

with height through the layer, the front would be of the warm type.

6.9.4. Thermal-Wind Indications of Frontal Zones. The magnitude of the thermal wind for a layer indicates the strength of the horizontal gradient of the mean temperature of the layer. Since a frontal zone defines a layer of maximum horizontal thermal gradient, it also represents a zone of maximum thermal wind. Furthermore, since the thermal wind blows parallel to the mean-temperature isotherms for the layer (with cold air to the left), the direction of the thermal wind vector will be roughly representative of the directional orientation of the front. The winds-aloft for the sounding shown in Figure 55 are seen plotted as a hodograph in Figure 56. The thermal wind is indicated by the shear vector connecting the wind vectors for the base and top of each layer.

The maximum thermal wind is found between 700 and 650 mb, supporting the previous frontal indications described in paragraph 6.9.3, above. The direction of the thermal wind vectors from 800 to 650 mb is roughly north-south; the frontal zone could thus be assumed to be oriented along a generally north-south line.

6.9.5. Wind Distribution as an indicator of the Dynamical Characteristics of Cold Fronts. Sansom [53], in an investigation of cold fronts over the British Isles, found a definite relationship between the variation of wind with height through a cold frontal zone and the weather characteristics associated with the front at the surface. He classified most of the cold fronts into Bergeron's two types (the lapse-rate indications for which were noted in par. 6.9.1), and listed the definitive upper-wind characteristics of each.

a. *Anafronts* are associated with widespread, heavy rain at the time of frontal passage, and with steady rain continuing for some time behind the front. The cloudiness resembles that of a warm front in reverse and clears slowly after frontal passage. Upper-wind variations through an anafront are as follows:
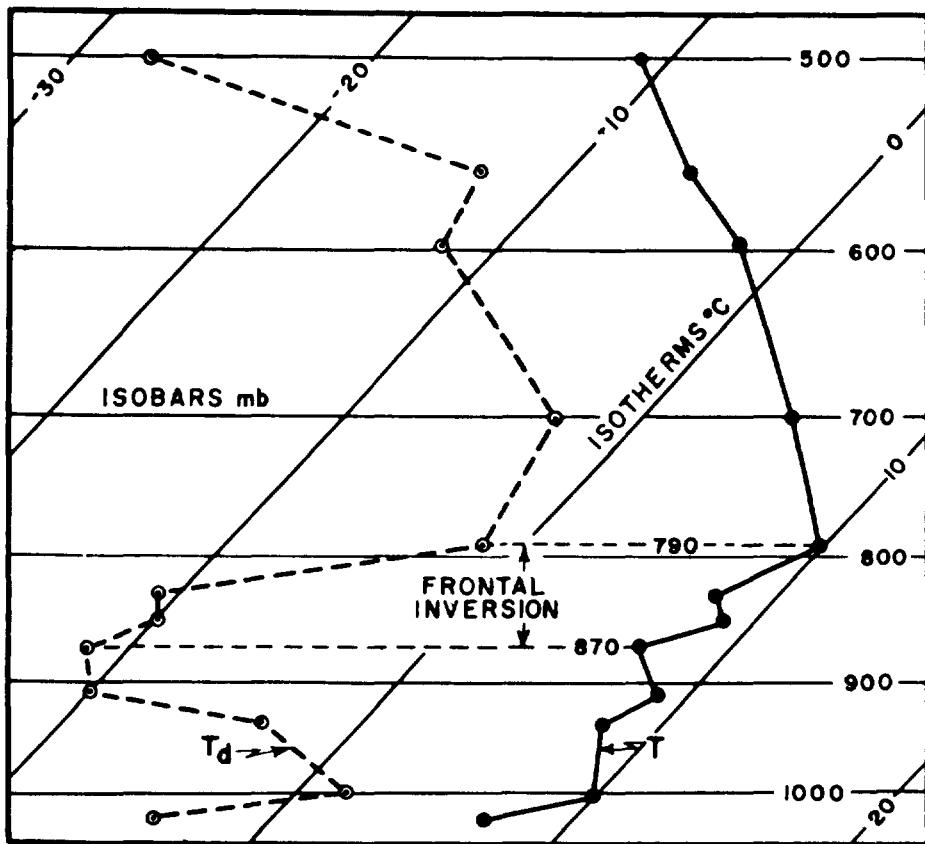
Figure 52. Frontal-Zone Indications from the Dew-Point Curve.

(1) Rapid backing of the wind with height (about 65 degrees between 950 and 400 mb); at 500 mb, the wind direction is inclined at a small angle (about 15 degrees) to the front.

(2) The wind component normal to the front decreases slightly with height, while the component parallel to the front increases rapidly. The mean speed of the front exceeds the wind component normal to the fronts, although the excess is insignificant below 800 mb.

(3) The thermal wind between 950 and 400 mb is almost parallel to the front.

b. *Katafronts* are associated with light, short-period precipitation and rapid clearing after frontal passage. The upper-wind variation through a katafront is as follows:

(1) Slight backing of the wind with height (about 20 degrees between 950 and 400 mb); at 500 mb, the wind direction is inclined at an average angle of about 42 degrees to the front.

(2) The wind components normal and parallel to the front both increase with height.

The wind component normal to the front exceeds the mean speed of the front at all levels above the lowest layers.

(3) The thermal wind between 950 and 400 mb is inclined at an average angle of about 30 degrees to the front.

The cold fronts which Sansom listed as "unclassified" were found to have upper-wind characteristics intermediate between those of anafront and katafronts. The wind component normal to the unclassified front was almost constant with height.

Sansom also investigated the vertical variation of the wind 50 to 150 miles ahead of the cold front; i.e., in the warm sector. He found little change of wind direction with height, but the angle between the warm-sector winds aloft and the surface fronts differed for anafronts
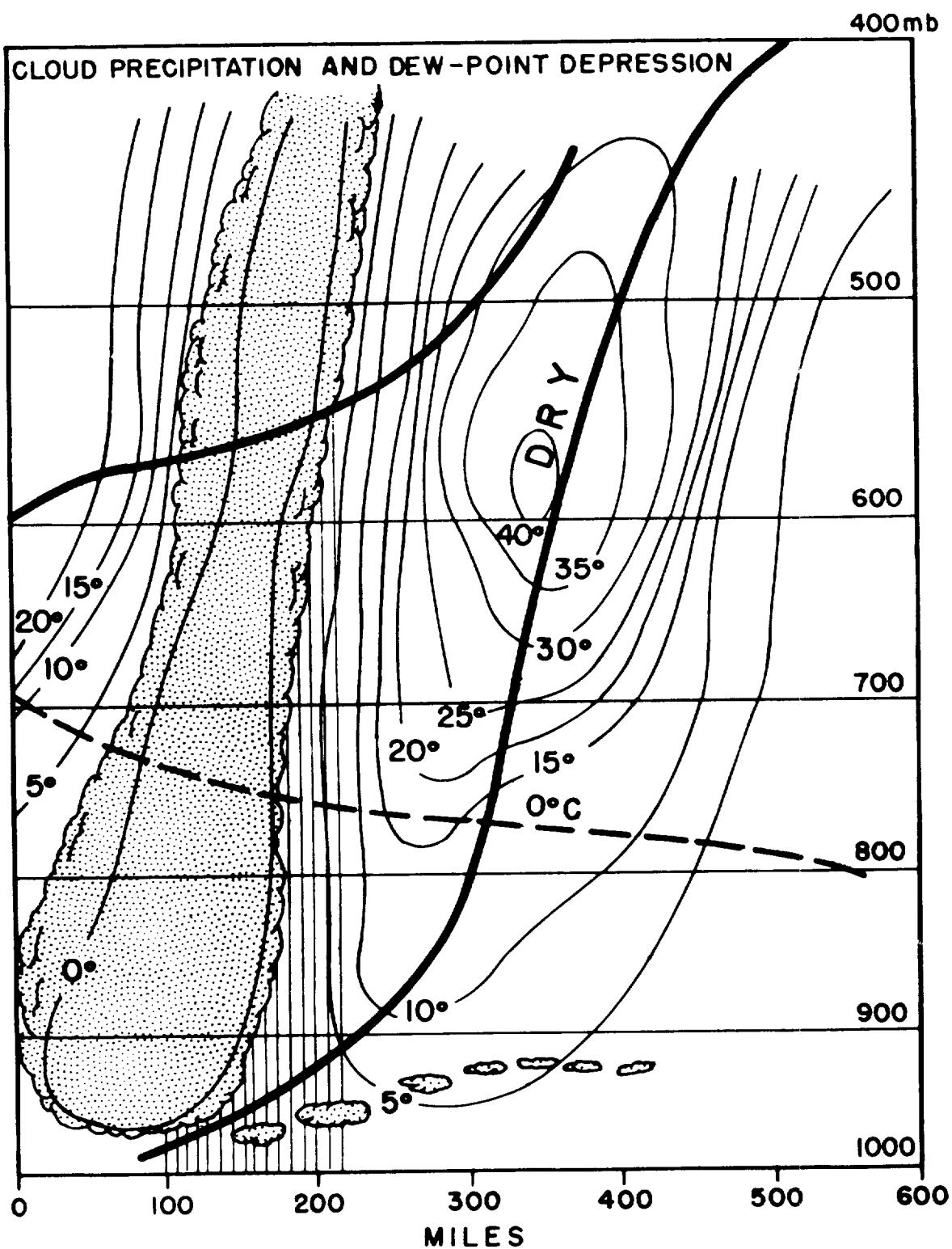
Figure 53. Vertical Cross-Section (Sawyer [56]) Indicating the Dry Tongue in a Warm-Frontal Zone. Cross-section is approximately normal to the front. Thick solid lines are boundaries of the frontal zone. Thin solid lines are isopleths of dew-point depression in °C. Shaded area indicates main features of the frontal cloud. Vertical hatching indicates precipitation outside of the cloud.
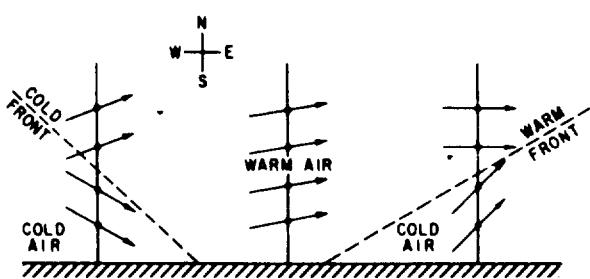
Figure 54. Vertical Distributions of Wind Direction in the Vicinity of Frontal Surfaces

and katafronts. The average angles between the surface fronts and the associated warm-sector winds at 700 and 500 mb are shown in Table 2.

TABLE 2

Angle between the Cold Front at the Surface and the Wind Direction in the Warm Sector.

	Anafront	Katafront
700 mb	18°	35°
500 mb	17°	35°
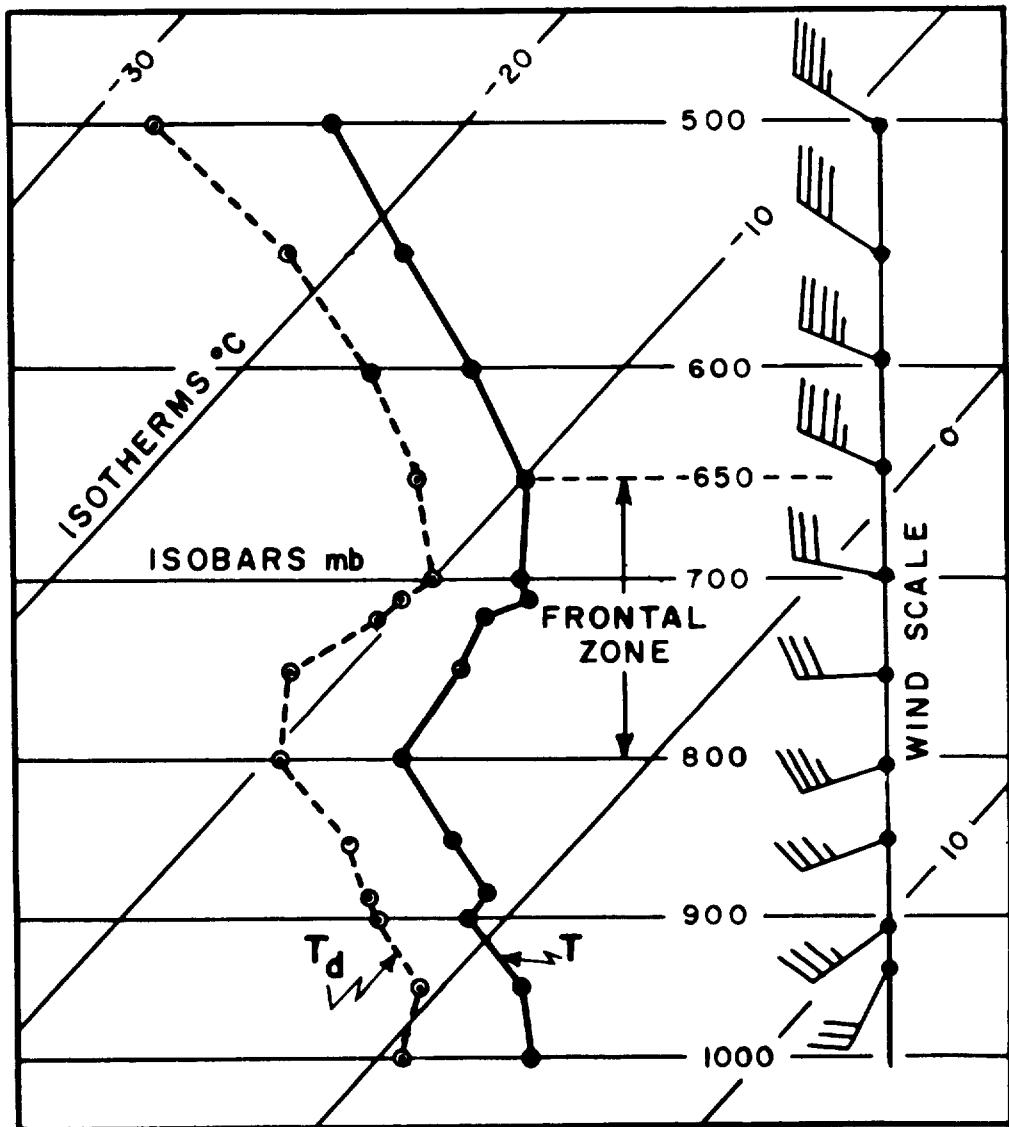
Figure 55. Distribution of Wind and Temperature Through a Frontal Zone.
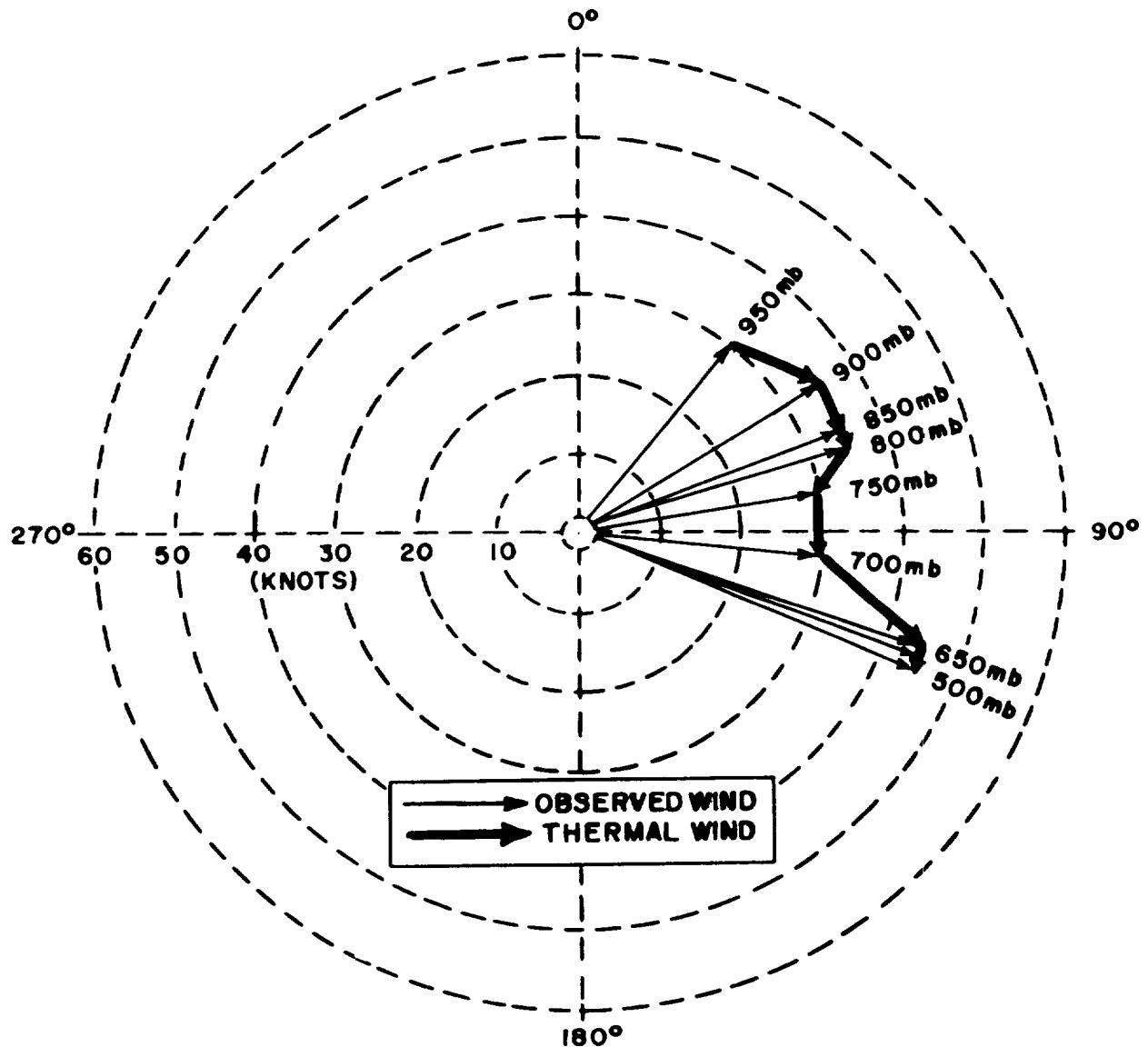
Figure 56. Hodograph of Observed and Thermal Winds for Sounding of Figure 55.

6.10.0. Tropopauses. Although the concept of a tropopause has been generally accepted for many years, there is still no agreement on how to apply the concept to synoptic analysis. Historically, the word was coined when the stratosphere was discovered, to describe the apparent "boundary" which separated the troposphere from the stratosphere. The scattered early soundings led meteorologists to believe that the tropopause was a single unbroken discontinuity surface, but later observations suggested that probably it is a varying transitional zone, often with several layers separated by overlapping discontinuities ("multiple tropopauses"). In any case, until recently it was generally assumed that the tropopause largely suppresses transfer of heat, air, or water vapor between the troposphere and stratosphere. However, with the large number of

soundings now reaching the stratosphere each day, it becomes possible to see [7] [23] that through the tropopause "breaks" quasi-horizontal air flow passes freely between the troposphere and stratosphere. An example can be seen in Figure 40.

There are many soundings on which the locating of a generally acceptable tropopause is very easy. These cases include those where a single strong inversion or marked stabilization of the lapse rate occurs. However, there are many other soundings where it is quite difficult to determine where the troposphere ends and the stratosphere begins. In these cases, the lapse rate may just gradually become more stable without any prominent sudden stabilization of the lapse rate with height, or there may be more than one point of stabilization; then it becomes a controversial problem to decide which point should locate the tropopause. The variation in structure in the tropopause region has led to many different ideas on how to define and analyze a tropopause. It has also been proposed to analyze a "tropopause layer" which would arbitrarily include the zone encompassing the various tropopauses occurring over a given area at a given time [1]; but this does not appear to be of practical value in operational forecasting. The conflict between the definitions officially advocated or used in different countries was finally compromised by the WMO who have standardized an arbitrary definition of the tropopause for operational use in internationally-exchanged uper-air sounding reports.

The present WMO definition does not attempt to settle the question as to what the tropopause is, which remains controversial. It defines, rather, an objective technique for locating the lowest height in the atmosphere where the lapse rate first decreases to an average lapse rate of 2°C/km for a two-kilometer layer. While the physical significance of this lowest height remains to be found, it does establish an international reference height to which other atmospheric phenomena can be empirically related. The main advantage is that the definition is objective, in that it allows the same height to be consistently selected by all technicians from a given sounding.

Various empirical and statistical relationships [34] [43] have been prepared in the past relating such things as the height of cirrus or the maximum wind to the height of the tropopause. These studies have probably been prepared using a more or less different definition of the tropopause than the WMO one. Before continuing to use these relationships, the difference(s) between the tropopause definition used and the current WMO definition should be determined to make certain that the relationships are still sufficiently valid when referred to tropopauses now being determined by the WMO definition.

6.10.1. WMO Tropopause Definition. As noted above, objective criteria for determining the tropopause height(s) transmitted in upper-air observations have been internationally standardized by the WMO. Within its definition, provision is made for identifying two or more tropopauses on a sounding. The WMO definition for the tropopause is as follows:

a. The "first tropopause" is defined as the lowest height at which the lapse rate[24] decreases to 2°C/km or less, provided also that the average lapse rate[25] between this height and all higher altitudes[26] within two

_____

[24]The *lapse rate* is the rate of decrease of temperature with height.

[25]The *average lapse rate* is the difference between the temperatures at the respective end points divided by the height interval, irrespective of the lapse-rate variations in the layer between the end points.

[26]All higher altitudes means that no point on the sounding in the two- (one-) kilometer interval above the "lowest height" can fall to the left of the 2° C/km (3°C/km) line extending from the "lowest height."

kilometers does not exceed 2°C/km. This tropopause will be termed the *conventional tropopause*.

b. If above the first tropopause the average lapse rate between any height and all higher altitudes[26] within a one-kilometer interval exceeds 3°C/km, then another tropopause is defined by the same criteria as under "a" above. This second tropopause may be either within or above the one-kilometer layer. There is no specific name given to this second tropopause nor to still higher tropopauses.

c. There are three qualifying r e m a r k s attached to the definition. They are:

(1) Whenever the sounding terminates at less than two kilometers above the altitude which otherwise appears to be a tropopause, the ascent is classified as *tropopause not defined*. This applies to both the conventional and the higher tropopause determinations.

(2) A height below the 500-mb surface will not be designated as a tropopause unless it is the *only* height satisfying the definition, and the average lapse rate in any higher layer fails to exceed 3°C/km over at least a one-kilometer layer. Further, the sounding must reach at least the 200-mb pressure surface. (The intention here is to admit that a discontinuity in the lapse rate at a height below the 500-mb surface is a tropopause only if it is reasonably certain that no other choice is possible.)

(3) When determining the s e c o n d or h i g h e r tropopauses, the one-kilometer interval with an average lapse rate of 3°C/km can occur at *any* height above the conventional tropopause and not only at a height more than two kilometers above the conventional tropopause.

Figure 57 illustrates how to apply the WMO tropopause definition to a sounding. The conventional tropopause is defined by criterion "a" of the definition. This criterion is satisfied above Point B of Figure 57. That is, the average lapse rate between Points B and D, the next two higher kilometers above Point B, is less than 2°C/km for all points of the two-

kilometer lapse rate (see Footnote 26). Thus, the conventional tropopause is established at Point B of the sounding.

T h e r e also is a possibility of a "second" tropopause at Point D. To find out, criterion "b" is used. This criterion requires a one-kilometer layer with a lapse rate greater than 3°C/km below the second tropopause height. This requirement is met through the layer CD, and in this particular case, qualifying remark "c(3)" applies also. When criterion "b" is met, then criterion "a" is again used to determine the location of a higher tropopause. Above Point D, the lapse rate DE again decreases to less than 2°C/km for the next two higher kilometers. Thus, a second tropopause is determined at Point D.

6.10.2. Character of the Tropopause.
A special code for the character of the tropopause (symbol S_t) has also been adopted by the WMO to help describe the tropopause more completely. This code is described in Table 3.

The following remarks are needed to help decide w h i c h code figure to select when describing any given tropopause:

a. All lapse rates should be determined over a one-kilometer interval when using the criteria in the table.

b. If the conventional tropopause does not coincide with any marked change in lapse rate and a marked change of lapse rate occurs at heights both above and below the conventional tropopause, then the larger of these changes should be used to determine whether code figure 5 or 6 is appropriate.

c. W h e n the conventional tropopause is best characterized by code figure 6 in arctic and antarctic regions in winter, a special case exists. Then the height of the marked change in lapse rate below the conventional tropopause should be referred to as an "arctic" or "antarctic" tropopause and recorded as such.
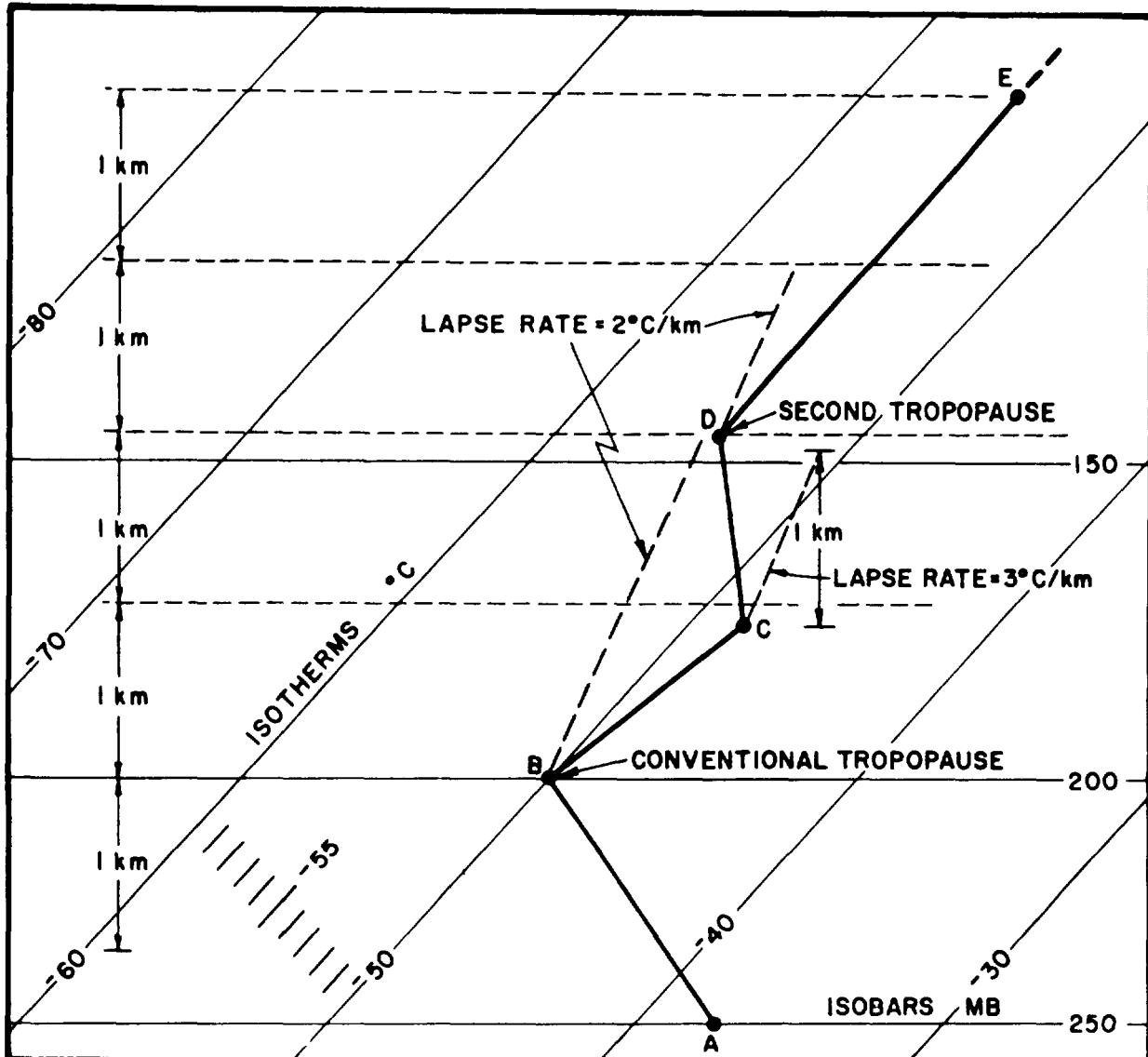
Figure 57. Tropopause Determinations Based on the WMO Definition.

This is done when there is not a one-kilometer interval between the "conventional" and "arctic" or "antarctic" tropopauses where the lapse rate exceeds 3°C/km.

If this occurs, the character of the "arctic" or "antarctic" tropopause should be given by code figure 9.
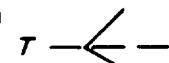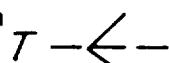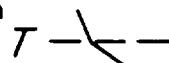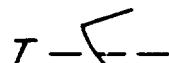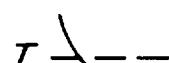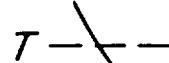
It is suggested that whenever a character of a conventional tropopause is given as code figure 5 through 9, the sounding be plotted and interpreted according to the use to be

made of the tropopause information. In some cases it may well be that a tropopause with such a characteristic has no operational significance.

The determination of the character of the tropopause is rather straightforward. For example, in Figure 57 the character of the conventional tropopause at Point B is established by noting the lapse rate for the one-kilometer layer above and below it. Above Point B, the lapse rate is less than 0°C for a one-kilometer layer, while below Point B

6—21

TABLE 3

S_t- CHARACTER OF THE TROPOPAUSE

CODE FIGURE		CODE FIGURE DESCRIPTION	
1.	CONVENTIONAL TROPOPAUSE COINCIDES WITH A MARKED CHANGE IN LAPSE RATE	LAPSE RATE ABOVE TROPOPAUSE $\leqslant$ 0°C/km LAPSE RATE BELOW TROPOPAUSE $\geqslant$ 5°C/km	T —< —
2.		LAPSE RATE ABOVE TROPOPAUSE $>$ 0°C/km LAPSE RATE BELOW TROPOPAUSE $\geqslant$ 5°C/km	T —< —
3.		LAPSE RATE ABOVE TROPOPAUSE $\leqslant$ 0°C/km LAPSE RATE BELOW TROPOPAUSE $<$ 5°C/km	T —< —
4.		LAPSE RATE ABOVE TROPOPAUSE $>$ 0°C/km LAPE RATE BELOW TROPOPAUSE $<$ 5°C/km	T —< —
5.	CONVENTIONAL TROPOPAUSE DOES NOT COINCIDE WITH ANY MARKED CHANGE IN LAPSE RATE	BUT A MARKED CHANGE IN LAPSE RATE $>$ 3°C/km OCCURS AT A HEIGHT ABOVE THE CONVENTIONAL TROPOPAUSE	T —< —
6.		BUT A MARKED CHANGE IN LAPSE RATE $>$ 3°C/km OCCURS AT A HEIGHT BELOW THE CONVENTIONAL TROPOPAUSE;	T —< —
7.		AND NO MARKED CHANGE OF LAPSE RATE $>$ 3°C/km OCCURS AT ANY OTHER HEIGHT.	T —< —

8. HEIGHT OF TROPOPAUSE UNCERTAIN BECAUSE TOP OF ASCENT IS LESS THAN 2 km ABOVE THE HEIGHT WHICH APPEARS TO BE THE TROPOPAUSE.

9. TROPOPAUSE IS NOT ALLOCATED TO ANY OF PRECEDING CATEGORIES.

the lapse rate is greater than 5°C for a one-kilometer layer. Thus, the character of the conventional tropopause is properly described by code figure 1 of the table.

.

ANALYSIS OF CLOUDS WITH AID OF RAOBS

7.1. Why the Raob is Important in Routine Synoptic Cloud Analysis. The cloud observations regularly available to forecasters in surface synoptic reports leave much to be desired as a basis for cloud forecasting. Some of their limitations may be noted:

a. Middle and high clouds are usually only observed and reported when visible from the ground. No heights are given in the synoptic reports, nor are amounts specifically reported, though they may sometimes be estimated from the amounts of low cloud and total cloud cover. In hourly reports, heights and amounts are sometimes estimated or obtained from aircraft.

b. At nighttime, reports of middle and high clouds (height, amount, and type) are less reliable than in daytime.

c. Cloud systems which have portions extending above 15,000 feet are usually associated with frontal systems and/or mid-tropospheric troughs and lows. Their central portions frequently have precipitation falling out of them, accompanied by abundant low clouds; here we usually get no direct information about how high the clouds extend. Only in the fringe area of the cloud systems, where the middle and high clouds often extend beyond the low clouds, are the middle and high clouds directly accessible to observation from the ground.

d. Tops of convective clouds are not reported either, except from a casual aircraft or radar observation. However, from the types of clouds reported and from the type and intensity of the precipitation falling from them, a rough estimate of tops can be obtained in many cases. Knowledge of the local or regional weather regime is important, of course, for this estimate. For example,

typical cumulus congestus at 60°N in wintertime may have a vertical extent of 6000 to 8000 feet; in the tropics, of 15,000 to 20,000 feet. Radar reports in the neighborhood often permit a close determination of the tops of convective clouds. Aircraft reports, particularly from aircraft flying in the middle levels are the most reliable.

e. CPS-9 and other radar installations can provide much useful information, particularly on the height of convective cloud, but the radar echo does not necessarily indicate the extent of the visible cloud. (See AWS TR 184.)

Radiosondes which penetrate cloud-systems reflect to some extent (primarily in the humidity trace) the vertical distribution of clouds. If the humidity element were perfect, there would usually be no difficulties in locating cloud layers penetrated by the sonde. Because of shortcomings in the instrument, however, the relationship between indicated humidity and cloud is far from definite, and an empirical interpretation is necessary. Nevertheless, radiosonde reports give valuable evidence which, when sifted with other available information, aids greatly in determining a coherent picture at least of

stratiform and frontal cloud distributions. Their value in judging air-mass cumulus and cumulonimbus distribution is negligible, however.

7.2.0 Frontal Cloud Structure.
A wealth of experience regarding cloud structures of fronts has been collected by meteorologists engaged in aviation forecasting, mainly through debriefing of flight crews. Very little of this experience has been summarized and presented in the form of scientific papers, although the consensus appears to be that frontal cloud is usually layered, that the high cloud is usually detached from the middle cloud, and that middle cloud is often well layered and many times does not extend very high [19] .

Only a few papers contain any statistical summaries which allow an assessment of a "typical" cloud structure with respect to features such as the type of front, distance from the depression center, and geographical area. Some of these papers [41] [42] [56] [57] are discussed in succeeding paragraphs.

Sawyer [56] investigated the cloud structure of 23 fronts over England or vicinity, based on data from the Meteorological Research Flight. He found that the cloud structure is variable. The main frontal cloud masses were usually formed within the warm air mass and extended into the transition zone by evaporation and recondensation of rain or snow. An example of such a situation is shown in Figure 53 and Figures 58a and 58b. The cross-section in Figure 53 shows the cloud mass of the warm front tilting much more steeply than the frontal zone. The thick frontal cloud does not extend much beyond the forward edge of the precipitation area at the surface. Ahead of the precipitation area at the surface, the frontal zone above 800 mb to 700 mb is very dry. These are features found in many fronts, particularly warm fronts.

7.2.1. Warm Fronts.
The probability of encountering cloud at any point in the region of an active warm front is shown in Figure 59, which is based on data published by Sawyer and Dinsdale [57]. The frequencies of cloud occurrence were based on 69 active warm fronts over Southern England. (An active warm front was defined as one having a rain belt at least 50 miles wide. The dimensions and slope of the schematic frontal zone were based on average values for the sample.) We notice again that the "ridge" in the probability pattern, coinciding with the locations of highest incidence of cloud, slopes upwards to the right more steeply than the frontal zone. Again, we notice that the frontal zone above about 10,000 feet is relatively cloud-free.

The authors [57] attempted to correlate the thickness of the cloud mass in active warm fronts with the following quantities:

  a. Slope of warm boundary.
  b. Thickness of frontal zone.
  c. Horizontal gradient of potential wet-bulb temperature.
  d. Change of geostrophic wind across the surface front.
  e. Six-hour change of parameter "d".
  f. Change (across the front) of wind component parallel to surface front.
  g. Change (across the front) of wind component normal to surface front.

Parameters "a" through "f" showed no correlation with frontal cloud but "g" gave a slight correlation, $r = 0.16$.

7.2.2. Cold Fronts.
Cold fronts appear to be just as elusive as warm fronts when it comes to "pinning down" the weather activity at the front by parameters that would characterize the front on the synoptic chart (other than the weather itself).

Austin and Blackmer [5] investigated by radar the precipitation patterns associated with warm-season cold fronts passing Boston, Mass., (30 cases). The fronts were divided into four main types, primarily according to their orientation. Other characteristics chosen to describe the fronts synoptically were:

  a. 700-mb temperature contrast across the front.
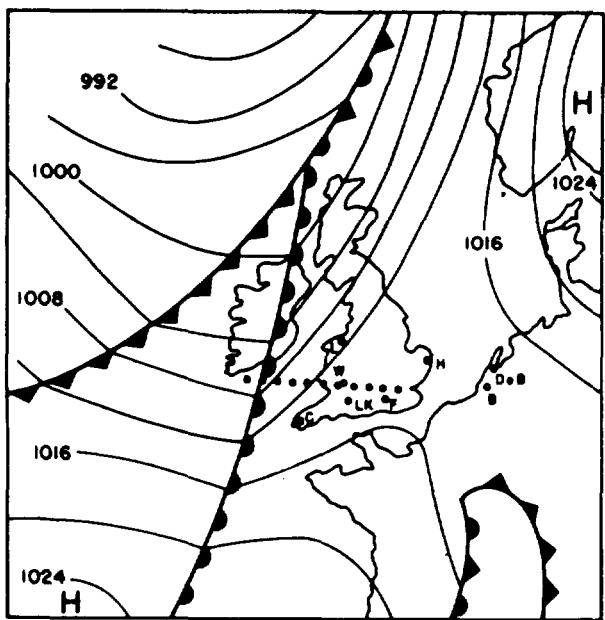
Figure 58b. 500-mb Chart, 1500 GMT, 19 March 1952.

b. Algebraic difference between 2-hour sea-level pressure tendencies before and after frontal passage.

c. 700-mb wind speed and direction immediately ahead of a front.

d. Stability of the warm air (850-mb temperature minus 500-mb temperature).

e. Potential stability of the warm air (850-mb minus 500-mb wet-bulb potential temperature).

f. 850-mb dew-point depression in the warm air.

g. Thermal advection, expressed as $k \cdot V_{500 \text{ mb}} \times V_{850 \text{ mb}}$, where k is the vertical unit vector in the warm air.

Neither the orientation classification nor the seven parameters listed above showed any significant relationship to the areal extent of the precipitation.

The precipitation areas, as they appeared on the radar scope, could be described as having three different structures: Isolated showers, bands, or masses. The distribution of these structures with respect to the front is given in Table 4. The highest frequency (23 out of 30 cases) is attached to "no postfrontal precipitation." The next highest is attached to "frontal and prefrontal bands of precipitation." Table 4 confirms the classical picture of the cloudiness extending in bands along or ahead of the cold front and usually breaking up behind the cold front, but it also points out that isolated showers occur nearly as frequently at, ahead of, and behind the front. The absence of postfrontal bands is particularly significant.

Table 5 gives the frequency of occurrence of precipitation as prefrontal, frontal, postfrontal, or combinations thereof, irrespective of structure. We notice the high incidence (30%) of frontal and prefrontal precipitation.

This study stresses the need for considering each cold front individually and finding its characteristics as revealed by the surface observations (clouds, precipitation) and

TABLE 4

Structure of Precipitation Areas Associated with April–September Cold Fronts Near Boston, Mass.

	Number of Cases			
	Frontal	Prefrontal	Postfrontal	Total
Bands	13	9	0	22
Masses	4	6	3	13
Showers	5	8	4	17
None	8	7	23	--
Total	30	30	30	--

TABLE 5

Percentage of Cold Fronts with Specific Precipitation Distribution (irrespective of structure), 30 Fronts, April–September, Boston, Mass.

	Percentage
Frontal Only	13
Prefrontal Only	23
Postfrontal Only	3
Frontal and Prefrontal	30
Frontal and Postfrontal	13
Prefrontal and Postfrontal	7
Frontal, Prefrontal, and Postfrontal	10

raobs, rather than forming a stereotyped picture of weather associated with the blue line on the chart. It is evident that the raobs spaced at 100 to 200 miles can easily give a misleading impression as to the cold-frontal cloud distribution, depending on whether the raobs happened to penetrate a band or cell or a "thin" area.

7.2.3. The Humidity Field in the Vicinity of Frontal Clouds. Figure 53 shows a tongue of dry air extending downward in the vicinity of the front and tilted in the same direction as the front. Sawyer [56] found that such a dry tongue was more or less well developed for all the frontal regions he investigated. This dry tongue was best developed near
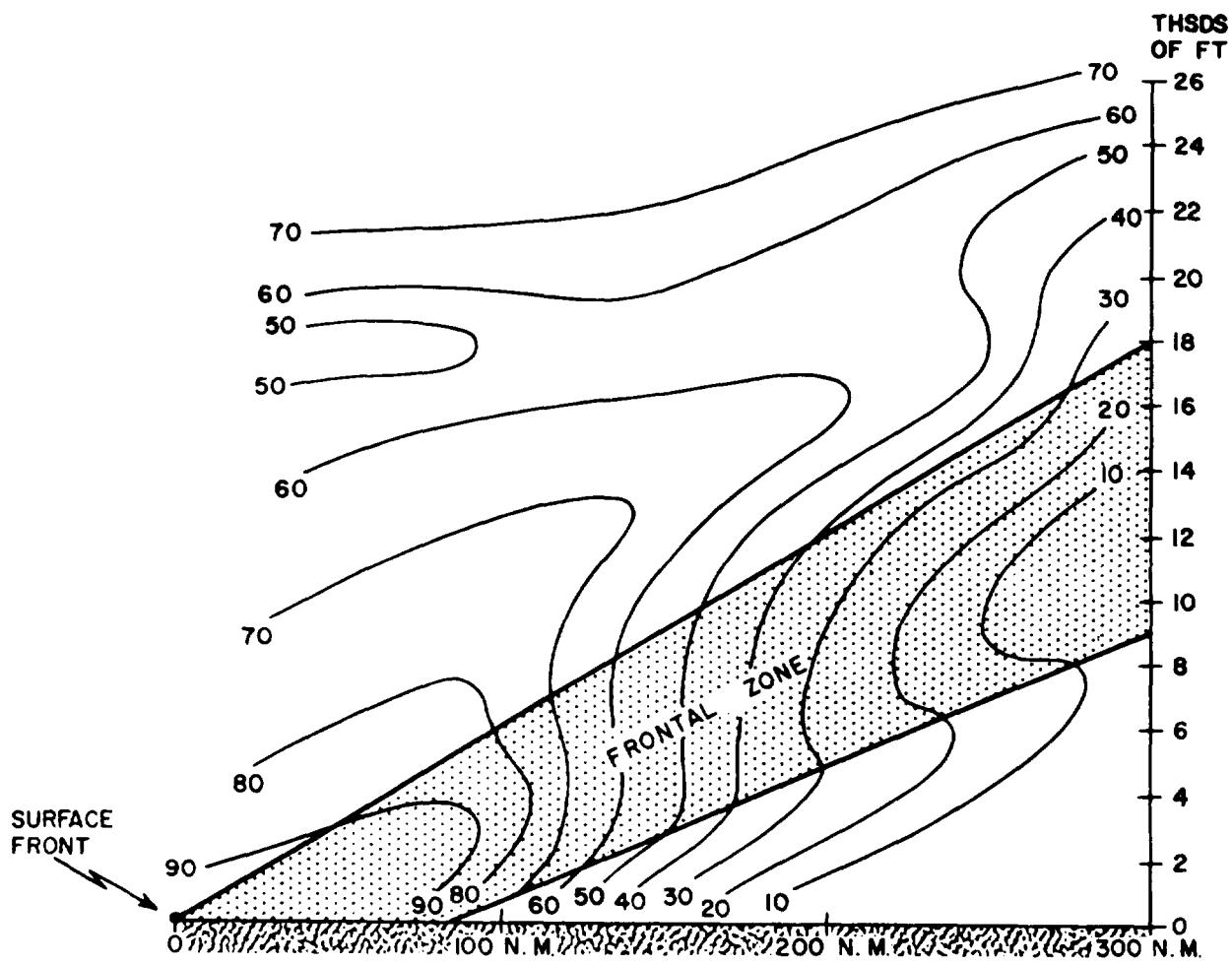
Figure 59. Frequency of Cloud Occurrence (In percent probability) In Active Warm Fronts Over Southern England (Sawyer and Dinsdale [57]).

warm fronts; it extended, on the average, down to 700 mb in cold fronts and 800 mb in warm fronts. In about half of the number of fronts, the driest air was found within the frontal zone itself; on occasions, it was found on both the cold and the warm sides of the zone. About half of the flights showed a sharp transition from moist to dry air, and the change in frost point on these flights averaged about 20°C in 35 miles. Some flights gave changes of more than 20°C in 20 miles.

As a frontal cloud deck is approached, the dew-point depression (or frost-point depression) starts diminishing rapidly in the close vicinity of the cloud (see Figure 60). Farther away than 10 to 15 miles from the cloud the

variation was much less, and it was less systematic. This fact should be borne in mind when attempting to locate the edge of a cloud deck from raob humidity data (at 500 mb, for instance). Linear extrapolation or interpolation of dew-point depressions cannot be expected to yield good results. For instance, when one station shows a dew-point depression of 10°C and the neighboring station shows saturation, the frontal cloud may be anywhere between them, except within about 10 miles from the driest station. Figure 60 points out an advantage as well. Since frontal cloud masses at mid-tropospheric levels are usually surrounded by relatively dry air, *it is possible to locate the edge of the cloud mass from humidity data on constant-pressure charts, at least to within the distance between*

7—5
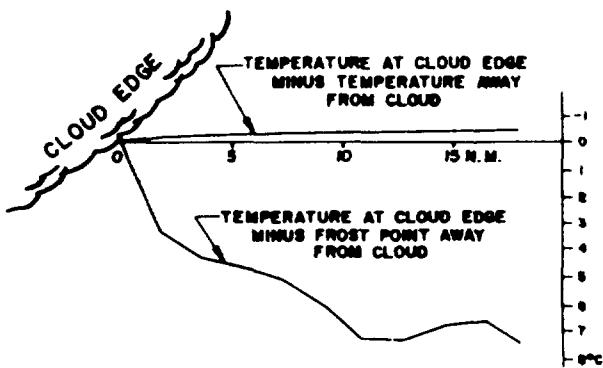
Figure 60. Average Horizontal Variation of Temperature and Frost Point in the Cloud-Free Air in the Vicinity of Frontal Cloud as a Function of the Distance from the Cloud Edge (Sawyer [56]).

neighboring soundings, even if the humidity data are not very accurate. This is so because the typical change of dew-point depression is going from the cloud edge to a distance of 10 to 15 miles or more into cloud-free air is considerably greater than the average error in the reported dew-point depression.

7.3. Temperature of the Cloud Top as a condition for Type of Precipitation.

The coalescence process may account for most of the precipitation which falls in the tropics and sub-tropics; the Bergeron-Findeisen theory, on the other hand, applies to most of the precipitation occurring in middle and high latitudes (in winter, at least). Whenever moderate or heavy rain falls in the temperature or arctic regions, it originates mainly in clouds that, in the upper portions at least, reach negative Celsius temperatures.

It has been found also that precipitating clouds usually extend for a considerable distance into sub-freezing temperatures. The difference in vapor pressure over ice and water reaches a maximum at -12°C. Mason and Howorth [40] found that over Northern Ireland, clouds less than 7500 feet thick with cloud-top temperatures warmer than -12°C and bases appreciably colder than 0°C rarely produced rain or snow.

Mason and Howorth [40] examined records from aircraft ascents through stratiform cloud over Northern Ireland (Aldergrove) and correlated these records with simultaneous hourly surface reports of precipitation. (The routine ascents rose to 400 mb.)

In the majority (87%) of cases when drizzle occurred, it fell from clouds whose cloud-top temperatures were warmer than -5°C, and which were, consequently, unlikely to contain ice crystals.

The frequency of rain or snow increased markedly when the cloud-top temperature fell below -12°C. When continuous rain or snow fell, the temperature in the coldest part of the cloud was below -12°C in 95% of the cases (41/43) and below -20°C in 84% of the cases (36/43).

Intermittent rain also was mostly associated with cold cloud tops, though cloud-top temperature above -12°C were somewhat more frequent with intermittent rain than with continuous rain. When intermittent rain was reported at the ground, the cloud-top temperature was below -12°C in 81% of the cases (46/57) and below -20°C in 63% of the cases (36/57). From this, it appears that *when rain or snow — continuous or intermittent — reaches the ground from stratiform clouds, the clouds, solid or layered, extend in most cases to heights where the temperature is below -12°C or even -20°C.*

This statement cannot, of course, be reversed. When no rain or snow is observed at the ground, middle cloud may well be present in regions where the temperature is below -12°C or -20°C. Whether precipitation reaches the ground or not will depend on the cloud thickness, the height of the cloud base, and on the dryness of the air below the base.

It is obvious that these findings may be of value in inferring the kind of precipitation to expect from forecasted cloud decks whose tops can be estimated as to height and temperature.

7.4. Inferring Clouds from Raobs. Theoretically, we should be able to infer from the radiosonde observations of temperature and humidity the layers where the sonde penetrated cloud layers. In practice, however, we find that the determinations we can make from the T and T_d curves are often less exact and less reliable than desired. Nevertheless, raobs give clues about cloud distribution and potential areas of cloud formation — clues which often cannot be obtained from any other source.

7.5.0. Systematic Errors in Radiosonde Humidity Elements. The great majority of humidity elements used in U.S. radiosondes are the carbon-impregnated plastic elements, ML-476/AMT. A limited number of sondes with the old lithium-chloride-coated plastic element ML-418/AMT-4 are still being used by the U.S. Navy and some foreign countries. The readings of this element tend to be too low.

7.5.1. Characteristics of the U.S. Lithium-Chloride Coated Humidity Element. Three characteristics of this humidity element combine to make the indicated relative humidity differ — at times appreciably — from the true (ambient) value.

a. The element has a variable time lag; i.e., a period of time must elapse before the element can adjust itself to the changing temperature and humidity in its surroundings. This adjustment is supposed to obey an exponential law, but the constants themselves in this exponential expression depend on the rate of change of both the temperature and the humidity. In practice, therefore, it is difficult to apply any corrections for this time lag except in a qualitative manner. It has been found experimentally that the time lag of this element can vary from 10 seconds to about 165 seconds. Also, the time lag, in general, increases with decreasing temperature [62]. The lag is largest when the element ascends from warm dry air into colder, moister air (this is usually the case when a radiosonde enters a more moist layer

or a cloud). The radiosonde will then indicate dew points that are too low; if the temperature decrease continues upward through the cloud (as it usually does) the radiosonde may fail altogether to report dew-point depressions small enough for the existence of a cloud to be inferred. In this case, if the existing cloud is only a few thousand feet thick, either the indicated cloud base will be too high, or no cloud will be indicated. Conversely, if the radiosonde emerges from a cloud or a moist layer into a drier layer above, the time lag is smaller, being of the order of 10 to 20 seconds [17]. Thus, when using this element, the height of the top of a cloud layer or a moist layer is usually indicated more accurately than is the base of such layers.

b. When a humidity signal is transmitted by the radiosonde, a pulsating direct current flows through the element, causing it to polarize. This effect, which becomes more pronounced with time (i.e., during the ascent), results in an increase in the resistance of the humidity element and an indicated humidity that is too low.

c. At high humidities (such as those in clouds and precipitation), the lithium-chloride coating on the humidity element is sometimes washed out. This also results in reported humidities which are too low. The "washout" effect is particularly troublesome when one is attempting to locate the base and top of thick cloud layers. These clouds often produce precipitation (even though it may not reach the ground), and they usually have a layer of lower, wet clouds associated with them. Consequently, the humidity element has had its sensing power weakened before it enters the higher cloud layer.

The net effect of these three characteristics of the lithium-chloride coated humidity element is that the relative-humidity values reported are usually too low. These errors led to the development of the carbon-impregnated humidity element.

7.5.2 Characteristics of the Carbon-Impregnated Plastic Humidity Element. The ML-476/AMT humidity element is used in the AN/AMT-4( ), AN/AMT-12, and AN/AMQ-9 radiosondes, and in the AN/AMT-6

( ) and AN/AMT-13 radiosondes (drop-sondes). The characteristics of this element are as follows:

a. The resistance of the element varies inversely with humidity changes of the atmosphere. The resistance ratio versus relative humidity characteristic of the ML-476/AMT is based on an absolute resistance at 33% relative humidity and a temperature of +25°C.

b. A limiting factor in making humidity measurements with this element is the fact that the time constant increases exponentially with decreasing temperatures; humidity values are unusable at temperatures colder than -40°C. The military specifications for the ML-476/AMT require that 63% of the total change in resistance of the element induced by a change in humidity from 20 ±5% to 90 ±5% shall occur in less than 2 seconds at +40°C and in less than 2 minutes at -40°C.

The accuracies of the ML-476/AMT are (as stated in the military specifications):

$T > 0°C, ± 5\%$
$0°C \geq T \geq -40°C, ± 10\%$
$T < -40°C,$ questionable.

The above accuracies refer to one ascent from 15% to 90% humidity. An additional ± 4% for humidities > 33% and ± 5% for humidities < 33% should be allowed for relative humidities changing in the opposite direction (hysteresis) from 90% to 15%.

c. The range of defined accuracies of relative humidity values is 15% to 96%. The sensitivity is only fair at humidities less than about 15% and above 96%.

d. In comparison with the old lithium chloride element, the ML-476/AMT provides more accurate measurement of relative humidity, has less hysteresis effects, operates over a wider range of relative humidity and temperature, and responds more rapidly to changes in humidity.

7.5.3. Characteristics of Other Humidity Elements.
The tests made several years ago at Payerne under WMO auspices indicated that most foreign radiosondes gave humidity readings which were acceptably compatible with those of the U.S. lithium-chloride element. Improvements in foreign humidity elements are being introduced which will tend to make them compatible with the carbon element at temperatures above freezing.

7.6. Dew Point and Frost Point in Clouds.
The data-trace recorded from the humidity strip is calibrated in terms of the relative humidity with respect to water at negative, as well as positive, temperatures. The T_d value, the humidity parameter that is transmitted over the teletype, is the temperature to which the air must be cooled isobarically and at constant vapor pressure if saturation with respect to a water surface is to be reached. The *frost point* (i.e., the temperature to which the air has to be cooled or heated isobarically in order to reach saturation with respect to ice) is higher than the dew point, except at 0°C, where the two coincide. In the graph shown in Figure 61, the difference between dew point and frost point is plotted as a function of the dew point itself.
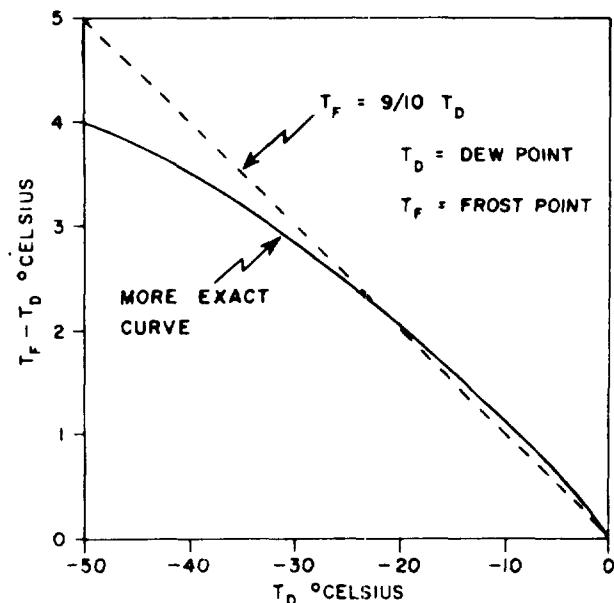
Figure 61. Difference Between Frost Point and Dew Point as a Function of the Dew Point.

In a cloud where the temperature is above freezing, the true dew point will coincide closely with the true temperature, indicating that the air between the cloud droplets is

practically saturated with respect to the water surface of the droplets. Minor discrepancies may occur when the cloud is not in an equilibrium state (e.g., when the cloud is dissolving or forming rapidly, or when precipitation is falling through the cloud with raindrops of slightly different temperatures than the air), but these discrepancies are theoretically small. In the subfreezing part of a cloud, the true temperature will be somewhere between the true dew point and the true frost point, depending on the ratio between the quantities of frozen and liquid cloud particles. If the cloud consists entirely of supercooled water droplets, the true temperature and the true dew point will, more or less, coincide. If the cloud consists entirely of ice, the temperature should coincide with the frost point. We cannot, therefore, look for the coincidence of dew points and temperatures as a criterion for clouds at subfreezing temperatures, even if the humidity element had no systematic errors of the nature discussed in paragraph 7.5.0. At temperatures below -12°C, the temperature is more likely to coincide with the frost point than with the dew point. The graph shown in Figure 61 indicates that the difference $(T_d - T_f)$ between the dew point and the frost point increases roughly 1°C for every 10°C that the dew point is below freezing; e.g., when $T_d = -10°C$, $T_f = -9°C$; when $T_d = -20°C$, $T_f = -18°C$; when $T_d = -30°C$, $T_f = -27°C$; etc. Thus, for a cirrus cloud that is in equilibrium (saturated with respect to ice) at a (frost-point) temperature of -40°C, the correct dew point would be -44°C (to the nearest whole degree).

We can state then, that in general, air in a cloud at temperatures below about -12°C is saturated with respect to ice, and that as the temperature of the cloud decreases (with height, e.g.), the true frost-point dew-point difference increases. The effects of these physical characteristics serve to reinforce the effects of the systematic faults of the humidity element itself (lag, polarization, and washout); i.e., they all conspire to make a radiosonde ascending through such a cloud indicate increasing dew-point depressions. Any attempt to determine the heights of cloud layers from the humidity data of a raob is, therefore, subject to errors from these effects. It is possible to overcome some of these errors by a subjective interpretation of the raobs, as discussed in the following paragraphs.

7.7. Examples of Interpretation of Raob with Respect to Cloud Layers, in Terms of Dew-Point Depression.

Various Skew-T charts of soundings[27] made over the United States have been chosen to illustrate the behavior of the radiosonde during cloud penetration (see Figures 62a through 62j). During the time these soundings were being made, aircraft observations (from Project Cloud-Trail flights, *AWS TR 105-130* and *AWS TR 105-145)* of the heights of cloud bases and tops were made from aircraft flying in the vicinity of the ascending radiosondes. The difference — in time and space — between the aircraft and sounding observations was usually less than two hours and 30 miles. Some of the aircraft reported only the cloud observed above 15,000 feet; others reported all cloud. In Figures 62a through 62j, the aircraft cloud observations are entered in the bottom left corner of each diagram under the heading CLOUD; the surface weather report is entered under the aircraft cloud report. Where low cloud was not reported by the aircraft, the height of the cloud base may be obtained from the surface report. Aircraft height reports are in pressure-altitude. The temperature, frost-point, and dew-point curves are indicated by T, T_f, and T_d, respectively.

---

[27] All of the soundings illustrated and discussed here were made with U.S. radiosondes. Certain foreign equipment appears to have performance characteristics similar to those of the U.S. instruments; however, no soundings from foreign equipment have been examined in this study (see par. 7.5.0.).
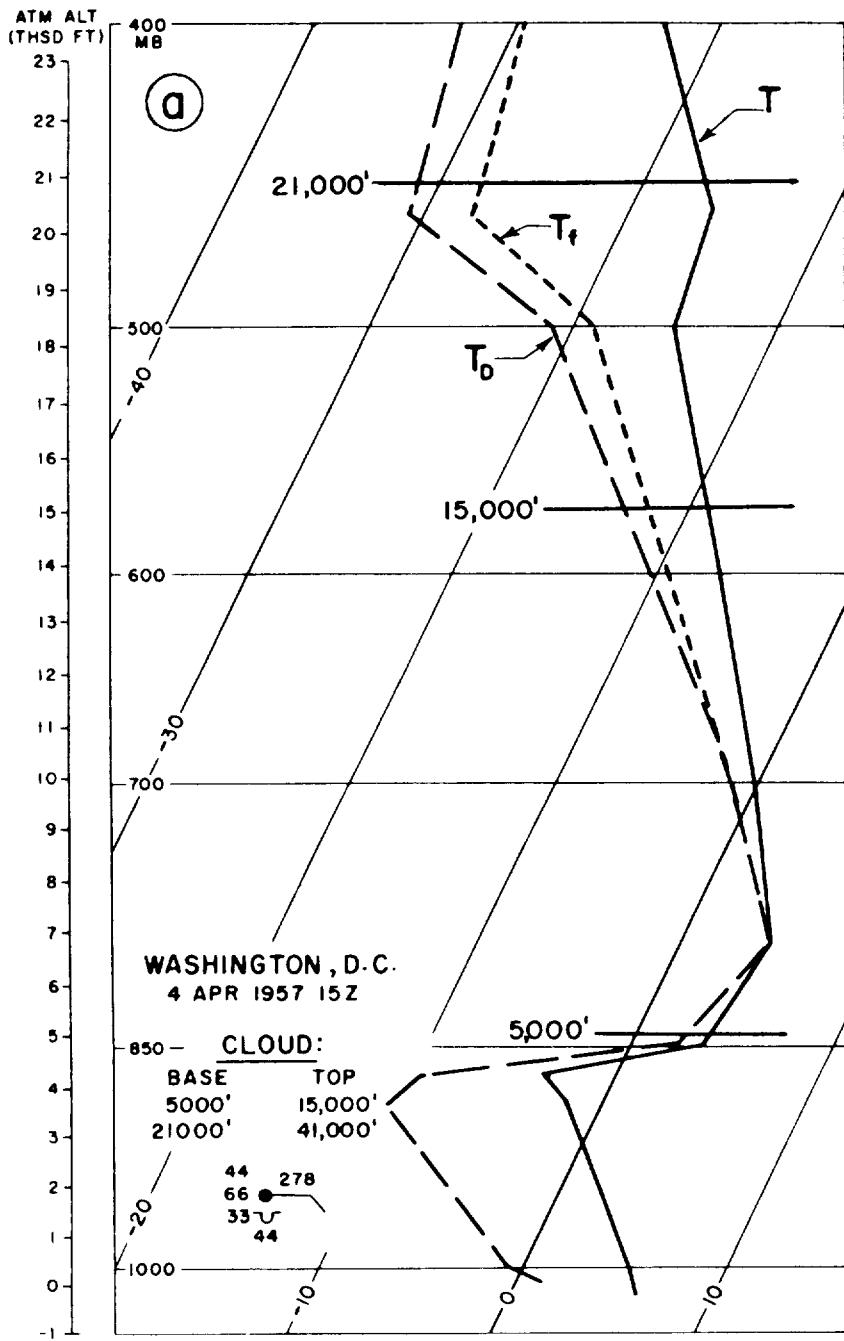
Figure 62a. Sounding in Marked Warm Front, Two Cloud Layers Indicated. A marked warm front is approaching from the south. Moderate, continuous rain fell two hours later. At 1830Z an aircraft reported solid cloud from 1000 to 44,000 feet (tropopause). The 15Z sounding shows an increasing dew-point depression with height, with no discontinuity at the reported cloud top at 15,000 feet. A definitely dry layer is indicated between 18,300 and 20,000 feet. The second reported cloud layer is indicated by a decrease in dew-point depression, but the humidity element obviously is slow in responding. The dew-point depression at the base of the cloud at 21,000 feet is 14°C and at 400 mb after about a 3-minute climb through cloud is still 10°C. From the sounding we should have inferred cloud from about 4500 feet (base of rapid humidity increase) to 500 mb and a second layer from 20,000 feet up. In view of the rapid filling of the cloud-free gap between 15,000 and 21,000 feet which followed as the warm front approached, the agreement between reported and inferred conditions is good.

7—10
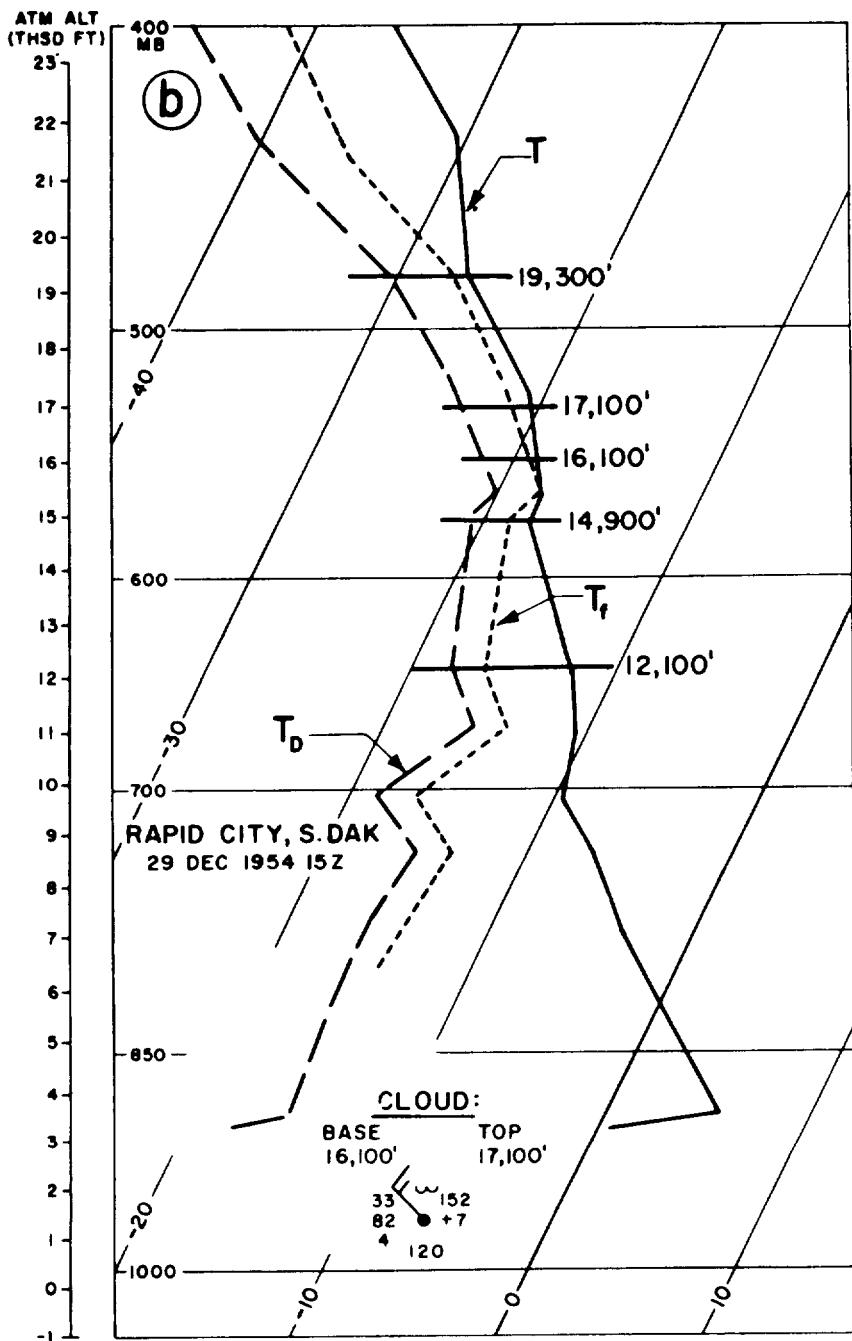
Figure 62b. Cold Front with Cloud Layer Thinner Than Indicated by Sounding. A cold front lay E-W across North Dakota at 15Z. The reported cloud layer was much thinner than would be inferred from the sounding. Using the rule that a cloud base is indicated by a fairly rapid decrease in dew-point depression to a dew-point depression of 6°C or less, we should put the base somewhere between 12,100 and 14,900 feet. Similarly, we should have expected the cloud to extend to 19,300 feet where the dew-point depression starts increasing again. The surface report places the base at 12,000 feet. It is possible that the difference in space and time between the aircraft and the sonde may account for the discrepancy. Of the two possibilities, 12,100 and 14,900 feet, we should choose the latter as base height. If a decrease in dew-point depression is followed by a much stronger decrease, choose the height of the base of the stronger decrease as the cloud-base height.
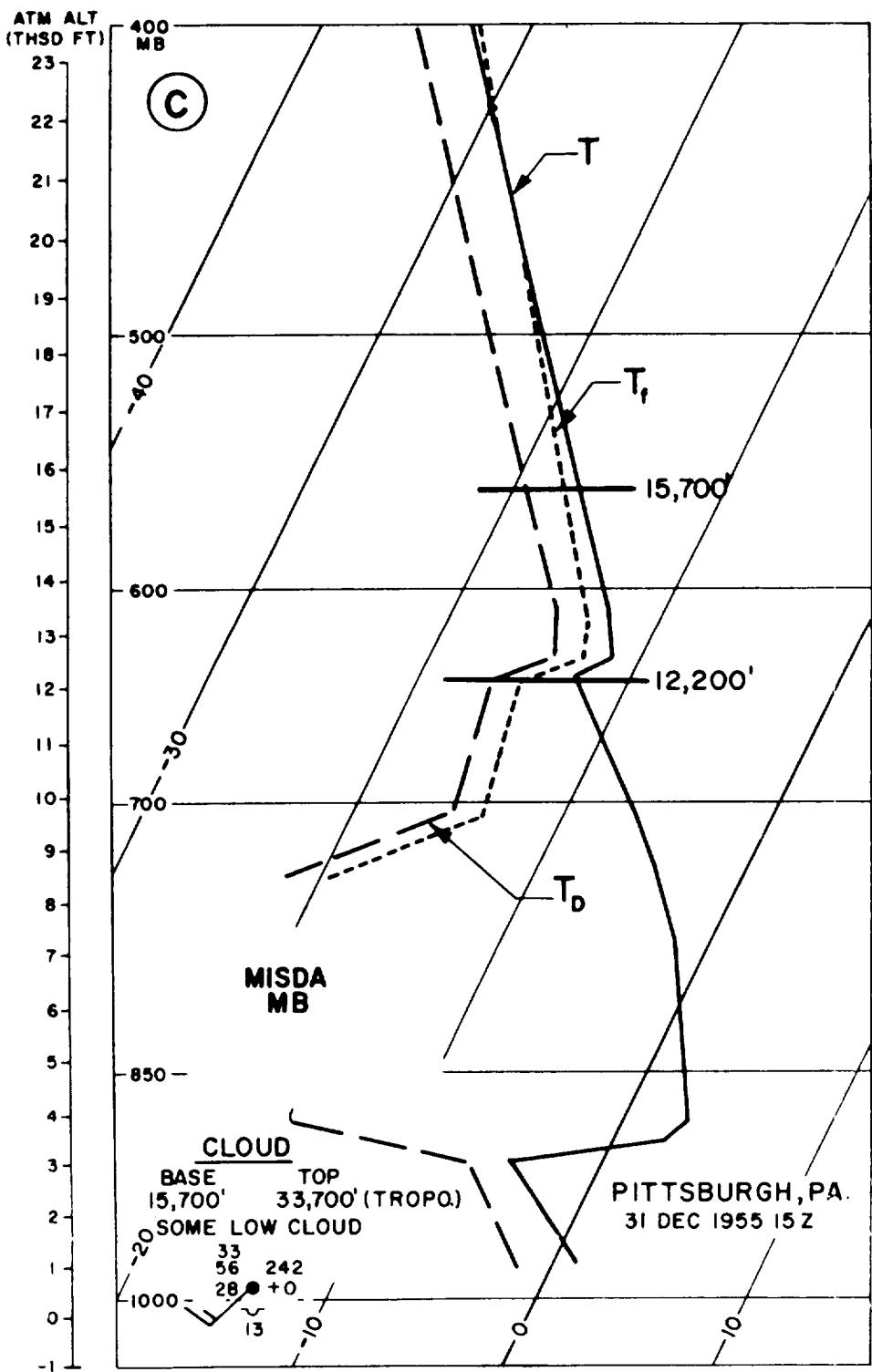
Figure 62c. Middle-Cloud Layer with No Precipitation Reaching the Surface. This is a case of cloud in the 500-mb surface with no precipitation reaching the surface; the nearest rain at the time was in Tennessee. The evidence from the sounding for putting the cloud base at 12,200 feet is strong, yet the base is inexplicably reported at 15,700 feet. The reported cloud base of 15,700 was probably not representative, since altostratus, with bases 11,000 to 14,000 feet, was reported at most stations over Ohio and West Virginia.
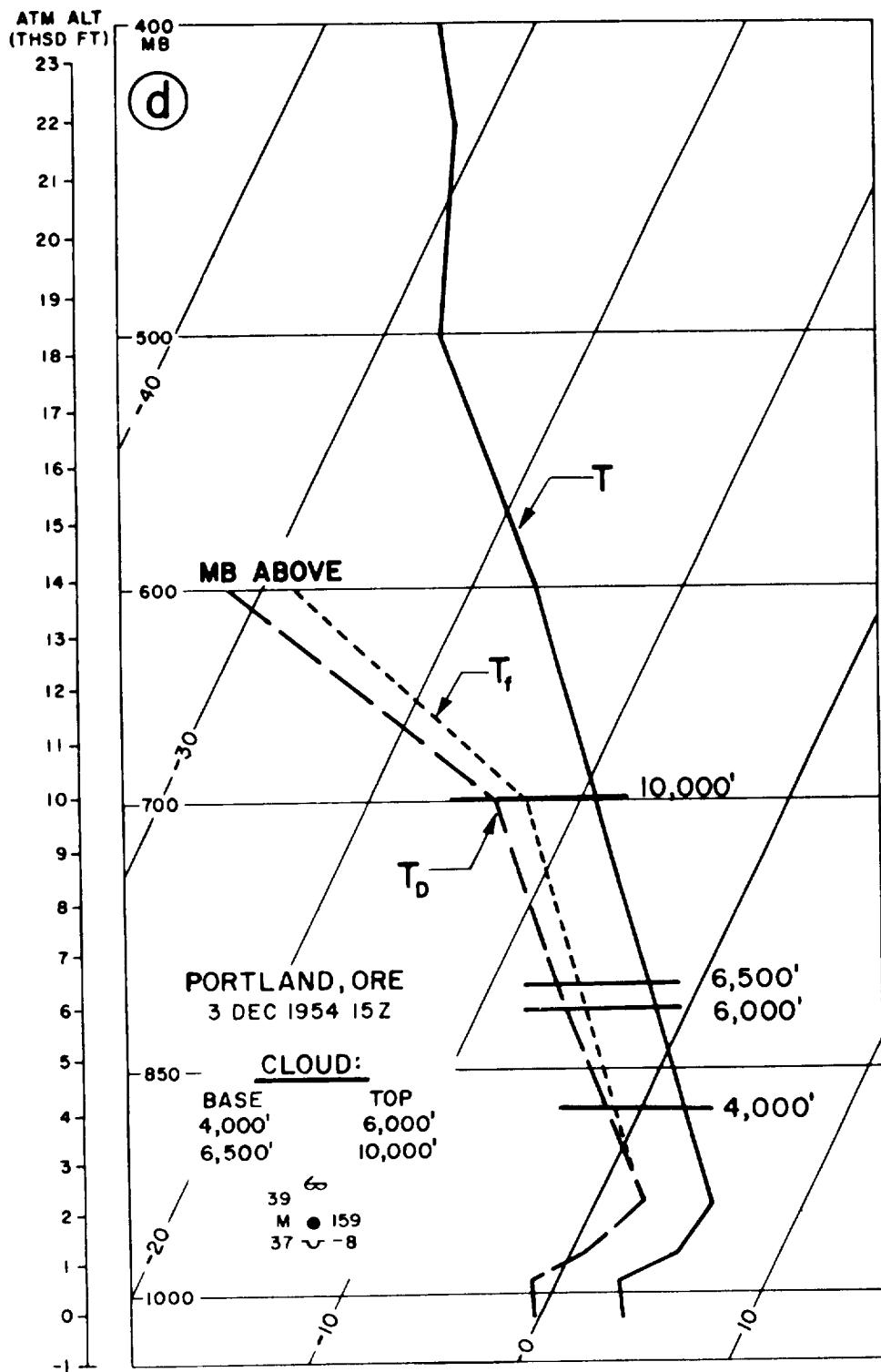
Figure 62d. Layer Clouds with Their Intermediate Clear Layers not Showing In Humidity Trace. There is good agreement between the sounding and the aircraft report. The clear layer between 6000 and 6500 feet is not indicated on the sounding. Thin clear layers as well as thin cloud layers usually cannot be recognized on the humidity trace.
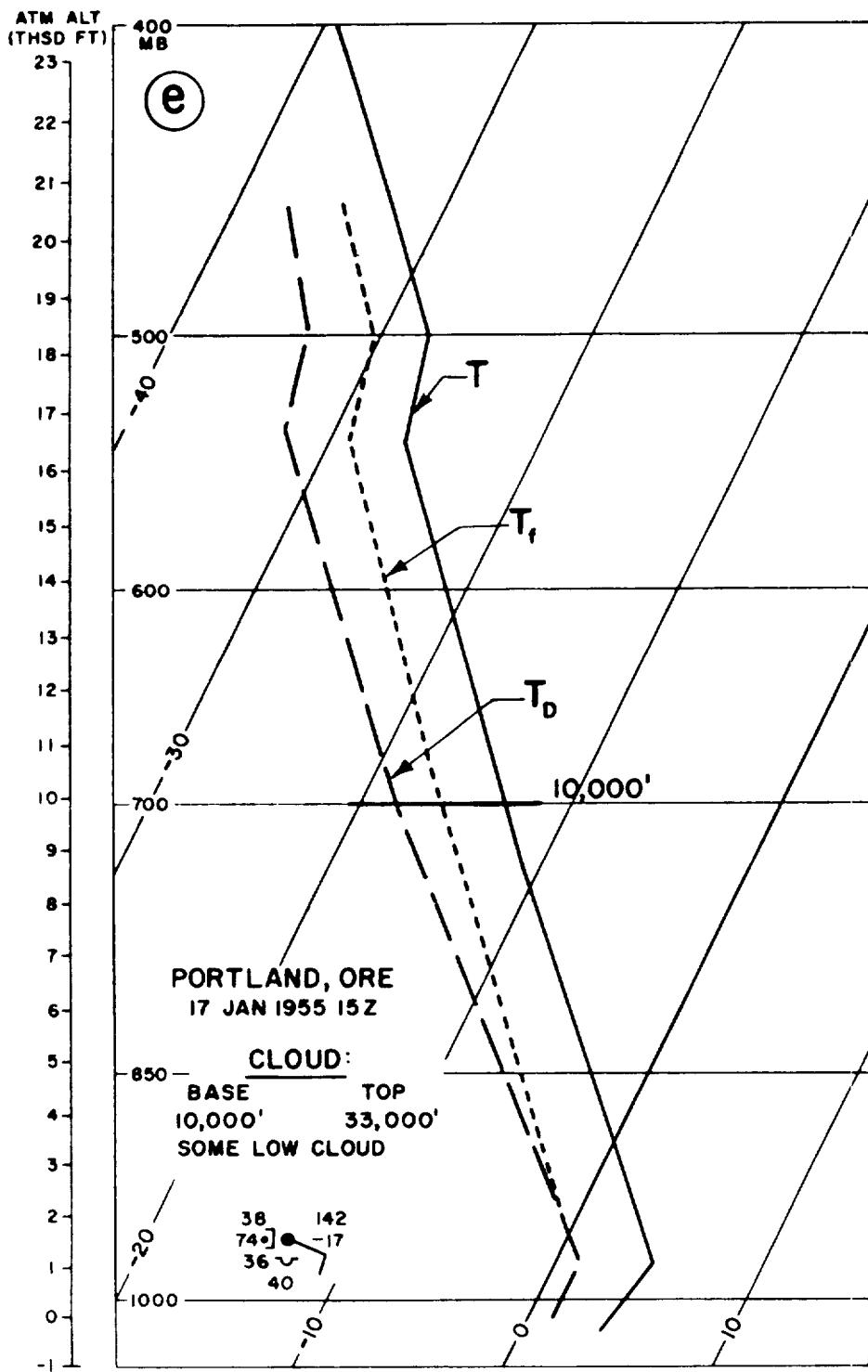
Figure 62e. Deep Layer of Cloud from Lower Levels to Tropopause with Some Clear Layers not Revealed by Sounding. There is cloud from 4000 feet to the tropopause, with the exception of an unspecified clear layer between the top of the low stratocumulus and the base of the middle cloud at 10,000 feet. From the sounding, there is little indication of any layering, and the dew-point depression is 4°C to 6°C throughout the sounding. This sounding is typical of solid or near-solid cloud from the surface to great heights in moderately cold atmosphere (500-mb temperature about -30°C).

7—14

ATM ALT (THSD FT)

400 MB

ⓕ

18,900'

500

T

600

T_f

700

850

PORTLAND, ORE
I FEB 1955 15 Z

T_D

CLOUD:

BASE	TOP
18,900'	24,900'
	(TROPOPAUSE)

41 176
74 -5
35

1000
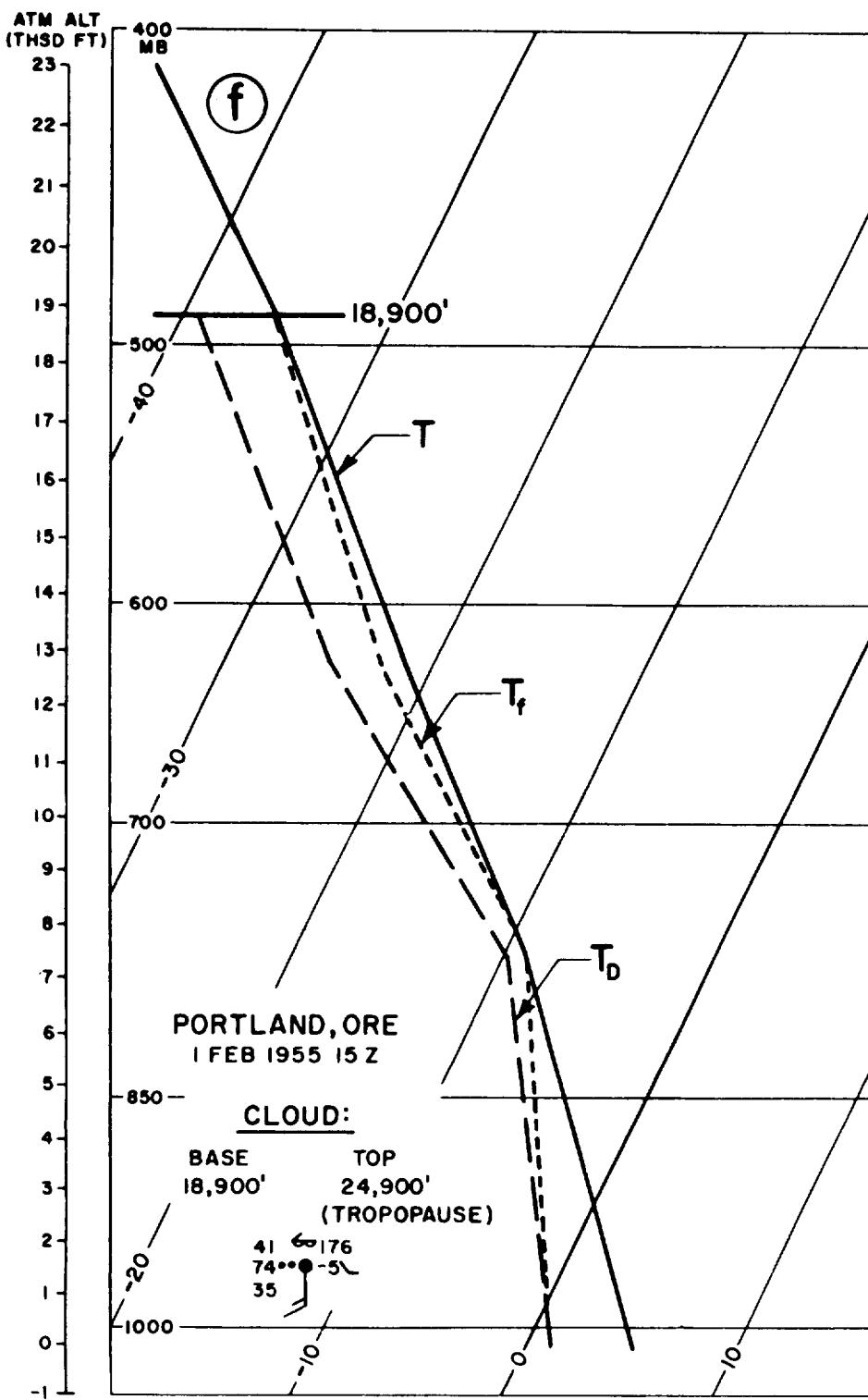
Figure 62f. This Sounding is Similar to that Shown in Figure 62e. From this sounding we should have infer-red solid cloud from near ground to above 500 mb. An occlusion was 30 miles west of Portland and was as-sociated with a widespread rain area. The discrepancy between sounding indications and observed cloud is hard to explain.
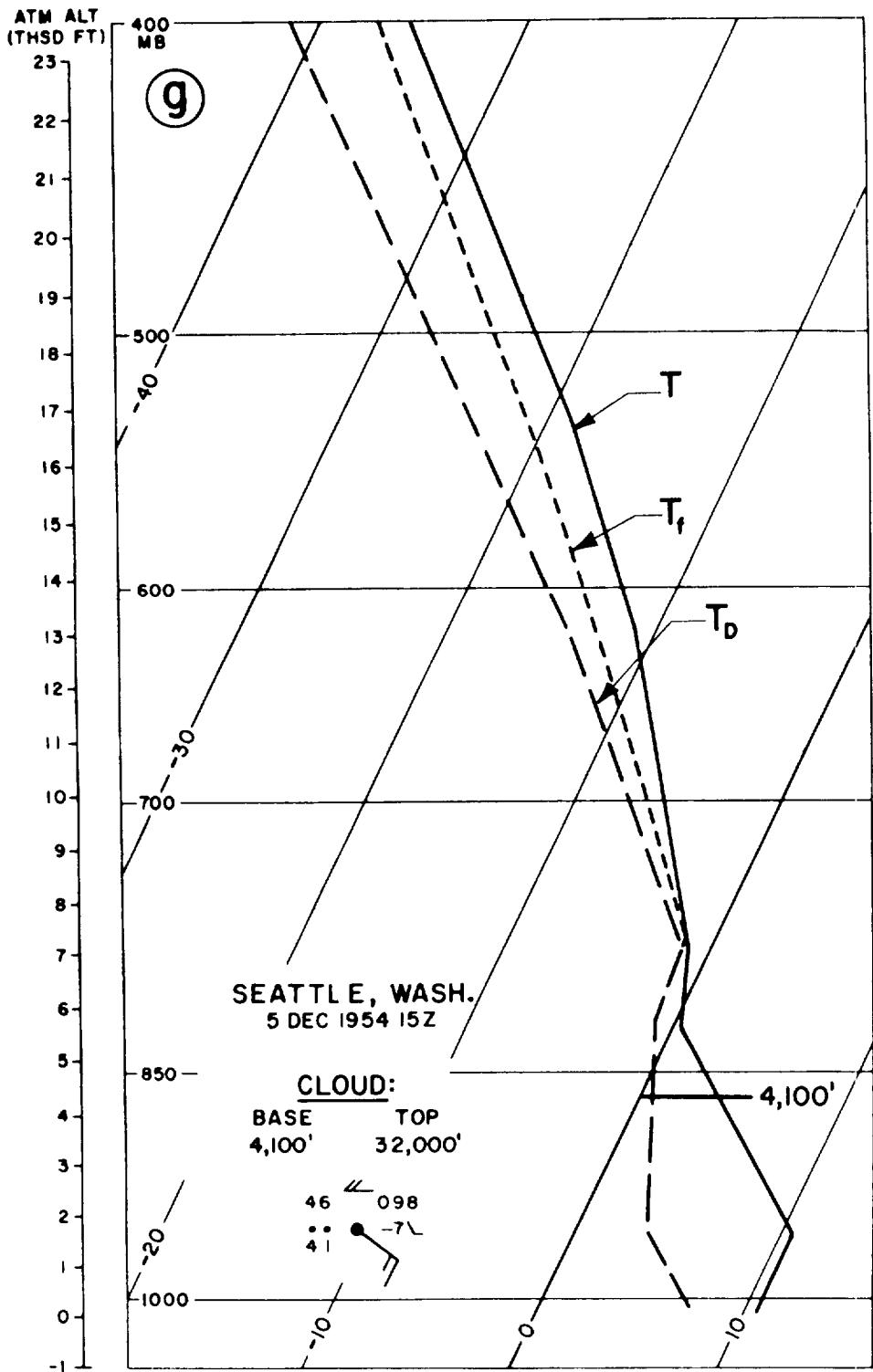
Figure 62g. Deep Cloud Layer, Sounding Showing Base Too High. There is good agreement between sounding indications and the observed cloud except for the cloud base, for which the sounding indicates the height to be at 5500 feet. (If a decrease in dew-point depression is followed by a much stronger decrease, choose the height of the base of the stronger decrease as the cloud-base height.)
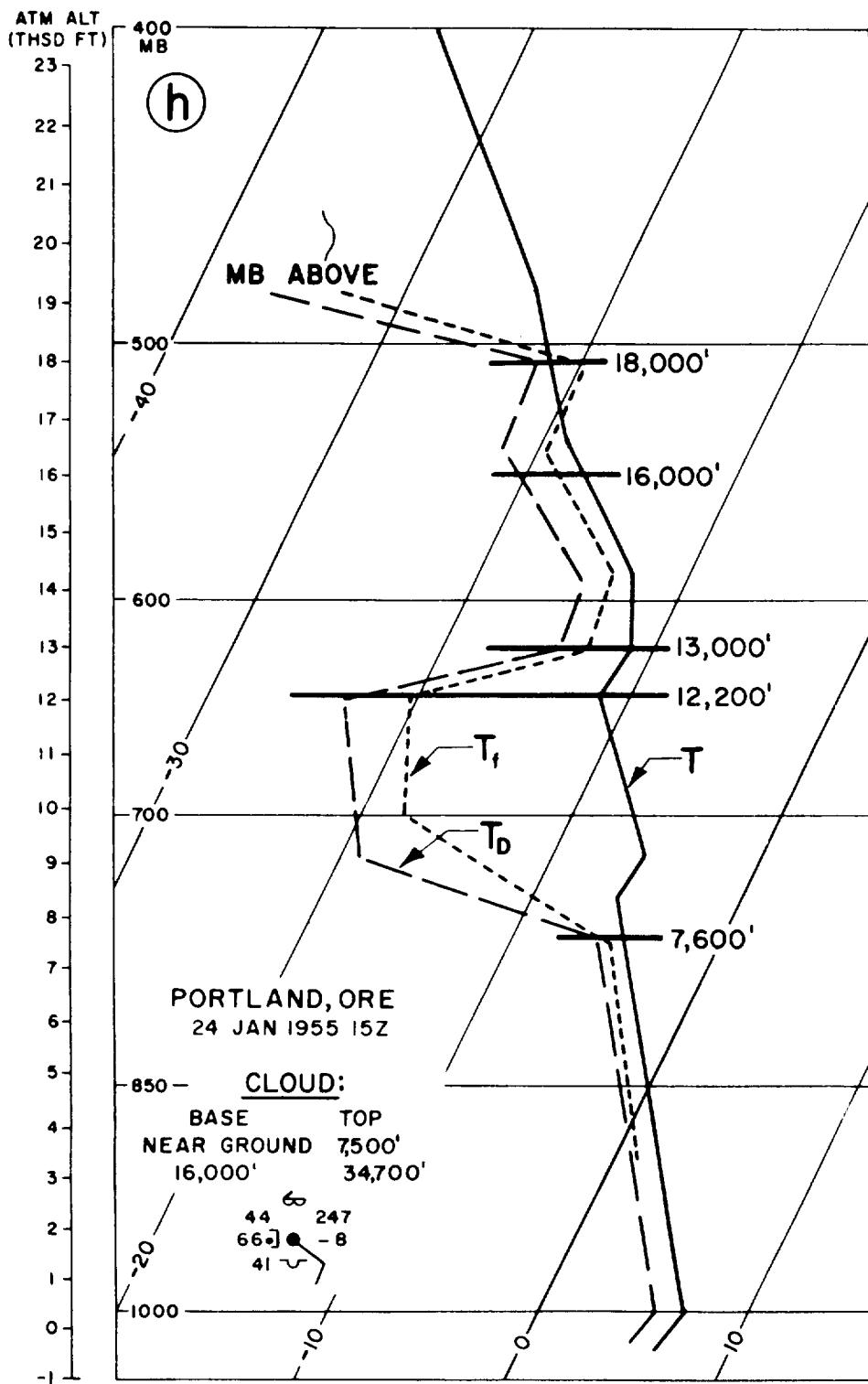
Figure 62h. Double Layer of Cloud, Top of Upper Layer not indicated by Sounding. A cold front was located 200 miles west of Portland. There is good agreement between observed and sounding-indicated cloud heights of the first layer. The sounding indicates a second layer based at 12,200 feet and definitely terminating at 18,000 feet. The aircraft reported solid cloud from 16,000 feet to near the tropopause. The most likely explanation: something went wrong with the humidity element above 18,000 feet.

7—17
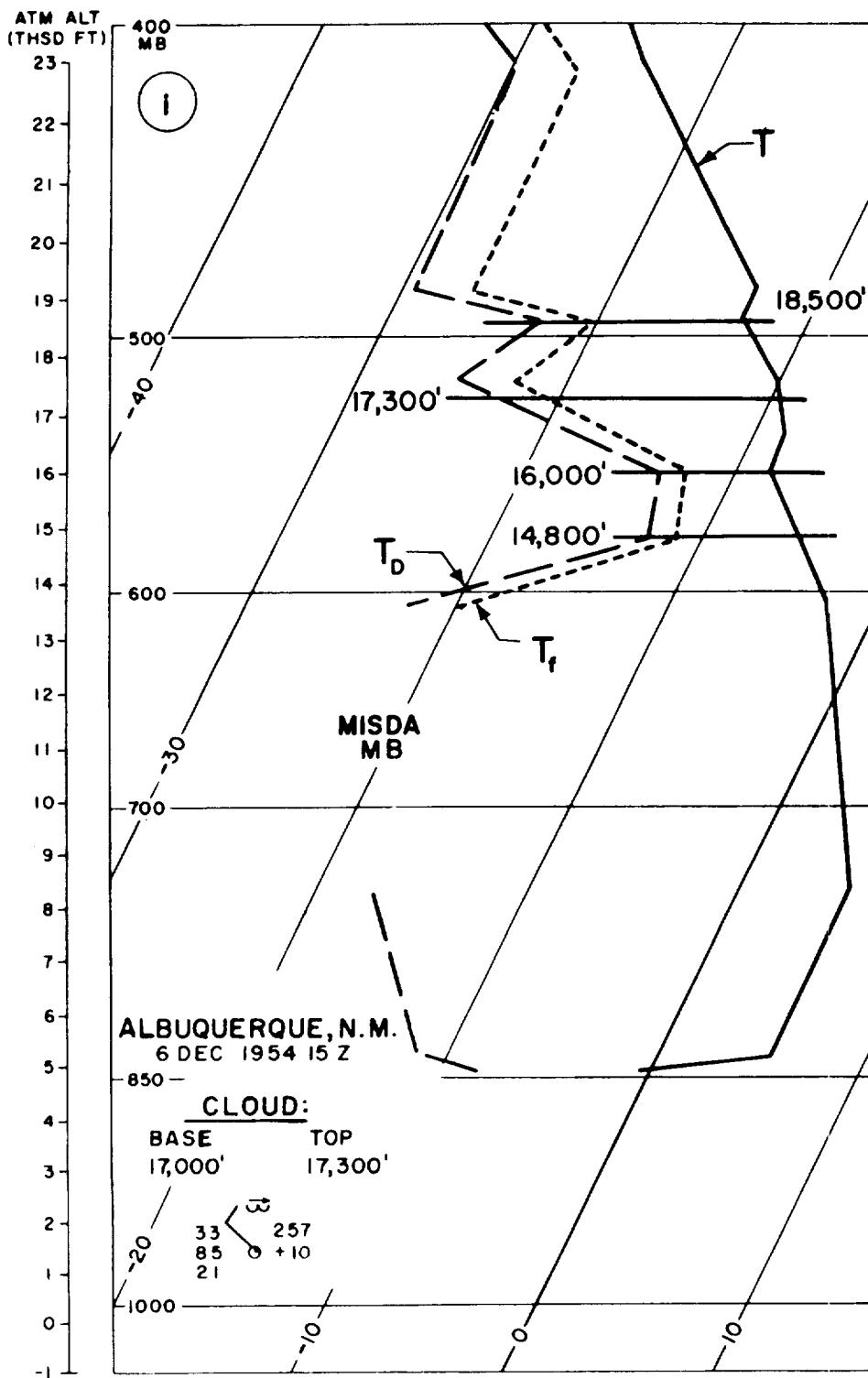
Figure 62i. Sounding Through Scattered Thin-Layered Middle Clouds Indicated by Variable Humidity. The sounding indicates considerable variability in the humidity trace. If any cloud could be inferred, it would be from 14,800 to 16,000 feet and at 18,500 feet. The height of the thin scattered layer observed at 17,000 feet is not well fixed by the sounding. This sounding is typical of thin layered middle clouds, usually scattered or broken.
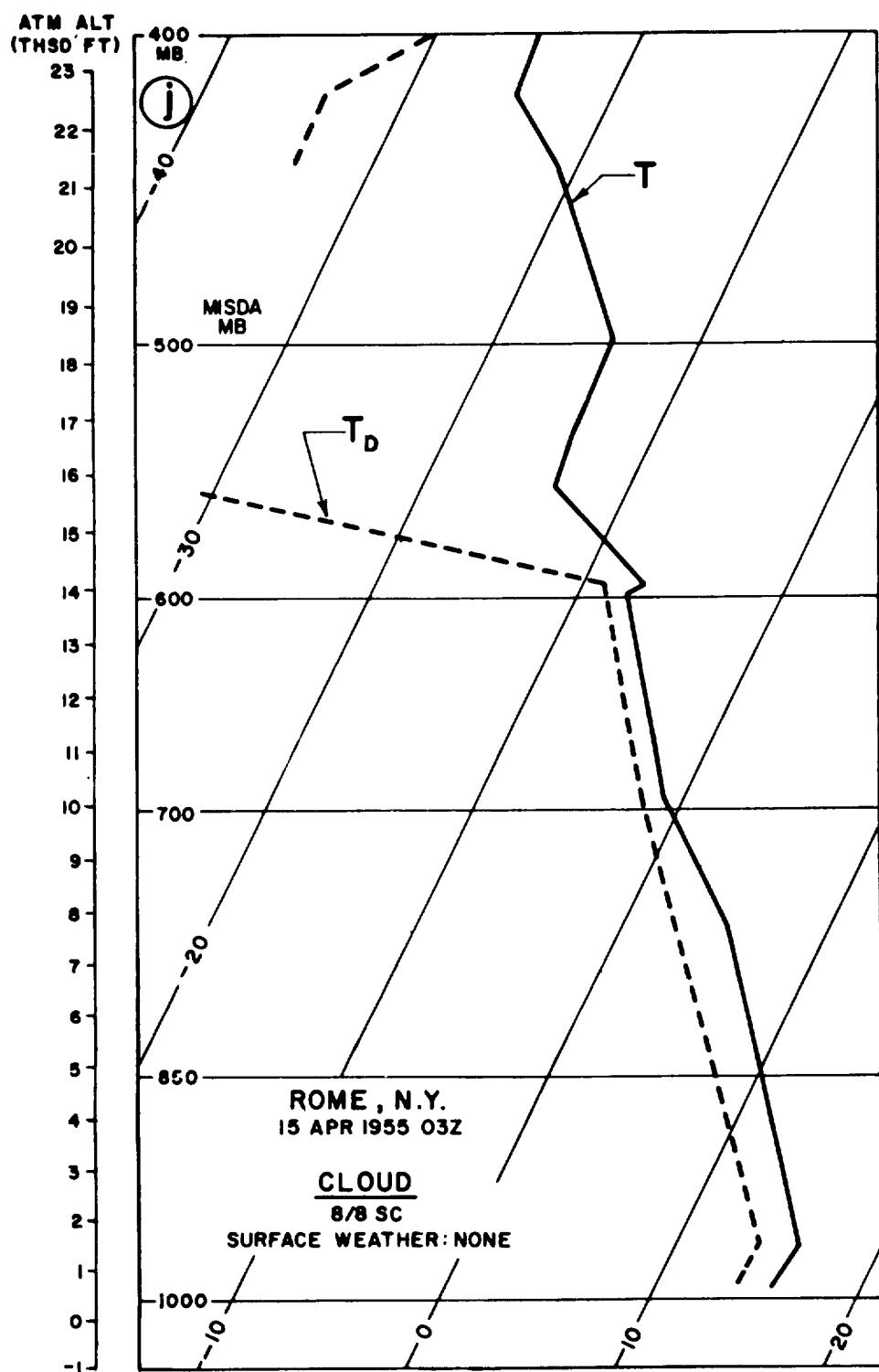
Figure 62J. Sounding Showing a Spurious Superadiabatic Lapse Rate where Sonde Leaves Top of Cloud. No aircraft reports were available. The sounding illustrates that the lapse rate is, at times, recorded as superadiabatic when the sonde leaves a cloud top and enters extremely dry air above the cloud. The phenomenon has been ascribed to a wet-bulb effect on the thermistor (see par. 5.6).

Comparisons of the type made above between soundings and cloud reports from aircraft provide us with the following rules:

a. A cloud base is almost always found in a layer (indicated by the sounding) where the dew-point depression decreases.

b. The dew-point depression usually decreases to between 0°C and 6°C when a cloud is associated with the decrease. In other words, we should not always associate a cloud with a layer of dew-point decrease but only when the decrease leads to a minimum dew-point depression < 6°C; at cold temperatures (below -25°C), however, dew-point depressions in cloud are reported as > 6°C.

c. The dew-point depression in a cloud is, on the average, smaller for higher temperatures. Typical dew-point depressions are 1°C to 2°C at temperatures of 0°C and above, and 4°C between -10°C and -20°C.

d. The base of a cloud should be located at the base of the layer of decreasing dew-point depression, if the decrease is sharp.

e. If a layer of decrease of dew-point depression is followed by a layer of stronger decrease, the cloud base should be identified with the base of the layer of strongest decrease.

f. The top of a cloud layer is usually indicated by an increase in dew-point depression. Once a cloud base is determined, the cloud is assumed to extend up to a level where a significant increase in dew-point depression starts. The gradual increase of dew-point depression with height that occurs on the average in a cloud is not significant.

In addition to the above analysis of Project Cloud-Trail data, another study was made in Hq AWS to see how reliable the dew-point depression is as an indicator of clouds. Raobs for January 1953 from 29 U.S. Weather Bureau stations were compared with cloud-base observations taken at the same location and approximate time of each raob. The results of this study are summarized in the two graphs shown in Figure 63. (A more complete discussion of this study is given in Attachment 1 to this manual.) Each graph shows the percent probability of the existence of a cloud layer in January for different values of the dew-point depression. On each graph one curve shows the probability of clear or scattered conditions as a function of the dew-

point depression; the other curve, that of broken or overcast conditions. Separate graphs are included for the 1000- to 850-mb and 850- to 600-mb layers. The graphs are based on 1027 observations, which are enough to indicate the order of magnitude of the dew-point depressions at the base of winter cloud layers. (The small irregularities in the curves were not "smoothed out" because
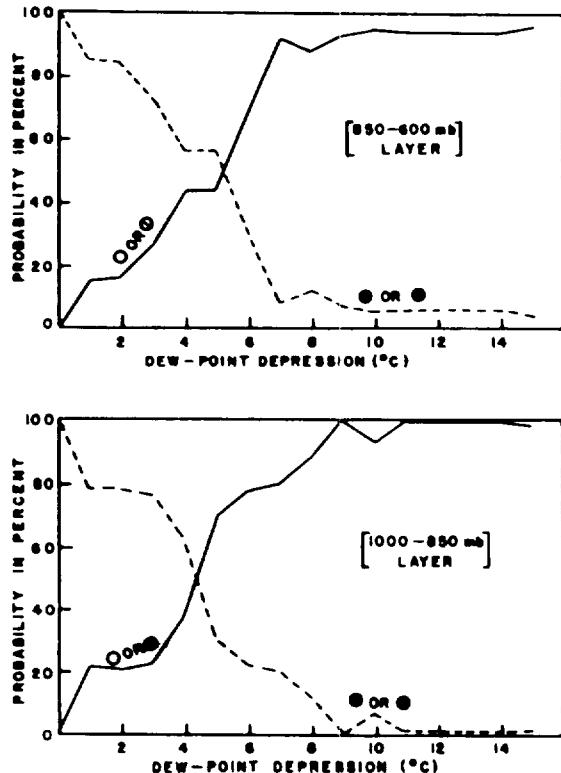
Figure 63. Percent Probability of the Existence of Cloud-Layer Bases for Different Values of Dew-Point Depression (°C). Solid lines represent probability of clear or scattered conditions; dashed lines, the probability of broken or overcast conditions with the cloud-layer bases between 1000 mb and 600 mb.

it is not certain that they are all due to insufficient data.) The graphs are applicable without reference to the synoptic situation. For a given winter sounding, one can estimate from the graph the probability of different sky-cover conditions with cloud bases between 1000 mb and 600 mb for layers of given minimum dew-point depressions.

7.8. Motorboating and Missing Data. "Motorboating" is a term used to describe the radiosonde's signal when the humidity is below the perceptible level of the element. A distinction must be made on the Skew-T
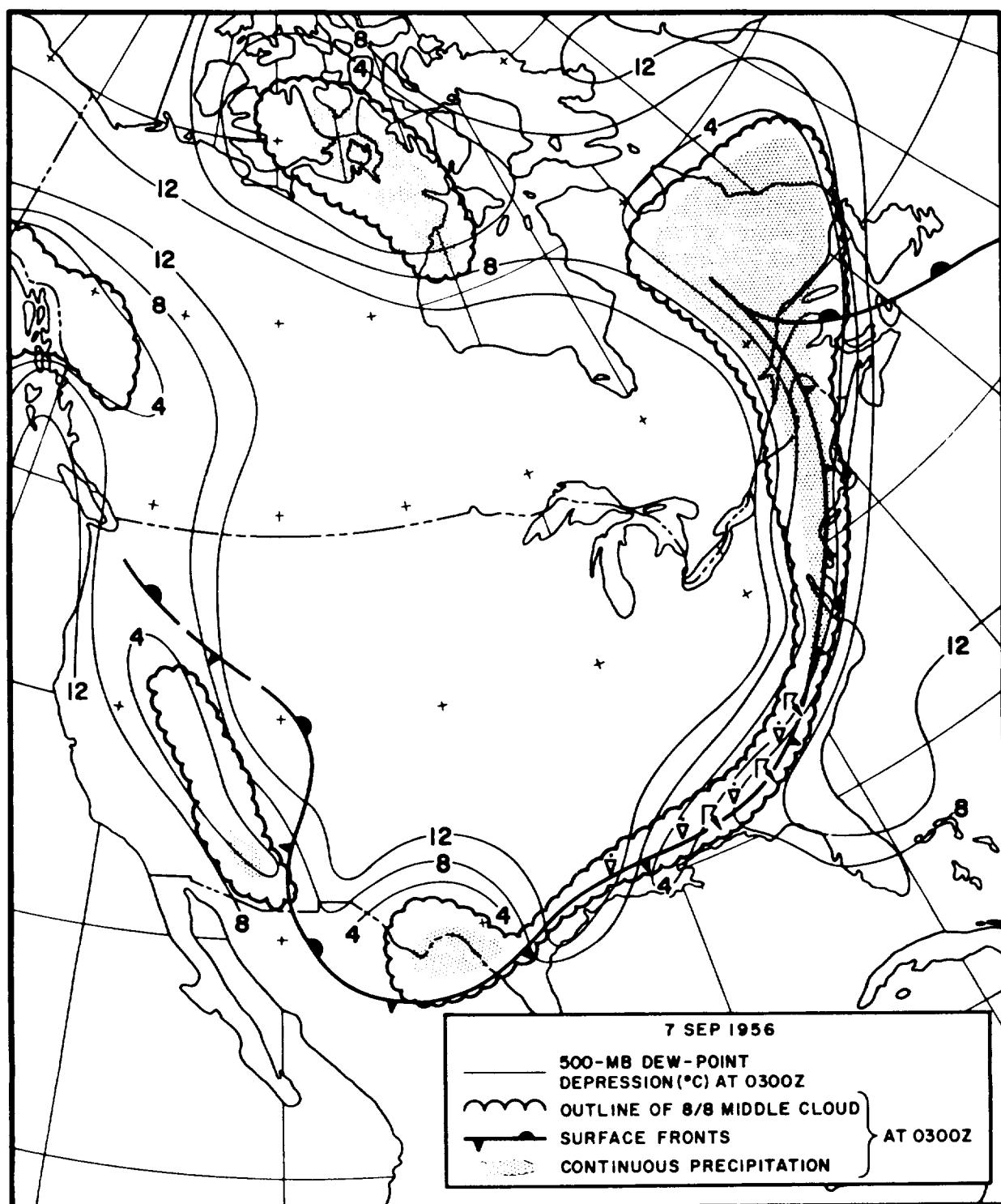
Figure 64. Surface Fronts, Areas of Continuous Precipitation, Areas Covered by 8/8 Middle Clouds, and Isolines of 500-mb Dew-Point Depression at 03Z, 7 September 1956.

plot between "motorboating" and "missing data." This distinction is often neglected. "Motorboating" should always be indicated as MB; "missing data" as MISDA (see par. 3.4). The confusion occurs because both cases are coded as a dew point of XX.

If the dew point is missing for reasons other than "motorboating," the case can be recognized by the additional data-group 10168 at the end of the transmission: The group 10168 is followed by one or more groups $OP_1P_1P_2P_2$, where P_1P_1 and P_2P_2 are the lower and upper levels of the stratum of missing data in tens of millibars.

When the temperature is below -40°C, no humidity data are sent; the humidity element is considered too unreliable at these low temperatures (see FMH No. 3, *Radiosonde Observations*, latest edition, as amended).

7.9. 500-mb Analysis of Dew-Point Depression.
Figure 64 shows an analysis of the 500-mb dew-point-depression field, superimposed upon an analysis (based upon the surface observations) of areas of continuous precipitation and of areas of overcast middle cloud. The 500-mb dew-point-depression isopleths were drawn independently of the surface data. The analyses show that:

a. The regions of high humidity at 500 mb coincide well with the areas of middle cloud and the areas of precipitation.

b. The regions of high humidity at 500 mb are separated from the extensive dry regions by strong humidity gradients. These gradients are, in all probability, much stronger than shown on this analysis, since this analysis has the defect of all continuous-field analyses which are based on discrete observations spaced widely apart; i.e., linear interpolation between observations smoothes out strong contrasts.

c. A dew-point depression of 4°C or less is characteristic of the larger part of the areas of continuous precipitation and also of the larger part of the areas of overcast middle clouds.

Since the 500-mb dew-point-depression analysis agrees well with the surface analysis of

middle cloud and precipitation, the possibility exists of replacing or supplementing one of these analyses with the other.

The characteristics (outlined above) of the 500-mb dew-point-depression analysis make it a valuable adjunct to the surface analysis. These analyses can be compared; and, by cross-checking, each can be completed with greater accuracy than if it were done independently.

A rough sketch of the dew-point-depression field may be completed on the facsimile chart in an few minutes. The dew-point depressions are now plotted on the upper-air analyses. Station circles are filled in where the depression is 5°C or less, which facilitates a quick appraisal of the dew-point-depression field.

7.10. Three-Dimensional Humidity Analysis — The Moist Layer.
A single-level (e.g., 500-mb) dew-point-depression analysis to find probable cloud areas does not indicate clouds above or below that level. For example, if the top of a cloud system reached only to 16,000 feet, and there were dry air above at 500 mb, we would never suspect, from the 500-mb analysis, the existence of cloud a short distance below the 500-mb level. (Admittedly, this is a hypothetical case; under such conditions, the raob would probably show humid conditions at 500 mb as well, even though the cloud top was actually below 500 mb.)

However, an analysis of the extension of the moist layers in three dimensions can be obtained simply by scrutinizing each individual raob. The raobs selected should be those for the general vicinity of, and the area 500 to 1200 miles upstream of, the area of interest, depending on the forecast period. (Most systems during a 36-hour period will move less than 1200 miles.) The moist layers, apart from the surface layers, can be determined by the methods described in paragraph 7.7. The heights of the bases and tops (labeled in thousands of feet of pressure altitude) are plotted at the raob-station location on the 500-mb chart. If more than one layer is present, this fact can be indicated, though there is little advantage in indicating a dry

7—22

layer 2000 to 3000 feet (or less) thick sandwiched between thicker moist layers. Usually, it is sufficient to indicate the entire moist layer, without bothering about any finer structure. A survey of the field is made easier by writing the heights of the bases in one color and the heights of the tops in another. It is not recommended that isopleths be drawn for the height of the bases and the tops, because the moist layer is not a well-defined entity.

If more specific and objective directions than those given in paragraph 7.7 are desired (as would be the case when non-professional persons are to select the moist layer), a moist layer may be defined as a layer having a frost-point depression of 3°C or less (i.e., a dew-point depression of 4°C at -10°C; 5°C at -20°C; 6°C at -30°C; etc.)

7.11. Limitations to Diagnosis of Tall Cumulus and Cumulonimbus Distribution from Raobs.
The cumulus and cumulonimbus of summer and tropical air-mass situations are generally scattered and in many, if not most cases, they do not actually cover over half of the sky. Under such conditions the probability of a radiosonde, released once to four times daily at a fixed time and place, passing up through a cloud of this type, appears. to be small. When a balloon does enter the base of a tall cumulus cloud it is likely to pass out of the side of the cloud rather than the top, or it may get caught for a time in a downdraft, giving an ambiguous record of the vertical-cloud distribution.

For the above reasons, experience indicates that little dependence can be placed on the usual soundings to indicate directly the existence of tall cumulus in the area. On the other hand, where the radiosonde samples the environment of such clouds, a stability analysis combined with consideration of surface-weather observations, radar and aircraft reports, and synoptic analysis for heating and convergence, will usually provide an estimate of the extent of cumulus sky coverage. This approach uses the same principles and procedures as in thunderstorm and severe-con-

vective weather forecasting, which are referenced in chapter 8 of this manual.

In those cases where the sounding passes up through a cumulus, it is well to keep in mind that the temperature in parts of such clouds is often colder than the environment just outside the cloud — especially due to "overshooting" or hail in regions of very strong updraft. These colder regions may still have buoyancy relative to other parts of the cloud surrounding them. Also, old dissipating cumulonimbus clouds are generally slightly colder than their environment.

The lapse rate in cumulus and cumulonimbus is not necessarily saturation adiabatic, owing to effects of "holes," downdrafts, melting of snow or hail, entrainment, mixing, etc.

Soundings made vertically through cumuliform clouds by means of aircraft or sailplanes are more indicative of their real structure than raobs; examples from various special projects are numerous in the literature (see, for example, [18] [37] [38] [45]).

7.12. Indications of Cirrus Clouds in Raobs.
True cirrus forms at temperatures near -40°C or colder and consists of ice crystals. At these temperatures as soon as the air is brought to saturation over water the condensate immediately freezes. The crystals then often descend slowly to levels of -30°C, and persist for a long time if the humidity below the formation level is high enough. In general, cirrus is found in layers which have saturation or supersaturation with respect to ice (at any temperature colder than 0°C, if the RH with respect to water is 100%, then the RH with respect to ice is >100%). Observations from special aircraft soundings with frost-point or dew-point hygrometers, indicated that the layers where cirrus occur are not always saturated with respect to ice and often occur with as much as 3°F frost-point depression; but this may be in part due to error in the instruments. When the aircraft noted "cirrus in the distance" at its height, a relative moist layer (frost-point depressions less than 15°F or 20°F) was usually being passed through [43] .

Present radiosonde humidity elements are far from capable of measuring humidity *values* satisfactorily at the temperatures of the cirrus levels. However, the elements will often show *change* in humidity at low temperatures that reflect the presence of the moist layers which contain cirrus. If the transmitted sounding data would include the heights at which the humidity trace at high levels indicates an increase, or the maximum height to which any humidity is shown, useful inferences of probability of cirrus could be made therefrom. This was suggested by an examination of some humidity traces on radiosonde records taken in conjunction with Project Cloud-Trail (*AWS TR 105-130* and *AWS TR 105-145*).

Several studies have pointed to indirect indications of cirrus presence whenever the dew-point depression at 500, 540, and 400 mb was relatively low [34] . Bannon [9] [10] found a correlation of 0.80 between temperature at 500 mb and frost point at 300 mb and 0.82 between $T_{(500)}$ and $T_{f(250)}$.

Results of efforts to find a relation between changes in lapse rate and the occurrence of cirrus have not been very convincing and it is doubtful on *a priori* grounds that any such simple universal relation should be expected (*AWS TR 105-130*).

Appleman has shown how his contrail-forecasting curves (when overlaid on the Skew-T Chart) can be used to improve the accuracy of ground-observer estimates of the height of *observed* cirrus layers (see *AWS TR 105-110* and *AWS TR 105-110A* for details of procedure and tests).

Chapter 8

FORECASTING USES OF RAOBS PLOTTED ON ADIABATIC CHARTS

8.1. General. Increasing dependence of detachments on centrally-produced analyses and prognoses has reduced the role of raob analysis. AWS philosophy on the use of the computer products and guidance on the use of raobs in conjunction with facsimile charts is outlined in AWSM 105-55 (rescinded, but can be used for background information). Some special techniques that require evaluations from analyzed and/or forecast soundings were developed by AWS for: severe convective storms, aircraft icing, contrails, anomalous propagation and refractive index, fog, and density altitude. Techniques for forecasting other phenomena from soundings, such as maximum temperatures and clouds, have been described in the literature.

8.2. Severe Convective Storms. The AWS Military Weather Warning Center (MWWC) employs specialized raob analysis techniques to identify airmass types favorable for severe weather, to evaluate various derived indexes of stability, to construct forecast soundings, and to semi-objectively evaluate hail size and maximum wind-gusts. Most of the MWWC routines are too sophisticated and time consuming for ordinary detachment use. The evaluation of many of these indexes has been computerized. However, several of the MWWC procedures that are described in AWS Technical Report 200 can be used in the detachment. A number of objective local-forecast studies for prediction of thunderstorms that use predictors taken from the sounding are listed in AWS TR 105-19.

8.3. Aircraft Icing. AWS/TR-81/001 describes procedures developed by AWS for forecasting icing. One procedure, which uses an overlay to the Skew-T diagram as an aid for determining the probable type and intensity of icing from a current or forecast sounding, has been computerized at the Air Force Global Weather Central (AFGWC).

8.4. Contrails. The AWS procedure for forecasting contrails is described in AWS/TR-81/001. This technique, which employs either curves overprinted on the Skew-T chart (DOD WPC-9-16) or a transparent overlay for this chart, has been computerized at AFGWC.

8.5. Anomalous Propagation and Refractive Index. The estimation of radio and radar refraction due to the atmosphere is treated comprehensively in AWS-TR-183 (2 Vols.) The various procedures are based on an evaluation of actual, forecast, or climatic soundings or on assumed model-atmospheric soundings. AWS has published a version of the Skew-T chart (DOD WPC-9-16-2) with a refractivity overprint. The construction and use of this chart was first described in AWS TR 169.

8.6. Fog Forecasting. The general aspects of fog forecasting are discussed in AWS-TR-239, as well as in standard textbooks of synoptic and applied meteorology. Certain specialized techniques require a detailed analysis of the lower level of the atmosphere sounding. Some objective fog-forecast techniques using sounding-derived variables are listed in AWS TR 105-19 and AWSP 0-13, but the ones that follow are new, and are included as part of the March 1990 revision:

Fog Stability Index (FSI).
The FSI, along with the "Fog Point" and "Fog Threat" that follow, may be useful for fog forecasting. The formula for FSI is:

$$FSI = 4T_s - 2(T_{850} + Td_s) + W_{850}$$

where:

$$T_s \quad = \text{Surface temperature in } °C$$

$$T_{850} = 850 \text{ mb temperature in } °C$$

$$Td_s = \text{Surface dew point in } °C$$

$$W_{850} = 850 \text{ mb wind speed in kts}$$

FSI	LIKELIHOOD OF RADIATION FOG
>55	Low
31-55	Moderate
<31	High

Fog Point.

This value indicates the temperature (°C) at which radiation fog will form. To determine fog point, find the pressure level of the LCL using the procedure described in Para 4.20. From the dew point at this pressure level, follow the saturation mixing ratio line to the surface. The isotherm value at this point is the fog point, or the temperature at which radiation fog will form.

Fog Threat.

This value indicates degree of the threat of fog formation by radiational cooling. It is calculated by subtracting fog point (see above) from the 850-mb wet bulb potential temperature.

Fog Threat = 850-mb wet bulb potential temperature minus fog point.

FOG THREAT	LIKELIHOOD OF RADIATION FOG
>3	Low
0-3	Moderate
<0	High

8.7. Density Altitude. A version of the Skew-T chart with an overprint grid to facilitate computation of density altitude was published in AWS TR 105-101 (Rev. 2); individual copies of this chart can be requisitioned from AWS. For operations at remote sites where soundings and observations are not available, use the special nomogram and tables in AWS TR 165.

8.8. Cirrus Cloud. Techniques for forecasting cirrus on the basis of lapse-rate parameters are summarized in AWS TR 105-130. However, other approaches described in the same report appear to be more successful.

8.9. Maximum Temperature Forecasting. Various objective methods for forecasting maximum temperature have been described in the literature (see U. S. W. B. Forecasting Guide No. 4). Most of these techniques involve a procedure for evaluating the solar energy input at the surface either by subjective synoptic considerations or by a physical approach. In either case, the Skew-T chart of a similar diagram is frequently used to convert the energy input into temperature gain. This conversion is facilitated by overlaying a set of parallel lines representing energy units and reading off corressponding temperatures on the Skew-T chart, adiabatic chart, or tephigram. Myers has devised an overlay for a Weather Bureau Adiabatic Chart (*Mon. Wea. Rev.*, Vol 86, 1985, pp. 149-164) and Kagawa has developed an overlay for the Canadian tephigram (DOT Canada, Met. Branch Tech Memo #683). A similar overlay can be prepared for the Skew-T chart.

8.10. Clouds. Use of adiabatic charts to estimate or forecast convective cloud amount, height, or intensity has been the subject of experiment for many years. In almost all this work it was necessary to adjust the procedure to local conditions, particularly as to place and time of soundings available, choice of representative surface temperature and moisture values, allowance for entrainment, and diurnal effects of convective mixing, topography, etc. Any success is usually attributed to the experimenter's experience and skill in such empirical modifications. One important difficulty is that in warm moist air masses small errors of several hundred feet in estimating or forecasting the height of the condensation level leads to very large differences in the forecast of cloud-top height, cloud coverage, and severity of associated convection weather. Recent literature of attempts to develop physical cumulus cloud-development models (for computer evaluation) and direct observation of cumulus structure, dynamics, and evolution by aircraft and radar suggest more realistic and sophisticated procedures for modifying parcel analysis on adiabatic charts. Studies of cloud populations over large areas also provide and background for better cloud forecasting with parcel analysis by allowing area probability considerations to be introduced.

REFERENCES

[1]   Albert, E. G. : "A Case Study of the Tropopause," Science Report #6, Contract
         No. AF 19(604) - 1755, New York Univ., Dept. of Met., 1959.

[2]   Anon: "Forecasting Tornadoes and Severe Thunderstorms," Forecasting Guide
         No. 1, US Weather Bureau, September 1956, 34 pp.; see also, Galway, J. G.:
         "The Lifted Index as a Predictor of Latent Instability," Bull. Amer. Met. Soc.,
         Vol. 37, No. 10, December 1956, pp. 528-529.

[3]   Anon: "Testing a Thunderstorm Forecasting Method," AWS Bulletin, November
         1952, pp. 24-27.

[4]   Anon: "Theta-E Charts and Thunderstorm Forecasting," AWS Bulletin, No. 3,
         1950, pp. 25-27.

[5]   Austin, J. M., and Blackmer, R. H.: "The Variability of Cold Front Precipita-
         tion," MIT, Dept. of Met., Research Report #27, Contract Report No. DA-36-
         039SC-71136, July 1956.

[6]   AWS-TR-239 : "General Aspects of Fog and Stratus Forecasting," April 1954 (AD-
         33689).

[7]   AWS TR 105-86: "Tropopause Analysis and Forecasting," March 1952 (ATI-162082).

[8]   Banerji, S. : "Forecasting Thunderstorms at Nagpur by Slice Method," Indian Jn.
         of Met. and Geophys., Vol. 1, No. 3, July 1950, pp. 184-189.

[9]   Bannon, J. K. : "An Analysis of Humidity in the Upper Troposphere and Lower
         Stratosphere," MRP 563, May 1950 (ATI-88400).

[10]   Bannon, J. K., Frith, R., and Shellard, H. C.: "Humidity of the Upper Tropo-
         sphere and Lower Stratosphere Over Southern England," Geophysical Memoirs
         No. 88, Met. Office, London, 1952.

[11]   Bellamy, J. C. : "Objective Calculations of Divergence, Vertical Velocity and
         Vorticity," Bull. Amer. Met. Soc., Vol. 30, No. 2, February 1949, pp. 45-49.

[12]   Bergeron, T. : "The Physics of Fronts," Bull. Amer. Met. Soc., Vol. 18, No. 9,
         September 1937, pp. 265-275.

[13]   Berry, F. A., Jr., Bollay, E., and Beers, N. R.: Handbook of Meteorology, 1st
         Edition, McGraw-Hill Book Co., Inc., New York, 1945.

[14]   Bjerknes, J. : "Saturated-Adiabatic Ascent of Air Through Dry-Adiabatically De-
         scending Environment," Quart. Jn. Roy. Met. Soc., Vol. 64, 1938, pp. 325-330.

[15]   Bjerknes, J., and Holmboe, J.: "On the Theory of Cyclones," Jn. of Met., Vol.
         1, Nos. 1-2, September 1944, pp. 1-22, plus Figures 9, 10, 14, 15, and 16.

[16]   Braham, R. R., Jr., and Draginis, M.: "Roots of Orographic Cumuli," 1st Con-
         ference on Cumulus Convection, May 19-22, 1959, 14 pp., plus figures.

[17]   Bunker, A. F.: "On the Determination of Moisture Gradients from Radiosonde
         Records," Bull. Amer. Met. Soc., Vol. 34, No. 9, November 1953, pp. 406-409.

[18]   Byers, H. R. , and Braham, R. R. : The Thunderstorm, Report of the Thunder-
         storm Project, U.S. Dept. of Commerce, US Weather Bureau, GPO, June 1949.

[19]   Conover, J. H. , and Wollaston, C. H. : "Cloud Systems of a Winter Cyclone," Jn.
         of Met. , Vol. 6, 1949, pp. 249-260.

[20]   Cressman, G. P. : "An Approximate Method of Divergence Measurement," Jn. of
         Met. , Vol. 11, No. 2, April 1954, pp. 83-90.

[21]   Cressman, G. P. : "The Influence of the Field of Horizontal Divergence on Con-
         vective Cloudiness," Jn. of Met. , Vol. 3, No. 3, September 1946, pp. 85-88.

[22]   Curtis, R. C. , and Panofsky, H. A. : "The Relation Between Large-Scale Vertical
         Motion and Weather in Summer," Bull. Amer. Met. Soc. , Vol. 39, No. 10, Oc-
         tober 1958, pp. 521-531.

[23]   Danielsen, E. F. : "The Laminar Structure of the Atmosphere and Its Relation to
         the Concept of a Tropopause," PhD Thesis, Univ. of Washington, Dept. of Met.
         and Clim. , 1958, 106 pp. ; also reprint from Arch. Met. Geoph. Biokl. , Series
         A, Vol. 11, No. 3, 1959, pp. 293-332.

[24]   Endlich, R. M. , and McLean, G. S. : "The Structure of the Jet Stream Core,"
         Jn. of Met. , Vol. 14, No. 6, December 1957, pp. 543-552.

[25]   Fawbush, E. J. , and Miller, R. C. : "A Method for Forecasting Hailstone Size
         at the Earth's Surface," Bull. Amer. Met. Soc. , Vol. 34, No. 6, June 1953,
         pp. 235-244.

[26]   Godson, W. L. : "Superadiabatic Lapse Rate in the Upper Air," Tech. Note No.
         16, WMO, Geneva, 1955.

[27]   Godson, W. L. : "Synoptic Properties of Frontal Surfaces," Quart. Jn. Roy. Met.
         Soc. , Vol. 77, No. 334, October 1951, p. 641.

[28]   Graham, R. D. : "A New Method of Computing Vorticity and Divergence," Bull.
         Amer. Met. Soc. , Vol. 34, No. 2, February 1953, pp. 68-74.

[29]   Graves, M. E. : "The Relation Between the Tropopause and Convective Activity
         in the Subtropics (Puerto Rico)," Bull. Amer. Met. Soc. , Vol. 32, No. 2, Feb-
         ruary 1951, pp. 54-60.

[30]   Herlofson, N. : "The T, log p — Diagram with Skew Coordinate Axes," Meteoro-
         logiske Annaler, Vol. 2, No. 10, Oslo, 1947, pp. 311-342 plus diagrams.

[31]   Hewson, E. W. : "The Application of Wet-Bulb Potential Temperature to Air Mass
         Analysis," Quart. Jn. Roy. Met. Soc. , Vol. 63, No. 266, July 1936, pp. 387-
         420; see also, Quart. Jn. Roy. Met. Soc. , Vol. 63, No. 268, January 1937, pp.
         7-30; and Quart. Jn. Roy. Met. Soc. , Vol. 63, No. 271, July 1937, pp. 323-337.

[32]   Hodge, M. W. : "Superadiabatic Lapse Rates of Temperature in Radiosonde Ob-
         servations," Mon. Wea. Rev. , Vol. 84, No. 3, March 1956, pp. 103-106.

[33]   Holmboe, J. , Forsythe, G. E. , and Gustin, W. : Dynamic Meteorology, John Wiley
         and Sons, Inc. , New York, 1945.

[34]   James, D. G. : "Investigations Relating to Cirrus Cloud," MRP 933, September 1955; see also Met. Mag., Vol. 86, No. 1015, January 1957, pp. 1-2; and Met. Mag., Vol. 88, No. 1041, March 1959, pp. 79-80.

[35]   Local Forecast Study for Wright-Patterson AFB: "Thunderstorms and Rain Showers," Terminal Forecast Manual, Section IV A, typescript, 14 November 1956 (AD-116123).

[36]   Ludlam, F. H., and Mason, B. J. : "Radar and Synoptic Studies of Precipitating Clouds," Tech. Rept. No. 1, Contract No. AF 61(514)-809, Dept of Met., Imperial College of Science and Techn., January 1956, 44 pp.

[37]   Malkus, J. S. : "On the Structure of the Trade Wind Moist Layer," Tech. Rept. No. 42, Ref. 57-9, Woods Hole Oceanographic Institute, January 1957, unpublished manuscript.

[38]   Malkus, J. S. : "Recent Advances in the Study of Convective Clouds and Their Interaction with the Environment," Tellus, Vol. 4, No. 2, May 1952, pp. 71-87.

[39]   Marshall, J. S. : "Effects of General Lifting or Subsidence on Convective Overturning," 1st Conference on Cumulus Convection, May 1959, Woods Hole, McGill Univ., Montreal, 1959, unpublished manuscript.

[40]   Mason, B. J., and Howorth, B. P. : "Some Characteristics of Stratiform Clouds Over North Ireland in Relation to Their Precipitation," Quart. Jn. Roy. Met. Soc., Vol. 78, 1952, pp. 226-230.

[41]   Matthewman, A. G. : "Cloud in Relation to Warm and Quasi-Stationary Fronts Near Bircham Newton in Winter," MRP 747, Met. Office., London, 1952.

[42]   Matthewman, A. G. : "Studies of the Structure of Fronts," Part I, MRP 597, Met. Office, London, 1950.

[43]   Murgatroyd, R. J., and Goldsmith, P. : "Cirrus Cloud Over Southern England," MRP 833, September 1953; (published later as) "High Cloud Over Southern England," Prof. Notes No. 119, Met. Office, London, 1956.

[44]   Namias, J. : "Subsidence Within the Atmosphere," Harvard Meteorological Studie No. 2, 1934.

[45]   Namias, J., et al. : "An Introduction to the Study of Air Mass and Isentropic Analysis," 5th Revised and Enlarged Edition, Amer. Met. Soc., October 1940.

[46]   Normand, C. W. B. : "On Instability from Water Vapour," Quart. Jn. Roy. Met. Soc., Vol. 64, No. 273, January 1938, pp. 47-69.

[47]   Petterssen, S. : Weather Analysis and Forecasting, McGraw-Hill Book Co., Inc., New York, 1940, p. 101.

[48]   Petterssen, S. : Weather Analysis and Forecasting, 2d Edition, Vol. II, McGraw-Hill Book Co., Inc., New York, 1956.

[49]   Petterssen, S., Knighting, E., James, R. W., and Herlofson, N. : "Convection in Theory and Practice," Geofysiske Publikasjoner, Vol. 16, No. 10, Oslo, 1946, 44 pp.

[50]   Priestley, C. H. B.: "Buoyant Motion in a Turbulent Environment," Austr. Jn. of Phys., Vol. 6, No. 3, September 1953, pp. 279-290.

[51]   Reihl, H.: Tropical Meteorology, McGraw-Hill Book Co., Inc., New York, 1954, pp. 53-70.

[52]   Rossby, C. G.: "Thermodynamics Applied to Air Mass Analysis," papers in Oceanog. and Met., Woods Hole Oceanog. Instn., and MIT, Vol. 1, No. 3, 1932, 41 pp

[53]   Sansom, H. W.: "A Study of Cold Fronts Over the British Isles," Quart. Jn. Roy. Met. Soc., Vol. 77, No. 331, January 1951, pp. 96-120.

[54]   Saunders, P. M.: "The Thermodynamics of Saturated Air: A Contribution of the Classical Theory," Quart. Jn. Roy. Met. Soc., Vol. 83, No. 357, July 1957, pp. 342-350; also Ludlam, F. A., and Saunders, P. M.: "Shower Formation in Large Cumulus," Tellus, Vol. 8, No. 4, November 1956, pp. 424-442.

[55]   Sawyer, J. S.: "Effect of Atmospheric Inhomogeneity on the Interpretation of Vertical Temperature Soundings," Met. Mag., Vol. 82, No. 975, September 1953, pp. 257-263.

[56]   Sawyer, J. S.: "The Free Atmosphere in the Vicinity of Fronts, Analysis of Observations by the Meteorological Research Flight," MRP 807, Met. Office, London, 1953: (published later as) "The Free Atmosphere in the Vicinity of Fronts," Geophysical Memoirs #96, Met. Office, London, 1955.

[57]   Sawyer, J. S., and Dinsdale, F. E.: "Cloud in Relation to Active Warm Fronts Near Bircham Newton During the Period April 1942 — April 1946," MRP 799, Met. Office, London, 1953.

[58]   Showalter, A. K.: "A Stability Index for Thunderstorm Forecasting," Bull. Amer. Met. Soc., Vol. 34, No. 6, June 1953, pp. 250-252.

[59]   Similä, A.: "Die Aerologischen Gewittertendenzkarten," Tellus, Vol. 1, No. 4, November 1949, pp. 18-23.

[60]   Smithsonian Meteorological Tables, 6th Revised Edition, Smithsonian Institute, Washington, D. C., 1951, p. 352.

[61]   Wagner, A. J., and Sanders, F.: "Some Relationships Between Air Mass Stability, Large-Scale Vertical Motion and Thunderstorm Frequency," Appendix 2 to "Some Application of Dynamical Concepts," MIT, Dept. of Met., Final Report on Contract No. AF 19(604)-1305, February 28, 1959, pp. 53-71 (AD-212267).

[62]   Wexler, A.: "Low-Temperature Performance of Radiosonde Electric Hygrometer Elements," Jn. Res. Nat. Bur. Stand., Vol. 43, 1949, pp. 49-56.

[63]   Wexler, H.: "The Cooling in the Lower Atmosphere and the Structure of Polar Continental Air," Mon. Wea. Rev., Vol. 64, No. 4, April 1936, pp. 122-136.

[64]   Wexler, R., Reed, R. J., and Honig, J.: "Atmospheric Cooling by Melting Snow," Bull. Amer. Met. Soc., Vol. 35, No. 2, February 1954, pp. 48-51.

[65]   WMO: Technical Regulations, Vol. I, WMO-No. 49, BD2, Secretariat of World Meteorological Organization, Geneva, 2d Edition, 1959.

A STUDY OF THE INTERPRETATION OF CLOUD
LAYERS FROM SOUNDINGS
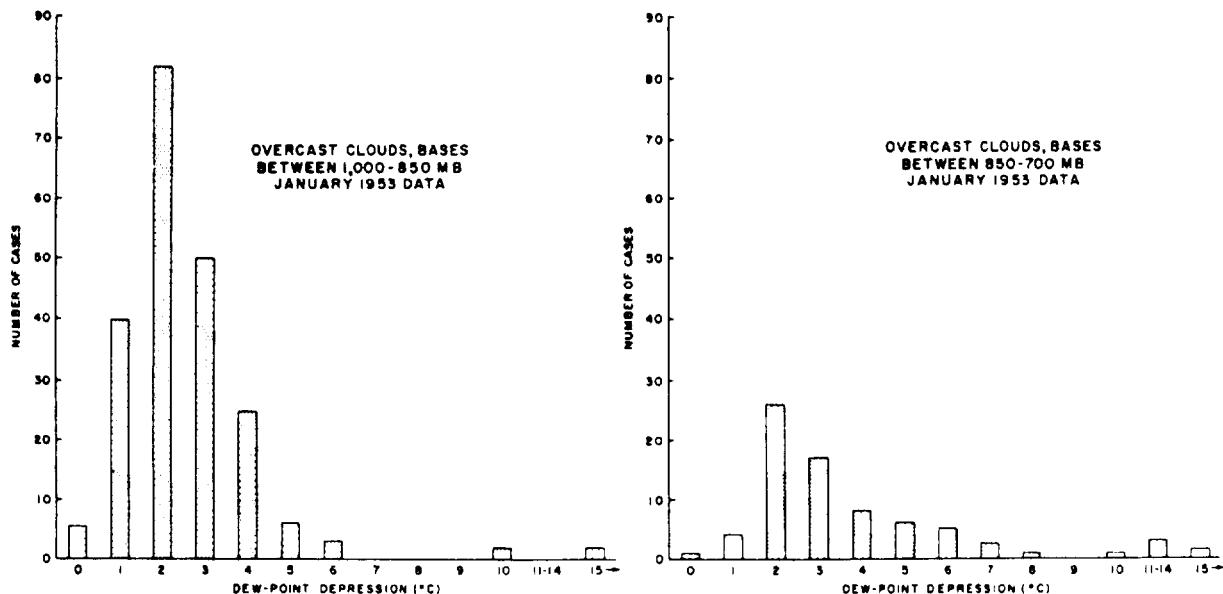
Figure A-1. **Frequency of Dew Point Depressions (°C) at the Cloud Base for Solid Overcasts with Bases Between 1000 and 700mb.**

In an unpublished study conducted by Romo at Hq AWS, raobs for January 1953 from 29 U. S. Weather Bureau stations were compared with the lowest-cloud-layer observations at the location and time of each sounding. Only reliable cloud observations were used, e.g., only those of the lowest observed cloud layer and those obtained from available pilot reports. The T_d value reported on the sounding at the base of the lowest cloud layer was then recorded for each cloud observation. For example, if Pittsburgh reported an overcast at 4000 feet at 0330Z, the 0300Z Pittsburgh sounding was examined for the dew-point depression at that height above the surface. To compensate for the probable lag in the humidity element, the smallest dew-point depression within the first 1000 feet above the reported cloud-base height was selected as representative.

Bargraphs showing the frequency of the January 1953 reports with the various dew-point depressions at the base of solid overcasts are shown in Figure 65.

One graph refers to the base of the overcasts observed within the 1000- to 850-mb layer, while the other refers to overcast cloud bases in the 850- to 700-mb layer. The graphs show that dew-point depressions of 1°C to 4°C are typical of overcast cloud decks in both layers during January. In these graphs the few cases of dew-point depressions greater than 5°C are attributed to either instrument failure or transmission errors.

Figure 66 shows the frequencies of various dew-point depressions at the cloud-layer base for both 1/10 to 3/10 and 4/10 to 7/10 cloud coverages, which are further subdivided into the 1000- to 850-mb and 850- to 700-mb layers.

Again, the greatest concentration is around a dew-point depression of 2°C to 3°C at the cloud base; but the 850- to 700-mb reports show a more even distribution.

Figure 67 shows the dew-point depressions at the 850-, 700-, and 600-mb surfaces when clear skies occur. As expected, clear skies
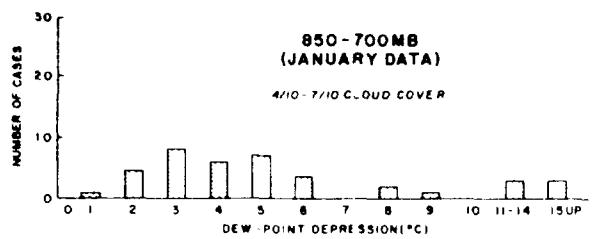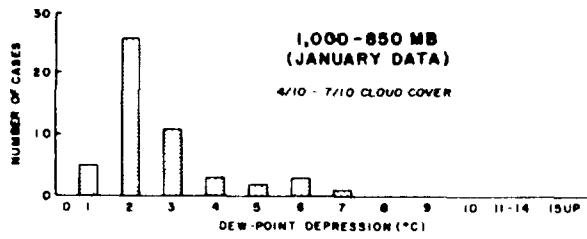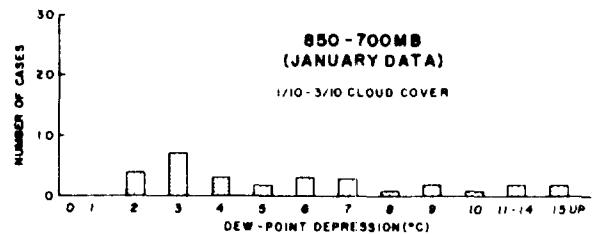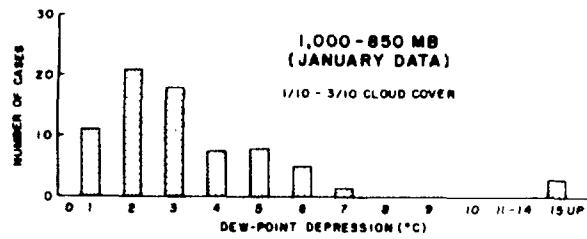
Figure A-2. **Frequency of Dew Point Depressions (°C) at Cloud Base in 1/10 to 3/10 and 4/10 to 7/10 Cloud Layers Between 1000 and 700mb.**

are generally associated with much bigger dew-point depressions.

The data from Figures 65, 66, and 67, can be summarized in a different way. Figure 68 (from which Figure 63 of the text was derived) shows the percent probability for clear, scattered, broken, and overcast cloud conditions in January as a function of the dew-point depression at the cloud base for the 1000- to 850-mb and 850- to 700-mb layers. These data represent 1027 individual January observations, enough to indicate the order of magnitude of the dew-point depressions at the base of winter cloud layers; but these

observations are not numerous enough to specify the actual percentages.

The above values are applicable during the winter months regardless of the synoptic situation. Given a sounding, one can determine from the graph the approximate probability of different sky-cover cloud layers with bases between 1000 mb and 600 mb for the layers of minimum dew-point depression up to 600 mb. During the warmer months of the year, the given probabilities are expected to increase for the smaller dew-point depressions and decrease for the larger depressions.
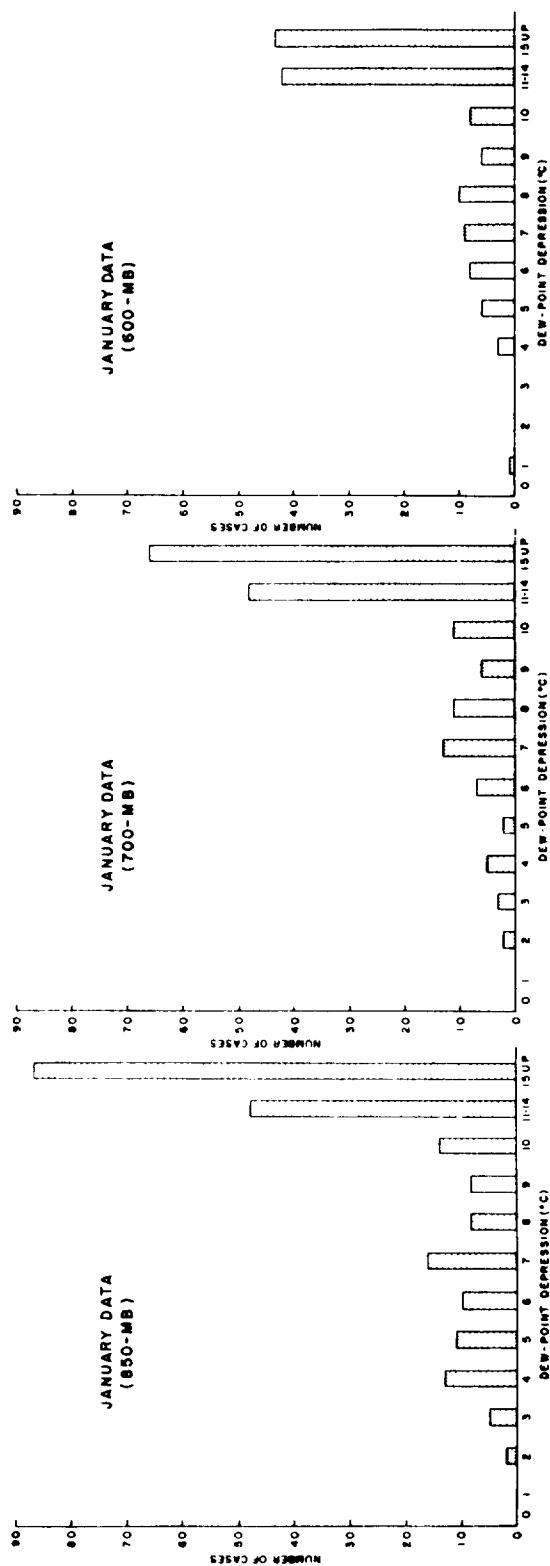
Figure A-3. *Dew Point Depressions at 850-, 700-, and 600-mb Surfaces with Clear Skies.*
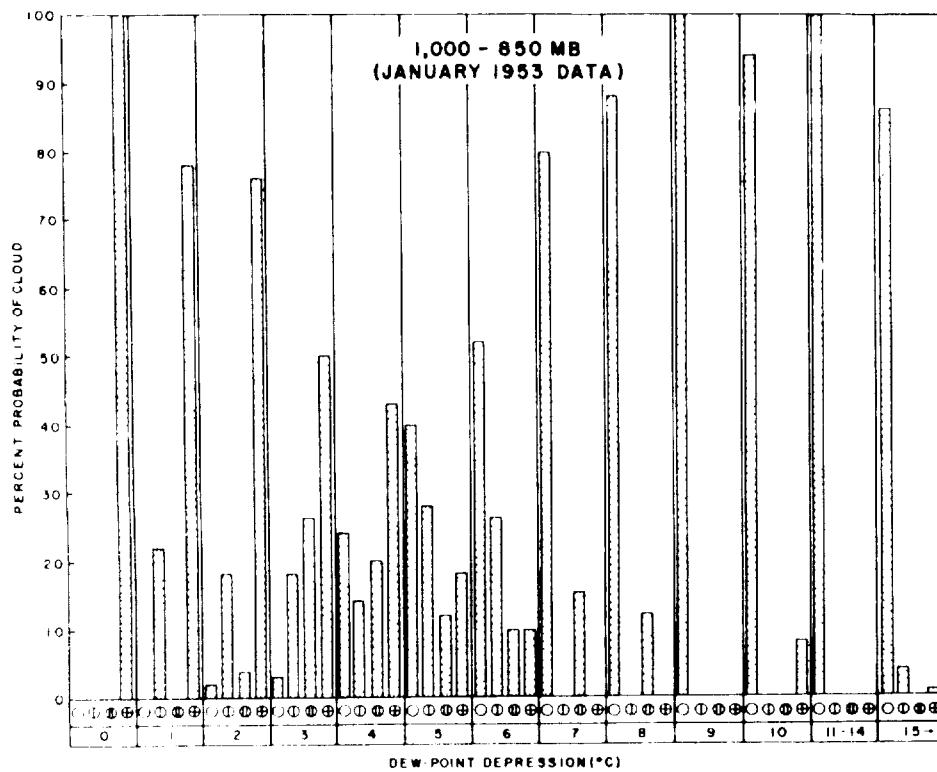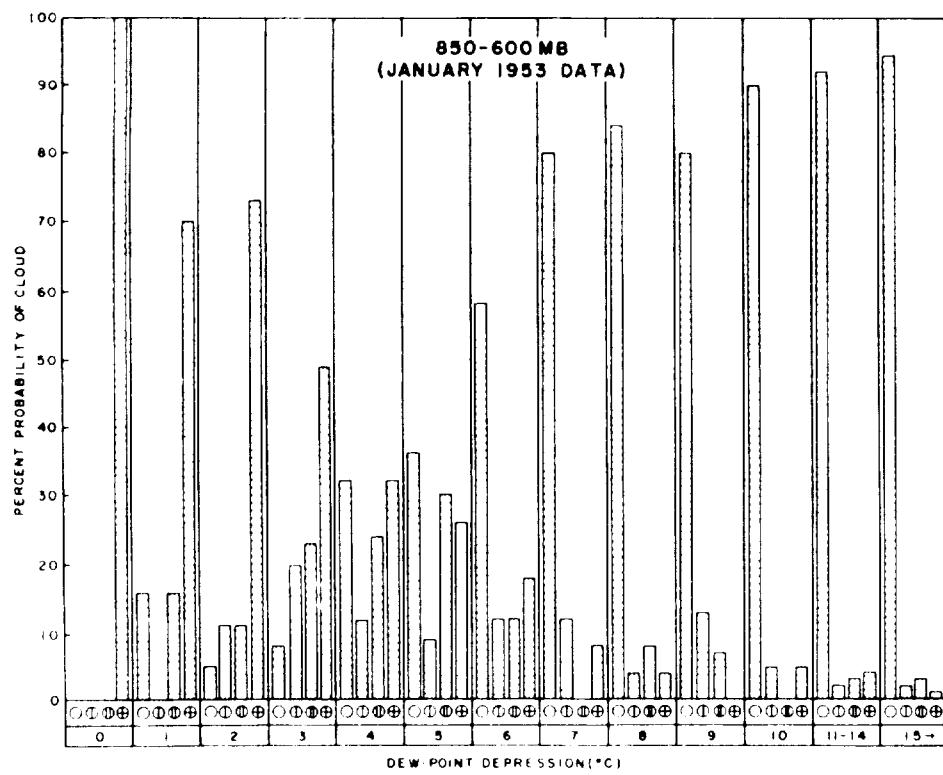
Figure A-4. The Approximate Percent Probability of Different Sky Coverages with Cloud Bases Between 1000 and 850mb Plotted Against the Dew Point Depression at the Cloud Base.

A-4

APPENDIX B

A MATHEMATICAL ANALYSIS OF LAPSE-RATE CHANGES

In an unpublished study (on file in Hq AWS), Johannessen mathematically described the processes in the atmosphere that lead to a change in the lapse rate at a station.

Denoting the lapse rate by:

$$\gamma = -\frac{\partial T}{\partial z} \qquad (1)$$

where T is temperature and z is height above the ground, we can write the identity:

$$\frac{\partial \gamma}{\partial t} \equiv \frac{\partial}{\partial t}\left(-\frac{\partial T}{\partial z}\right) \equiv -\frac{\partial}{\partial z}\left(\frac{\partial T}{\partial t}\right)$$

$$= -\frac{\partial}{\partial z}\left(\frac{dT}{dt} - \mathbf{v} \cdot \nabla T + w\gamma\right) \qquad (2)$$

where $\mathbf{v}$ is the horizontal wind vector and w is the vertical motion.

From the first law of thermodynamics:

$$\frac{dQ}{dt} = c_p \frac{dT}{dt} - \alpha \frac{dp}{dt} \qquad (3)$$

where Q is heat supplied to a mass unit of air, c_p is specific heat, α is specific volume, and p is pressure. In the atmosphere we can further write with sufficient accuracy (after considering the magnitude of the various terms in the expansion of $\frac{dp}{dt}$):

$$\frac{dp}{dt} \approx w \frac{\partial p}{\partial z} = -wg\rho \qquad (4)$$

where ρ is density and g acceleration of gravity. Applying Equations (4) and (3) into (2) results in:

$$\frac{\partial \gamma}{\partial t} = -\frac{\partial}{\partial z}\left[\frac{1}{c_p}\frac{dQ}{dt} - \mathbf{v} \cdot \nabla T - w(\Gamma - \gamma)\right] \qquad (5)$$

where we have written:

$\Gamma = g/c_p = 0.01\ °C\ m^{-1} =$ dry adiabatic lapse rate.

In Q above is included the latent heat exchanged during condensation and evaporation. If we want to exclude the latent heat from Q and let Q stand only for heat transfers by radiation and turbulence, we may do so by interpreting Γ as the saturation adiabatic lapse rate during the condensation phase, but as the dry adiabatic lapse rate otherwise.

Writing Equation (5) down, term by term (after performing the indicated differentiations of products):

$$\frac{\partial \gamma}{\partial t} = \begin{cases} \text{increasing stability when} < 0 \\ \text{decreasing stability when} > 0 \end{cases}$$

$$= -\frac{1}{c_p}\frac{\partial}{\partial z}\left(\frac{dQ}{dt}\right) : \begin{cases} \text{differential heating in the} \\ \text{vertical} \end{cases}$$

$$-\mathbf{v}\cdot\nabla\gamma \qquad : \begin{cases} \text{advection of air of different} \\ \text{stability} \end{cases}$$

$$+\frac{\partial \mathbf{v}}{\partial z}\cdot\nabla T \qquad : \begin{cases} \text{shearing advection of} \\ \text{different temperature} \end{cases}$$

$$+\frac{\partial w}{\partial z}(\Gamma - \gamma) \qquad : \begin{cases} \text{shrinking and stretching of} \\ \text{column} \end{cases}$$

$$-w\frac{\partial \gamma}{\partial z} \qquad : \begin{cases} \text{vertical advection of lapse} \\ \text{rate} \end{cases}$$

A brief discussion of each term follows:

a. $- \dfrac{1}{c_p} \dfrac{\partial}{\partial z} \left(\dfrac{dQ}{dt} \right)$: This very im-

portant term is responsible for the pronounced diurnal change in lapse rate. By day, insolation heats the ground layers more than the layers above, thus $\dfrac{\partial}{\partial z} \left(\dfrac{dQ}{dt} \right)$ is negative and the whole term is positive; i.e., destabilization occurs. This effect may also be of importance away from the ground, e.g., night cooling from the top of cloud layers may destabilize the cloud tops and cause them to grow upwards. This effect has been offered as an explanation for nocturnal thunderstorms.

b. $- \mathbf{v} \cdot \nabla \gamma$: When a gradient of lapse rate exists and the wind blows across the isolines of lapse rate, air of a different lapse rate is simply replacing the air *in situ* and a corresponding change takes place. This process cannot, for instance, create an area of instability where none existed before. The process can merely translate already existing areas of stability and instability. However, it is one of the main effects to watch for on the map, since, for example, showers may occur as air of less stability is moving into an area.

c. $\dfrac{\partial \mathbf{v}}{\partial z} \cdot \nabla T$: The shearing advection process is identically zero if the winds are geostrophic, since $\dfrac{\partial \mathbf{v}_g}{\partial z} \approx \mathbf{k} \times \nabla T$ and $\mathbf{k} \times \nabla T \cdot \nabla T = 0$.

Hence, if we write: $\mathbf{v} = \mathbf{v}_g + \mathbf{v}_a$, where $\mathbf{v}_g$ is the geostrophic wind, then

$\dfrac{\partial \mathbf{v}}{\partial z} \cdot \nabla T = \dfrac{\partial \mathbf{v}_a}{\partial z} \cdot \nabla T$; i.e., only the *ageostrophic* wind components accomplishes anything. This term may create areas of instability where none existed before and may thus have greater prognostic importance if it can be evaluated properly by chart methods.

d. $\dfrac{\partial w}{\partial z} (\Gamma - \gamma)$: This process stabilizes a shrinking column and destabilizes a stretching column. A stretching column may, for instance, be one where the top ascends more rapidly than the bottom, hence, the top will cool more rapidly than the bottom and result in less stability. In a shrinking column, the top may ascend more slowly than the bottom and result in increased stability.

e. $- w \dfrac{\partial \gamma}{\partial z}$: This effect is a shifting up or down of existing lapse rates along the vertical. An example is that subsidence may spread stable inversion lapse rates downwards, almost to the ground in extreme cases.

The analysis above is a mental exercise that may be considered necessary to understand the way radiation, turbulence, release of latent heat, advection, shearing motion, and stretching and shrinking of atmospheric air columns contribute to changing the local lapse rate. At times one of the effects may be dominant to the extent that the other effects are only feeble reflex processes of smaller magnitude. In such cases the sign of the total is at least easy to determine. At other times, two or more of the processes are of the same and considerable magnitude but opposite sign so that the outcome may be hard to guess.

INDEX OF TERMS

(Shows paragraph where certain terms and concepts are defined, introduced, or primarily discussed.)